DESIGN AND COMMISSIONING OF A COMPUTER CONTROLLED OSCILLATING HYDROFOIL DYNAMOMETER

DAVID L. GREENING

Design And Commissioning Of A Computer Controlled Oscillating Hydrofoil Dynamometer

by

© David L. Greening, B.Eng.

A thesis submitted to the School of Graduate Studies in partial fulfilment of the requirements for the degree of Master of Engineering

Faculty of Engineering and Applied Science
Memorial University of Newfoundland

April, 1996

St. John's Newfoundland Canada

ISBN 0-612-17595-2

Design And Commissioning Of A Computer Controlled Oscillating Hydrofoil Dynamometer

David L. Greening, B.Eng.

Abstract

High propulsive efficiencies can be realised from oscillating foil propulsors. Information on these propulsors can be obtained by systematically studying the geometry's and motions of manufactured foils and the fins and flukes of cetacean mammals and fast swimming fish, which propel themselves through oscillations of a high aspect ratio lunate fin or fluke.

The development of a dynamometer for studying the flow patterns and propulsive characteristics of oscillating foil propulsors is described. The dynamometer was designed to measure the effect of variations in foil parameters such as planform, sweep back, foil section, pitching axis location, and foil flexibility for a series of oscillating motions. It was designed primarily for use in a cavitation tunnel, to study the flow over the foils and their cavitational characteristics and, secondarily, for use in a towing/wave tank, to study the propulsion efficiency of the foils. Two foils were mounted in a central mounting pod which in turn was connected to the drive system. Mounting the foils in this manner did not disturb the flow over the tips of the foils which are thought to play a prime role in the propulsive performance of the foils. The drive system consisted of two numerically controlled direct current servo motors connected to a 80286 computer through a Unidex 14 series multi-axis motion controller. The system was programmed to produce a small sine wave oscillating motion and to allow the oscillating motion to be modified easily.

The dynamometer was capable of producing a series of motions which were obtained by modifying the motion subroutine in the Unidex control program. The first

motion programmed for use with the dynamometer was a small pitch angle sine wave motion with a constant phase angle of 90° between pitch and heave.

This thesis project was the first in a series of thesis projects aimed at developing a fully functional oscillating foil dynamometer to 1) Oscillate test foils with a substantial variety of oscillating motions; 2) Study the development of the flow over the test foils; 3) study the formation of cavitation on the test foils; and 4) To determine the propulsion efficiency of the test foils. The aim of this thesis was 1) design and fabricate the prototype dynamometer, 2) program its control system to produce the initial oscillating motion, 3) conduct a series of tests to determine the systems abilities and limitations, and 4) make recommendations on how to overcome its limitations. The implementation of the recommendations is left as part of the next thesis project in this series.

The performance and evaluation of the dynamometer in a series of preliminary tests is described. These tests were aimed at evaluating the performance of the dynamometer and its computer control system and not as a complete study of the foils. The foils which were used in the initial tests had a rectangular planform with an aspect ratio of six and a NACA 0019 section (this section is similar to the section through the flukes of a fin whale).

The initial test consisted of running the dynamometer with a sine wave motion for a series of pitch and heave amplitudes, pitching axis locations, oscillating frequencies, and water flow velocities. These tests demonstrated the operational capabilities of the dynamometer, the accuracy of the obtained motion compared with the requested motion and the quality of the data retrieved from the data acquisition system.

Acknowledgements

I would like to take this opportunity to thank my Supervisor Dr. Neil Bose, for offering me this research topic and providing both moral and financial support. He provided invaluable guidance with my studies and research and helped make my master's program an enjoyable and interesting learning experience. Thank you Dr. Bose, I enjoyed working with you on this project.

I extend my thanks to the School of Graduate Studies and the Faculty of Engineering and Applied Science for providing me with financial support through teaching assistantships and an award for outstanding progress in my research. Thanks are also owed to the Atlantic Career Development Board for a Career Development Award.

I thank the professors in my four graduate courses for their informative courses. I would like to pay special thanks to Dr. J. Sharp and Dr. N. Hookey for presenting courses which I found to be particularly helpful in my research as well as challenging. I would also like to give special thanks to the members of my study group Mr. Antonino Calderon, Mr. Krishnan Ramanathan, and Mrs. Yihong Xie for their many discussions during our course work.

Thanks are also due to the technical staff of Technical Services at Memorial University of Newfoundland for their many design suggestions and for fabricating many of the dynamometer's components. I thank the National Research Council of Canada, Institute For Marine Dynamics, for allowing me the use of their cavitation tunnel to run the initial tests on the dynamometer.

I thank my fellow graduate students for their informative conversations and companionship throughout my studies. I would especially like to thank my office mates Bin Zou and Dan Walker for all their help and moral support.

Last but not least, I would like to thank my family for their unending moral support during my research. I would also like to pay very special thanks to my wife Mrs. Dan Yang for all her support, understanding and encouragement. Thank you.

Contents

List of Figures

List of Tables

Chapter 1

Introduction

1.1 Oscillating Propulsors

The peak efficiency for the flukes of an immature fin whale has been estimated using a strip theory to be 87% (Bose and Lien 1989). The screw propeller, which is the most efficient and widely used type of propulsor in use today, may be capable of achieving a propulsion efficiency of 70% for an exceptional propeller, however most propellers have efficiencies in the range of 45% to 65% (Van Manen 1973). Clearly there is room for improvement.

A new type of propulsor which shows promise of achieving higher efficiencies and lower risk of cavitation is the oscillating propulsor. A large number of creatures that travel in a fluid medium are propelled by oscillating foils. Birds, cetacean mammals and fish are propelled by oscillating foils in the form of wings, flukes, and fins.

In today's economic environment it is important to keep costs to a minimum and one of the largest costs in operating marine vehicles is the cost of fuel. Cetaceans, which are comparable in size to survey submersibles, are known to travel thousands of miles during migrations with minimal feeding. For example blue whales travel from their feeding grounds in polar and sub-polar regions to subtropical and tropical waters where they calve and then complete their eight month trip back to their feeding grounds with only minimal feeding (Kshatriya and Blake 1988). Human developed submersibles do not even begin to emulate this level of endurance.

It may be that we can learn valuable lessons from these swimming animals by looking into the design of bio-engineered propulsors, such as oscillating foils, designed based on the flukes of cetacean mammals. We may also be able to develop "smart" materials, for example materials similar to those in the tips of a whale's flukes which deflect under loading to reduce the strength of tip vortices and thus increase efficiency.

To determine the most efficient foil geometry's, materials, and oscillating motions these parameters should be varied systematically in a series of experiments to determine their effects on the propulsion efficiency, the flow characteristics around the foil and the cavitation characteristics of the foil. This thesis covers the design and commissioning of an oscillating foil dynamometer for this purpose.

There are many other uses for the dynamometer described in this thesis besides testing oscillating propulsors. Many ships use foils as roll stabilisers. These stabilisers can be divided into two categories, either passive or active. One type of passive stabilisers are attached to a boom by a cable and allowed to oscillate freely as they are towed alongside the ship, while active stabilisers are attached to the ship's hull and the oscillation motion controlled. This dynamometer could be used to determine the best foil geometry's to produce a large lift force while keeping drag to a minimum for both types of stabilisers. The dynamometer could also be used to determine the best point to attach the cable to the passive foils and to determine the most efficient motions for the active stabilisers. Another use for the dynamometer might be in the study of control surfaces for marine vehicles such as rudders, submersible control fins, and depressors for sonar buoys.

1.2 Scope of the Present Work

The work covered in this thesis is divided into three major areas: design and fabrication of the dynamometer, setting up and programming the dynamometer's motion control system, and finally the commissioning of the dynamometer. The first stage of the work involved determining the design requirements for the dynamometer and developing a conceptual design which best satisfied these requirements. Once this was completed, the detailed design of the dynamometer's components was carried out, including specifying all fabrication processes required. This stage of the work also involved the supervision of the dynamometer's fabrication and its assembly.

The second stage of the work consisted of setting up and programming the dynamometer's control system to produce a sinusoidal oscillating motion. The control program which was written in Microsoft QuickBasic interacted with a Unidex 14 Motion Controller to produce the desired motion. It should be noted that the program was written in modular form to allow the easy addition of other motion subroutines.

The final stage of the work consisted of commissioning the dynamometer. First the control structure of the computer program was tested to determine if it was operating correctly and producing the desired motion commands. Once the functioning of the program was proven to be correct the dynamometer was connected to the controller and operated for a series of motions in air without the foils installed to compare the obtained motions with the requested motions. The foils were not installed, so that there would be no physical connection between the two drive shafts. If the shafts were connected by the

pod holding the foils and the motion had malfunctioned the dynamometer may have been damaged. The final stage of the commissioning involved performing a series of experiments in a cavitation tunnel to determine the capabilities and limitations of the dynamometer and to assess the performance of the data acquisition system in use and to put forward recommendations on how to enhance the dynamometer's performance and eliminate any of its deficiencies.

1.3 Description of Oscillating Propulsion

Oscillating foils work on the principle of oscillating a foil in such a way as to cause a flow of water over the foils. The foil section produces a lift force when the water flows over it in the same manner as a screw propeller or an airfoil produces lift. These propulsors may have single or multiple foils which are oscillated vertically, horizontally, or orbitally. The dynamometer described in this thesis oscillates two foils vertically.

Figure 1.1 shows a plot over time of a single foil being oscillated vertically in the same manner as the dynamometer oscillated the foils. When the foil was oscillated with a given heave amplitude h and a pitch angle amplitude α in a water flow, parallel to the x axis, it produced a lift force.

As the foil is oscillated it pitches around a pitching axis b which is perpendicular to the chord line of the foil. The pitch angle continuously varies from 0° of pitch to the maximum pitch angle, which is equal to the pitch angle amplitude, as it is heaved up and

down. The time between the points where the foil is at its maximum heave displacement and maximum pitching angle is the phase difference between pitch and heave ϕ_1.

As stated above, the dynamometer was designed to study the effects of different foil geometry's, materials and motions. Some of the motion variables that it is necessary to vary are the heave amplitude, pitching amplitude, pitching axis location, phase angle between pitch and heave, oscillating frequency and oscillating motion. These variables are thought to play a major role in the development of the flow over an oscillating foil propulsor and its efficiency.

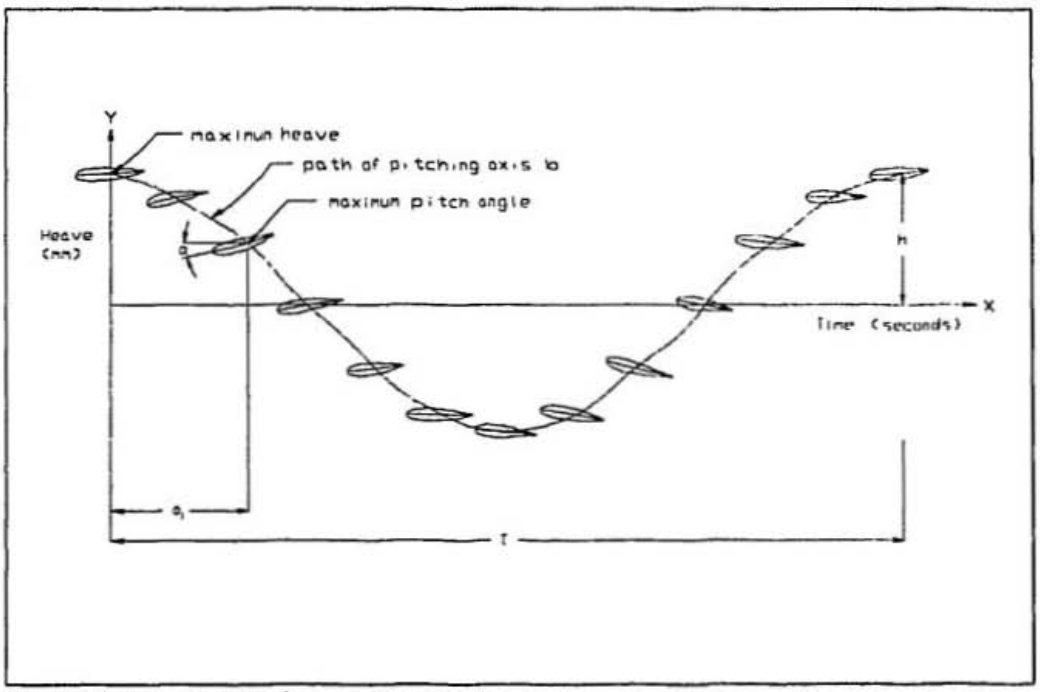

Figure 1.1 Oscillating motion of foil

In this work the foils were oscillated in a water flow. As the water flowed over the foils it either generates thrust and hence absorbed power, or extracted power from the fluid stream to drive the motion of the foils. In this study only the former was of interest. The product of the mean thrust developed over time multiplied by the free stream velocity of the water gave the power absorbed by the foils. The water flow was generated by the cavitation tunnel's impeller and the oscillating action of the foils and was measured using a set of water manometers installed in the cavitation tunnel. The mean thrust was measured with a strain gauged section installed in the aft drive shaft of the dynamometer.

Chapter 2

Literature Survey

2.1 Oscillating Propulsors

Many creatures that live or travel in a fluid, be it air or water, propel themselves by oscillating foils. The process of evolution ensures that the most beneficial traits of a species are passed on to its offspring while limiting the traits which are not beneficial (Krebs and Davis 1978). Therefore, it can be assumed that the oscillating foil is a highly efficient type of propulsor, since such a large variety of creatures use them as propulsors.

Lighthill (1969) suggests that the optimisation of the hydromechanical efficiency may have been one of the most important factors guiding the evolutionary process of fast swimming aquatic animals and flying birds. Lighthill defined hydromechanical efficiency as the mean forward velocity of the animal multiplied by the mean thrust required to overcome the total drag on the animal divided by the mean rate at which the animal does work on the surrounding fluid.

The efficiency of an oscillating foil is highly dependent upon the mode of its oscillation (Chopra 1974). Aquatic animals employ a wide range of oscillating modes to propel themselves (See Table 2.1 (Hoar and Randall 1978)). Lighthill (1969), divided the oscillating motion of many aquatic animals into two main categories. The first category being the anguilliform mode of oscillation and the second the carangiform mode of oscillation. The carangiform mode of oscillation as defined by Lighthill (1969) includes the subcarangiform, carangiform, and thunniform modes of oscillations.

Table 2.1 Oscillating modes employed by aquatic animals

anguilliform	ostraciiform	balistiform
subcarangiform	tetraodontiform	rajiform
carangiform	labriform	gymnotiform
thunniform	diodontimodes	amiiform

In the anguilliform mode of oscillation the entire body of the animal is involved in the oscillation. The oscillation begins at the foremost part of the animal and travels, in a wave of increasing amplitude, along the entire length of the animal's body (Chopra 1976). This mode of oscillation is used mainly by animals having low hydromechanical efficiency, such as eels, which maintain their body depth over their entire length while the breadth of their bodies tapers off towards the tail to form a long continuous foil all the way to a vertical trailing edge.

The carangiform mode of oscillation is characterised by small or even zero amplitude motions in the forward half or two-thirds of the animals body and large amplitude motion of the trailing portion of the body (Chopra 1976). Most of the fast swimming aquatic animals such as the scombroid fishes, including the tunny fishes, fast sharks, and cetacean mammals use this mode of oscillation (Lighthill 1970). All of these animals have evolved the high-aspect-ratio lunate shaped tail in the pursuit of high hydrodynamic propulsion efficiency (Lighthill 1970). This mode of oscillation develops thrust by producing sudden acceleration of the water surrounding the foils. This produces a reactive thrust by changing the momentum of the surrounding water (Chopra 1976).

The main problem with mechanically powering oscillating propulsors results from the fact that almost all marine power plants supply power through rotating shafts which do not lend themselves to efficient production of oscillatory motions. If the problem of powering full size oscillating propulsors is set aside in the experimental study of these propulsion devices, it may be that highly efficient oscillating motions and foil geometry's can be developed.

The first human developed oscillating foil was the sculling oar (Barnaby 1887). An oar can produce a propulsive thrust when it is oscillated transversely to the vessel's direction of travel, while being coupled with a pitching motion. The pitching motion is such that it produces a forward thrust over the entire oscillating cycle.

The sculling oar was widely used as the propulsors for classical Chinese junks and is still employed to propel some large junks. The main limitation of the sculling oar is not its efficiency, but the limited amount of power which a human can provide. The first patent for a mechanically powered sculling propeller was issued to Torger Thompson in 1904 (Saunders 1957). Further study of powered sculling propellers was carried out at the David Taylor Model Basin by J.E. Allen in the 1940's (Saunders 1957). Although no numbers were given, good efficiencies were claimed.

In the early 1800's a number of people developed oscillating propulsors which operated by pushing water astern on the aft stoke and feathering to reduce drag on the forward stoke. One of the first propulsors of this type was developed in 1826 by Narim (Taggart 1969). Narim's propulsor consisted of two foils hinged together in such away that they opened up on the aft stroke to push water astern and folded up parallel to the

direction of motion on the forward stroke. A 30 foot yacht was built in 1881 with a 36 inch oscillating blade suspended over the stern, which work on the same principle as Narim's propulsor (Taggart 1969). This propulsor had an oscillating frequency of 120 cycles per minute. High speeds were predicted for this yacht based on calculations, however, there are no records of how well the yacht actually performed.

Other similar devices were developed by Anderson in 1853 and de Berque in 1854 (Taggart 1969). J.E. Allen developed a similar device in the late 1940's at the David Taylor Model Basin (Taggart 1969). He utilised a more efficient type of hydrofoil than his predecessors and proved that good propulsive efficiency could be obtained from such a device. The main problem with this type of propulsor was that it only developed a propulsive thrust over half the oscillating cycle and it is primarily a drag rather than a lifting device.

If we look back to nature, we see that the creatures that use oscillating foils as propulsion devices oscillate the foils in such away as to produce thrust over most if not the entire oscillating motion. This is done by oscillating the foils in a direction perpendicular to their direction of travel and by pitching the foil so that it has an angle of attack relative to the water flowing over it. This produces a thrust in the same manner as an aerofoil.

One of the first human developed propulsors to work on this principal was patented by Robert Fowles in 1848 (Taggart 1969). This device, which can be seen in Figure 2.1, consisted of one or more foils fixed to two vertical rods, one of which was fixed in position and the other free to oscillate vertically. Fowles also suggested that if the

foils were turned and oscillated horizontally behind the vessel then they could be used as a steering mechanism as well as a propulsion device.

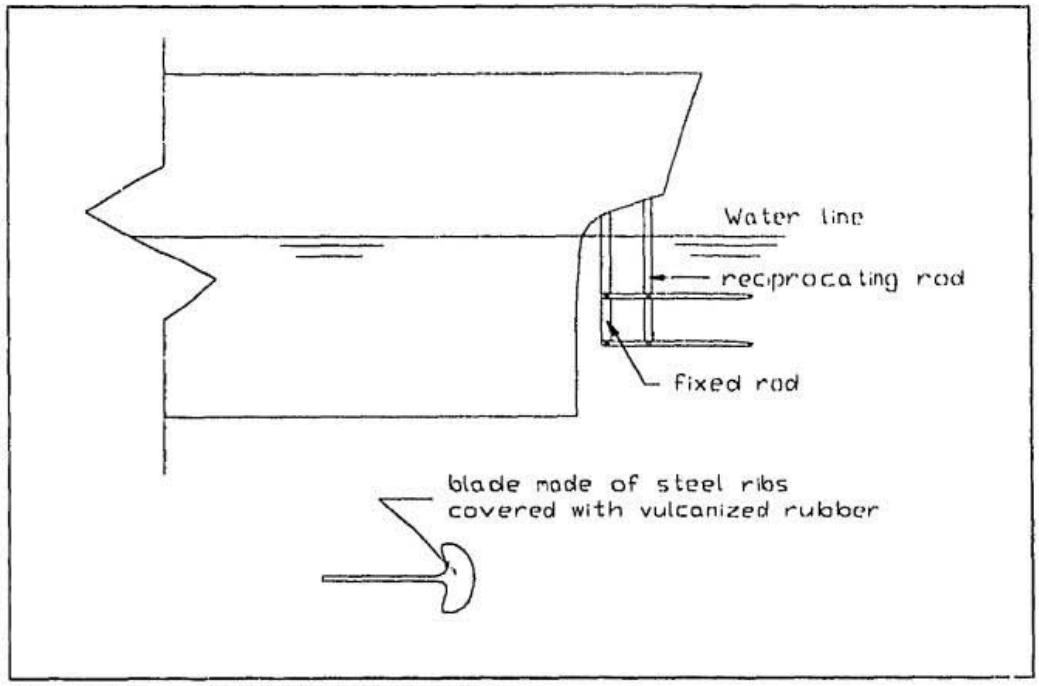

Figure 2.1 Fowles fish tail propeller

Carl Henning was issued a patent in 1874 for a propulsor which used foils to convert energy from waves into propulsive energy (Taggart 1969). His devices consisted of inclined foils placed at both the bow and stern of a boat. These foils produce thrust in the same manner as Fowles's propulsors, however, the oscillating motion was provided by the movement of the water particles in the waves and the pitching and heaving motion of the boat.

A more successful propulsor utilising this principal was patented by Herman Linden in 1898 (Taggart 1969). His propulsor consisted of two foils mounted horizontally, one at the bow and the other at the stern of a boat. The pitching motion of

the boat in a sea provided the oscillating motion of the foils. He mounted a set of 20 inch long by 10 inch wide foils on a thirteen foot long boat named *Autonaut*. This boat obtained speeds of three knots while running into the wind and sea. Linden built other boats with similar propulsors; the largest being 24 feet in length. This boat achieved a speed of four knots.

William Johnson patented a device which simulated the anterior portion of a fish in 1862 (Taggart 1969). This propulsor consisted of two flexible foils mounted on rigid arms that oscillated transversely behind a vessel as shown in Figure 2.2. He claimed that flexible foils were capable of higher efficiencies, however, no results are available to support this claim.

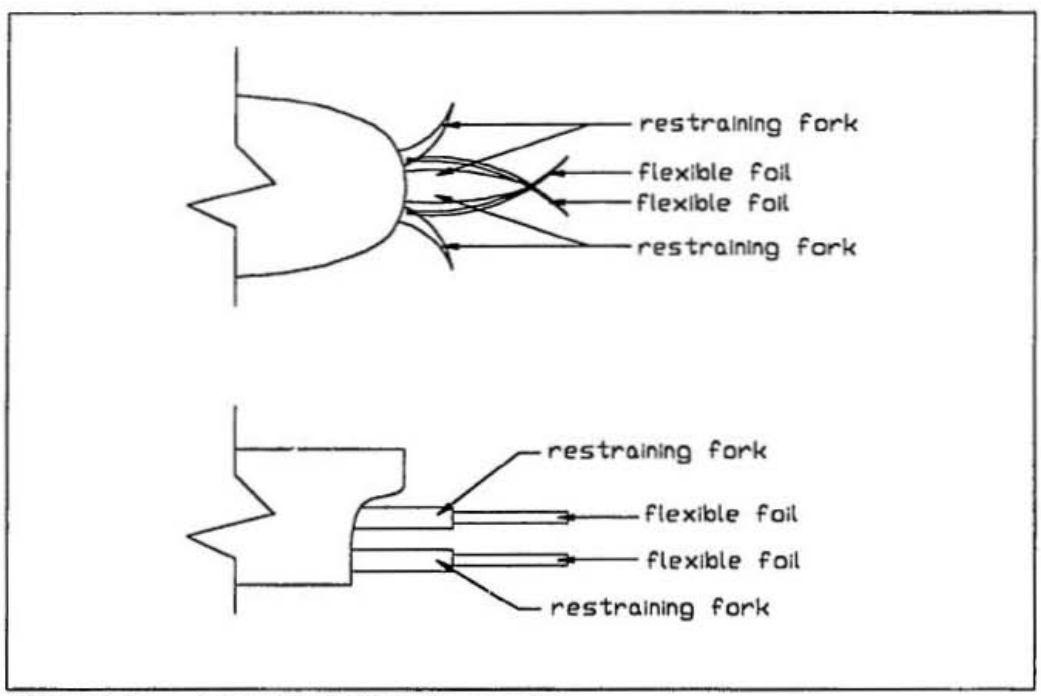

Figure 2.2 Johnson's flexible fin propeller

In 1929, Curry recommended the construction of a boat with a flexible fin propulsor, which would simulate the anterior portion of a fish (Taggart 1969). This type of boat which can be seen in Figure 2.3, utilised human power to drive the foil and has proven successful for certain applications, such as commando boats in Burma during the Second World War (Taggart 1969).

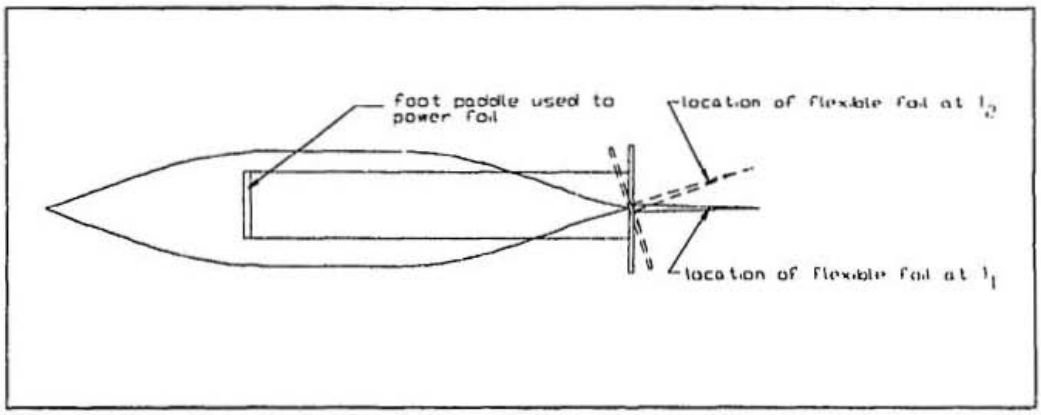

Figure 2.3 Curry's flexible fin propulsor

Currently a research group at the Massachusetts Institute of Technology have developed a tail-driven robotic tuna (Popular Mechanics 1995). The research team is conducting experiments aimed at finding the most efficient swimming motions for this robotic tuna. The overall goal of this project is the development of highly efficient fully autonomous underwater vehicles.

To date none of these forms of oscillating propulsors have enjoyed any amount of extended success. This may be due to the lack of systematic study of the foil's geometry and oscillating motions, the difficulty of powering the oscillating motion and the variable nature of the developed thrust.

The only type of oscillating propulsor which has proven to be successful so far is the rotating vertical axis propellers. These propellers take advantage of the rotating motion provided by marine engines and since they utilise many foils, which produce thrust over the entire rotation, the obtained net thrust is constant.

Robert Hooke proposed the design of a vertical watermill, which was similar to today's vertical axis propellers, in 1681 (Taggart 1969). However his device was designed to extract energy from the water and not as a propulsor. An early successful vertical axis propeller was patented by Hunter in 1842 (Taggart 1969). This propulsor, which was fitted to the 184.5 foot U.S. naval ship *Union*, consisted of a number of blades attached to a rotating drum mounted under the vessel. The blades were attached to the drum by hinges so that they folded up against the drum when they were moving forward and dropped down against stops when moving aft. In 1874 a feathering paddle wheel, which rotated about a vertical axis and operated in such a way that the blades produced thrust over the entire rotation cycle, was installed on the USS *Alarm* (Taggart 1969).

The modern version of the vertical axis propeller consists of a number of foil sections mounted on a rotating drum mounted under the vessel with the foils extending downward. As the drum is rotated about its vertical axis, the individual foils also rotate about a separate vertical axis in such a way that all the foils produce a constant net thrust in the same direction. By moving the position of the axis which the foils rotate about, the direction of the thrust can be changed.

There are two main types of vertical axis propellers in use today. These are the Kirsten-Boeing propeller developed by Frederich Kirsten and William Boeing in 1921 and

the Voith-Schneider propeller developed by Ernst Schneider and J. Voith in 1926 (van Manen and van Oossanen 1988). These propellers are described in van Manen and van Oossanen (1988), Harvald (1983), and Rawson and Tupper (1984).

Although oscillating propellers in one form or another have been considered as propulsion devices for marine vehicles for hundreds of years, they have not been studied systematically. This may be one of the major reasons for their lack of use.

2.2 Previous Experiments and Studies

In the latter part of this century a large amount of research has been carried out on oscillating propulsion. One of the main areas of research has focused on the study of aquatic animals, in the hope of determining how these animals produce such high speeds and efficiencies. An overview of some of these studies is presented here in order to determine the important parameters related to this type of propulsion and to determine the direction which further work on this topic should take.

Wu (1961 and 1971a) carried out numerical studies on oscillating propulsors by modelling the swimming of a fish as a two-dimensional flexible waving plate of negligible thickness. In the 1961 study Wu showed that it is advantageous to have the oscillating motion propagate with increasing amplitude from the leading edge of the plate to the trailing edge. Wu (1971a) expanded on this conclusion by showing that the wave travelling along the plate should have a phase velocity greater than the desired swimming

velocity. However, he did not determine an exact motion shape uniquely. He also concluded from this study that a flexible plate had a higher thrust than a rigid one.

Wu (1971b) analysed data from tests conducted by Lang and Daybell in 1963 on a porpoise swimming in a wave tank. His analysis showed the pitching axis of the porpoise's fluke to be at the 0.793 chord point from the leading edge. Wu approximated the performance of the porpoise using a two-dimensional linearized invisid flow theory and found the porpoise to have an efficiency of 99% assuming the pitch axis to be located at the 0.8 chord position from the leading edge and a 90° phase angle between the pitch and heave motion. This over estimated efficiency since viscous effects were not taken into account (neglected friction). Wu concluded that high efficiencies can be achieved with large heave amplitudes combined with small pitching amplitudes, provided the phase angle between pitch and heave are correct.

Wu (1971c) and Lighthill (1960 and 1969) conducted numerical studies which showed that the mean values of thrust, work done, and energy lost to the wake was wholly dependent on the geometry and motion of the after portion of an aquatic animal. Both Wu and Lighthill assumed that the trailing edge of the tail shed a trail of vortices as shown in Figure 2.4. This resulted in a jet like stream which is assumed to be responsible for the developed thrust. Wu also suggested that a reduced motion of the forward body would help in reducing the body recoil of the animal.

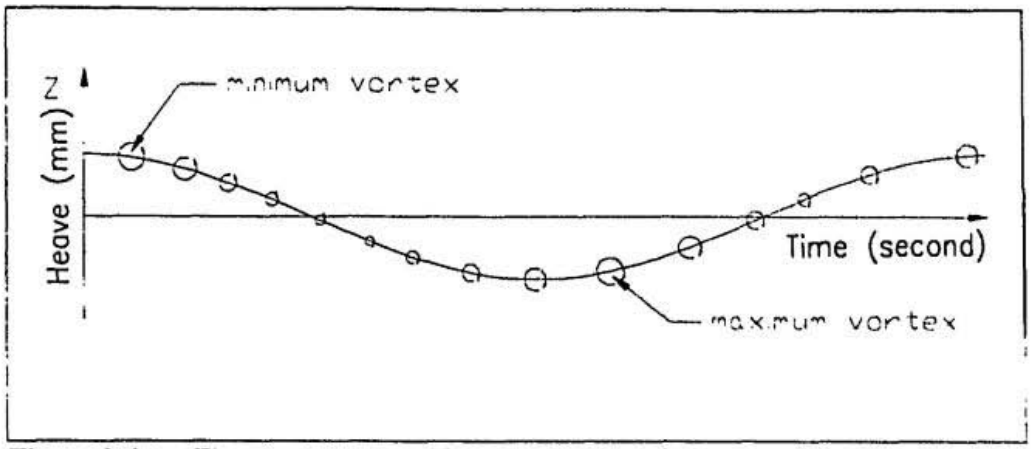

Figure 2.4 The vortex wake behind an oscillating foil

Lighthill (1970) carried out an analysis of the oscillating motion of aquatic animals with high aspect ratio lunate tails. He showed that the best location for the pitching axis of the tail from a thrust and efficiency point of view was at a position between the mid chord and trailing edge position of the tail. This was in agreement with the findings of Wu's (1971b) calculations of the pitching axis location for the flukes of a porpoise.

Chopra (1974) extended the two dimensional analysis of lunate-tail propulsion conducted by Lighthill (1970) to a three dimensional analysis. His analysis showed that a reduction in the aspect ratio of the tail results in a reduction in the predicted thrust and propulsive efficiency and that the best location for the pitching axis was between the mid chord and the trailing edge of the tail. He suggested, however, for pitching axis positions in this area the thrust is highly dependent on the leading edge suction which may not be obtained in actual foil motions due to separation at the leading edge at high angles of attack. These conclusions are in agreement with Lighthill (1970).

Chopra (1976) extended the theory of lunate-tail propulsion to motions of arbitrary amplitude (large amplitude motions). His analysis showed that lunate-tailed animals should oscillate their tails with a large heave or sideslip at high frequencies in order to achieve good efficiencies and that the thrust increases as the angle of attack increases. However, this was partly due to high values of leading edge suction; and if the angles of attack were too high separation would occur at the leading edge causing a decrease in thrust. A swept leading edge may lead to these leading edge suction forces being realised in practice.

Chopra and Kambe (1977) studied the propulsion of a finite aspect ratio flat wing planform oscillating with a small amplitude motion. The parameters which they considered to be important were: the aspect ratio (span^2/ planform area), the reduced frequency (oscillating frequency * a typical length/ speed of advance), the feathering parameter (the ratio of the tail slope and the slope of the path of the pitching axis) which was introduced by Lighthill (1969), the pitching axis location, and the shape of the leading and trailing edges. Their analysis, which was based on potential flow theory, suggested that a curved leading edge such as the edge of a lunate tail reduces the component of the thrust dependent upon leading edge suction and that a sweep back angle larger than 30° reduces efficiency.

Katz and Weihs (1978 and 1979) developed a two-dimensional theory for the study of large amplitude unsteady motion of a flexible oscillating propulsor. This study showed that flexibility of the foil increased the propulsive efficiency by up to 20% while slightly decreasing the overall thrust compared to a rigid foil. The flexibility of the foil

allows the hydrodynamic pressure to distort the foil, decreasing the instantaneous lift. However, the orientation of the lift force is redirected so as to be closer to the direction of travel. The analysis also showed that a phase difference of 90° between pitch and heave is probably optimal for this type of propulsor; the thrust grows as the ratio of heave amplitude to chord length of the foil increases and as the pitch angle increases as long as separation does not occur; and the best location for the pitching axis is in the aft quarter of the foil.

Katz (1981) developed a vortex method to study the separated non-steady flow over a cambered foil. He was successful in calculating the foil's lift and drag forces for a wide range of angles of attack, the periodic varying forces on the foil, and the vortex-wake roll-up. However, the chordwise separation point had to be assumed to be known from experiments or flow-visualisation.

Grue et al. (1988) presented the results of a mathematical study of foils oscillating under the influence of waves at a free surface. In this study they found that up to 75% of the encountered wave energy could be extracted and used for propulsion by a large aspect ratio foil. They also estimated the propulsion performance of a 40m ship by such a foil. It was found that for the ship operating in head seas a speed of advance of 8m/s was predicted while a speed of advance of 4m/s was predicted for following seas.

The fin whale is the fastest of the large whales, it is capable of obtaining speeds of 19.5 knots (Gambell 1985) and speeds of 5 knots over many days have been reported by (Ray et al. 1978). The performance of these whales, which use an oscillating foil in the

form of flukes for propulsion, demonstrate the potential of oscillating foils for marine applications.

Bose and Lien (1989) developed a strip theory to study the hydrodynamic performance of an immature fin whale's flukes. The flukes of a whale have both spanwise and chordwise flexibility, however, to simplify the analysis the foils were assumed to be rigid. They found that the maximum peak efficiency for the flukes to be 87% at a pitch angle of 30° and an advance ratio of 4.5. Where the advance ratio was defined as π multiplied by the forward speed of advance divided by the product of the oscillating frequency and the heave amplitude. The calculations also showed that the maximum speed range for the flukes of the whale studied was 20 - 25 knots, if cavitation, which could cause damage to the surface of the flukes, was to be avoided.

A rigid foil, with an aspect ratio of 4, mounted on a flexible armed drive mechanism was studied in a set of experiments and the results compared to a linearized mathematical model by Lai et al. (1989). A maximum efficiency of 70% was obtained in the experiments and the mathematical model indicated that this could be increased by increasing the aspect ratio of the foil to 10. Calculations were also carried out to show that a flexible foil with a span of 5.3m, chord of 1.3m oscillating at 2.2 radians/second could be used to replace a 2.65m diameter propeller on a 66m long ship with a breadth of 10.5m and a depth of 5.2m.

Bose (1992) developed a two-dimensional constant potential panel method to calculate the forces developed by a flexible oscillating foil. The result of an analysis on

two dimensional oscillating rigid and flexible foils indicated that a thin foil is more efficient and develops more thrust than a similar thick foil and that a flexible foil produces less thrust than a rigid one. However, a flexible foil has a higher efficiency.

Lai et al. (1993) carried out experiments aimed at studying the extraction of wave energy from ocean waves by an oscillating foil. They mounted a flexible plate over the stern of a 0.33m sailing yacht model and tested it in a miniature wave tank for different head sea conditions. When the plate was attached to the model it advanced into the wave and drifted astern when the plate was removed. Once the idea was shown to be feasible, they mounted a flexible foil on a 0.5m long flexible arm which was attached to the stern of a 1/5 scale model of a racing yacht and tested it in head seas for two different depths of submergence and a range of wave frequencies. The tests showed that the pitch and heave response of the model was reduced at frequencies near the resonance frequency and slightly increased for low frequencies. It was also shown that this motion reduction effect and the thrust developed by the foil decreased as the depth of submergence increased. The highest thrust coefficient measured during the tests was 0.5 corresponding to a 53% reduction in the model's resistance.

Lui and Bose (1993) developed a quasi-vortex lattice method to predict the propulsive performance of three naturally occurring oscillating foils; namely the fluke of a fin whale (*Balaenoptera physalus*), white-sided dolphin (*Lagenorhynchus acutus*), and a white whale (*Delphinaptera leucas*). The maximum propulsion efficiencies were found to be 96%, 96%, and 90% for the fin whale, white sided dolphin, and white whale

respectively. However these values do not take into account the frictional drag on the flukes.

Bose (1993) developed a two-dimensional constant potential panel method which he used to study oscillating propulsors with chordwise flexibility. The following parameters were studied to determine their effect on the propulsion efficiency and the thrust coefficient: reduced frequency; pitch amplitude and feathering parameter; heave amplitude/chord ratio; pitching axis location; phase angle between pitch and heave; and deflection shape. It was found that the efficiency varied most strongly with the heave amplitude ratio and pitch amplitude. The best efficiencies were 82% for a heave amplitude ratio of 0.78; 83% for a pitch amplitude of 27.5°; 78% for the pitch axis located at the three-quarter chord point; and 81% for a flexibility ratio of 0.09.

Yamaguchi and Bose (1994) numerically analysed the performance of both a rigid and flexible oscillating foil propulsor for a 200,000 ton tanker. Both foils gave an increase in the propulsion efficiency over the optimum screw propeller for the ship. The rigid foil had an increase in efficiency of 17% while the flexible foil gave an increase of 25% for a total efficiency of 72%. It was suggested that the increases in efficiency from the foils was primarily due to the increase in the working area of the oscillating foils over the screw propeller. This increase in area decreased the pressure load per unit area on the propulsor required to produce a given level of thrust.

Most of these studies are based on numerical theories. This indicates that some of the future work in this area should be aimed at obtaining experimental data to confirm and help modify these theories. Experiments should be conducted to study the flow

characteristics over oscillating foils. In particular these experiments should be aimed at providing a better understanding of the flow separation and the development of cavitation and vortices around an oscillating foil. The effects of varying the geometry and flexibility of the foils and the following motion parameters: heave and pitch amplitude, phase difference between pitch and heave, pitch axis location, oscillating frequency, angle of attack, and type of oscillating motion should also be studied to determine the most efficient combinations.

2.3 Oscillating Foil Testing Apparatuses

Other testing apparatuses, which have been used in the study of oscillating foils, are presented in this section to help develop ideas about the design of the dynamometer covered in this thesis. Lai et al. (1989) conducted experiments on an oscillating foil at the University of Glasgow. The diagrammatic drawing of the experimental set-up can be seen in Figure 2.5. The foil to be tested was attached to a flexible arm which was in turn connected to two vertical arms, one of which was fixed while the other was oscillated vertically by an electric motor through a wire and pulley system. The motor drove through a reduction gear to a Scotch yoke mechanism to produce a pure sinusoidal motion. The wire was then oscillated up and down sinusoidally rotating arm A angularly in a sinusoidal manner which drove the oscillating arm up and down in a sinusoidal manner. This rotated the arm which is connected to the flexible arm in a sinusoidal angular oscillation. The fixed arm supported the lower pinned joint, but was also pinned

at its top end independently of the arm A. The fixed arm had a vertical and a horizontal leg rigidly attached to each other, so that the load cell picked up the fore and aft loads on the pinned joint at the lower end of the vertical leg of the fixed arm.

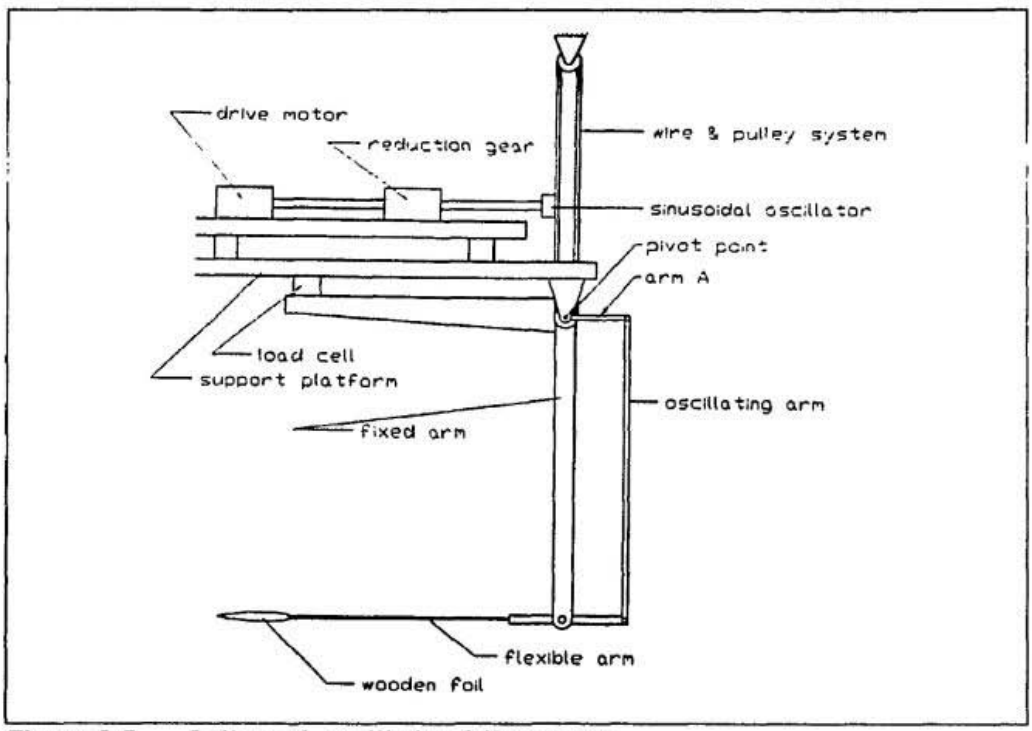

Figure 2.5 Lai's et al. oscillating foil apparatus

This set-up allowed the study of the efficiencies of different foils. However, due to the use of the flexible arm the exact motion of the foil could not be determined. Lai had problems with inertia modes but he was able to calibrate the apparatus so that these could be subtracted from the fore and aft drag/thrust loads.

Lai et al. (1993) conducted a series of experiments on a flexible foil propeller as a wave propulsion device. In these experiments a foil was attached to the stern of a one-

fifth scale model of a three-quarter ton racing yacht by a 0.5m long flexible bar. The model was tested in a wave tank in head seas over a range of different frequencies and forward speeds. The foils oscillated passively as the model heaved and pitched. The resistance of the model was measured by towing the model with a pendulum-type force dynamometer.

This experimental set-up allowed the usefulness of an oscillating foil as a wave propulsion device to be proven. However, it did not allow for the determination of the foil's motion or its efficiency.

Hoppe (1989) performed experiments on a dynamo-elastic oscillating propeller. His test apparatus consisted of a rigid rectangular foil connected to a vertically oscillating arm with an elastic spring arrangement. This arm was sinusoidally oscillated vertically by an electric motor while the springs allowed the foil to pitch under the influence of the hydrodynamic forces. The developed thrust was measured by a double beam strain-gauge instrument. This set-up allowed the measurement of the input power and the thrust developed by the foil and thus the efficiency of the foil. However, it did not allow the study of the foil's motion.

Triantafyllou et al. (1993) tested an oscillating foil with both a heaving and pitch motion in the MIT testing tank. A diagrammatic drawing of their apparatus can be seen in Figure 2.6. This apparatus consisted of a foil supported at its ends by vertical struts which were oscillated by a personal computer (PC) controlled motor. A second similar motor was used to provide the pitching motion of the foil through a chain pulley system. The forces acting on the foil were measured using a piezoelectric force transducer inserted at

the lower end of the vertical strut while the torque was measured by a dynamometer at the pitching drive motor. The motion was monitored by a linear variable differential transducer (LVDT) and a potentiometer.

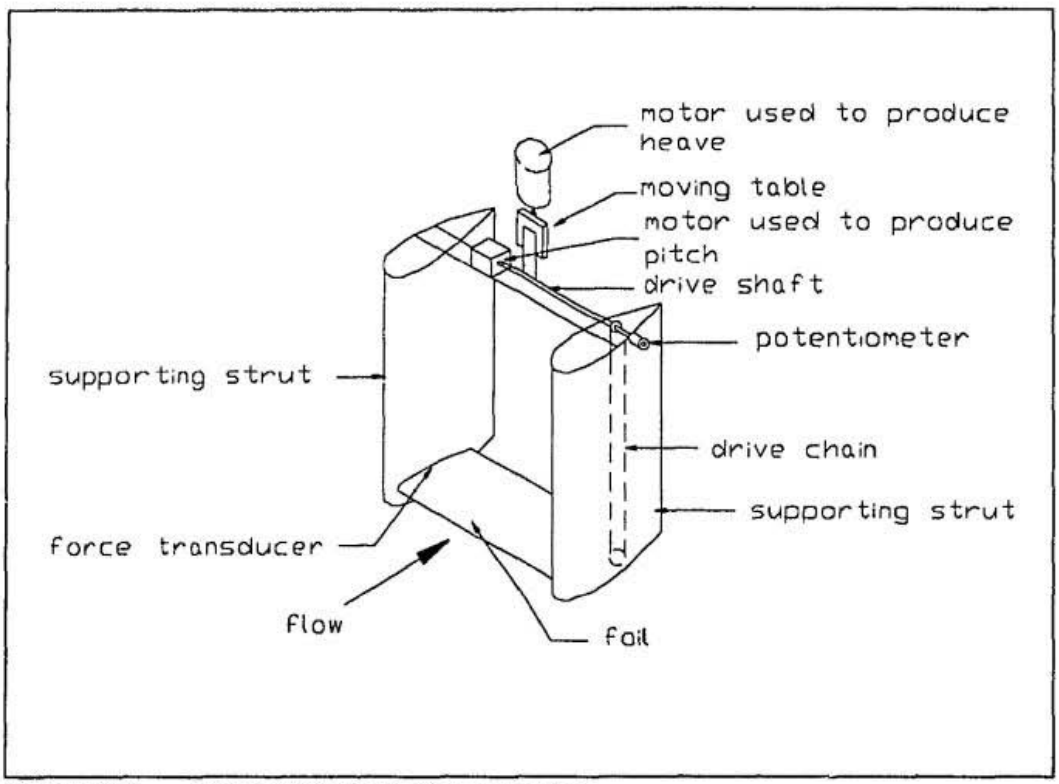

Figure 2.6 Triantafyllou's testing apparatus

This apparatus allowed both the propulsive performance of the foil and its motion to be studied. However, it did not allow the study of the flow over the tips of the foil, which is thought to play a prime role in the performance of an oscillating foil.

Yamamoto et al. (1993) developed an oscillating foil test apparatus which oscillated a foil with a sway and yaw motion (see Figure 2.7). This system allowed the input power and the developed thrust to be determined and thus the efficiency of the

tested foils could be found. The motions were developed by computer controlled servo motors. However, no measuring instrumentation devices were installed to monitor the accuracy of the obtained motions.

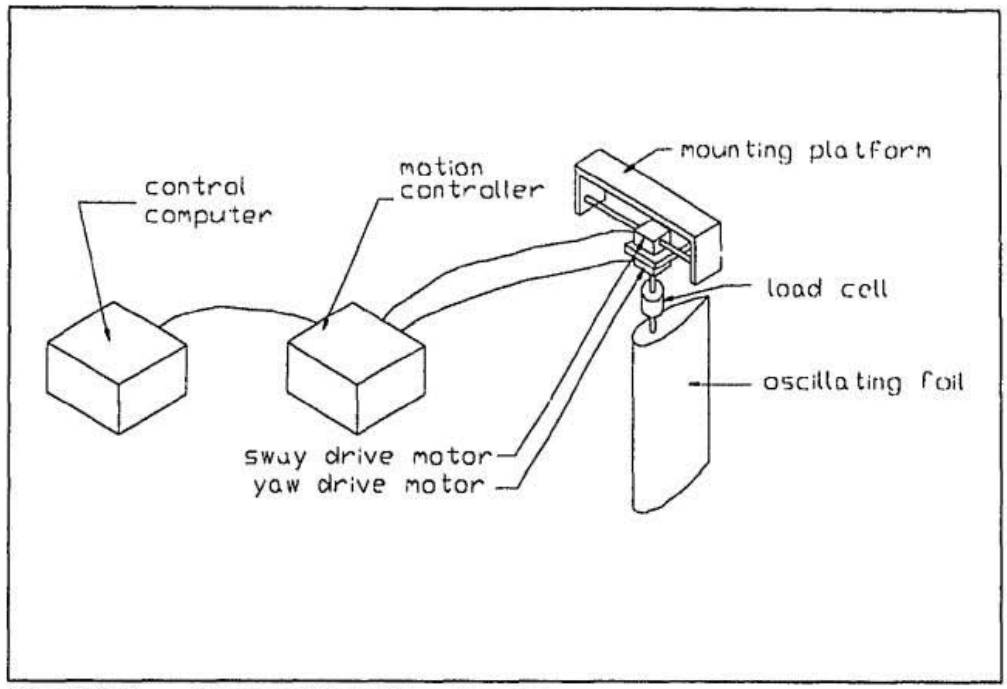

Figure 2.7 Yamamoto's testing apparatus

Chapter 3

Design of Dynamometer

3.1 Design Requirements

A dynamometer is an instrument which is used to measure forces and or power. This dynamometer's main function, however, will be to produce the different oscillating motions and secondarily to measure the forces on the foils. These motions will have variable pitch and heave amplitudes, pitch axis locations, phase angles between pitch and heave, and oscillating frequencies.

The design of any apparatus is governed by the proposed uses and function of the apparatus, the facilities that the apparatus will be used in conjunction with and the use of any existing equipment which has to be incorporated into the design (Ullman 1992) .

The dynamometer was to be used to study the effects of variations in foil geometry's, foil flexibility, and oscillating motions on propulsion efficiency and flow characteristics around oscillating foils. The cavitation and stall characteristics of different foils and foil motions was also to be studied using the dynamometer.

The following were the design requirements:

1) A means of measuring the input power to the foils and the thrust developed by the foils had to be provided so that the propulsion efficiency of the foils could be calculated. The propulsion efficiency of the foils was defined as the mean thrust developed by the foils multiplied by the free stream velocity divided by the mean power absorbed by the foils.

2) The data acquisition system had to be shielded from all electro magnetic fields in the testing area, so as to minimise electronic noise and offsets.

3) A quick and easy way of changing the test foils had to be incorporated into the design.

4) Since the foils were to be tested in a water flow, all the dynamometer's components, which were to be operated in the flow had to be corrosion resistant.

5) The components of the dynamometer, which operated in the flow, had to be designed in such away as to minimise the drag forces on them and to minimise their effects on the flow characteristics around the foils.

6) To produce the desired oscillating motions a means of moving the pitch axis of the foils along their chord lines and oscillating the foils with a phase difference between pitch and heave had to be incorporated into the design.

7) To allow for accurate measurements and to minimise the dynamometer's effects on the flow characteristics around the foils all vibration had to be kept to a minimum.

8) The desired operating frequency range for the dynamometer was 0.00 to 1.00 Hz (0.00 to 6.28 radians/second).

9) The supporting assembly should have a natural frequency that will minimise the transfer of vibrational forces to it from the oscillating components (foils and drive shaft system). Since the operating frequency range for the dynamometer will be 0.00 to 1.00 Hz, the supporting assembly should not have a natural frequency

between 0.71 to 5 Hz (4.44 to 31.42 radians/second) in order to avoid operating in the resonance zone of the supporting assembly.

10) The oscillating components should have a natural frequency sufficiently above that of the desired oscillating frequency of the dynamometer to ensure that they are not operated near their resonance frequency. If possible the oscillating components should have a natural frequency greater than 5.00 Hz.

As mentioned above, the facilities which the dynamometer was to be used in conjunction with imposed some limitations on the design of the dynamometer. The dynamometer was designed primarily for use at the National Research Council of Canada's Institute For Marine Dynamic's cavitation tunnel and for secondary use in Memorial University's towing/wave tank. The Cavitation tunnel was to be used to study the flow characteristics around the foils while the towing tank was to be used to study the propulsive performance of the foils (especially efficiency).

It was decided to use the cavitation tunnel to study the flow characteristics around the foils, since it is more convenient to view these characteristics in the tunnel, rather than in the towing tank. Also, when studying the cavitation characteristics of the foils it is necessary to lower the water pressure to help initiate cavitation; this can be done in the cavitation tunnel but not in the towing tank.

It is necessary to use the towing tank for the propulsion efficiency test since, these tests require the foils to be tested at a low speed of advance and from experience, gained by operating both the cavitation tunnel and the towing tank, it is known that it is much easier to control the speed of advance in the towing tank than it is in the cavitation

tunnel. Also, since the motors were not water proof all possible designs required the motors to be outside the tunnel and the drive shaft/shafts to penetrate the tunnel's walls. This shaft/shafts would have to be sealed. Since, all sealing systems have some level of friction it was believed that it would be difficult to measure the input power to the foils at the cavitation tunnel. However, the seals are not necessary when conducting propulsion test in the towing tank.

The cavitation tunnel greatly influenced the design of the dynamometer. Therefore, a brief description of the tunnel and how it influenced the design will be given here. The tunnel has a 1.2m long test section, with a square cross section of 500mm which allows the testing of model propellers with a maximum diameter of 250mm or of foils with a maximum span of 250mm. The tunnel influenced the design in the following way:

1) The dynamometer was designed so that it could be mounted on the circular brass port in the top window of the cavitation tunnel. This required the fabrication of a duplicate port to be used with the dynamometer, thus having no permanent effect on the cavitation tunnel.

2) The tunnel had to remain water and air tight, when the dynamometer was installed.

3) The frictional force from the drive shaft seals had to be relatively constant and low in comparison with the input force to the foils. This was necessary to ensure that the performance of the drive motors were not limited and if the frictional forces were low enough (relative to the input forces and the expected lift forces on

the foils) and constant, then some of the propulsion efficiency test could be conducted at the cavitation tunnel. Note the efficiency tests conducted to evaluate the effects of the speed of advance of the test foils should still be carried out at the towing tank.

4) The width of the foils could not exceed 250mm and the maximum heave amplitude of the foils had to be less than 125mm to avoid operating the foils in the boundary layer of the cavitation tunnel's walls.

The use of existing equipment also imposed design requirements on the design of the dynamometer. The dynamometer had to incorporate a set of direct current (D-C) Servo motors and a Unidex 14 multi-axis motion controller. This imposed the following requirements:

1) the design had to incorporate and conform to the operational characteristics of the D-C Servo Motors;

2) the weight of the dynamometer's moving parts had to be kept to a minimum so as not to unduly limit the acceleration of the drive motors;

3) the rotational movement of the motor shafts had to be converted into translational motions;

4) the motion control program for the motors was limited to the use of the built in subroutines supplied with the Unidex 14 motion controller; and

5) the number of motion commands that could be sent from the motion control program was limited to the number of commands that the Unidex motion

controller could store in its storage buffers and the speed at which the controller could execute these commands.

3.2 Conceptual Design

Once the design requirements are defined, the next step in the design process is the development of a conceptual design to fulfil those requirements. This involved generating as many solutions as possible and choosing the solution which best satisfied the design requirements for the lowest cost (Shigley and Mischke 1989, Siegel et al. 1965, Spotts 1978 and Earle 1983).

The design solution which was selected is presented in Figures 3.1, 3.2 and 3.3. Note, that the parts numbered in Figures 3.1 and 3.2 are listed in Table 3.1. Figures 3.4, 3.5, 3.6, and 3.7 present photographs of the completed dynamometer.

The remaining portion of this section will be devoted to explaining how the dynamometer functions. The detailed design of the major components of the dynamometer will be covered in section 3.3.

As mentioned above, the dynamometer had to fulfil two major functions. The first to provide the oscillating motions to the foils and the second to measure the forces experienced by the foils.

The oscillating motion was accomplished by connecting the foils to two drive shafts which could be oscillated vertically by two D-C servo motors. The test foils were

mounted one on either side of a central mounting pod (See Figure 3.2) which was in turn connected to the two drive shafts by pin connections. The forward drive shaft had a link

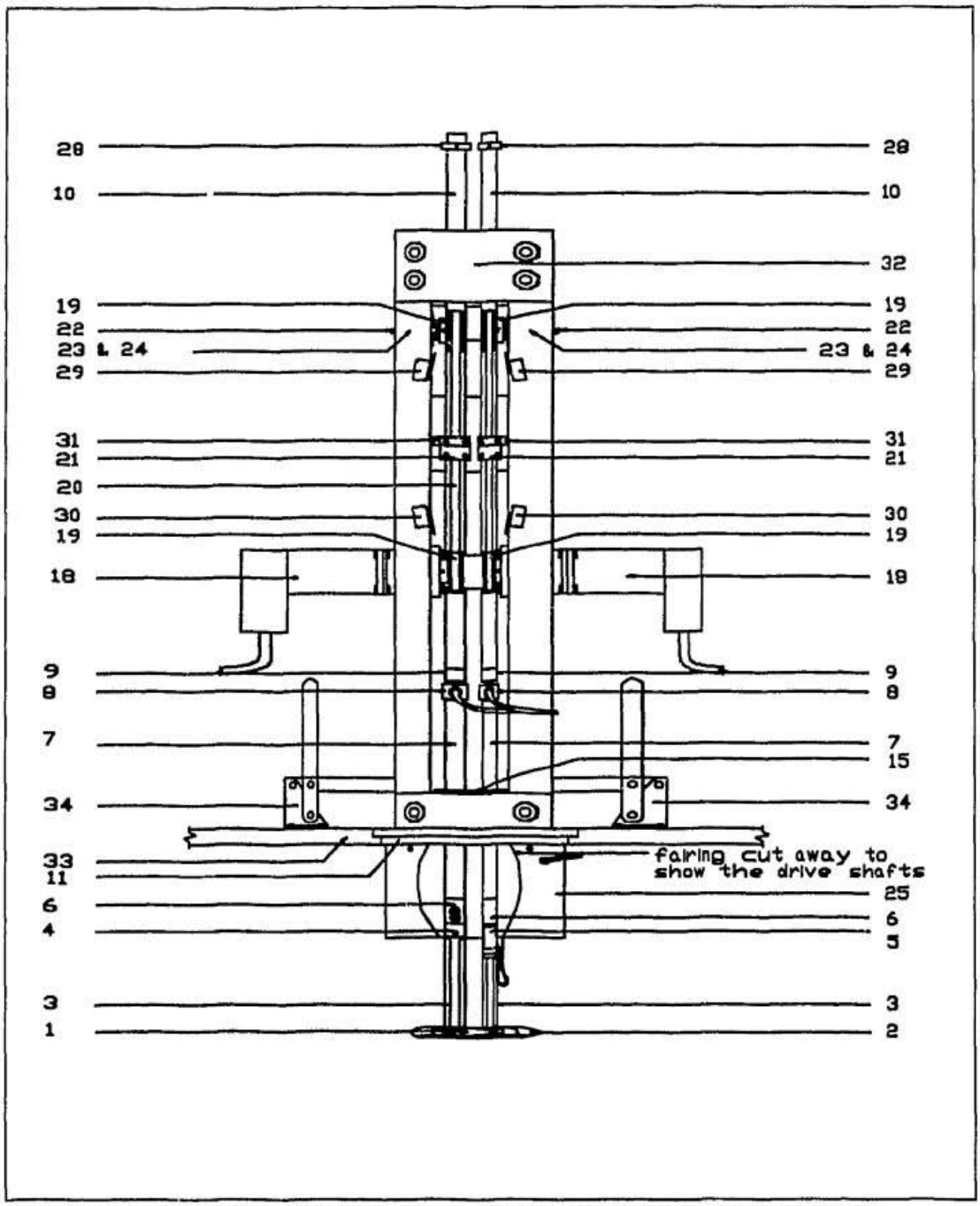

Figure 3.1 Profile view of dynamometer. Forward end of the dynamometer is towards the left hand side of the page.

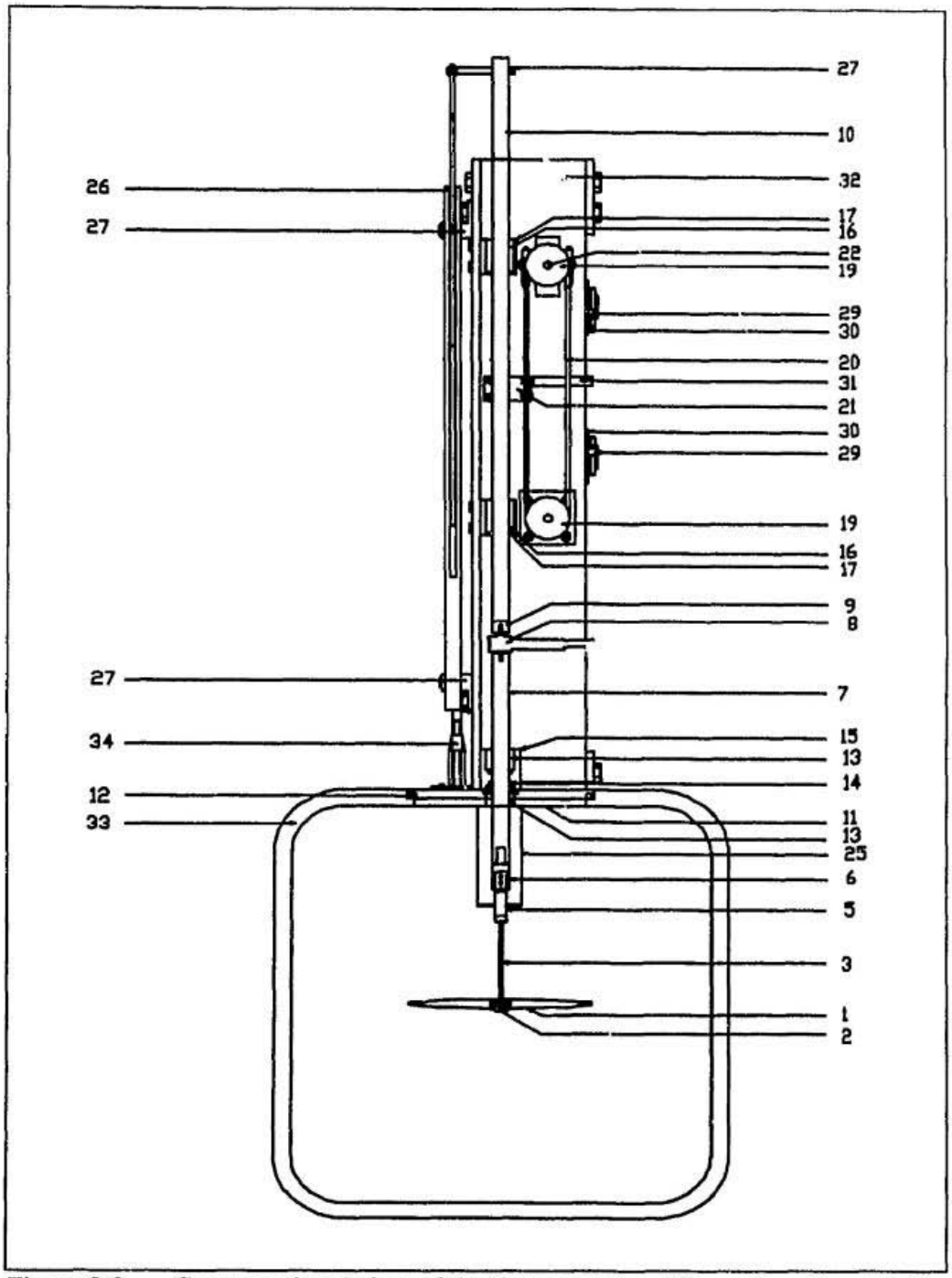

Figure 3.2 **Cross sectional view of the dynamometer. View taken through the aft drive shaft**

Table 3.1 Parts list corresponding to Figures 3.1 and 3.2

Part #	Part	Part #	Part
1	foils	18	DC servo drive motors
2	mounting pod	19	pulleys
3	lower forward drive shaft	20	drive belts
4	pivot joint	21	drive belt /drive shaft connectors
5	lower aft shaft strain gauged section	22	upper pulley shafts
6	drive shaft connection inserts	23	upper pulley shaft housings
7	intermediate drive shafts	24	rotary bearings
8	load cells	25	fairing
9	load cell to drive shaft inserts	26	LVDT
10	upper drive shafts	27	LVDT brackets
11	window port	28	LVDT to drive shaft connections
12	window port o-ring	29	limit switch
13	bushings	30	limit switch bracket
14	drive shaft seals	31	limit switch flags
15	bushing/drive shaft seals housing	32	mounting bracket
16	linear bearings	33	cavitation tunnel
17	linear bearing brackets	34	port window clamp

incorporated in it to allow the drive shafts to oscillate out of phase with each other in order to allow the development of a pitching motion (See Figure 3.1 and 3.3).

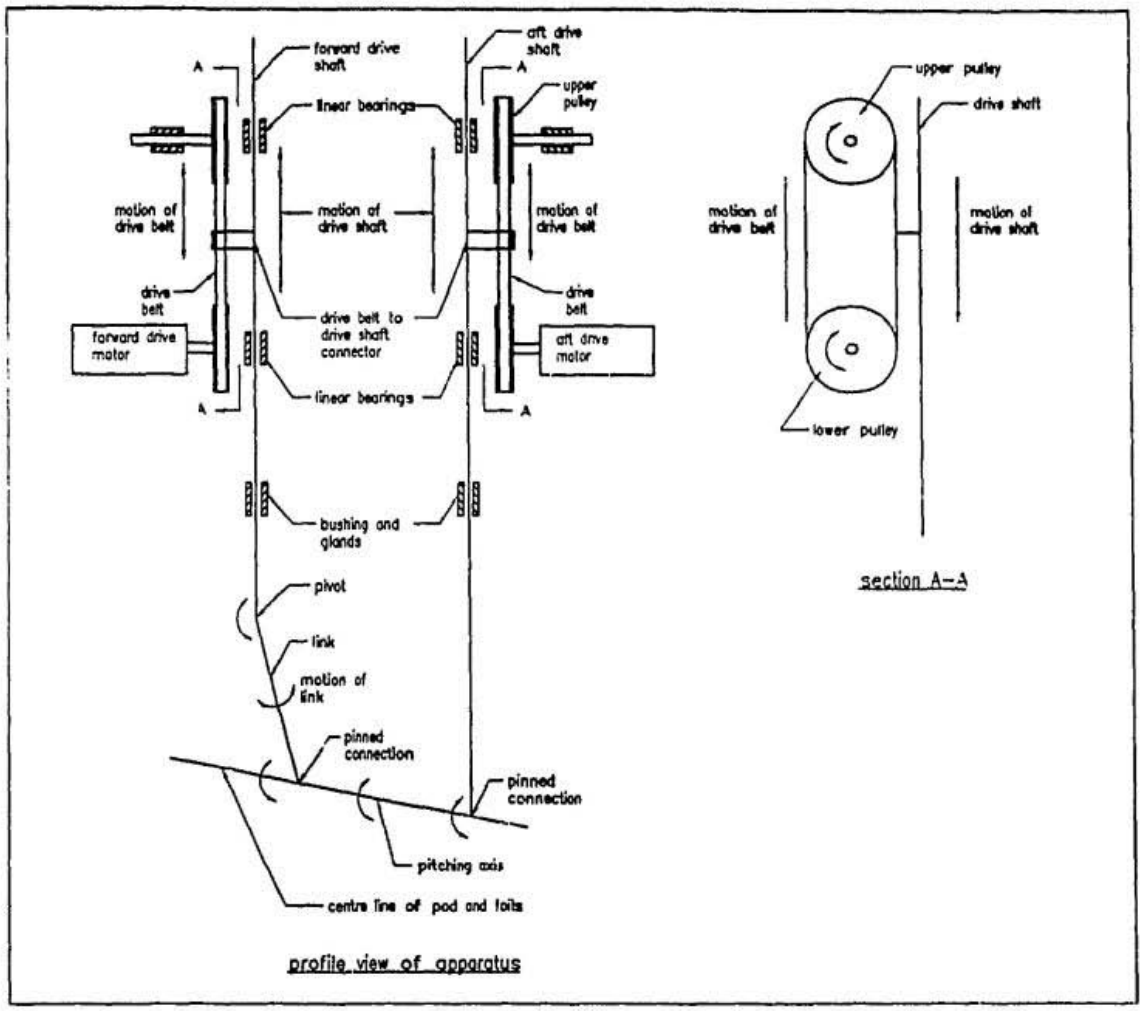

Figure 3.3 Kinematics of the dynamometer

By adjusting the phase difference between the two drive shafts a pure heave, pure pitching, or a combination pitching and heaving motion could be obtained. The location of the pitching axis along the chord line of the test foils and the phase angle between pitch and heave could also be varied by adjusting the phase difference between the oscillating motion of the two drive shafts.

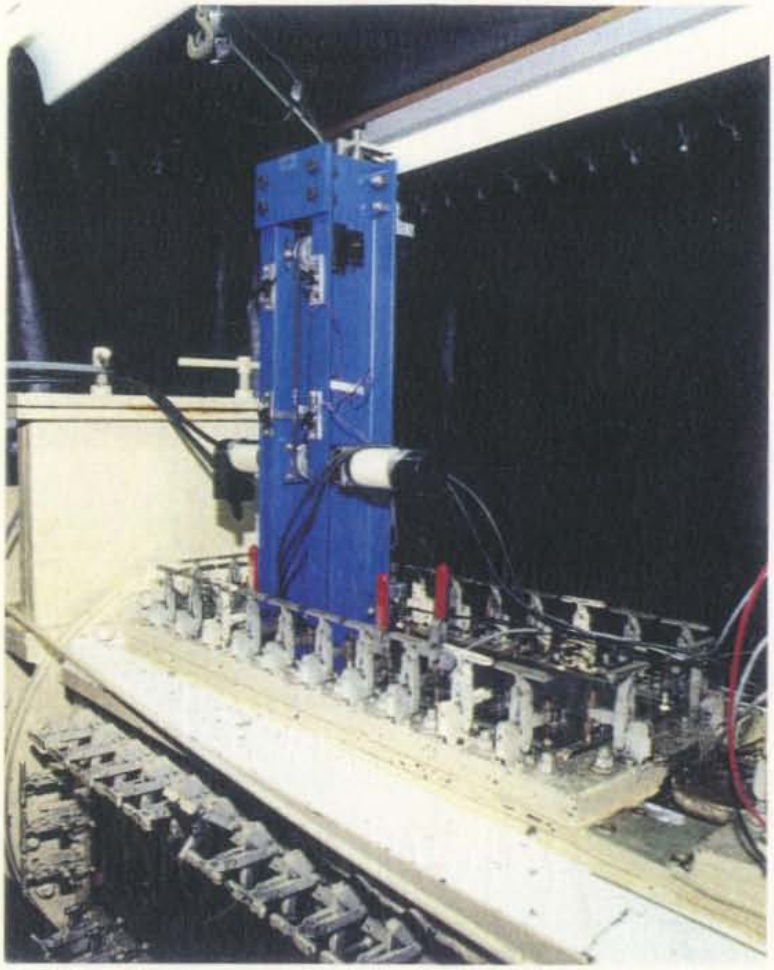

Figure 3.4 Photograph of the dynamometer. Looking at the left hand side of the dynamometer from a position aft of the dynamometer.

The drive shafts were aligned vertically by two linear bearings and two Teflon bushings for each shaft and were oscillated by two D-C Servo motors (See Figures 3.1 and 3.18). The power was transmitted from the motors to the drive shafts through two timing belt pulley systems. The belt pulley system for the aft drive shaft can be seen in

Figures 3.2 and 3.3. The lower pulleys were mounted directly on the motor's drive shafts while the upper pulleys were mounted on freely rotating shafts, which could be adjusted vertically to tension the drive belts.

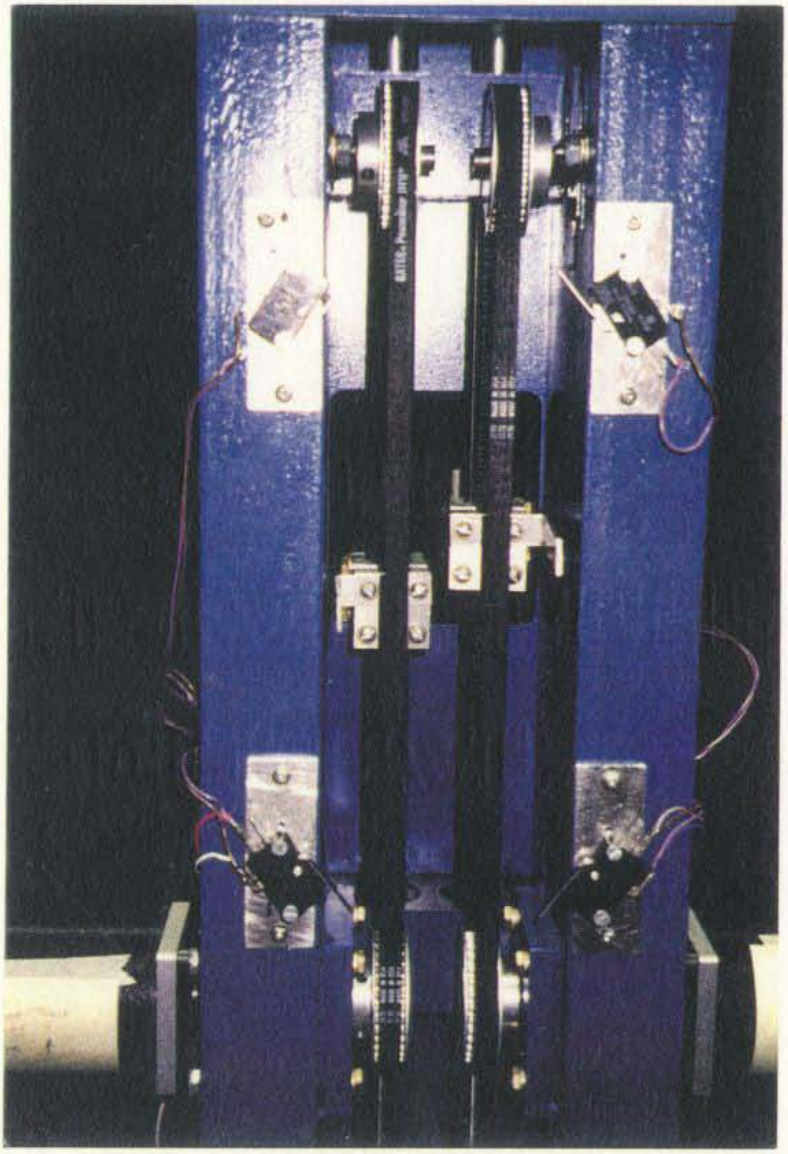

Figure 3.5 Photograph of the top section of the dynamometer. Looking horizontally at the left face of the dynamometer with the forward drive shaft to the left hand side of the page.

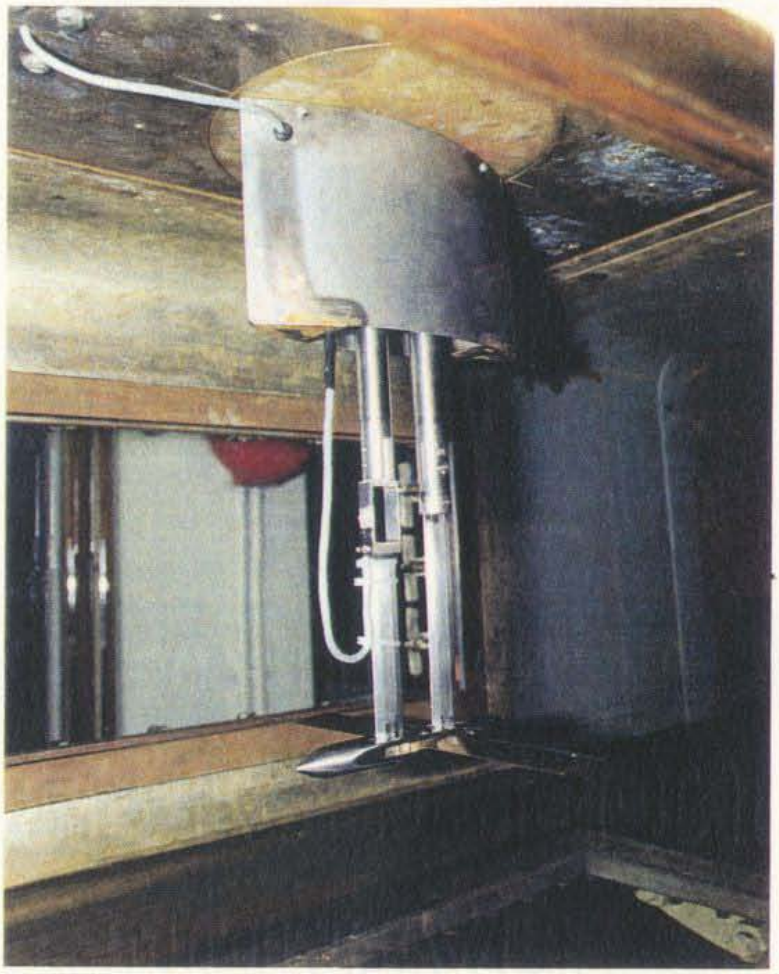

Figure 3.6 Photograph of the dynamometer inside the tunnel. Looking horizontally from the right hand side of the dynamometer with the aft drive shaft closest to the left hand side of the page.

When the two drive shafts were operated out of phase with each other the link in the forward drive shaft rotated from the vertical position causing the pod and foils to pitch (See Figure 3.3). This link was required, since the upper portion of the drive shafts remained parallel to each other and at a constant distance from each other.

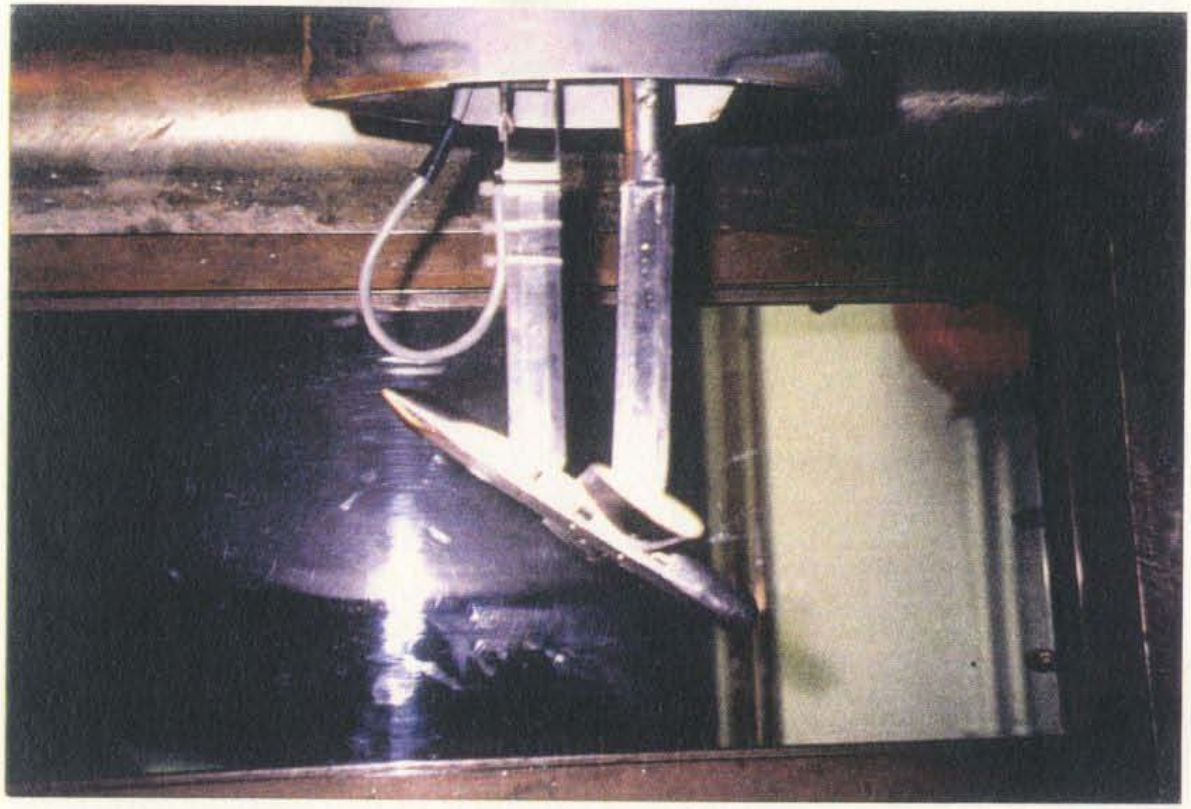

Figure 3.7 Photograph of the lower section inside tunnel with a pitch angle. Looking horizontally at the right hand side of the dynamometer with the aft drive shaft towards the left hand side of the page.

The motors were controlled by a Unidex 14 motion controller which received motion commands from a Unidex encoder installed in a 80286 personal computer (PC). This computer used a QuickBasic Program to allow the operator of the dynamometer to interact with the motion controller to produce the desired motion. Each motor was connected to two limit switches, as shown in Figures 3.1 and 3.2 above, to ensure that the motors could not produce a heave amplitude greater than 110mm. A displacement greater than 110mm, would have resulted in damage to the dynamometer.

The dynamometer was equipped with two LVDTs to monitor the motion developed by the dynamometer during testing. The output from these LVDTs was fed to a Keithley data acquisition system which converted the signal from an analogue signal to a digital signal. The digital signals were then fed to a second computer for initial analysis and storage.

The second function of the dynamometer, the measurement of the forces exerted on the foils, was accomplished by installing a strain gauged section in the lower end of the aft drive shaft and by a load cell in both drive shafts as can be seen in Figures 3.1 and 3.2. The forward drive shaft had a pivot joint inserted in it, therefore, the majority of the forces experienced by the foils, in the direction of the free steam water flow were resisted by the aft drive shaft. Thus, the resultant drag and thrust forces on the foils could be measured by the strain gauged section in the aft drive shaft, while the input forces to the foils and the vertical components of lift could be measured by the load cells. It should be noted that a small portion of the forces in the free stream direction will be resisted by the forward drive shaft. However this portion of the forces should be small since the maximum angle of the forward drive shaft from the vertical will be 2.36 degrees for a pitch angle of 30 degrees.

The exact portion of the forces in the free stream direction which will be carried by the forward drive shaft can not be determined by a static analysis, since these forces will be influenced by the dynamic forces resulting from the motion of the different components making up the oscillating assembly of the dynamometer. Since, these motions

are oscillatory in nature it will only be possible to estimate the order of magnitude of these forces and to calibrate the dynamometer by running a series of tests in air.

Figure 3.8 shows the loads acting on the link in the forward drive shaft (labelled link A) and the pod (labelled link B). During a test these links are accelerating vertically, horizontally, and rotationally. The following assumptions can be made about the associated forces.

1) The vertical accelerations and associated inertia forces are picked up by the load cells but do not influence the strain gauged section in the aft drive shaft.

2) The horizontal accelerations do influence the thrust/drag measurements from the strain gauged section.

3) The rotational accelerations also influence the thrust/drag measurements from the strain gauged section.

4) Link A will transmit forces to the upper portion of the forward drive shaft at its upper end and to the pod (link B in Figure 3.8) at its lower end. However, it can be assumed that the forces in the free stream direction, which are transmitted to link B from link A due to rotational accelerations of link A about its upper end will be small, since the maximum angular amplitudes are approximately three degrees. The horizontal component of the axial force in link A is defined by Equation 3.1. It should be noted, that the axial load in link A includes the inline inertia forces of link A itself.

$$F_{fsh} = F_{alA} * \mathrm{Sin}\theta \qquad (3.1)$$

Where:

F_{fsh} = the horizontal component of the axial forces in link A carried by the forward drive shaft

F_{alA} = the axial force carried by link A

θ = the angle between the forward drive shaft and a vertical line at a given time during the motion

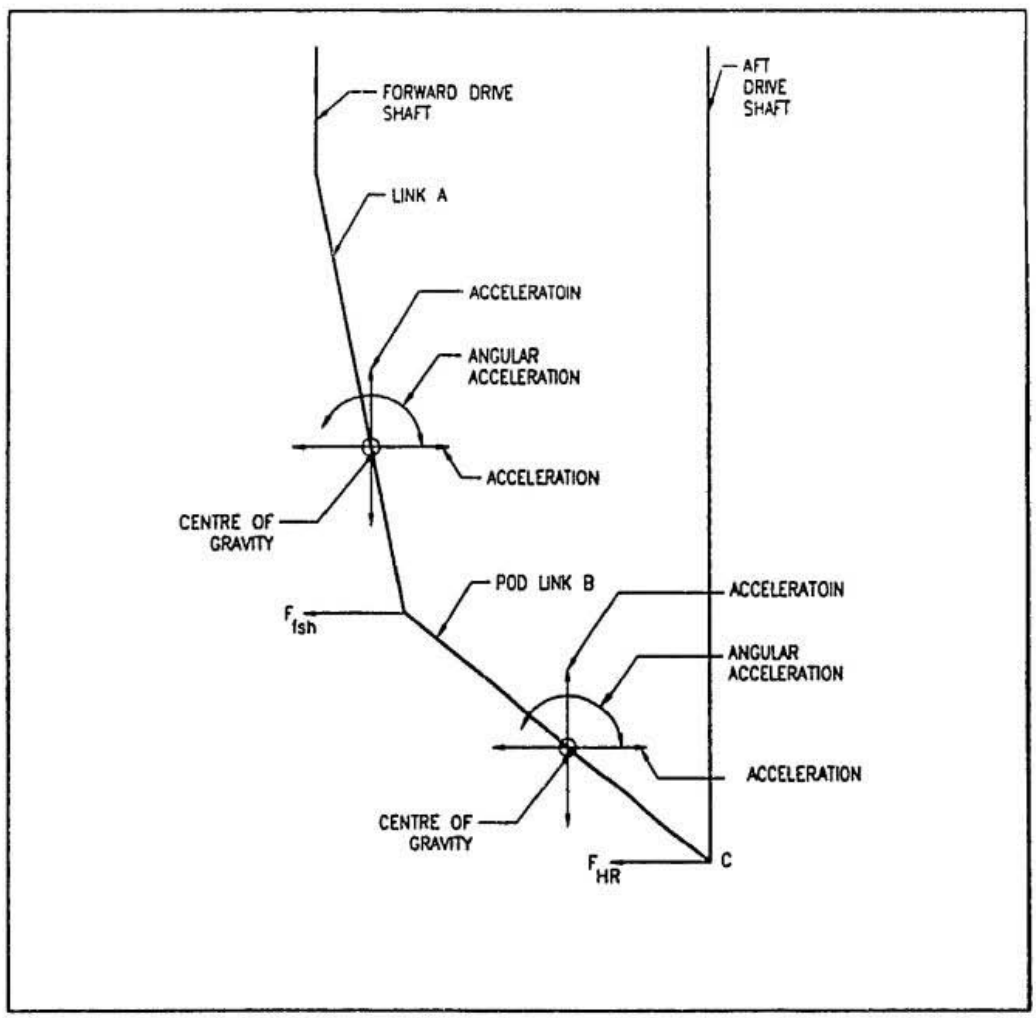

Figure 3.8 Loads acting on the aft drive shaft resulting form the motion of the forward drive shaft , link in forward drive shaft and the pod.

From Figure 3.8 we can see that the motion of link A and link B will transmit the following loads to the aft drive shaft.

1) A vertical load which will be picked up by the load cells but should not affect the strain gauge output, since the gauges are arranged in a wheatstone bridge configuration which is designed to pick up a difference in the strain in the four separate legs of the bridge. This configuration will not pick up axial loads since axial loads will produce equal amounts of strain in all four legs of the bridge.

2) An oscillating moment which should be small due to the pin connection between link B and the aft drive shaft.

3) A horizontal force due to the axial load in link B and the horizontal component of the force resulting from the rotational acceleration of link B.

The maximum force F_{HR} on the aft shaft due to the rotation of Link B was estimated to be 0.03N (See Appendix 'D' Page 203). This Force is relatively low, since the oscillating frequencies for all the dynamometer's motions are low. The maximum horizontal component of the axial force in link A was estimated to be 2.4N(See Appendix 'D' page 203). It should be noted that these forces are oscillatory in nature and that they are relatively low compared with the maximum expected thrust loads of 67N (3.6%) developed by the foils.

The signals from the strain gauged section and the load cells were amplified and sent to the same Keithley data acquisition system as the signals from the LVDTs. Sending

the signals in this manner allowed the motion of the foils at a given time to be directly synchronised with the signals from the strain gauged section and the load cells.

3.3 Detailed Design

The detailed design of the major components of the dynamometer will be covered in this section and a complete set of design drawings are included in Append "A". These components are listed below in Table 3.2.

Table 3.2 Dynamometer components

1	Mounting bracket	6	Drive system
2	Foils and mounting pod	7	Fairing
3	Drive shafts	8	Limit switches
4	Seals	9	Data acquisition system
5	Shaft alignment system		

3.3.1 Mounting Bracket

The mounting bracket which was the main structural component of the dynamometer can be seen in Figure 3.9. Both steel and aluminium were considered for the mounting bracket. Steel was chosen because of its lower cost and higher material strength. The lower end of the mounting bracket was a duplicate of the port in the top window of the cavitation tunnel and was fabricated out of brass. To this was bolted two 800mm long steel channel sections, which were held together at the back by an 800mm

long steel plate and two smaller sections of plate located at the front top and bottom of the mounting bracket. A connection plate was welded to the bottom of each channel section. These plates were then bolted and doweled to the duplicate window port. The dowels were used to ensure the alignment of the bushings, mounted in the duplicate window port, and the linear bearings mounted on the plate at the back of the mounting bracket.

It can be seen from Figures 3.1, 3.2, 3.4, and 3.5 that the mounting bracket forms the core of the dynamometer and to this were connected the following components: the motors, the linear bearing housing, limit switches, upper pulley assembly, window port, and the LVDTs.

To avoid the transmission of vibrational forces from the oscillating components to the mounting bracket the transmission ratio, which is defined as the fraction of the maximum force that is transmitted through to the foundation (See Equation 3.2) must be kept to a minimum (Steidel 1989). From Figure 3.10 it can be seen that a frequency ratio between 0.2 and $\sqrt{2}$ is undesirable. It is preferable to have a natural frequency for the mounting bracket substantially above that of the desired oscillating frequency of the dynamometer. However, this in not possible, since the mounting bracket must have high stiffness. Therefore, the mounting bracket should have a natural frequency substantially below the desired oscillating frequency. The natural oscillating frequency for the mounting bracket is 7217Hz (45343radians/second) about the centre line of the tunnel and 1895168Hz (11907691radians/second) perpendicular to the centre line of the tunnel, this gives transmission ratios of one, therefore, the transference of vibrational forces from the

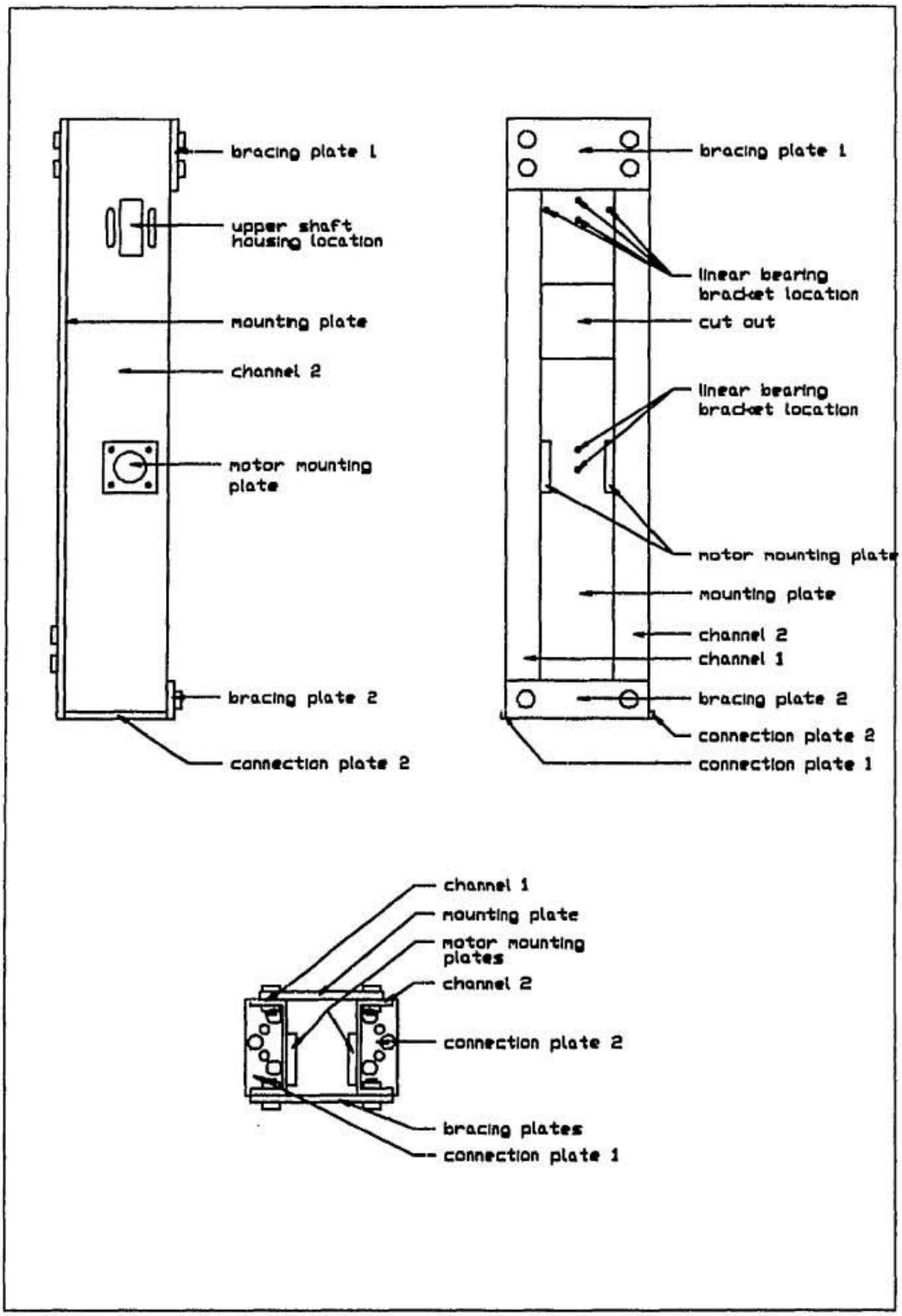

Figure 3.9 Mounting Bracket. Part number 32.

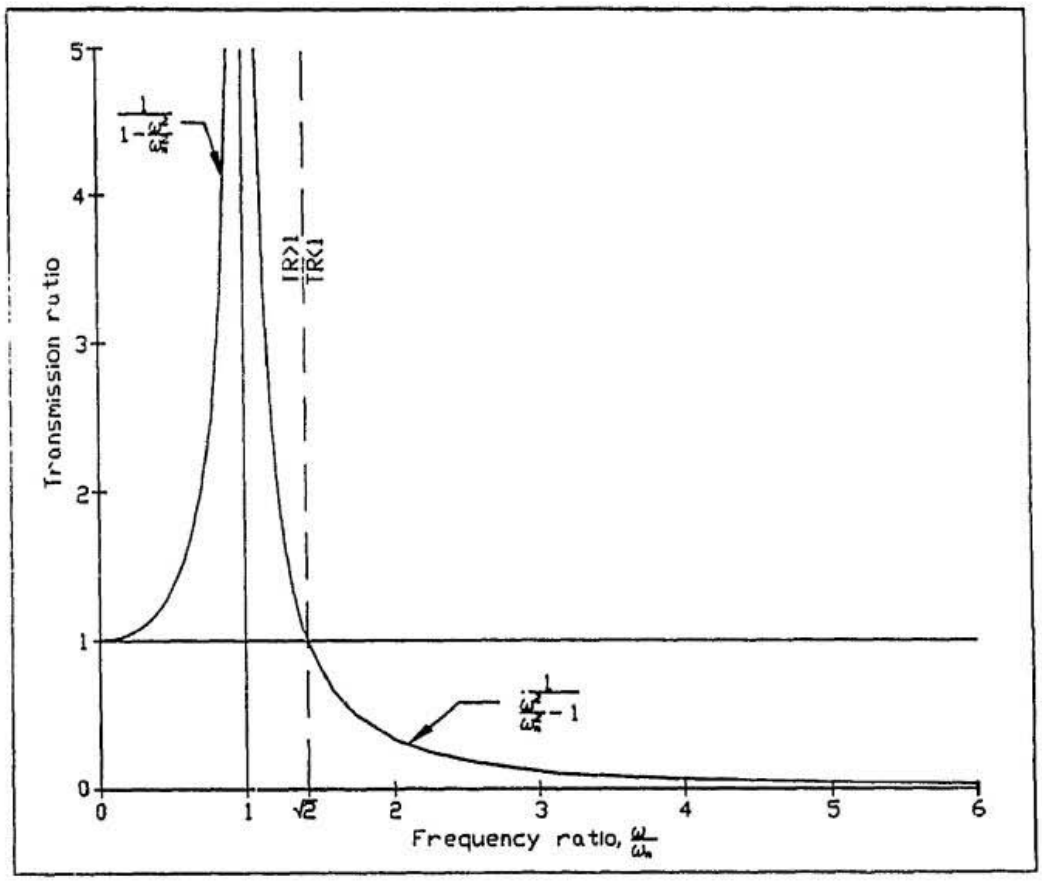

Figure 3.10 Transmission ratio

oscillating components to the mounting bracket should not be a problem (See Appendix 'D' for the calculation of natural frequencies and transmission ratios page 200 to 202).

$$\text{T.R.} = \text{transmission ratio} = |\,1/[1-\omega^2/\omega_n^2]\,| \qquad (3.2)$$

where: ω = the oscillating frequency of the forcing function

ω_n = the natural oscillating frequency of the supporting assembly

3.3.2 Foils and Mounting Pod

Three sets of foils were designed and fabricated for use with this dynamometer. The foils were fabricated out of brass since it has good machinability, good corrosion properties and was relatively inexpensive to machine compared with the other lighter materials which could have been used such as clear polycarbonate plastic and titanium.

The first set of foils had a rectangular planform with an aspect ratio of six and a NACA 0019 section (this section was similar to the section through the flukes of a fin whale). The second set of foils had the same aspect ratio and section, but with a sweep back of thirty degrees (this sweep back was similar to that of a fin whale's flukes) and a taper ratio of 0.18. The third set of foils were tapered with the same aspect ratio and section, but with a planform based on the geometry of the flukes of an immature male fin whale (Bose and Lien 1989).

The three sets of foils can be seen in Figures 3.11, 3.12, and 3.13 below. All foils were made in two identical sections having a span of 100mm and standardised roots, so that they would fit one in either side of a central mounting pod. A span of 100mm was selected to ensure that the flow over the foils would not be affected by the boundary layer of the cavitation tunnel's walls.

The mounting pod was designed to allow a series of different foils to be easily mounted and oscillated while keeping the flow disturbances around the foils to a minimum. A photograph of the mounting pod with a set of foils inserted can be seen in Figure 3.13. The entire assembly had a total width of 222mm.

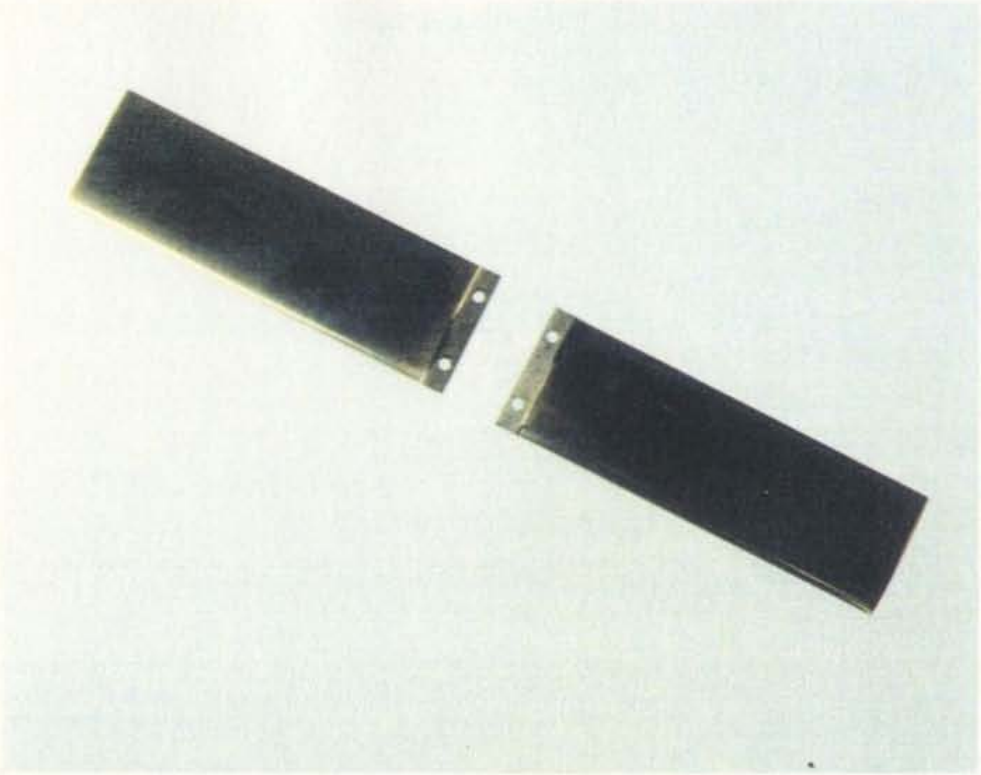

Figure 3.11 Foil one. Looking down on the foils with the leading edges towards the top of the pages. Part number 1.

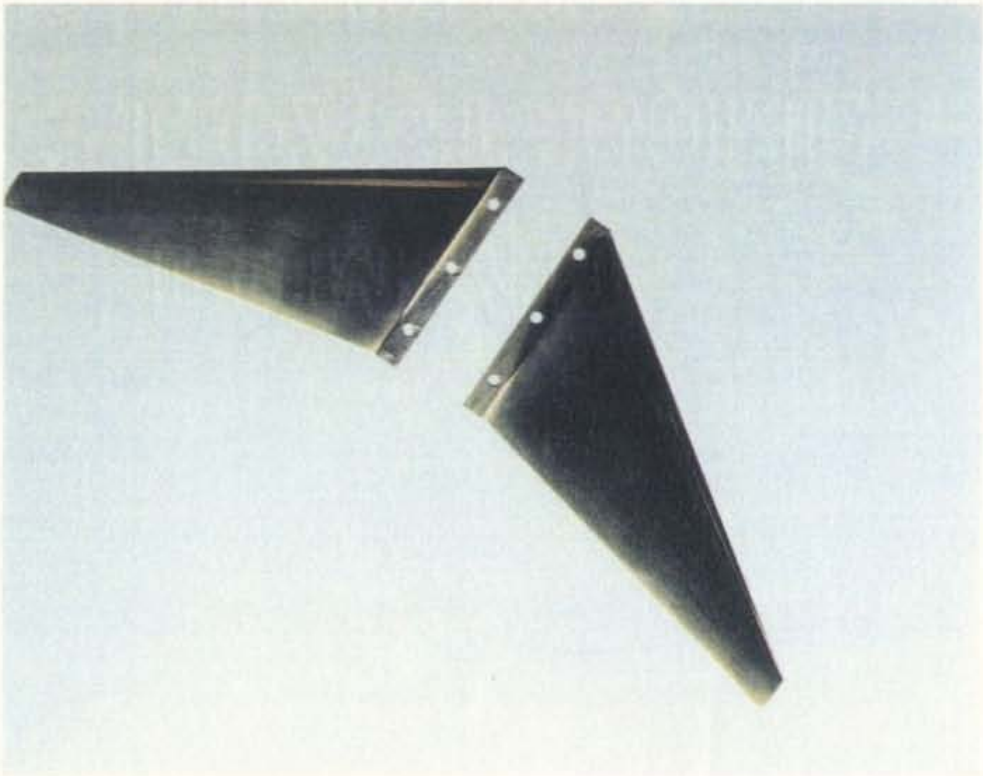

Figure 3.12 Foil two. Looking down on the foils with the leading edges towards the top of the pages. Part Number 1.

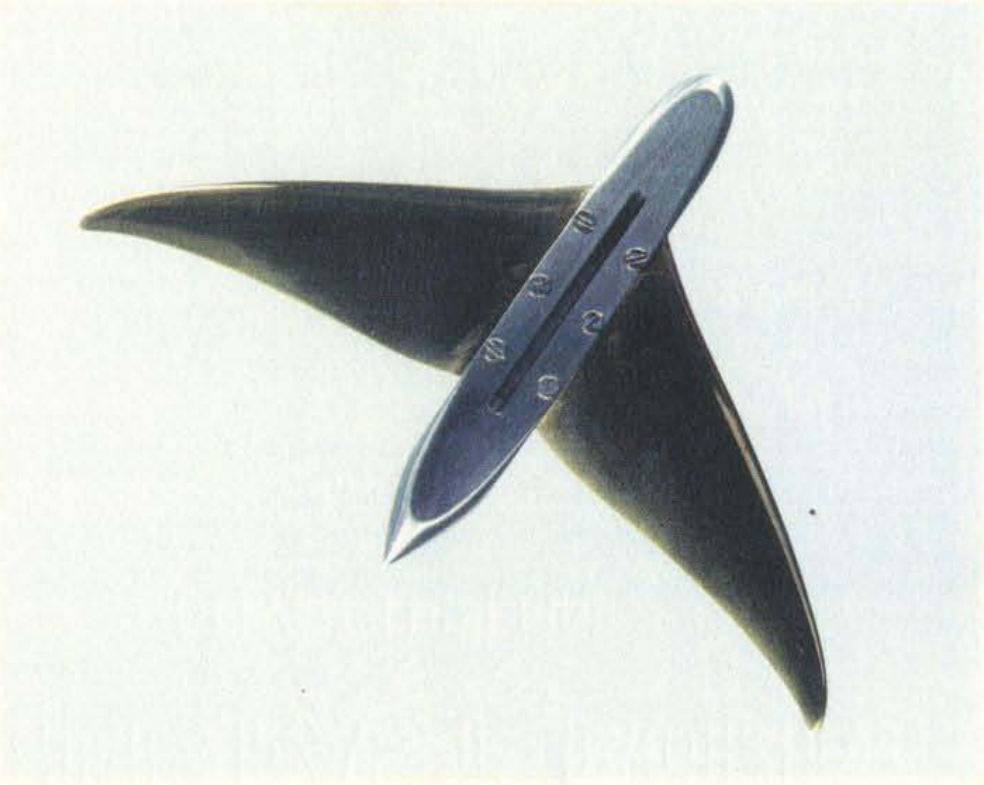

Figure 3.13 Foil three installed in mounting pod. Looking down on the foils with the leading edges towards the top of the pages. Part number 1.

The design drawing of the mounting pod is presented in Figure 3.14. The mounting pod had an overall length of 146mm, a breadth of 22mm, and a depth of 14mm. The forward end of the mounting pod had a sectional shape defined by an ellipse rotated about the mounting pod's central axis. This shape was chosen to reduce the chance of flow separating from the forward shoulders of the pod and thus to decrease the drag on the mounting pod and flow disturbances around the foils. A longer smoother forward

section would have been ideal but such a section would have increased the mass of the pod which had to be kept to a minimum. The ellipse was centred on the centre line of the pod to reduce any lift forces which may be developed by the pod. The after end of the mounting pod had a sectional shape defined by a circular arc, which provided a long tapered after section that decreased the chance of flow separating from the aft end of the pod. This decreased the wake behind the pod and thus the drag forces on it.

The pod was fabricated from stainless steel to give high strength and good corrosion resistance. Three grooves were cut in it one on either side to allow for the mounting of the foils and one in the top to allow the connection of the drive shafts. It was decided to cut one long groove for the connection of the drive shafts instead of two shorter grooves in order to decrease mass and make fabrication easier. Two diagonal flats were also cut along the bottom surface of the pod to decrease its mass.

It should be noted that stainless steel was chosen as the fabrication material for the mounting pod, even though the mass of all moving parts had to be kept to a minimum, because a high strength material was required to ensure that the mounting pod did not collapse while the grooves were being fabricated or while in use. Also the screws for holding the foils in place were threaded into the pod and if a softer material had been used these screw threads may have stripped when the screws were tightened. The screws must be tightened enough to cause the sides of the grooves to clamp the roots of the foils. A high strength material was also required for the bearing surfaces of the pins connecting the mounting pod to the drive shafts.

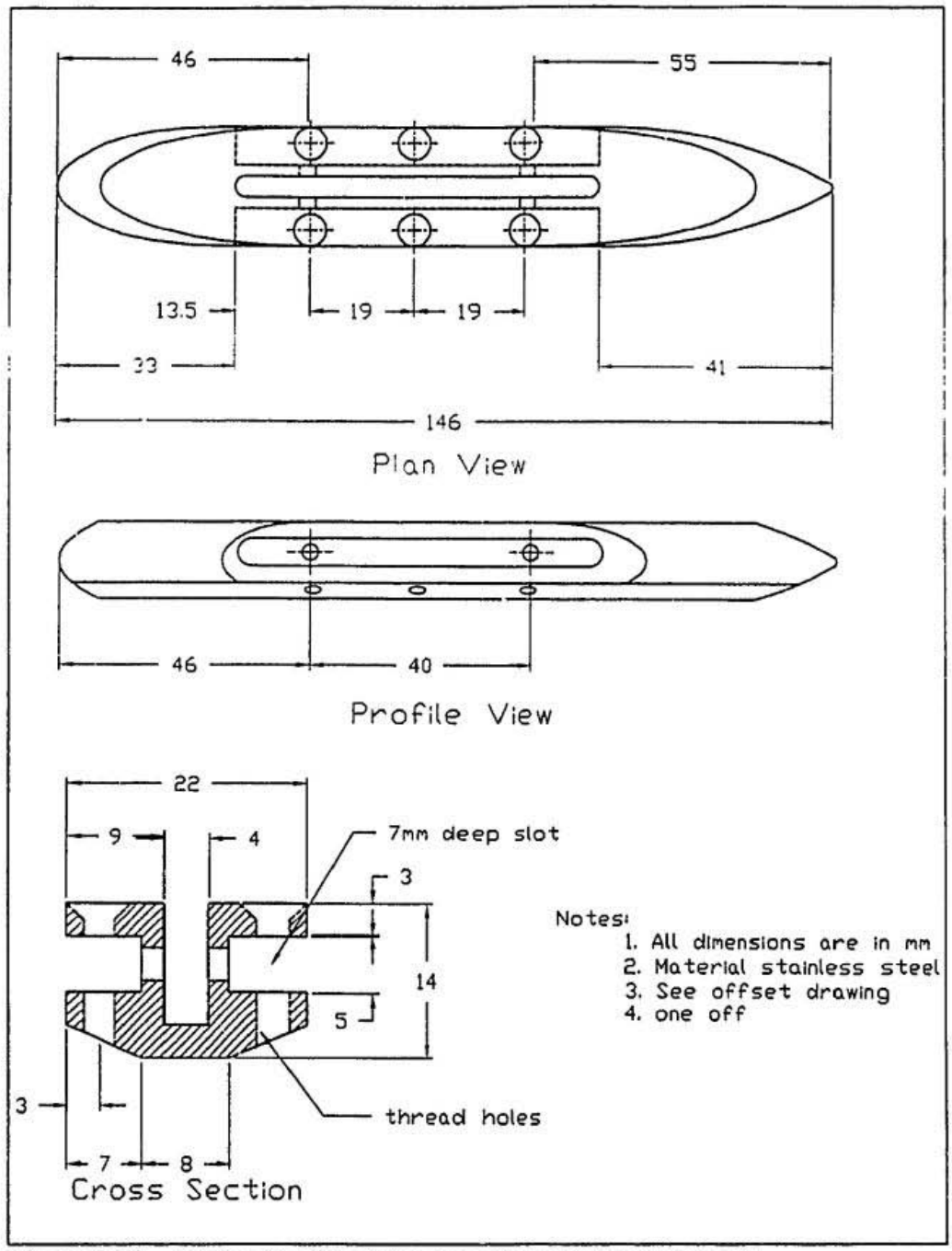

Figure 3.14 Design drawing of the mounting pod. Part number 2.

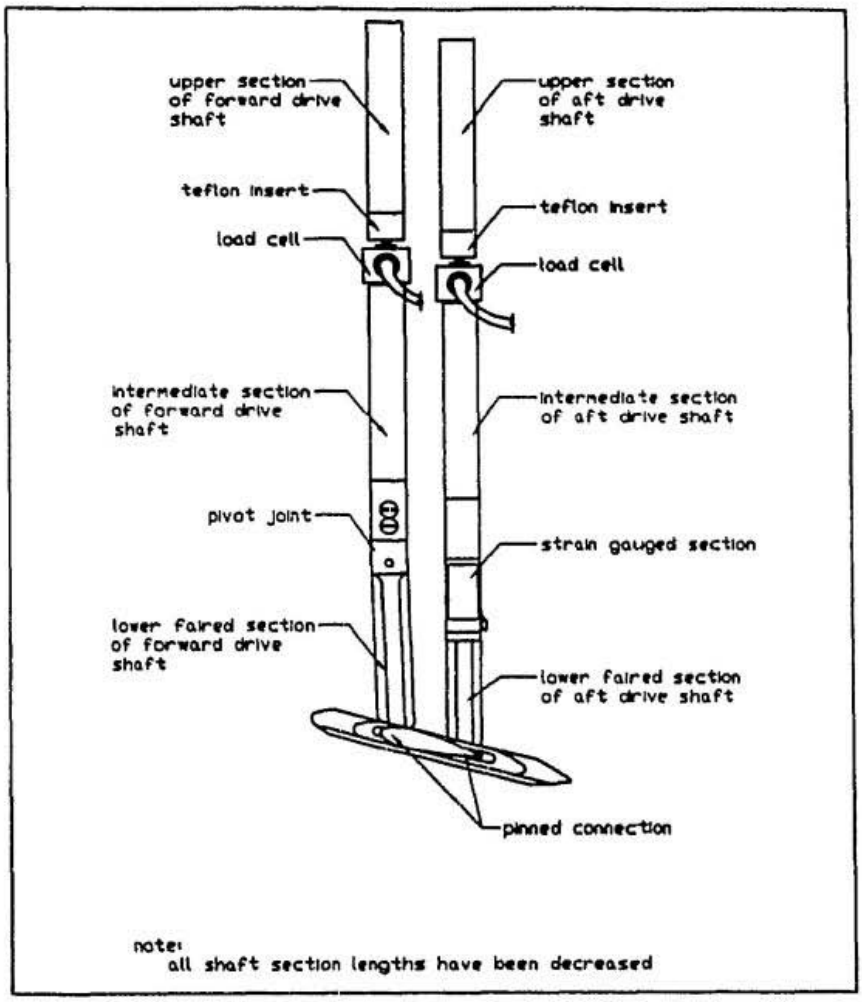

Figure 3.15 Layout of the drive shafts

3.3.3 Drive Shafts

Tne power to drive the foils was transmitted from the motors through two drive shafts. Each of the drive shafts consisted of a number of different sections which can be seen in Figures 3.1, 3.2, and 3.15. Both the forward and aft drive shafts are identical

except that the forward drive shaft has a pivot joint inserted in it 131.5mm above the mounting pod (between the pod and the tunnel window). The pivot joint is connected to the pod by a faired link. The aft drive shaft has a strain gauged section 103.5mm above the mounting pod (between the pod and the tunnel window). The link in the forward drive shaft allows the drive shafts to move out of phase with each other, without them binding up at the point where they penetrate the cavitation tunnel's walls, while the strain gauged section allows the measurement of the bending forces, developed by the foils, on the aft drive shaft. Four strain gauges were mounted in a wheatstone bridge configuration on the 1mm thick section of the aft drive shaft in such away as to measure only bending strain due to forces along the longitudinal axis of the mounting pod.

The upper sections of both drive shafts were made out of stainless steel ground hardened shafts 3/4in. in diameter (See Appendix 'D' page 187 to 192 for sizing of the shafts). Ground hardened shafts were used to ensure that the linear bearings used to align the drive shafts would not wear grooves in the shafts and to provide a smooth dimensionally accurate surface to ensure that a good seal could be made at the point where the shafts penetrated the walls of the cavitation tunnel. To obtain a good seal a shaft with a dimensionally accurate surface is required (Martini 1984). It would have been preferred, to use hollow shafting or stainless steel tubing to minimise mass but it was difficult to obtain and much more expensive than the solid shafting used.

The upper sections of both drive shafts had a load cell inserted at their base to allow the measurement of the forces in the drive shafts generated by the drive motors and the dynamic (the dynamometer will be calibrated to eliminate the dynamic loads) and

hydrodynamic forces from the foils (see Figures 3.2 and 3.15). The load cells were screwed into Teflon inserts which were in turn screwed into the steel shafts. The threads in the Teflon were oversized (25% of the load cells threads were held by the teflon) so that the load cells would pull out of the Teflon insert if the shafts experienced a load greater than 12lbs. This was done to ensure that the load cells never reached their maximum overload of 15lbs. The thread size for the inserts was determined by running a number of tensile tests at Memorial University's Materials laboratory.

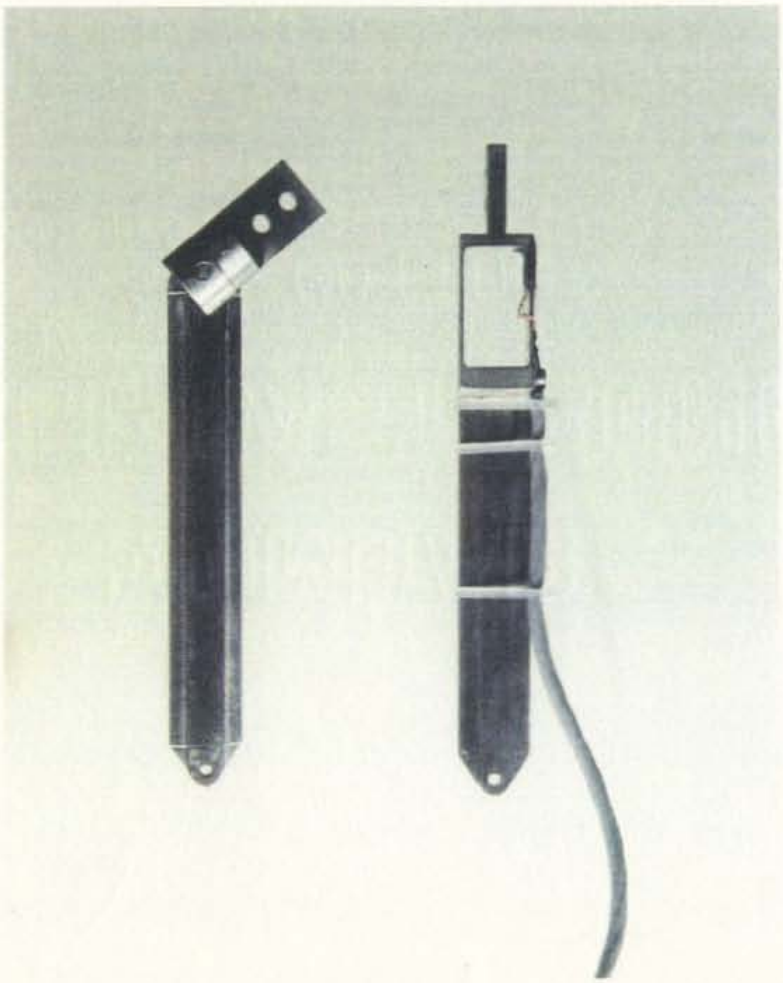

Figure 3.16 Photograph of the lower faired section of the drive shafts. The forward drive shaft (part No. 3 and 4) is shown to the left hand side of the page while the aft drive shaft (part No. 5) is shown to the right hand side of the page.

To the lower ends of each load cell was attached an intermediate section of shaft identical to the upper shaft section. Attached to the lower ends of these intermediate sections were the pivot joint, faired link, and strain gauged sections mentioned above.

Attached to the lower ends of the pivot joint and strain gauged section were faired sections of stainless steel (See Figure 3.16) which extended down into the mounting pod and were connected to the mounting pod by pin connections. The lower ends of the shafts were faired to reduce the drag on them and to reduce the flow disturbances around the foils.

The natural vibrational frequency for the drive shafts, mounting pod, and foil system was estimated by modelling the system as a mass supported by two cantilever beams. The drive shafts were assumed to be rigidly clamped at the point were they penetrated the cavitation tunnel for these calculations and the mass of the beams (drive shafts) was included in the calculations. The calculation of the natural frequency was done for two positions corresponding to the upper and lower limits of the dynamometer's motion which correspond to the maximum and minimum natural frequencies for the dynamometer. The calculated natural frequencies, in the fore and aft direction, were: 9.58Hz (60.2radians/second) for the upper limit and 2.37Hz (14.9radians/second) for the lower limit (The calculations are included in Appendix 'D' page 192 to 194). This resulted in frequency ratios in the range of 0 for the lower frequency motions to 0.42 for the highest frequency motions (See Figure 3.10). Therefore, there may be a small problem of attenuation of the signals from the measurement system when the dynamometer is operating at its maximum oscillating frequency and heave amplitude.

To avoid this the natural frequencies of the drive shaft system should give a frequency ratio outside the range of 0.2 and $\sqrt{2}$. It would have been preferable to have the frequency ratio above 3 (See Figure 3.10). This was not possible, since it would have required the shafts system to have a low stiffness and a high mass (See Equation 3.3 (Steidel 1989)). Therefore, the system should have a maximum frequency ratio of 0.2. This problem may be solved if the solid shafts are replaced by hollow shafts in the future. The hollow shaft would have approximately the same stiffness but a much lower mass than the solid shafts. Since the natural frequencies is a function of the stiffness of the shafts divided by the mass of the shafts, the hollow shafts should have a higher natural frequency than the solid shafts.

$$\omega_n = \sqrt{(k/m)} \qquad (3.3)$$

Where:

ω_n = the natural frequency of the system

k = the stiffness of the system

m = the mass of the system

3.3.4 Seals

The edge of the window port, the two penetrations for the drive shafts and the penetration for the strain gauge cable had to be made both water and air tight to prevent water from leaking out of the tunnel during atmospheric testing and prevent air from entering the tunnel during testing at pressures below atmospheric pressure (The pressure

in the cavitation tunnel will range from one to minus one atmosphere). The seals for the drive shafts also had to be designed to have low and constant frictional resistance's to allow smooth running of the drive shafts and if possible the measurement of the input forces to the foils.

One of the best methods of sealing a port is by use of a O-ring while the best method of sealing an oscillating shaft is by using U-cup rings opposing each other (Martini 1984). Therefore, the window port was sealed by a 7mm diameter rubber O-ring and the strain gauge cable was sealed by a screw down seal provided in the window of the tunnel. Each drive shaft penetration was sealed by two urethane U-cup rings, positioned in grooves cut into the window port (See Figure 3.17). Two single acting seals opposing each other were used, for each drive shaft, to seal a vacuum in one direction and water pressure in the other. Note, that the size and spacing of the seals were based on recommended seals given in the Dowty Silcofab catalogue for a working pressure of plus or minus one atmosphere and a reciprocating shaft.

3.3.5 Shaft Alignment System

The alignment of the drive shafts was accomplished by running each drive shaft through two linear bearings and two Teflon bushings. At the point where the drive shafts entered the cavitation tunnel there were two 25mm long Teflon bushings placed 21mm apart. These were placed here to align the shafts where they penetrated the cavitation tunnel's window port. These bushings provided the reactions required to balance the

horizontal thrust on the foils and the drag on the lower drive shafts. This allowed the shafts to run smoothly through the window, thus reducing the frictional forces and preventing the wearing of the brass window port and the U-cup rings used to seal the drive shaft penetrations in the window port. The bushings were also required at this location to eliminate any bending loads from being transmitted to the load cells which would have been damaged by such loads.

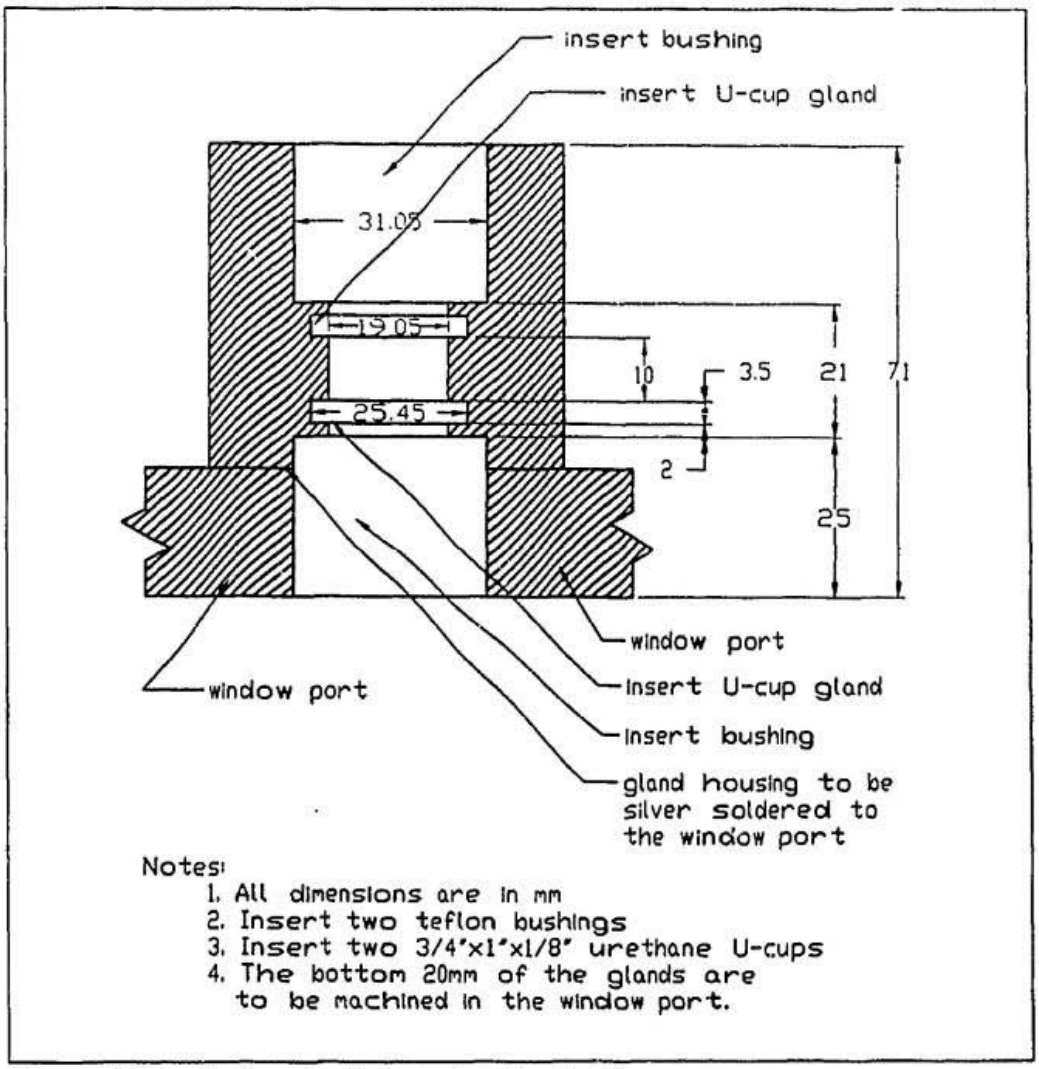

Figure 3.17 Shaft seals. Part number 11 and 15.

Each drive shaft runs through two linear bearings above the top of the cavitation tunnel's window port (See Figure 3.1, 3.2, and 3.18). These bearings were placed at 345mm and 677mm above the port (measured to the centre of the bearings) to minimise the deflection of the drive shafts and to allow a heave amplitude of at least 110mm.

3.3.6 Drive System

The drive system for the dynamometer consisted of two programmable D-C servo motors each of which drove a pulley drive belt system connected to the dynamometer's drive shafts. A timing pulley was mounted on the shaft of each motor (See Figures 3.2 and 3.3). These pulleys were connected by fibreglass reinforced timing belts to identical pulleys mounted on freely rotating shafts. The upper pulley shafts were each mounted in a vertically adjustable housing which allowed the tensioning of the drive belts. The belts were connected to the drive shafts with a clamp connection which can be seen in Appendix 'A' (drawing number A-15 page 152). Timing belts were used since they do not allow any slippage in the motion (Shigley and Mischke 1989).

In order to provide a range of motions two Aerotech programmable D-C Servo motors model 1050 with 10/1 ratio gear boxes with low backlash were selected to oscillate the drive shafts. The motors operational parameters are listed in Table 3.3.

These motors were controlled by a Unidex 14 motion controller and could be programmed to produce an infinite series of motions. The motion controller was capable of simultaneously moving both motors independently of each other. By oscillating the

shafts out of phase with each other, a heaving and pitching motion could be developed with the pitching axis located anywhere along the chord line of the foils. The versatility of this system allowed the position of the pitching axis of the foils to be programmed into the computer.

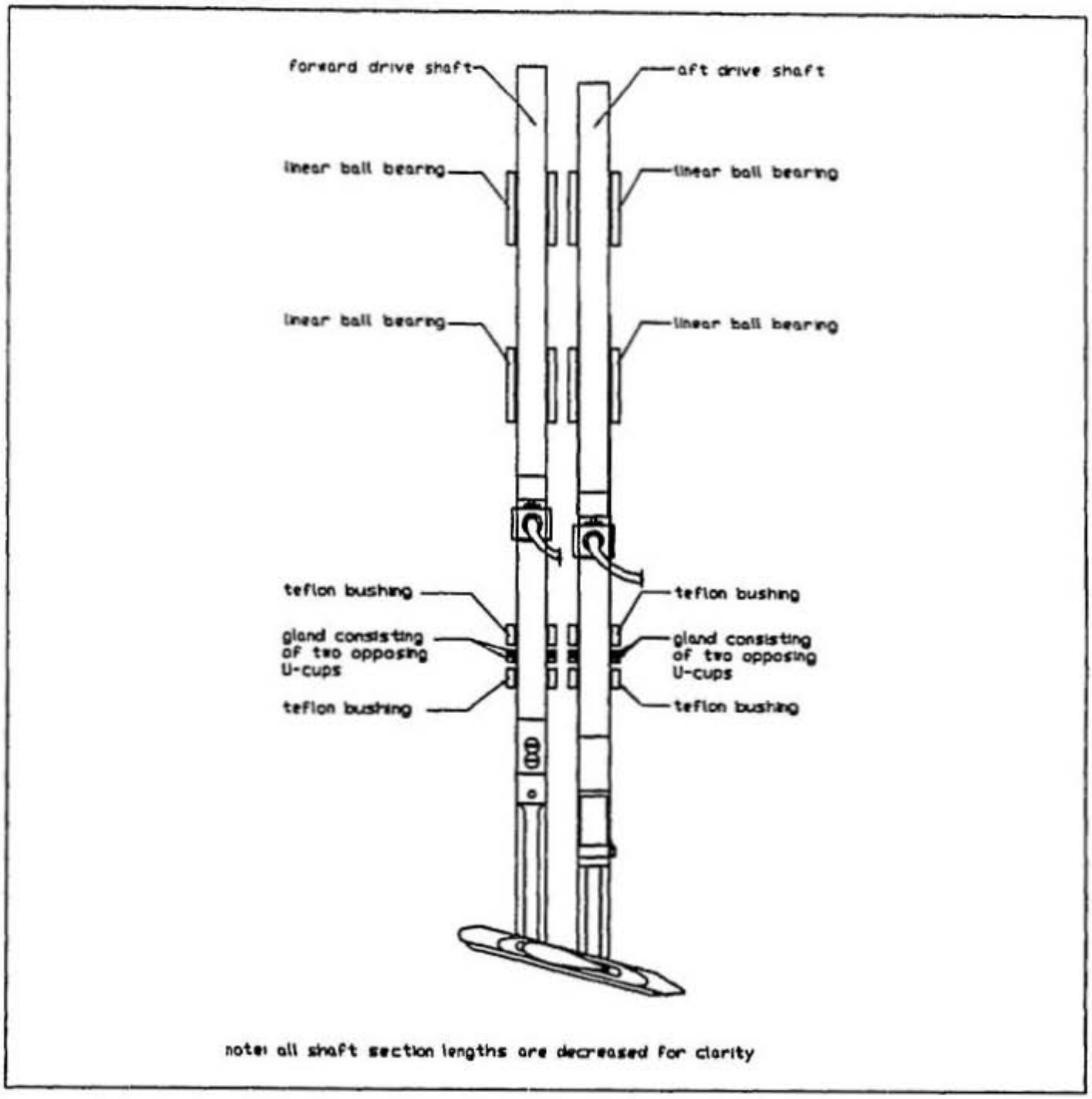

Figure 3.18 Drive shaft alignment

Table 3.3 Motor operational parameters

stall torque, continuous	0.35N-m
peak torque	2.52N-m
maximum speed	6000rpm
maximum power output, continuous	146watts
maximum acceleration	44000radian/second^2
weight	1.59kg

3.3.7 Fairing

To reduce the flow disturbances around the foils and to reduce drag on the drive shafts the upper portions of the drive shafts operating inside the tunnel were encased in a fairing. This fairing, which can be seen in Figure 3.19 was made of two stainless steel sheets rolled into circular arcs and welded together at both ends. The fairing was connected to the bottom of the tunnel's window port and the drive shafts oscillated freely through it.

3.3.8 Limit Switches

Each motor was equipped with a connection for limit switches which could be used as a home position for the motors and to limit the motor's motions. Four limit switches were installed to ensure that the dynamometer was not damaged by motor over runs. A flag was attached to each of the clamps connecting the drive shafts to the drive belts. Two limit switches were placed 110mm below these flags and two switches were placed 110mm above these flags to allow a total maximum heave motion of 220mm (See Figure 3.1 and 3.2). All four limit switches were wired together so that if any switch was

tripped both motors would stop. This was necessary, since both drive shafts were connected together by the mounting pod and if one motor stopped while the other continued to move it would damage the dynamometer.

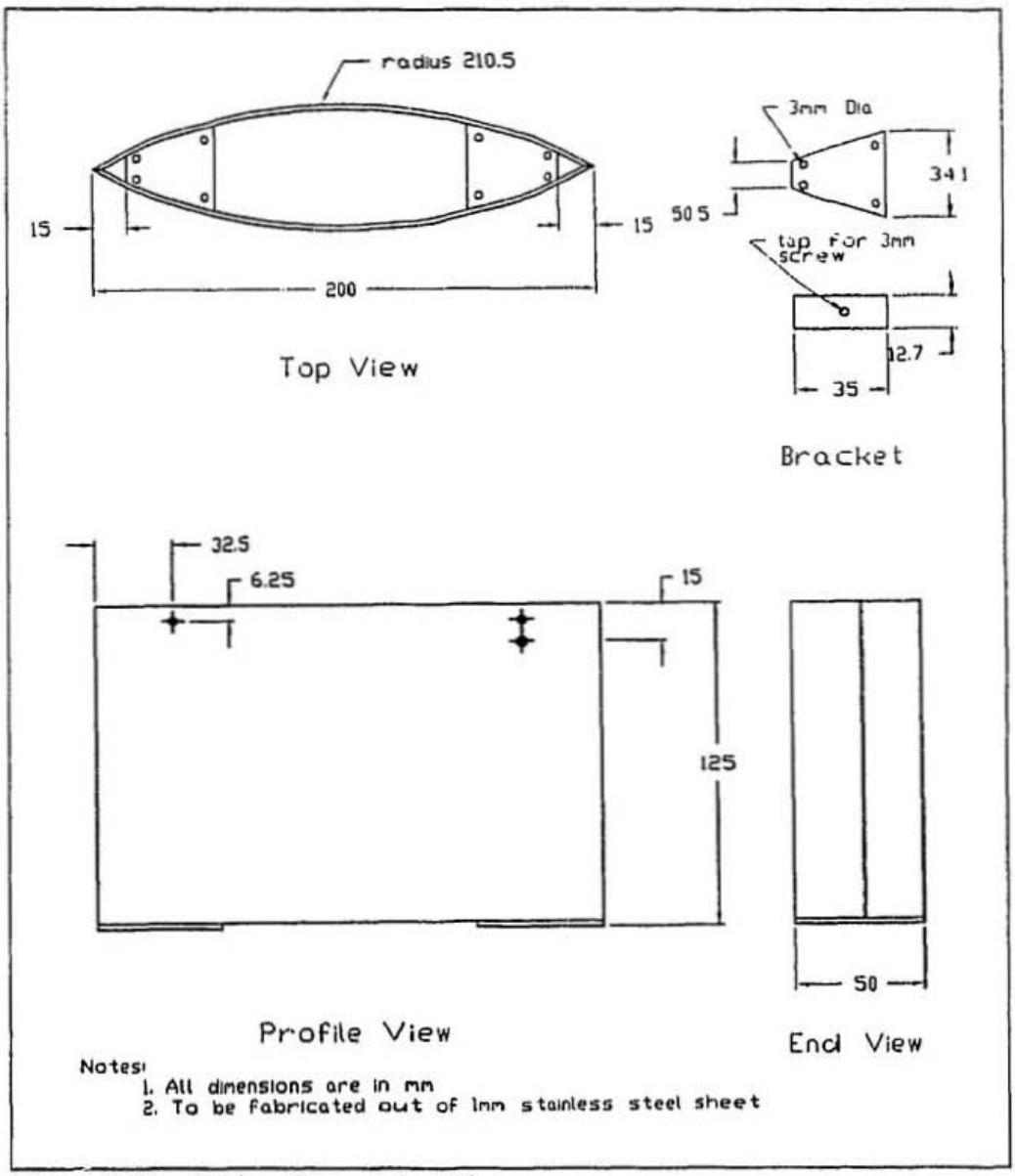

Figure 3.19 Fairing. Part number 25.

3.3.9 Data Acquisition System

The instrumentation system was made up of: a full Whetstone bridge strain gauged section inserted in the aft shaft of the dynamometer, two miniature load cells with a range of 10lbs tension/compression capacity (one inserted in each shaft) and a LVDT connected to each shaft. An amplifier with a built in DC power supply excited and amplified the output signals from the strain gauges and load cells. A separate power supply was used for the LVDTs because the signals from them did not have to be amplified. The signals from the instruments were processed by a Keithley 570 data acquisition system and fed to a 80286 computer used to store the data and perform initial data processing.

The dynamometer's data acquisition system was designed to fulfil the following two functions: 1) To record the exact motion of the test foils so that the effects of different motions could be studied; and 2) To measure the resultant axial forces in the drive shafts produced by the drive motors and the vertical component of the lift/drag forces from the test foils and the horizontal component of the lift/drag forces in the direction parallel to the water flow (See Figure 3.20). This information will allow the propulsion efficiencies of the test foils for different propulsion parameters and motions to be calculated using Equation 3.4.

$$\eta_P = (V_A' * T')/P' \qquad (3.4)$$

Where:

η_P = propulsion efficiency

$\dot{T}$ = mean thrust developed by the tests foil during a complete motion cycle

$\dot{V_A}$ = mean speed of advance of the test foil during a complete motion cycle

$\dot{P}$ = mean power supplied to the test foils during a complete motion cycle.

= the mean of the force supplied to drive the test foils * the speed of advance of the test foils

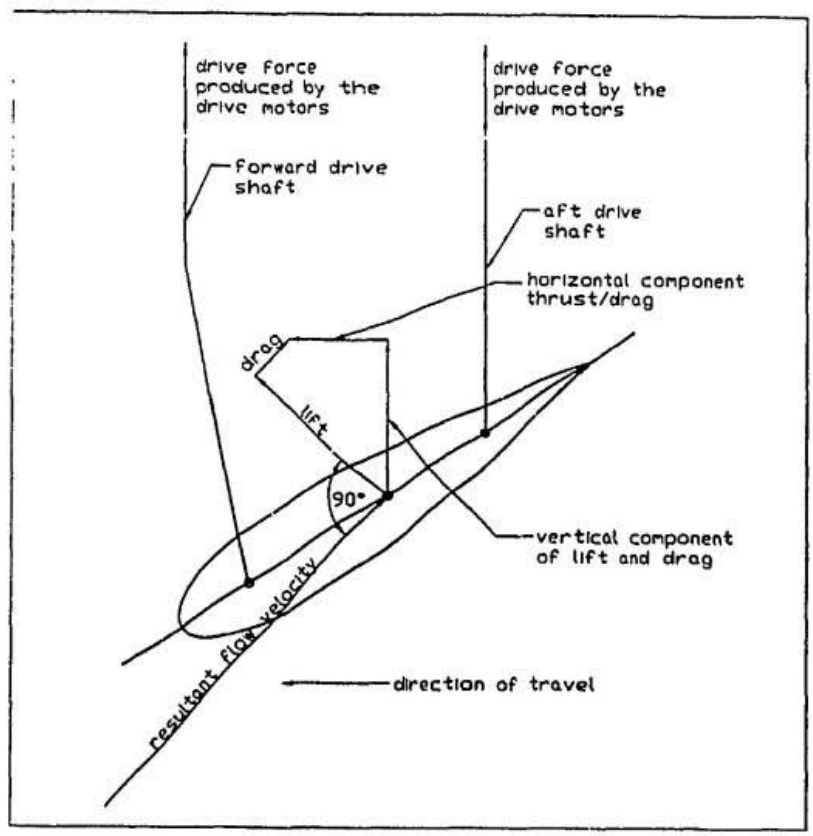

Figure 3.20 Forces to be measured by the data acquisition system

The maximum movement of the drive shafts was 220mm (an heave amplitude of 110mm), while the maximum expected axial loads in the drive shafts were 46N and the

maximum thrust loads on the aft drive shaft were 67N. See Appendix 'D' pages 176 to 187 for the calculation of the forces.

The LVDTs were used to determine the exact displacement of the foils over time, while the load cells measured the end loads on the drive shafts. These loads could be used in combination with the foil's velocities, obtained from the LVDTs displacement data, to determine the power absorbed by the foils. The purpose of the strain gauged section was to measure the drag and thrust forces exerted on the aft drive shaft. These forces were used to determine the thrust developed by the foils.

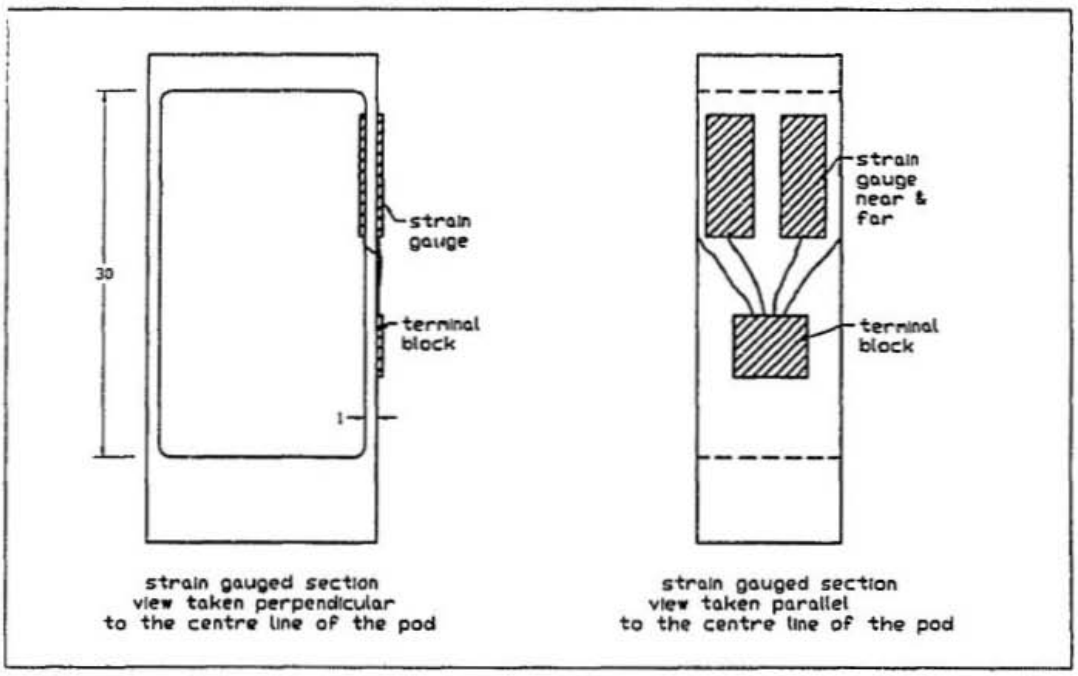

Figure 3.21 Layout of strain gauges

The strain gauged section can be seen in Figures 3.16 and 3.21. The centre portion of the section was milled out to form two 1mm thick bending beams at the outer

sides of the section (See Appendix 'D' page 194 to 196). These were designed to develop a maximum strain of 1700 micro-strain (See Appendix 'D' page 197 to 200 for calculations). Four strain gauges were mounted at the upper end of the aft bending beam in a Wheatstone bridge configuration and sealed in a water proof clothing (See Figure 3.21). The natural oscillating frequencies of the reduced strain gauged section were much higher than the operational frequencies of the dynamometer. Therefore, the strain gauged signals should not be influenced by vibrational noise due to the oscillating motion of the lower assembly. Note, that both the natural frequencies about an axis parallel and an axis perpendicular to the water flow were checked (See Appendix 'D', page 196 for the calculations).

Figure 3.22 shows the forces which will act on the dynamometer while Figure 3.23 shows the forces that will act on the foils. From these figures it can be seen that the load cells will experience the following forces:

1) forces exerted by the drive motors,

2) frictional forces from the bearings, bushing, and seals,

3) frictional forces due to friction in the pivot joint and pins,

4) dynamic forces due to the vertical acceleration of the shafts, pod, and test foils,

5) vertical components of the centripetal forces due to the rotational movement of the lower forward drive shaft, pod, and test foils,

6) lift forces from the foils, and

7) lift forces from the pod.

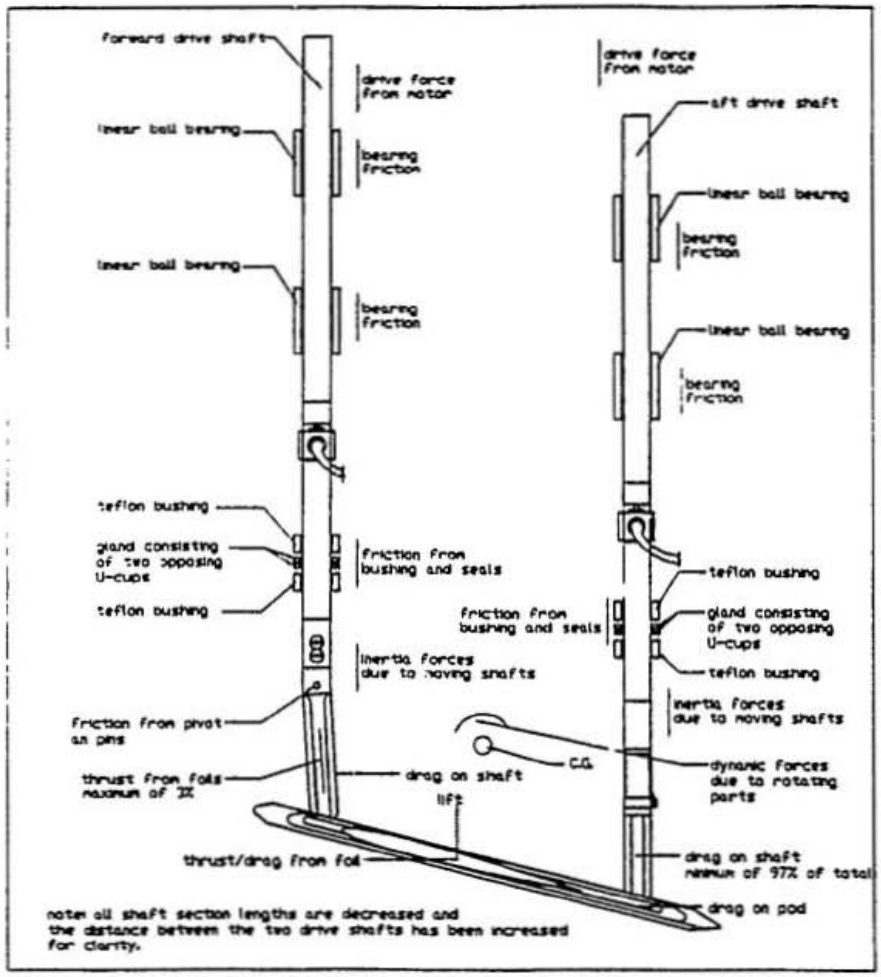

Figure 3.22 Forces experienced by the dynamometer

The strain gauged section will experience the following forces:

1) thrust/drag forces from the tests foils,

2) thrust forces from the pod,

3) drag forces on the lower drive shafts, pod, and test foils,

4) axial forces transferred from the forward drive shaft due to the rotation of the faired link, and

5) horizontal components of the centripetal forces due to the rotational movement of the lower forward drive shaft, pod, and test foils.

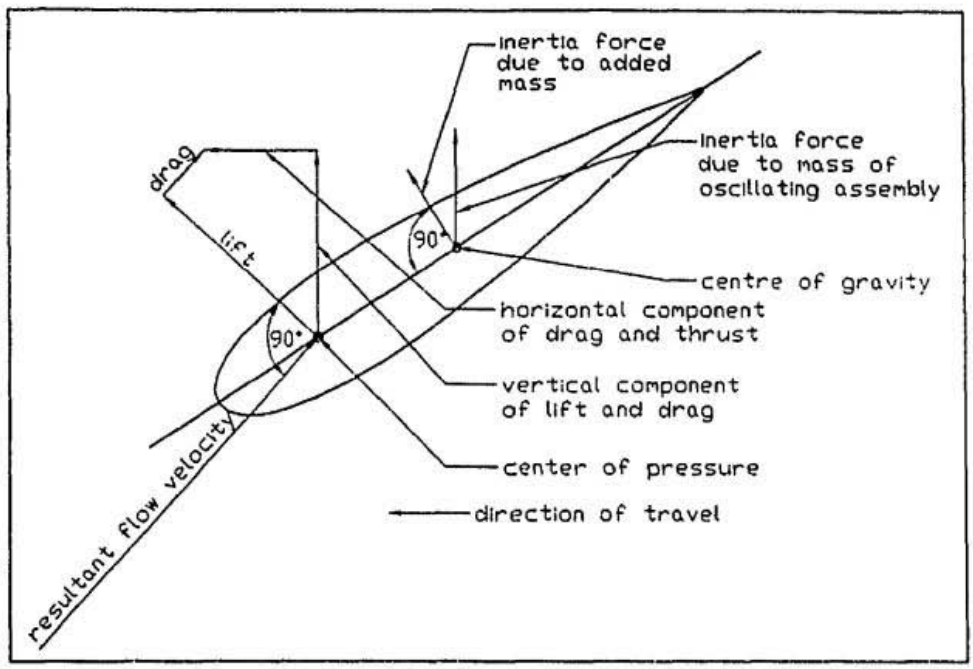

Figure 3.23 Forces acting on the test foils

It can be seen from Figures 3.22 and 3.23 that the load cells will experience forces which will interfere with the measurement of the forces which the dynamometer was intended to measure. If the frictional forces from the bearings, bushing, and seals are too great to allow the desired measurements the seals and bushing can be replaced by an additional set of linear bearings and the propulsion efficiency tests conducted in the wave tank. The frictional forces in the pivot joint and pins should be relatively low once the dynamometer is broken in. The maximum dynamic forces due to vertical accelerations of the oscillating components will be approximately 46% of the total axial loads carried by the drive shafts (See Appendix 'D' page 186 to 187 for the calculations). The vertical

components of the centripetal forces due to the rotation of the lower assembly will be small due to the small angles and low oscillating frequencies. All these forces can be calibrated for by running the desired test conditions in air before and after the actual test in water. The lift/drag forces from the pod should be relatively small compared to those from the test foils and can be calibrated for by running the desired test parameters in water without the test foils installed. If after a series of test conditions the lift/drag on the pod is determined to be constant or negligible it can be ignored.

The drag forces on the lower drive shafts should also be small compared to those produced by the test foils and can be easily calibrated for in the same manner as the lift/drag forces on the pod. The component of the thrust forces which will be carried by the forward drive shaft and the horizontal component of the dynamic forces from the centripetal motion of the pod, test foils, and lower forward drive shaft were shown to be relatively low compared to the expected loads in Section 3.2 (approximately 3.6%) and can be calibrated for by running a series of test in air (See Appendix 'D' Page 203). It should also be noted that the maximum inertia loads will occur at different phases than the maximum hydrodynamic loads. If a series of tests conducted in both air and water can be conducted to show that the phase and or frequency of these loads are far enough apart, then the inertia loads can be filtered out of the desired measurement signals.

The data acquisition system was completely shielded from electronic and magnetic noise. To achieve this, all cables used in the system were twisted pairs with double shielding. Each individual wire was shielded and then the entire cable was wrapped in an additional metallic foil shield. These shields were grounded to the Keithley data

acquisition system. Since the strain gauges, LVDTs, and load cells were also shielded, the signals from the measuring instruments were shielded from all sources of electronic and magnetic noise all the way from the measurement devices to the Keithley data acquisition system. The Keithley data acquisition system converted the electronic signals into digital signals which are not affected by electronic and magnetic noise.

Chapter 4

Motion Control

4.1 The Control System

A schematic diagram of the dynamometer's control system is presented in Figure 4.1. The control system is made up of a 80286 PC Computer with a Unidex 14 Control Board installed in it, a Unidex 14 Drive chassis, and two D-C programmable servo motors.

Figure 4.1 shows how the operator of the dynamometer can interact with the control system to develop the desired motion. The operator interacts with a QuickBasic program running on the PC to define the desired motion. Once the desired motion has been defined the QuickBasic program then calculated a series of displacements, velocities, and accelerations to approximate the desired motion. It then creates a series of ASCII strings, which call the built in Unidex subroutines needed to produce the desired motion. These ASCII strings are sent to the Unidex 14 control board which uses the built in subroutines to develop a set of parameters defining the electrical pulse train which have to be sent to each motor to produce the desired motion. These parameters are then sent from the control board inside the PC to the Unidex 14 drive chassis which generates the pulse trains for each motor independently and then sends them to the motors, which produce the desired motion.

4.2 Motion Development

This section will cover the development of the computer program written to control the motions of the dynamometer. The program was written in modular form so that all the motion specific computer code, was contained in one subroutine. This allows new subroutines, to produce different motions, to be written and added to the main control program in the future. For this project a subroutine to produce a small amplitude sinusoidal wave motion with a constant 90° phase angle between pitch and heave was written.

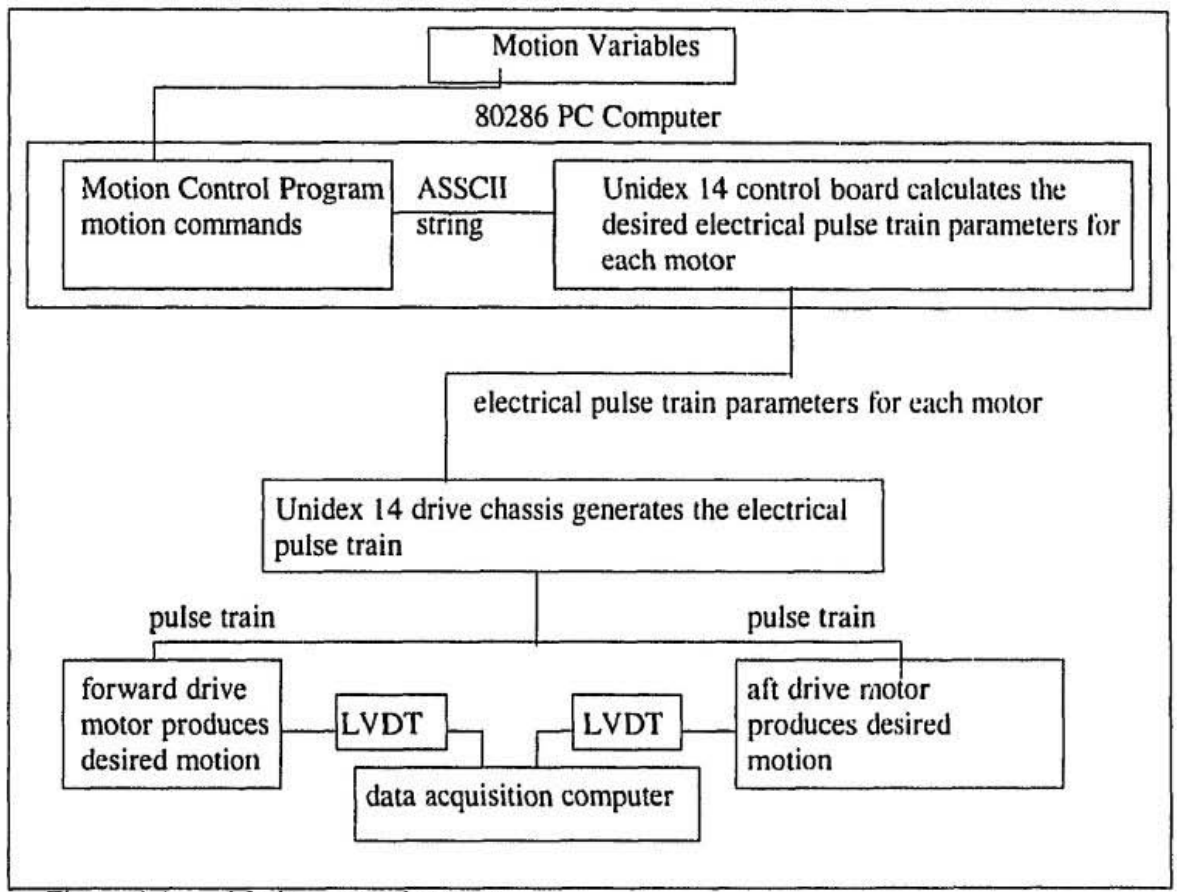

Figure 4.1 Motion control system

A 90 degree fixed phase angle was chosen to help simplify the initial programming of the motion controller and was justified by the high efficiency found in Wu's (1991b) study on porpoises. In his study, he assumed a 90 degree phase angle between pitch and heave. Again it should be noted that in this project the main objective was to test the dynamometer and not the foils. Further work on this project will involve developing new motions with a greater degree of flexibility. This will involve both fixed and variable phase angles and will be accomplished by writing the equations of motion in their general form with the phase angle supplied as an operator definable constant or cyclic function. This added complexity will not affect the operation of the dynamometer since the calculations are performed off line.

4.2.1 Development of The Equations of Motion

For a sinusoidal small amplitude motion with a constant 90° phase angle between pitch and heave, the displacement of any point x on the foil is defined by equation 4.1 (after Lighthill 1970). See Figure 4.2.

$$Z = Re[h - i\alpha(x - b)]e^{i\omega t} \qquad (4.1)$$

Where:

$e^{i\omega t} = \cos(\omega t) + i\sin(\omega t)$

Z = vertical displacement of a point x on the centre or nose tail line of the foil (m)
Re = the real part
h = amplitude of heave motion (m)
α = amplitude of pitch (radians)
ω = radian frequency of oscillation (radians/second)

x = position along the chord line of the foil from the centre chord location (m)

b = the pitching axis location relative to the mid chord of the foils (m)

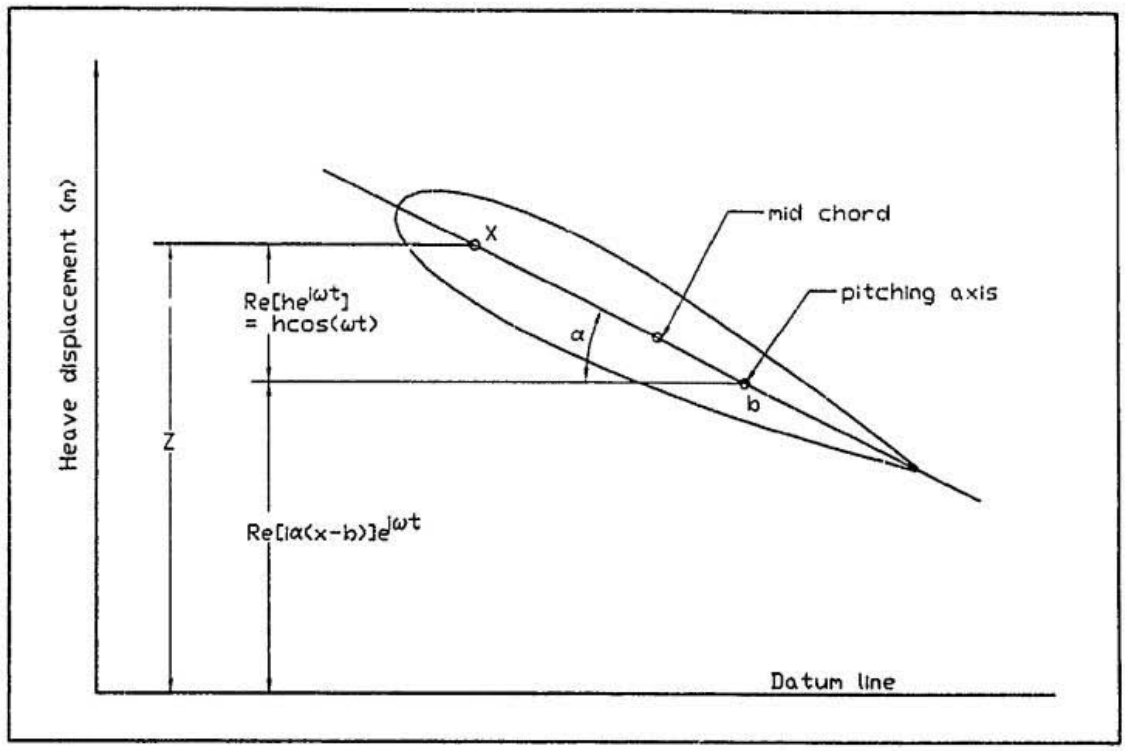

Figure 4.2 Components of a sinusoidal small amplitude motion

This equation is only valid for small pitching amplitude motions, due to a simplifying approximation in the equation. It is assumed, in the equation, that the tangent of the angle between an horizontal line through the foil's pitching axis and its centre chord line is equal to the angle in radians. Thus, the errors in this equation increase as the pitching amplitude of the motion increases. For a five degree pitch the error will be

0.25% and for a 23 degree pitch angle (the maximum obtainable by the dynamometer) it would be 6%.

As mentioned above, Equation 4.1 describes the displacement of any point x on the centre line or nose tail line of the foil. If we define the point of intersection of the foil's centre line and the forward shaft as 'a' and the aft shaft as 'c' (See Figure 4.3) then the equations of displacement for the drive shafts and the pitching axis are:

$$Z_a = h\cos(\omega t) + \alpha(a - b)\sin(\omega t) \quad (4.2)$$

$$Z_c = h\cos(\omega t) + \alpha(c - b)\sin(\omega t) \quad (4.3)$$

$$Z_b = h\cos(\omega t) \quad (4.4)$$

Using equations 4.2 and 4.3 to define the motions of the drive shafts introduces a second error. The equations do not take into account the pivot point in the forward drive shaft (the forward drive shaft is assumed to remain vertically straight). This results in an error since the forward drive shaft does not remain vertically straight. This error also increases as the pitching amplitude of the motion increases. For a requested pitch angle amplitude of 30° a pitch angle amplitude of 30.18° is obtained (0.62% error).

This error can be corrected by using equation 4.5 to calculate a new pitch angle amplitude α_o (slightly lower than the desired angle α_d) to be inserted into the motion program to obtain the desired pitch angle amplitude (See Appendix 'D' page 176 for the development of Equation 4.5). When the motion program is updated the movement of the link can be incorporated into the motion. It was left out during this stage of the project to simplify the initial programming of the motion.

$$\alpha_o = \arcsin[AB*SIN\alpha_d - BD + BD*COS\theta/AB] \quad (4.5)$$

where: AB = the distance between the drive shafts
BD = the length of the link in the forward drive shaft
$\theta = \arcsin[AB - AB*COS\alpha_d/AB]$

Differentiating equations 4.2, 4.3, and 4.4 with respect to time gives the velocity equations.

$$V_a = -\omega h\sin(\omega t) + a\omega(a-b)\cos(\omega t) \quad (4.6)$$
$$V_c = -\omega h\sin(\omega t) + a\omega(c-b)\cos(\omega t) \quad (4.7)$$
$$V_b = -\omega h\sin(\omega t) \quad (4.8)$$

Differentiating the equations of velocity with respect to time gives the following equations for acceleration:

$$A_a = -\omega^2 h\cos(\omega t) - a\omega^2(a-b)\sin(\omega t) \quad (4.9)$$
$$A_c = -\omega^2 h\cos(\omega t) - a\omega^2(c-b)\sin(\omega t) \quad (4.10)$$
$$A_b = -\omega^2 h(\omega t) \quad (4.11)$$

The equations for displacement (Equation 4.2, Equation 4.3, and Equation 4.4) can be rewritten as:

$$Z_a = [h^2 + (\alpha(a-b))^2]^{1/2}\cos(\omega t - \phi_a) \quad (4.12)$$
$$Z_c = [h^2 + (\alpha(c-b))^2]^{1/2}\cos(\omega t - \phi_c) \quad (4.13)$$
$$Z_b = h\cos(\omega t) \quad (4.14)$$

Where:

$$\phi_a = \tan^{-1}\left[\frac{\alpha(a-b)}{h}\right] \quad (4.15)$$
$$\phi_c = \tan^{-1}\left[\frac{\alpha(c-b)}{h}\right] \quad (4.16)$$

Since the equations of motion could not be fed directly into the control system a means of approximating the desired motion had to be developed utilising the subroutines which were built into the Unidex motion controller. This was accomplished by dividing

the desired motion (see Figure 4.4) into a number of equal time intervals and calculating the displacement for each time interval using Equations 4.12 and 4.13 (See Figure 4.5).

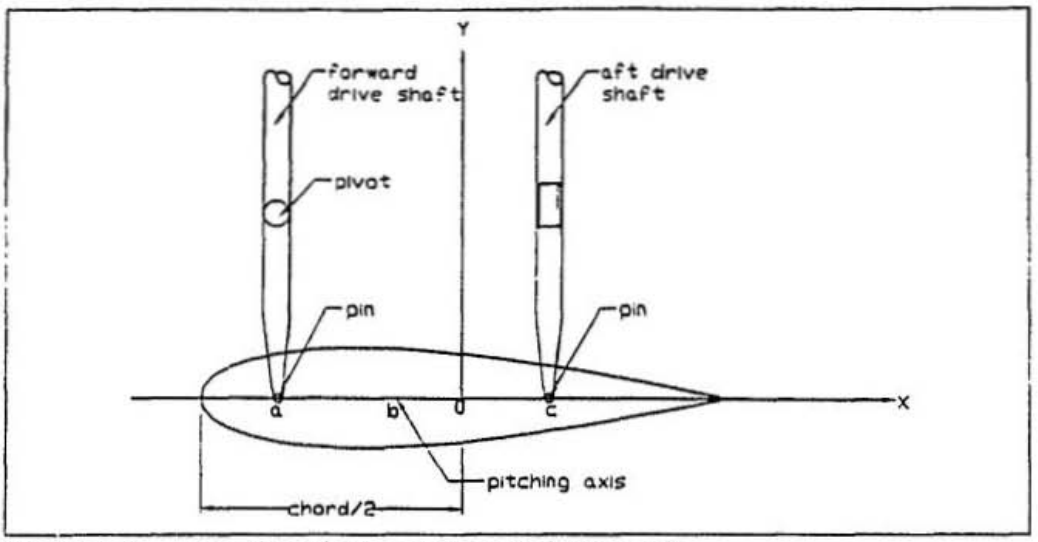

Figure 4.3 Location of drive shafts and pitching axis

note: the X and Y axes are centred at the mid chord of the foil with the positive X axis pointing toward the trailing edge and the positive Y axis pointing upward.

For each time interval the velocity and accelerations required to reach the desired displacement in the time interval was calculated based on the displacement, velocity, and acceleration profiles presented in Figure 4.6. The equations for the peak velocity and acceleration are given in Equations 4.17 and 4.18.

These profiles allowed time for the motors to ramp up to their peak velocities and then ramp back down to a stop at the end of each segment. This allowed the required accelerations to be reduced, thus reducing the vibrations. It would have been preferable not to stop the motors at the end of each segment or time interval, but this has not been

possible to date given the limitations of the available subroutines built into the motion controller.

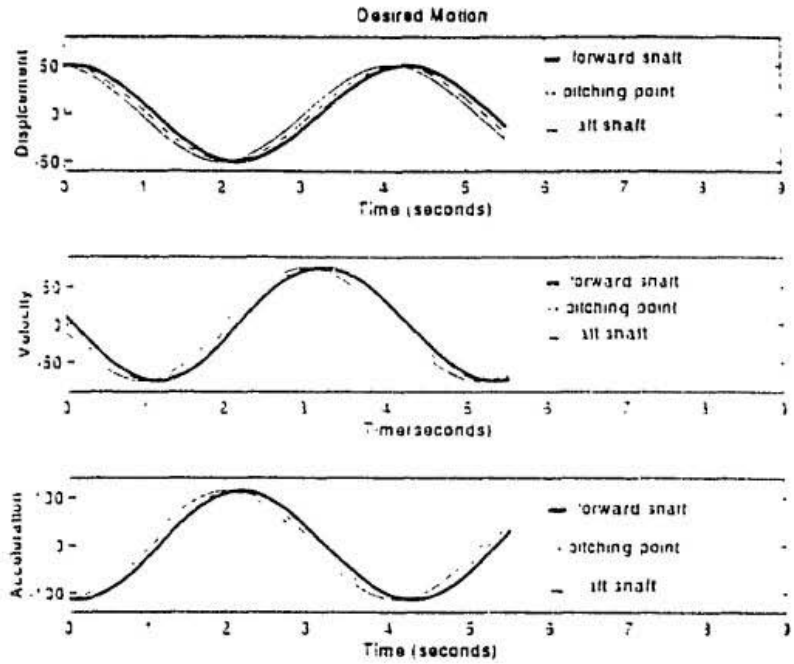

Figure 4.4 Desired motion

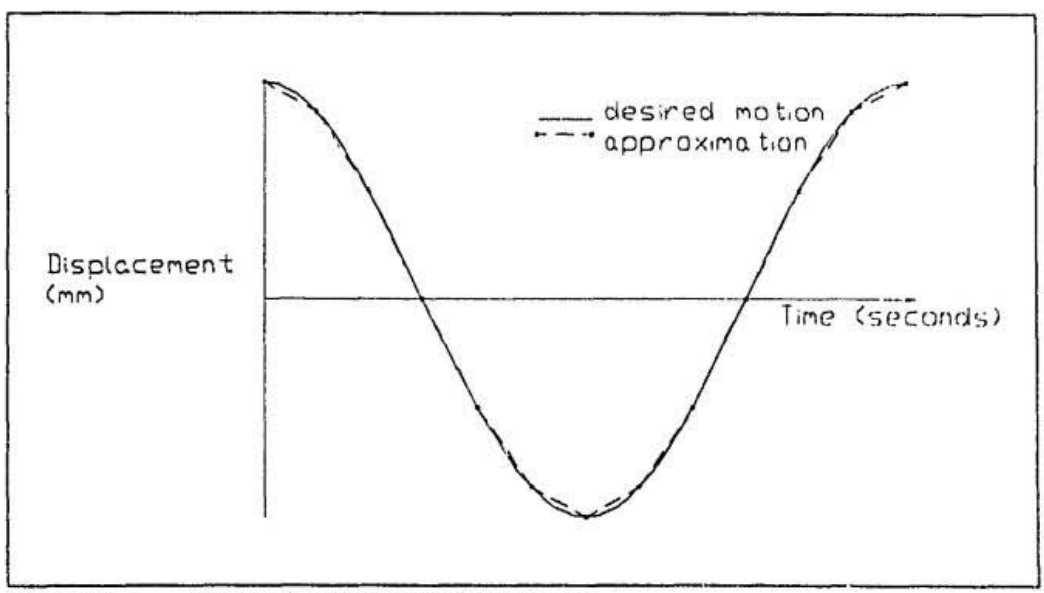

Figure 4.5 Approximation of desired motion

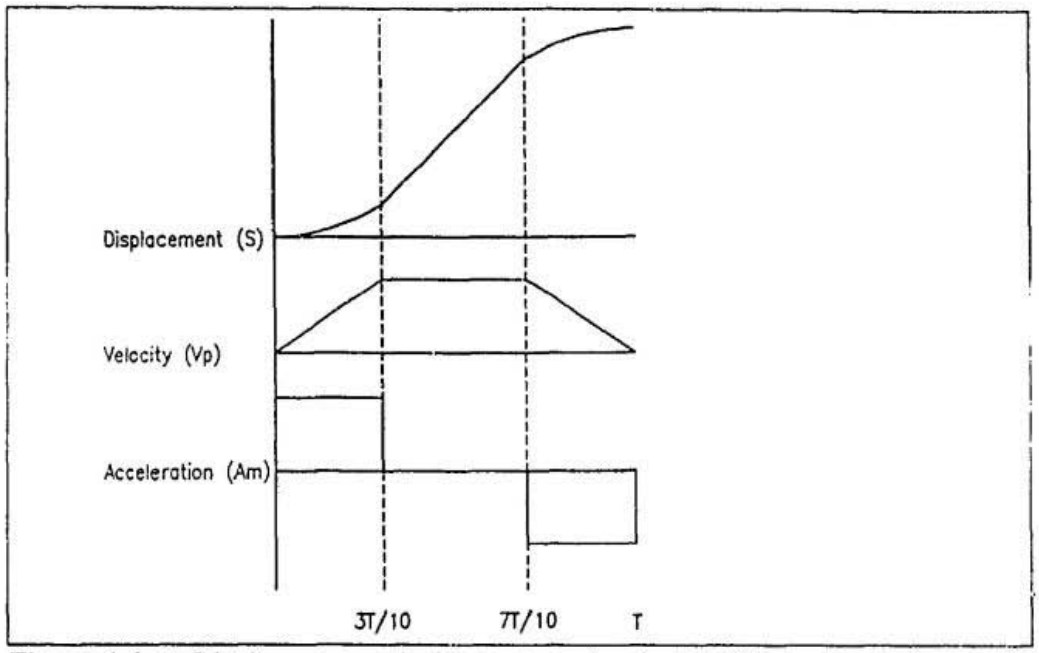

Figure 4.6 Displacement, velocity, and acceleration profiles

$$V_p = \frac{3S}{2T} \tag{4.17}$$

$$A_p = \frac{9S}{2T^2} \tag{4.18}$$

Where:

V_p = the peak velocity (m/s)

A_p = the peak acceleration (m/s^2)

S = displacement during time interval (m)

T = interval time (s)

The motion controller was designed in such a way that the desired motion had to be built up using a combination of the base commands supplied with the motion control system. These commands were encoded in the hardware of the system and were not accessible by the operator. Therefore, it was not possible to modify these command subroutines to allow a continuous motion.

4.2.2 The Control Program

The control program was written in QuickBasic. Due to the excessive size of the program, the actual code is not included in this thesis. However, some flow charts needed to help explain the operation of the program are presented in this chapter while the remaining flow charts are presented in Appendix 'C'. Some of the subroutines used in this program were taken directly from the software provided with the controller. The flow charts for these subroutines are not included.

The flow chart for the main program is presented in Figure 4.7a and b. It can be seen from this figure that the first set of operations, which the main program performed, initialised the system to a known state. This involved setting all Unidex encoder and user units to one, resetting all the Unidex error flags and interrupts to indicate that there were no errors, setting the Unidex's sendmode to one which allowed the Unidex controller to send information back to the control program, disabling the Unidex echo so that the commands being executed by the controller would not be printed on the computer screen,

clearing the storage buffers, and resetting the default velocities and accelerations for the motors.

Once the system was reset the program then created four dialogue boxes on the computer screen (See Figure 4.8) to display an history of the operator's requests, what was being asked of the operator, the responses, and the available options. The program then gave the operator the option to position the foils at the centre line of the cavitation tunnel. If the option to centre the foils was chosen then the main program switched control to a subroutine called CENTRE, which allowed the operator to move the foils up or down using a series of either displacement or levelling moves and then returned control to the main program after the foils were in position. The displacement move consisted of both drive shafts moving the same distance. A levelling move allowed the operator to move either the forward or aft shaft alone, in order to level the foils.

Next the main program entered a control loop. This allowed the operator to run a test and then return back to the beginning of the control loop after the test was completed to start another test with the same or a new set of motion variables. The first operation which the control program performed in the control loop was to ask the operator if the motion variables had to be changed. If so the control program switched control to a subroutine called INFO. then asked for values for the motion heave and pitch amplitude, and the oscillating frequency, before switching control back to the main program. This subroutine also contains a check to ensure that the heave amplitude is less than 100mm (the maximum allowed to ensure that there is no damage to the dynamometer).

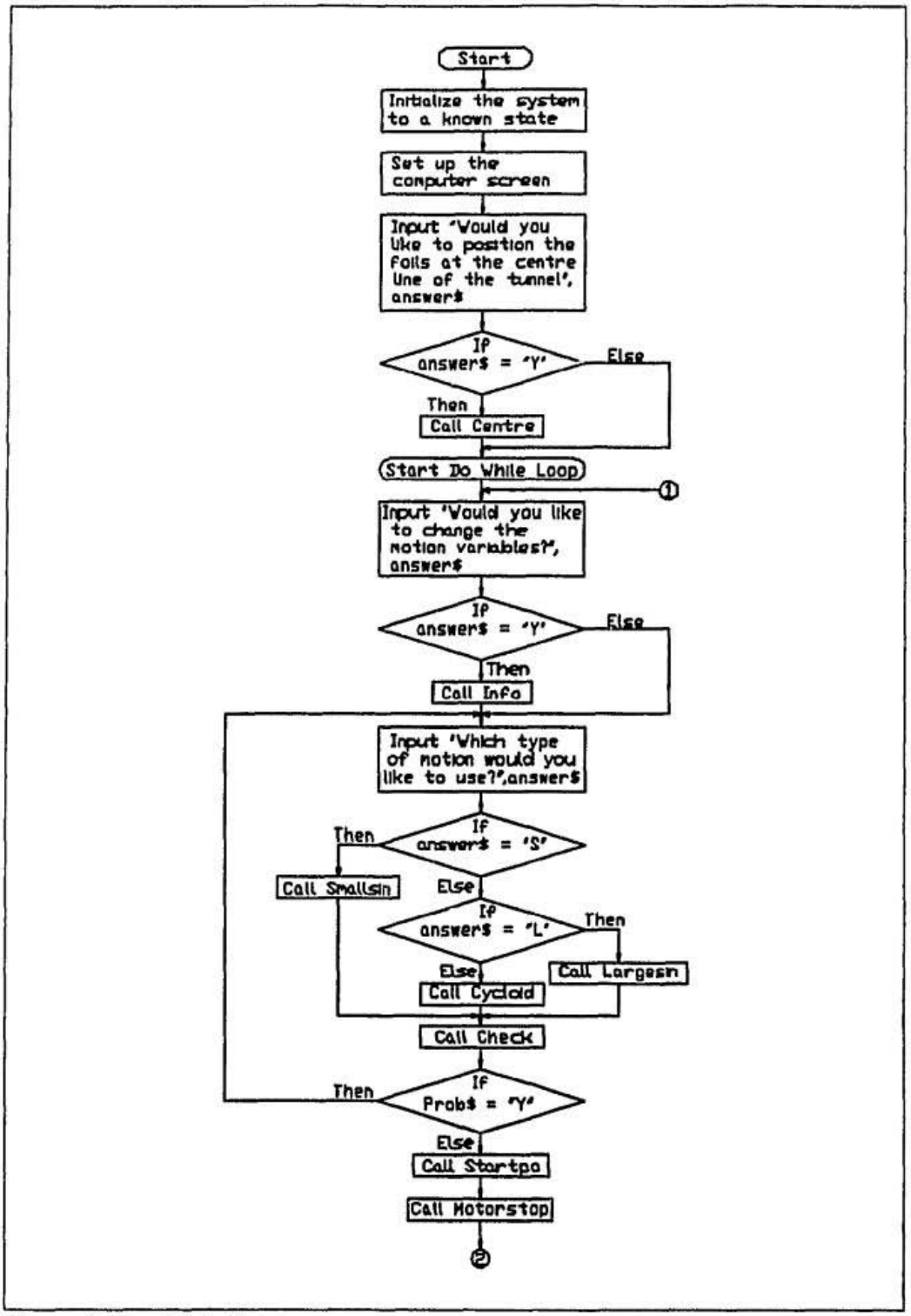

Figure 4.7a Main Program

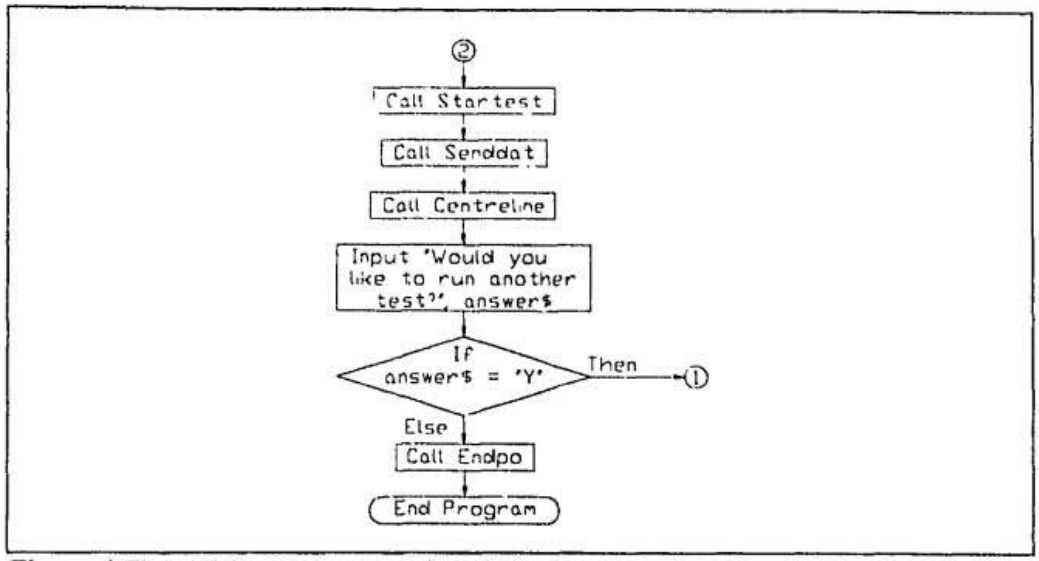

Figure 4.7b Main Program continued

The second operation in the control loop involves the selection of the desired type of motion. Currently there is only one motion available, a small amplitude sine wave, but the program was designed so that other motions could be added at a later date: e.g., large amplitude sine, cycloidal, etc. The "If" statement in the flow chart in Figure 4.7a shows how two additional motion subroutines, namely a large amplitude sine wave and a cycloidal wave motion, could be incorporated.

After the type of motion was selected, the main control program switched control to the selected motion subroutine. In this case the subroutine called SMALLSIN was used (See Figure 4.9). This subroutine calculated a series of displacements, velocities, and accelerations to approximate a small pitch amplitude sinusoidal motion based on Equations 4.12, 4.13, 4.17, and 4.18. Before these calculations could be performed, the subroutine calculated the phase angle required between the displacements of the two drive

shafts, to produce the requested motion. This was done since the phase difference was produced by adding the phase, in seconds, to the time value fed into Equation 4.12. Thus, the phase had to be a multiple of the time required per segment. Once this was done the subroutine calculated the minimum number of segments that the motion had to be divided into if an accurate value of phase difference was to be achieved. It then asked the operator to select a number of segments to divide the motion into. This had to be a multiple of two

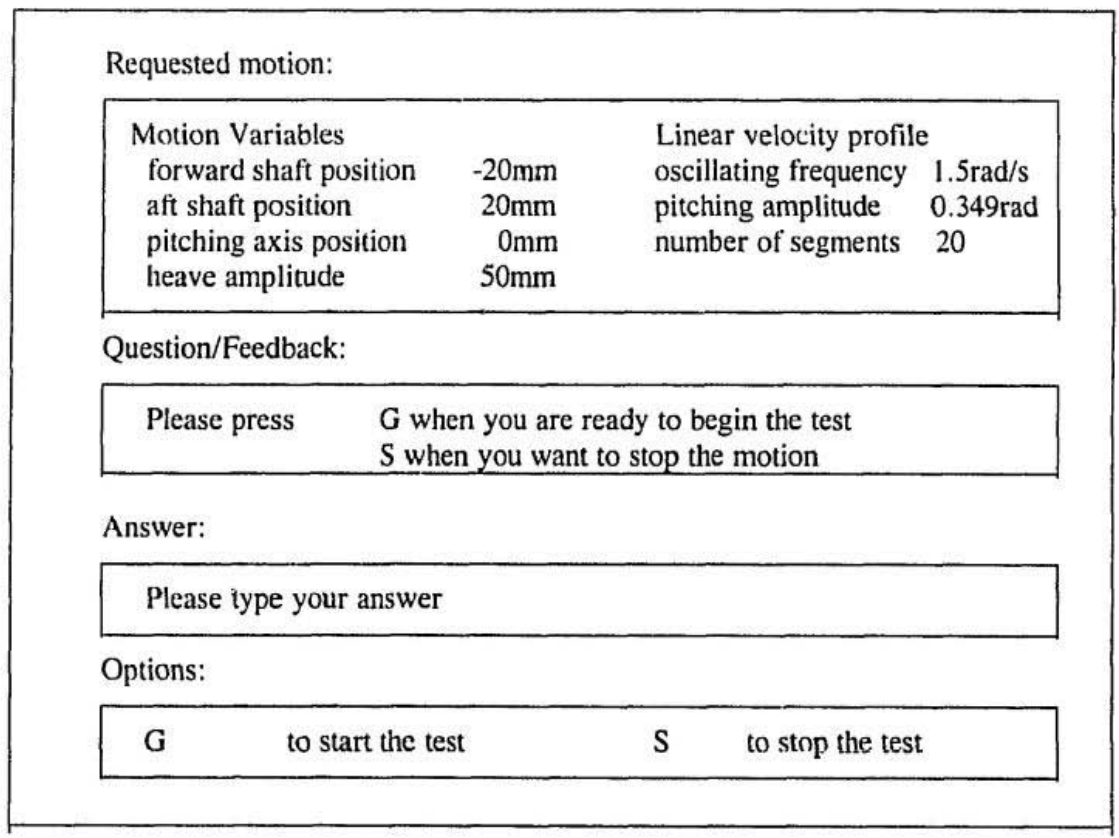

Figure 4.8 Computer screen showing dialogue boxes

multiplied by the minimum number of segments. To ensure that the maximum displacement in the cycle was achieved. See the approximated motion plots for 3 segments in Figure 4.10a and for 6 segments in Figure 4.10b.

Once the number of segments had been selected, the displacements, velocities, and accelerations for each segment were calculated. This information was then stored in a data file for use with other subroutines and control was switched back to the main program: see Table 4.1 which presents a typical motion command data file. The first line in the file gives the number of commands in the file, the second line gives the type of velocity profile to be used by the controller, and the remaining lines are velocity, acceleration, and displacement commands. MA, VC, and AC are the absolute displacement, peak velocity, and peak acceleration commands respectively. Note, the first number following the command defines the command for the forward drive shaft and the second number defines the aft drive shaft. The units for displacement, velocity, and acceleration were given in motor steps, motor steps/second, and motor steps/second/second respectively. There were 20,000 steps in one revolution of the motor shafts.

The next subroutine called by the main program was call CHECK. The purpose of this subroutine was to check the data file containing the motion commands to ensure that none of the moves required a displacement greater than 110mm, a pitch angle of the foils greater than 50 degrees, or extreme velocities and accelerations. This was checked to ensure that the requested motion did not require moves that could damage the dynamometer. If there was a problem with any of the move commands the subroutine

printed a message to the screen indicating how the requested motion exceeded the allowed motions. The subroutine then returned control to the main program. The main program

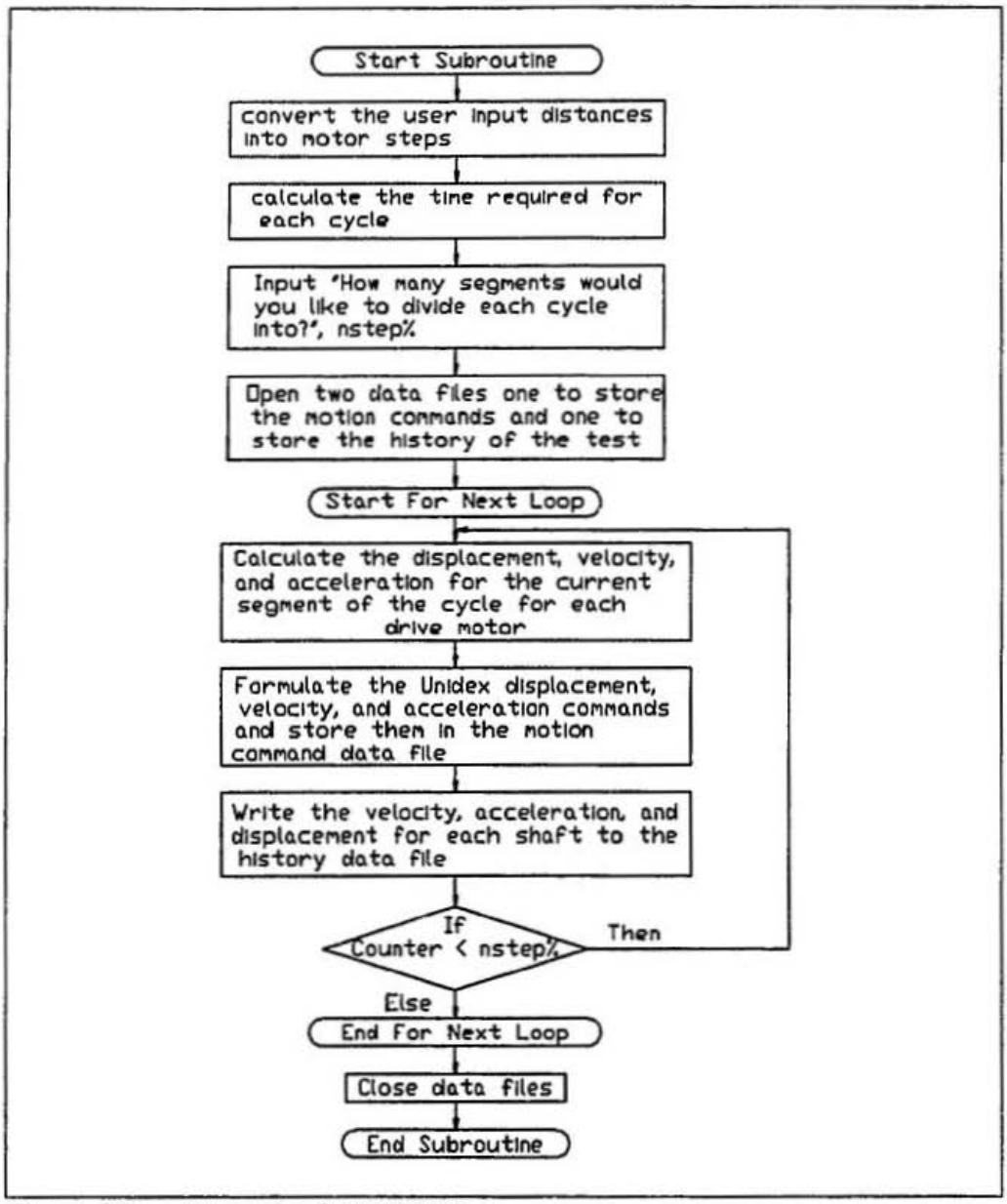

Figure 4.9 Subroutine SMALLSIN

then checked to see if the subroutine CHECK had found any problem with the requested motion. If there was a problem the main program looped back to the subroutine INFO so that a new set of motion variables could be fed into the program. If the subroutine CHECK did not find a problem with the requested motion the main program switched control to a subroutine called STARTPO.

The subroutine STARTPO located the foils at the correct starting position. It did this by opening the data file created by the motion subroutine and getting the first displacement command in the data file. It then sent this command to the Unidex controller for execution. Once the foils had been sent to their starting position, the data file was closed and control was switched back to the main program. The main program then switched control to a subroutine called MOTORSTOP. This subroutine was used to check if the motors were stopped. It did this by executing a control loop which sent a

Table 4.1 Typical motion data file

Line number	Command	Line number	Command
1	26	14	"MA0,0;GO"
2	"linear"	15	"VL7154,7154;"
3	"VL7154,7154;"	16	"AC13664,13664;"
4	"AC13664,13664;"	17	"MA-1873,1873;GO"
5	"MA-10915,10915;GO"	18	"VL17269,17269;"
6	"VL17269,17269;"	19	"AC32981,32981;"
7	"AC32981,32981;"	20	"MA-6394,6394;GO"
8	"MA-6394,6394;GO"	21	"VL17269,17269;"
9	"VL17269,17269;"	22	"AC32981,32981;"
10	"AC32981,32981;"	23	"MA-10915,10915;GO"
11	"MA-1873,1873;GO"	24	"VL7154,7154;"
12	"VL7154,7154;"	25	"AC13664,13664;"
13	"AC13664,13664;"	26	"MA-12788,12788;GO"

command to the controller to return the position of the motors. The subroutine kept checking the position of the motors until the positions for both motors remained constant. It then returned control to the main program.

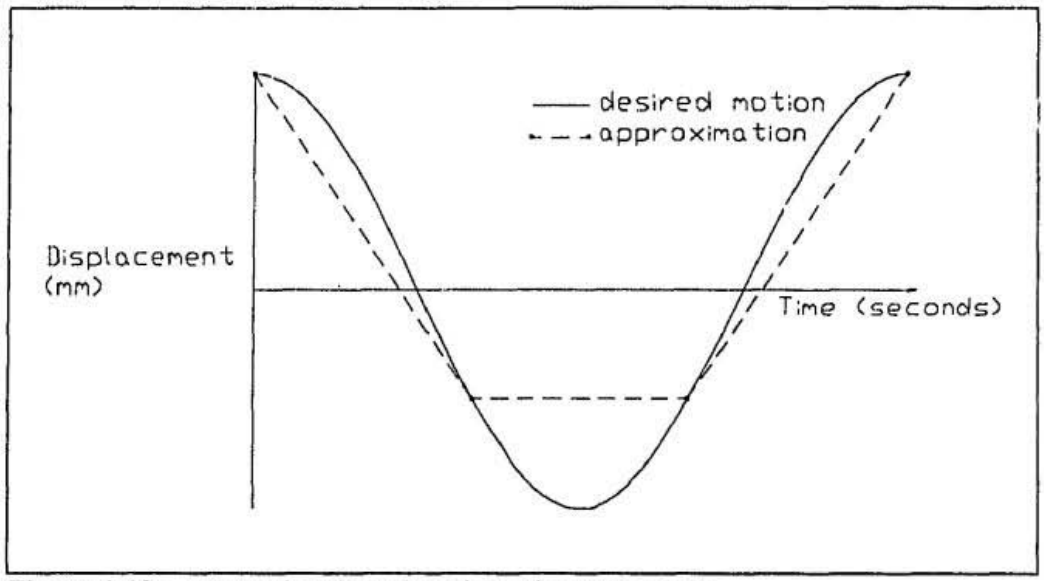

Figure 4.10a Approximation of motion using 3 segments

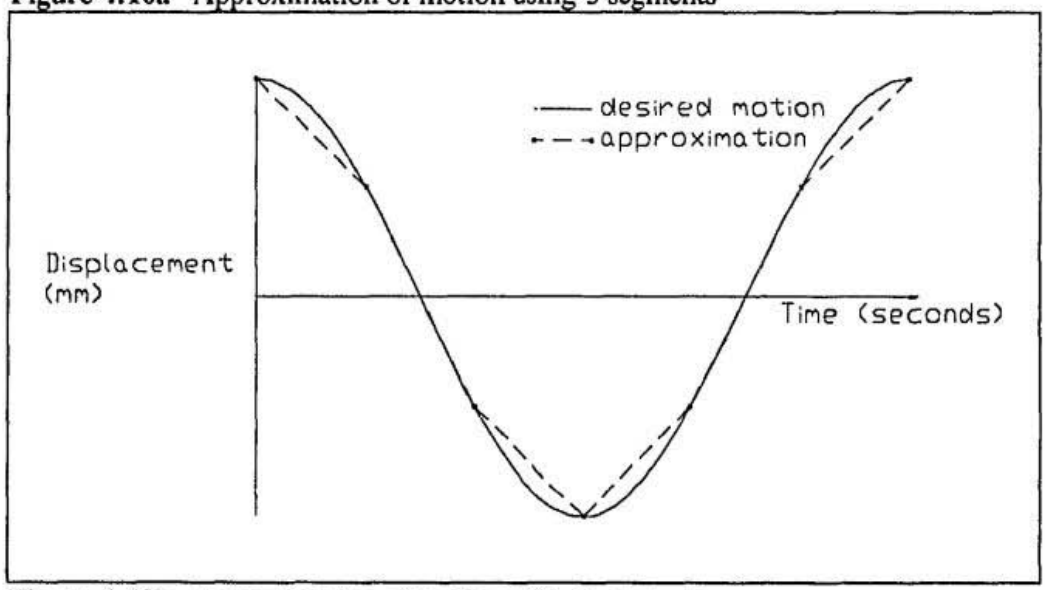

Figure 4.10b Approximation of motion with 6 segments

The main program then switched control to a subroutine called STARTEST which was used to stop the program execution until the operator was ready to start the test. When the operator was ready he/she presses the letter G on the keyboard and the subroutine switched control back to the main program, which immediately switched control to the subroutine SENDDAT (See Figure 4.11).

This subroutine read the motion commands in the data file into an array and then sent these commands to the controller. The subroutine checked to see if there was room for a command in the Unidex's storage buffers before sending each command. Once all the commands were sent, the subroutine checked to see if the operator had requested the motion to stop. If the request to stop the motion had not been made then the subroutine looped back to the first motion command and sent the commands again. It continued to do this until the request to stop the motion had been made. Then it switched execution control back to the main program which switched control to a subroutine CENTRELINE.

The subroutine CENTRELINE returned the foils to the initial position that they were in prior to the execution of the subroutine STARTPO and then switched execution control back to the main program. The operator was then given the option to run another test. If the operator wished to run another test the main program looped back to the beginning of the control loop. Otherwise the program switched execution control to a subroutine called ENDPO which sent the commands to reduce the motor's velocity and acceleration and then moved the drive shafts down to their lower limit switches.

Then control was switched back to the main program and the program executions were completed.

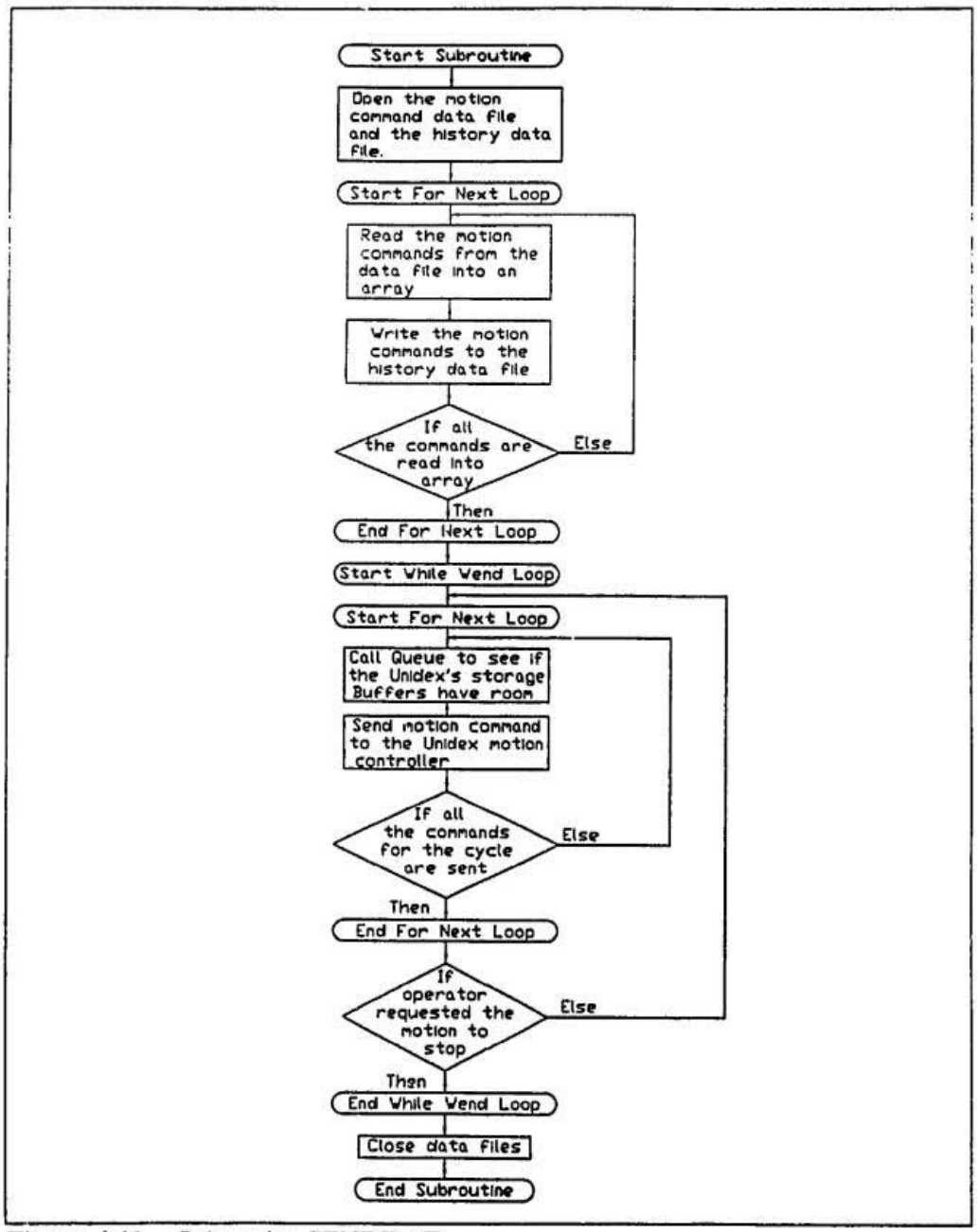

Figure 4.11 Subroutine SENDDAT

Table 4.2 presents a list of all the subroutines and functions that were used in the motion control program. This table also gives a brief description of the purpose of each subroutine and function along with its origin. These functions and subroutines have one of two origins, they were either taken from the Unidex software supplied with the motion control system or they were written by the author for this project. It can be seen from Table 4.2 that most of the subroutines and functions along with the main program were written specifically for this project. Only the subroutines and functions used to send or receive characters from the Unidex motion controller were taken from the supplied software.

Table 4.2 Program subroutines and functions

Subroutine or Function name	Purpose	Origin
MOTION	This was the main program used to control the motion of the dynamometer.	author
CENTRE	This subroutine allowed the dynamometer's operator to interact with the Unidex controller to position and level the foils at the centre line of the cavitation tunnel or some other position.	author
CENTRELINE	This subroutine returned the foils to the centre line of the cavitation tunnel after each test run.	author
CHECK	This subroutine was used to check the commands generated by the motion subroutines to ensure that none of the commands would produce a motion that would exceed the limitations of the dynamometer.	author
CHECKSTATUS	This subroutine was used to check if the Unidex controller was flagging an error.	Unidex software

Table 4.2 Continued

CLEAN1 CLEAN2 CLEAN3 CLEAN4	These four subroutines were used to clear information from the different dialogue boxes.	author
ENDPO	This subroutine was used to reduce the velocity and acceleration of the motors and move the foils down to their lower limits at the end of a testing session	author
EXCEED	This subroutine was used to print an error message indicating how the requested motion exceeded the limits of the dynamometer if the motion exceeded the limits.	author
FILENDING	This subroutine created the file names for the files used to store the motion commands and the motion history.	author
HISTORY	This subroutine was used to create a data file that contained a history of the test run. It wrote the requested parameters and motion command to a data file stored on the computers hard drive.	author
INFO	This subroutine asked the operator of the dynamometer to feed in the following information defining the desired motion: heave and pitch amplitude, position of the two drive shafts and the pitching axis, the oscillating frequency, and number of segments to divide the motion cycle into.	author
INITSYS	This subroutine was used to reset the Unidex motion controller to a known state at the beginning of program.	Unidex software and modified by author
MISTAKE	This subroutine printed an error message to the feedback dialogue box if an invalid response was given by the operator.	author

Table 4.2 Continued

MOTORSTOP	This subroutine was used to check if the motors were stopped. If they were not stopped the subroutine continued to monitor them until they came to a stop.	author
QUEUE	This subroutine was used to check if there was room in the storage buffers, of the two motors, for another command before a command was sent. If there was no room the subroutine would keep monitoring the buffers until there was room.	author
SCR	This subroutine was used to create the dialogue boxes used to display information on the computer screen.	author
SENDDAT	This subroutine was use to send the commands in the motion data file to the Unidex controller for execution.	author
SMALLSIN	This subroutine was used to approximate a small amplitude sinusoidal motion.	author
STARTEST	This subroutine was used to stop the program, immediately before the beginning of the test run, Until the operator was ready to begin.	author
STARTPO	This subroutine was used to position the foils at the correct position for the beginning of a test run.	author
WRITECHR	This subroutine was used to send one character at a time to the Unidex motion controller.	Unidex software
WRITESTRING	This subroutine was used to take a command string and send it one character at a time to the subroutine WRITECHR.	Unidex software
LIMIT$	This function was used to ensure that a command string was limited to the correct number of characters.	Unidex software
READCHR$	This function was used to retrieve information sent back by the Unidex controller one character at a time.	Unidex software

Table 4.2 Continued

READDATA$	This function was used to check if the Unidex controller was sending information back. If so it got one character at a time.	Unidex software
READLF$	This function read data sent back from the Unidex controller until it found a CR LF then it read characters until it reached the end of the string.	Unidex software
REMOTE$	This function switched control from the PC to the remote clock or visa versa depending on the information in the subroutine INITSYS	Unidex software
RESPONSE$	This function took the first character in the response of the operator and capitalized it to reduce the amount of code needed in the decision statements.	author
VALID$	This function was used to determine if the information being sent back from the Unidex controller was a valid character or a space, return, or line fed. If it was not a valid character it was discarded.	Unidex software

Chapter 5

Commissioning of Dynamometer

5.1 Tests in Air without the Mounting Pod and Foils Installed

When the design, fabrication and installation of the dynamometer and the motion control program was completed and checked, the commissioning of the dynamometer was performed. The first part of this process consisted of running the dynamometer in air for a wide range of motion parameters to test the functioning of the motion control system.

During these test runs the motion of the dynamometer was monitored by a pair of LVDTs, one connected to each drive shaft. The first set of tests was aimed at determining if the dynamometer could produce a pure heaving motion and a combined pitching and heaving motion. The strain gauges were mounted on the section in the United Kingdom and did not arrive until the final stages of the commissioning of the dynamometer. Therefore, the strain gauged section was not tested in air. It was also decided not to mount the load cells during this phase of the testing to reduce wear on them.

It was found that the dynamometer was capable of producing a pure heaving motion with a maximum heave amplitude of 110mm and a pitching and heaving motion with a maximum pitch angle amplitude of 23°, where the total displacement of either drive shaft did not exceed 110mm. It was not possible to obtain a pure pitching motion since heave equals zero for a pure pitching motion (See Equations 4.15 and 4.16) and

this resulted in a division by zero error in the calculation of the phase angle between the two drive shafts. However, it was possible to approximate a pure pitching motion by setting the value of heave amplitude very close to zero.

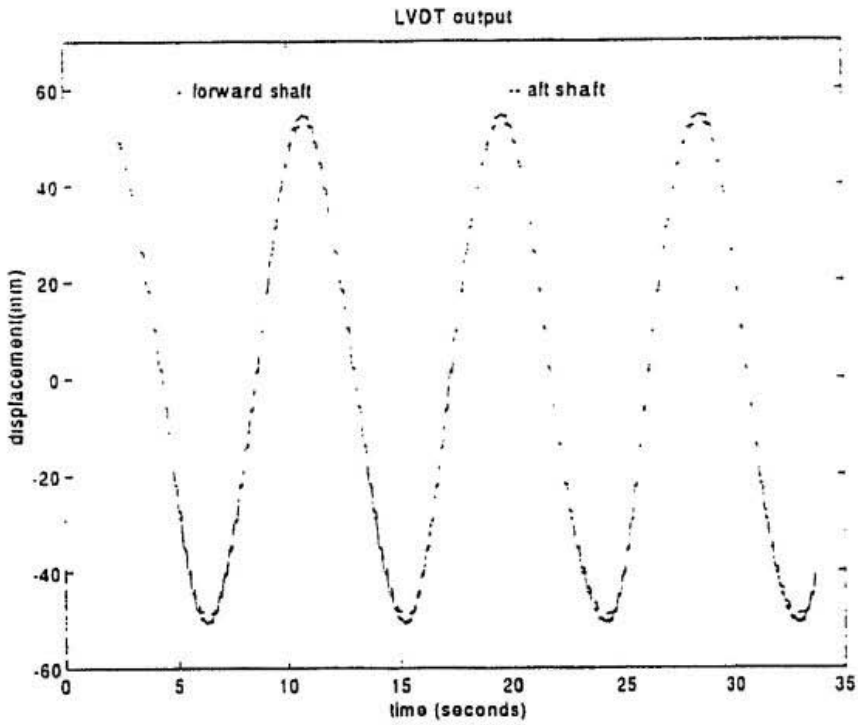

Figure 5.1 LVDT output for a pure heave motion. Note: motion defined by the following parameters: pitching axis located 20mm forward of the aft shaft (x=0), heave amplitude 50mm, pitch angle amplitude 0 degrees, and oscillating frequency 1radians/second.

Figure 5.1 shows the LVDT output for a pure heaving motion while Figure 5.2 shows the LVDT output for a combination of a pitching and heaving motion with a phase difference of 0.3491 radians (0.233 seconds) between the motion of the two drive shafts. Figure 5.3 shows the LVDT output for a motion which approximated a pure pitching motion with an heave amplitude of 1mm and a pitch angle amplitude of 20°.

The 1mm heave is at the pitching axis which is positioned 10mm forward of the forward drive shaft. It may be possible to obtain a pure pitching motion by modifying the motion subroutine SMALLSIN so that if a heave amplitude of zero is requested a set of modified equations, which neglects heave, can be used to calculate the required displacements.

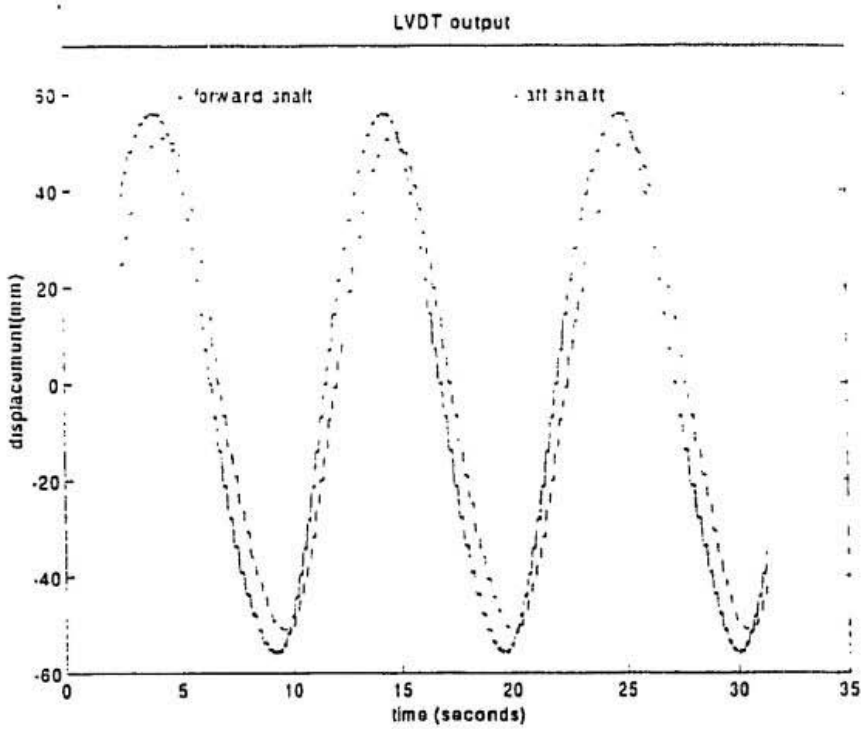

Figure 5.2 LVDT output for a combined heaving and pitching motion. Note: Motion defined by the following parameters: pitching axis located 10mm aft of the aft shaft (x=30), heave amplitude 50mm, pitch angle amplitude 20°, and oscillating frequency 1.5radians/second.

The requested frequencies for the motions shown in Figures 5.1, 5.2, and 5.3 were 0.159Hz (1.0radians/second), 0.239Hz (1.5radians/second) and 0.239Hz (1.5radians/second) respectively while the obtained frequencies were 0.114Hz (0.72radians/second), 0.10Hz (0.63radians/second), and 0.077Hz (0.48 radians/second)

respectively. The reasons for these errors are related to the limitations of the motion controller and will be explained later in this section.

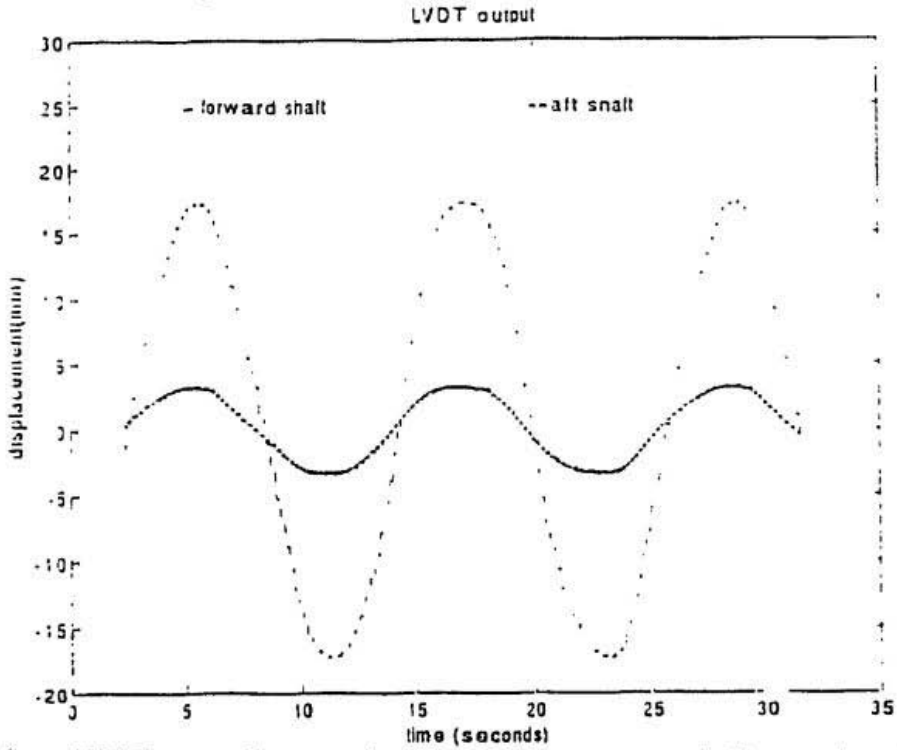

Figure 5.3 LVDT output for a motion approximating a pure pitching motion. Note: Motion defined by the following parameters: pitching axis located 10mm forward of the forward shaft (x=-30), heave amplitude 1mm, pitch angle amplitude 20°, and oscillating frequency 1.5radians/second.

The next set of tests performed was aimed at ensuring that the oscillating frequency and phase angle between the two drive shafts remained constant for every cycle of the motion over the entire test. Tests were run for a wide range of motion parameters and some tests were repeated. They all showed that the oscillating frequency and phase angle between the two drive shafts stayed constant for a given test and that the test results were repeatable.

The third set of tests was aimed at determining the accuracy of the approximated motions. Figure 5.4 presents the LVDT output for the forward shaft for a set of test run with the same motion parameters except that the number of segments which each motion cycle was divided into was changed. It was found that as the number of segments in the cycle increased, the motion became smoother and closer to that of a sinusoidal wave motion. However, as the number of segments increased the obtained oscillating frequencies decreased below that requested for the motion. This was due to a finite time lag occurring between commands for each segment. The larger the number of segments, the larger the number of these delays in a cycle. The effects of these delays can also be seen from the obtained frequencies for the motions plotted in Figures 5.1, 5.2, and 5.3.

Since the errors in the obtained frequencies are a direct function of the number of segments which the motion is divided into it is possible to calibrate the system so that a frequency higher than the desired frequency can be requested in order to obtain the desired frequency. Also a control feedback loop could be programmed to analysis the motion after the first few cycles and inform the operator if the obtained frequency is close enough to the desired frequency. The control loop could allow the operator to define an exceptable frequency tolerance.

The effect of the number of segments which a cycle is divided into can be seen from the desired motion plotted alongside the obtained motions in Figure 5.4. The percent error in the obtained frequencies for the motions plotted in Figure 5.4 were:

3.6%, 4.9%, 36.9%, and 52.5% for 6, 20, 30, and 40 segments per cycle respectively. These errors were calculated by fitting a sinusoidal function, of the form given in Equation 4.1, to the output from the LVDT to determine the obtained frequencies. The percent error was taken as the difference between the requested and obtained frequencies taken as a percentage of the requested frequencies.

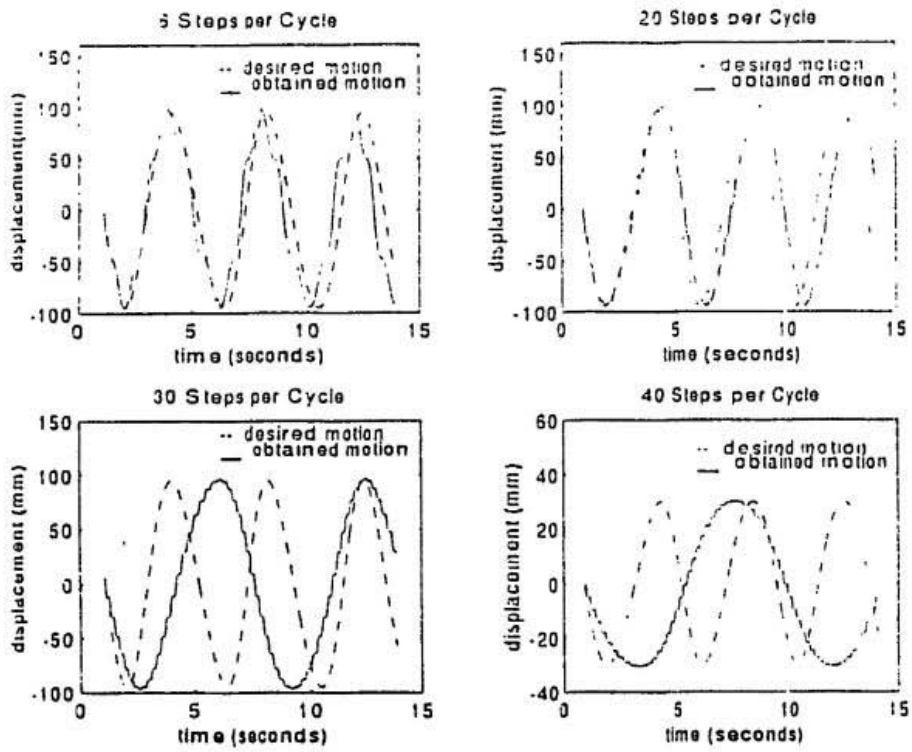

Figure 5.4 Obtained motions compared to the requested motions. Note: All motions were defined by a pitching axis located 20mm forward of the aft shaft (x=0), heave amplitude 95mm (except the motion divided into 40 segments which had a heave amplitude of 30mm), pitch angle amplitude 0°, and oscillating frequency 0.24Hz (1.5radians/second).

The accuracy of both the magnitude of heave and the frequency of the motion had to be evaluated. Therefore, these obtained motions are re-plotted in Figure 5.5 along with plots of the desired motions corrected for the obtained frequencies. From this figure it can be seen that if the obtained frequencies are used in the calculation of the desired motion, the errors in the approximations of heave amplitude due to approximating a curve with a series of linear functions are very small for motions divided into more than 20 segments per cycle. The root mean squared error for the motions plotted are: 9 (9.5%), 3.5 (3.6%), 2.8 (2.9%), and 0.7 (2.3%) for 6, 20, 30, and 40 segments per cycle respectively. The terms in the brackets are the percent errors based on dividing the root mean errors by the maximum displacement. These calculations were based on data collected at a sampling rate of 45 samples/second. The calculated errors will vary slightly for different data sampling rates for a given requested motion.

The fourth set of tests was done to further determine the effect of the number of segments in each motion cycle on the obtained oscillating frequency. It can be seen from Figure 5.6, that as the requested oscillating frequency increased the effect of increasing the number of segments in each cycle resulted in the obtained frequency dropping off at a faster rate. This is believed to be caused by the increased accelerations required to obtain higher frequencies and the time delays between each segment. It is

believed that the accelerations developed by the motors may be slightly lower than those requested. This effect would be larger for the higher frequencies.

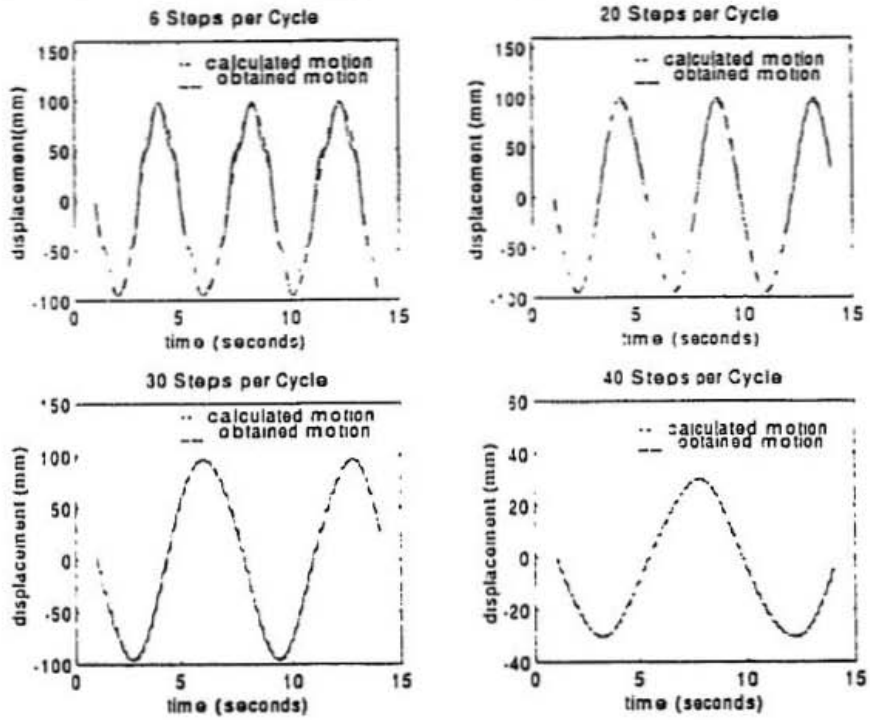

Figure 5.5 Obtained motions compared to the desired motions calculated for the obtained frequency. Note: All motions were defined by a pitching axis located 20mm forward of the aft shaft (x=0), heave amplitude 95mm (except the motion divided into 40 segments which had a heave amplitude of 30mm), pitch angle amplitude 0°, and oscillating frequency 0.24Hz (1.5radians/second).

The final set of tests in this series was aimed at determining the upper limits of the oscillating frequencies which could be requested without the motion becoming too uneven or rough, due to excessive accelerations. Figure 5.7 presents plots which define the upper limits for the number of segments that the motion cycle can be divided into, for a particular requested heave amplitude and oscillating frequency, if the motion is not to be uneven or rough. The second plot in Figure 5.7 defines the limits where the

motion is beginning to become rough while the first plot defines when the motion becomes so rough that it vibrates the dynamometer. Heave amplitude also affected the roughness of the motion, since larger heave amplitudes resulted in higher accelerations for a given oscillation frequency.

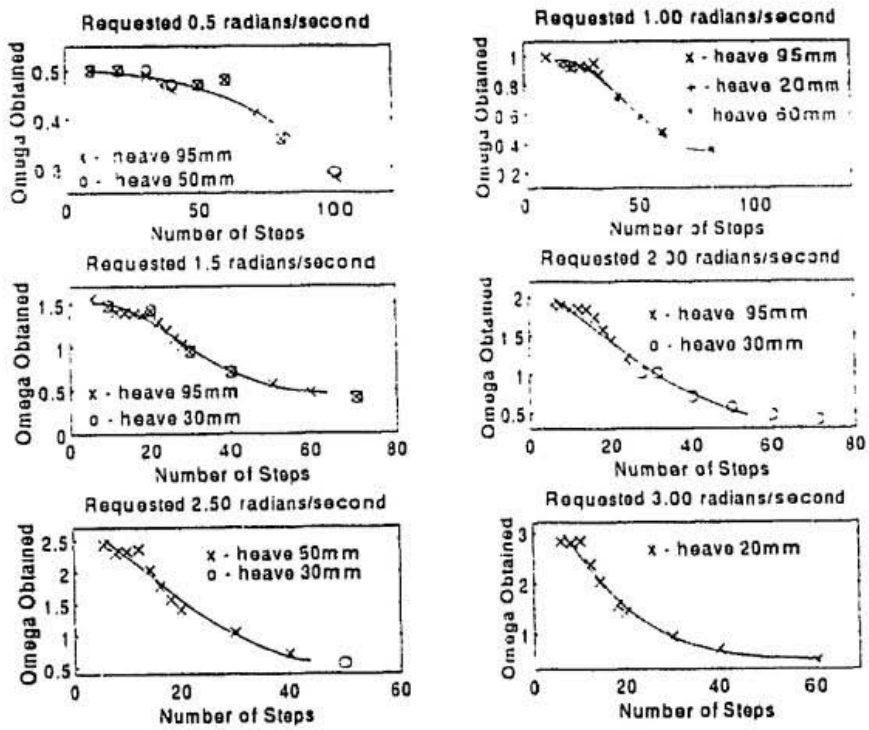

Figure 5.6 Plot of the obtained frequency against the number of segments in the cycle for different oscillating frequencies.

The plots in Figure 5.7 can be used as a guide in selecting the maximum number of segments to divide a motion cycle into. For example, if a heave amplitude of 50mm and an oscillating frequency of 0.32Hz (2 radians/second) is requested then, according to the second plot in Figure 5.7, the number of segments that the motion should be divided into should be less than 45, to ensure that the motion is even and smooth.

According to the first plot if the motion is not to be excessively uneven or rough then the number of segments requested should be less than 61.

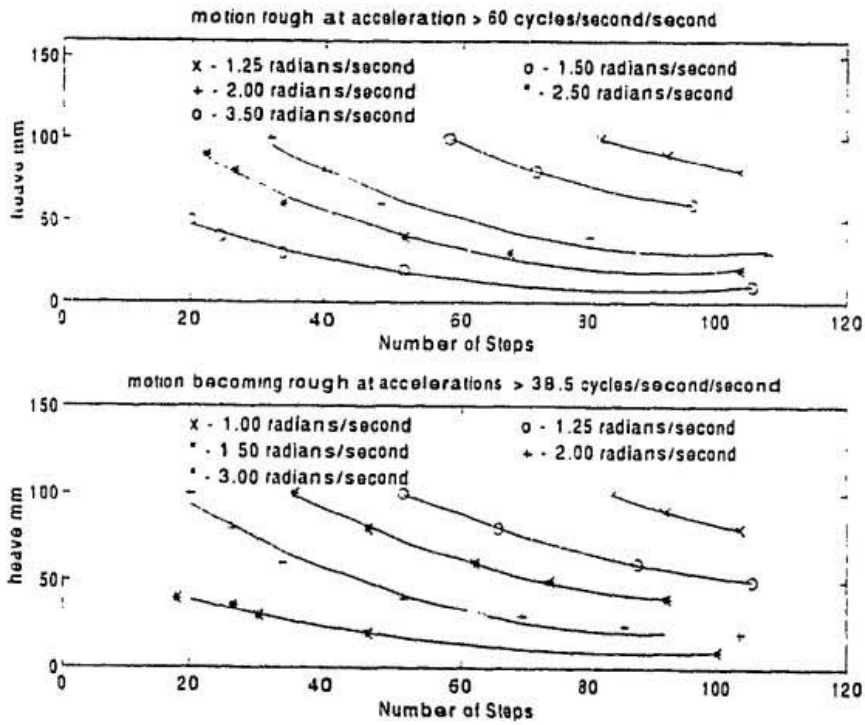

Figure 5.7 Plot of heave amplitude against the number of segments in a cycle defining the roughness limits.

To develop the plots presented in Figure 5.7 tests were run for ten different heave amplitudes ranging from 10mm to 100mm for increasing oscillating frequencies until the motion was judged to be too uneven or rough. This judgement was based on the plots of the output from the LVDTs. After these tests were completed the data files containing the motion commands for the motions, which were deemed to be becoming

uneven or rough and those that were excessively uneven or rough, were analysed to determine the maximum accelerations required for those motions. The average maximum accelerations for the two conditions were calculated to be 38.5 cycles per second squared for the motion becoming uneven and 60 cycles per second squared for the motion becoming excessively uneven.

These accelerations were then used along with the motion equations to calculate the maximum number of segments which a given motion cycle could be divided into without the motion starting to become uneven and the motion being excessively uneven, for different heave amplitudes and oscillating frequencies. These calculated results were used to produce the plots in Figure 5.7.

5.2 Calibration of Dynamometer's Instrumentation System

As mentioned in Chapter 3 the dynamometer's data acquisition system was made up of a full Wheatstone bridge strain gauged section, two miniature load cells, and two LVDTs. The strain gauged section was designed as part of this project while the load cells and LVDTs were off the shelf. The calibration of the instruments was done using a Keithley S570 data acquisition system and software.

The LVDTs were excited by twelve volts direct current during calibration and testing. Seventeen sample points with 480 samples per point and a sampling rate of 45 samples per second were used. The points ranged from a positive displacement of

120mm to a negative displacement of -120mm. Typical slopes, offsets, and Rsquared value for the calibration of the two LVDTs are given below.

Table 5.1 Forward drive shaft LVDT calibration

slope	0.1049023
offset	-228.486527
Rsquared value	0.9999750

Table 5.2 Aft drive shaft LVDT calibration

slope	0.0733322
offset	-166.3131066
Rsquared value	0.9999820

The Rsquared values, are a measure of the accuracy of the fit of a linear equation to the data points obtained during the calibrations. An Rsquared value of one indicates a perfect fit. As can be seen the calibrations for the LVDTs are good and show that the LVDTs are linear.

The load cells were powered by five volts direct current and amplified with a gain of 400. The calibration was done using twenty five sample points with 1000 samples per point and a sampling rate of 45 samples per second. The points ranged from a tensile force of 34.9 N to a compressive force of 34.9 N. Typical slopes, offsets, and Rsquared value for the calibration of the two load cells are given below.

Table 5.3 Forward drive shaft load cell calibration

slope	0.042407
offset	-86.7822649
Rsquared value	0.9996583

Table 5.4 Aft drive shaft load cell calibration

slope	0.0418954
offset	-85.8653840
Rsquared value	0.9990014

The strain gauged section was excited by five volts direct current and amplified with a gain of 500. The calibration was done using thirty sample points with 1000 samples per point and a sampling rate of 45 samples per second. The points ranged from a positive force of 50.0 N (positive thrust forward) to a negative force of 50.0 N. Typical slopes, offsets, and Rsquared values for the calibration of the strain gauged section is given below.

Table 5.5 Aft drive shaft strain gauge calibration

slope	0.0346949
offset	-70.8067863
Rsquared value	09990152

The Rsquared values for the load cells and stain gauged section were a little low (a minimum value of 0.9999 is preferred). This may have been a result of slight inaccuracies in the calibration weights which were used for the calibrations. However, it was decided that these calibrations were ok for the initial testing of the dynamometer. These instruments must be re-calibrated before any foil performance tests are conducted. When the instruments are re-calibrated the load cells and strain gauged section should be calibrated for a range of forces up to 50N and 70N respectively.

5.3 Test in a Fully Operational State

After the initial tests on the motion control system of the dynamometer were completed, the dynamometer was installed at the cavitation tunnel, the LVDTs were re-calibrated and the load cells and strain gauged section were calibrated in place. Once

this was completed the last stage in the commissioning of the dynamometer was carried out. This involved running a set of tests with the dynamometer in the completely operational state (note the strain gauged section did not arrive from England until the last stage of the commissioning tests). These tests were aimed at determining the quality of the data obtained from the data acquisition system and not as a complete study of the foils used.

The only problem resulting from the installation of the dynamometer was a small air leak in through the insulation on the cable of the strain gauged section, when a vacuum was drawn on the tunnel. This was not considered serious since it could be easily sealed with silicon rubber or similar sealant.

The first set of tests involved running a series of tests to ensure that the dynamometer could produce the same range of motion which it had produced when tested in air. It was found that the dynamometer was still capable of the same range of motions and that the water in the tunnel had a small damping effect on the roughness of the motion when operated at the upper limits of the oscillating frequency. During these tests the drive pulleys mounted on the aft drive shaft motor kept working loose after about 30 minutes of testing.

The next set of tests involved running a series of tests with different tunnel water speeds for a motion with a heave amplitude of 50mm, pitching axis location 19.5mm forward of the aft drive shaft, a pitch amplitude of 20°, and a requested oscillating frequency of 1.5 radians per second. These tests were aimed at determining

the quality of the data obtained from the load cells and the strain gauged section. Figure 5.8 shows typical output from the load cells inserted in the forward and aft drive shafts. It can be seen from these plots that every time the drive shafts change direction, at the upper and lower limits of the motion, there is a large jump in the measured forces compared to the forces measured while the shafts are moving between these points. These jumps were a result of the high static frictional forces in the seals around the two drive shafts and inertia forces resulting from the maximum accelerations at the reversal points of the motion. The dynamometer will have to be calibrated so that the effects of the inertia forces can be subtracted from the output from the load cells and the shaft seals and bushings will have to be replaced by a set of linear bearing and the propulsion test conducted in the wave tank. Also, the A/D range for the load cells were exceeded during part of the data acquisition time. This resulted in the loss of some of the data peaks. This could have been corrected by changing the gain on the amplifier, however it was not deemed to be necessary since the high frictional forces in the seals and bushing around the drive shaft and the inertia forces caused this problem and made it impossible to obtain reliable data from the load cells. For accurate tests for propulsive efficiency, this indicates that it is likely that better results would be obtained by removing the shaft seals and testing in the towing tank.

Figure 5.9 presents a typical plot of the output from the strain gauged section. The plot of thrust in Figure 5.9 has a high noise to signal ratio despite the shielding of the entire data acquisition system from electronic and magnetic noise. This is believed

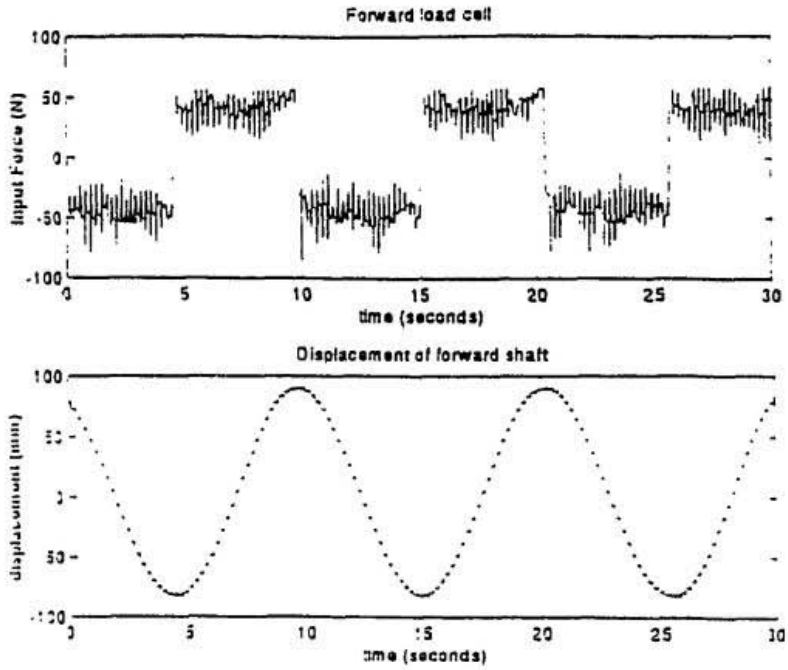

Figure 5.8 Typical output from the load cells

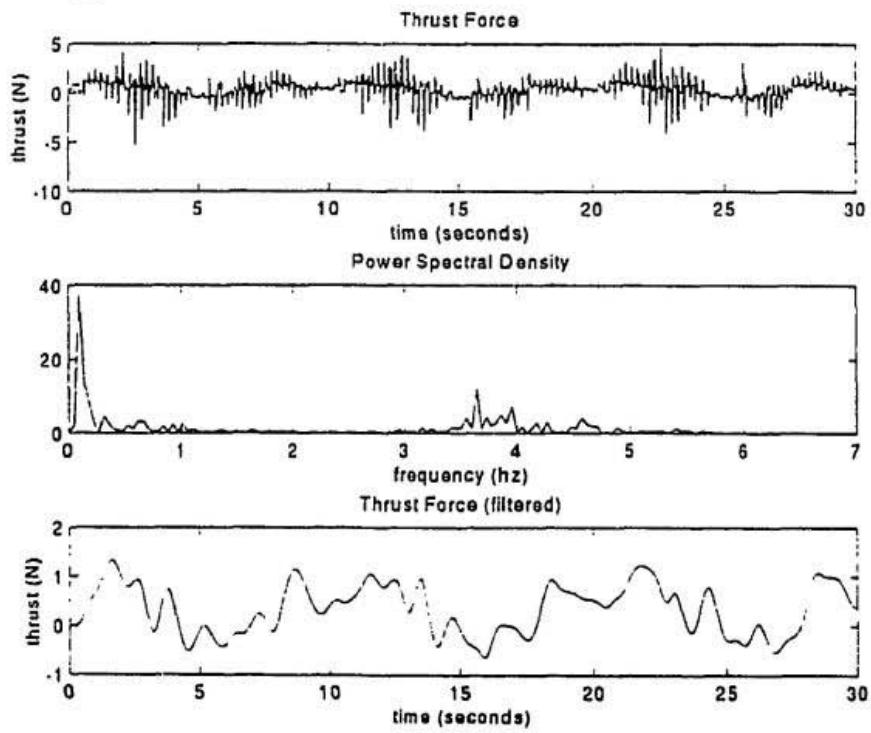

Figure 5.9 Typical output from strain gauged section

to be due to mechanical noise. As can be seen from the LVDT output plotted in Figure 5.10, the mechanical noise present in the motion is due to the motors starting and stopping at the ends of each segment of the motion cycle.

From the plot of the power spectrum density in Figure 5.10 it can be seen that the vibrations caused by the starting and stopping of the motors occurred at a frequency of around 4Hz to 5Hz. The plot of the power spectrum for the thrust signal shows substantial (compared to that at the oscillating frequency of 0.1Hz) energy in the signal between 3.5Hz to 5Hz. The energy in the thrust signal between 3.5Hz and 5Hz was thought to have resulted from the vibration in the oscillating motion. Therefore, both the signals from the strain gauged section and the LVDT were filtered using a 5th order Butterworth low pass filter to eliminate all frequencies above 1Hz (which is ten times the oscillating frequency of the motion). The filtered signals from the strain gauged section and the LVDT are presented in Figures 5.9 and 5.10 respectively.

It can be seen that the vibrational noise has been removed from the signals. However, it is not possible to make any conclusion on the operation of the strain gauged section. Figure 5.11 presents a plot of the transfer function for the oscillating motion to the thrust signal. It can be seen from this plot that there is very little energy transferred from the input oscillating motion to the output thrust at 0.1Hz but there is considerable energy transferred from the vibrations at frequencies above 2.8Hz. This indicates that the vibrations caused a force on the aft shaft which is not related to thrust

generated by the foils. Therefore, before the operation of the strain gauged section can be evaluated the vibrational problem with the motion must be solved.

Figure 5.12 shows a plot of developed thrust against water speed which was produced using the output from the strain gauged section. This plot shows the thrust dropping off as the water speed increases. A similar trend for the thrust developed by an oscillating foil was observed by Hoppe (1989). This indicates that the strain gauged section may be functioning properly.

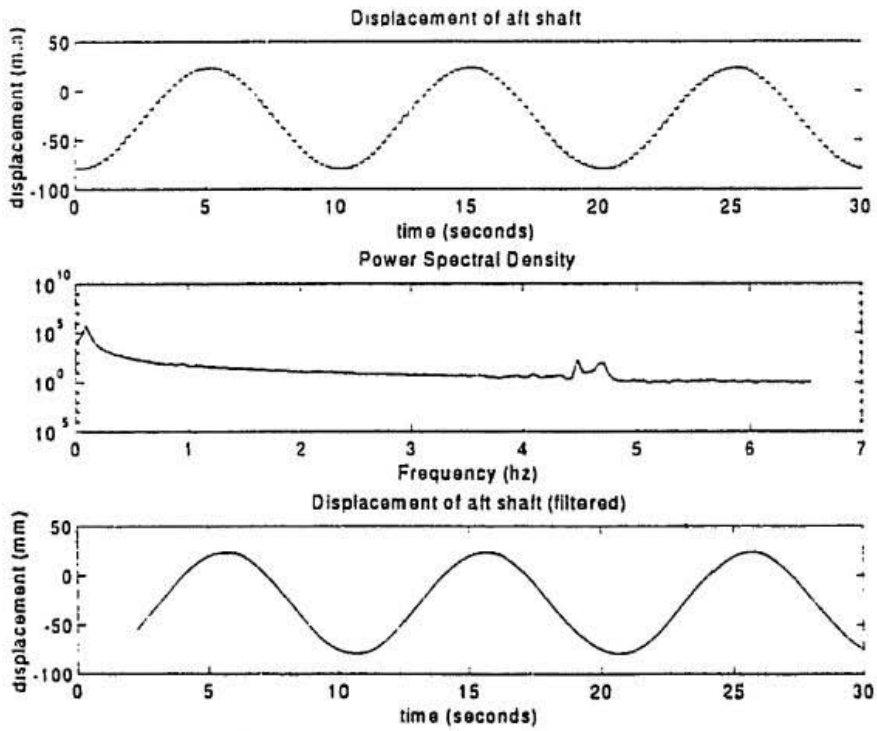

Figure 5.10 Typical output from the aft LVDT

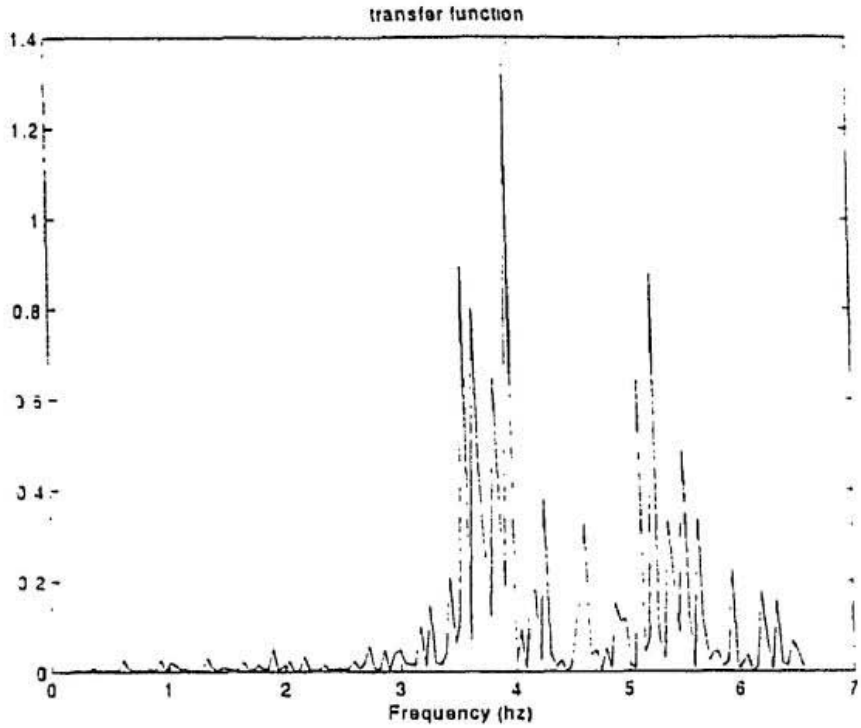

Figure 5.11 Energy transfer function between the input oscillating motion and the output thrust

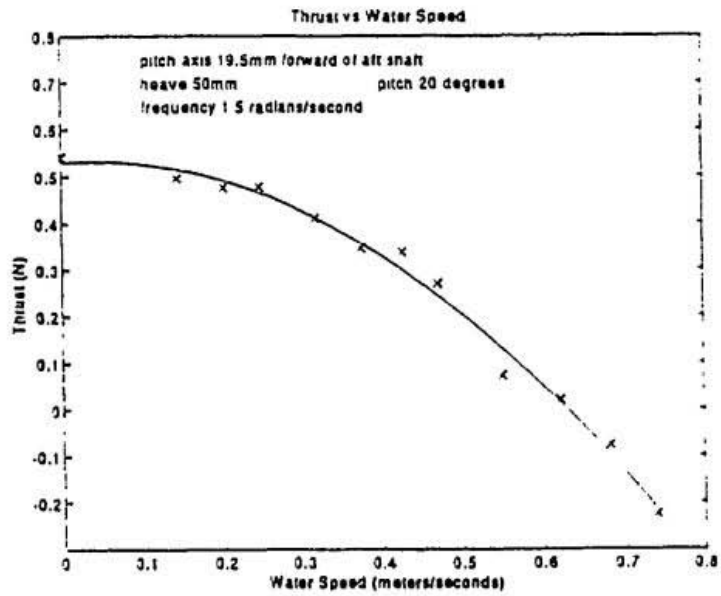

Figure 5.12 Thrust against tunnel water speed

Chapter 6

Conclusions

The main objective of this project was the development of a dynamometer to be used in the study of the propulsion and flow characteristics of oscillating foils. This involved the complete mechanical design of an oscillation foil dynamometer and overseeing its manufacture; the design of the data acquisition system and its installation; the programming of two D-C servo motors to produce the foils oscillating motion; the commissioning of the entire system; and the presentation of recommendations on how to improve the performance of the system.

The installation of a load cell in each of the two drive shafts provided a means of determining the power absorbed by the foils being tested (when used in conjunction with the velocity record), while the insertion of a strain gauged section in the aft drive shaft, allowed the measurement of the thrust/drag developed by the foils. The entire data acquisition system was completely shielded from all sources of electronic and magnetic fields to minimise the electronic noise in the obtained signals. Also, the drive shafts and strain gauged section were designed so that their natural frequencies were outside the operational oscillating frequencies of the dynamometer. The operational frequencies of the dynamometer were between 0 and 1.0Hz (0 and 6.28radians/second) while the natural frequencies of the drive shafts were between 2.37 and 9.58Hz (14.9 and 60.20radians/second) and 78.1Hz (491radians/second) for the strain gauged section about an axis perpendicular to the direction of the water flow.

This data acquisition system will allow the propulsion efficiency of the foils being tested to be determined once the dynamic, inertia, and frictional forces are calibrated or eliminated. The inclusion of a pair of LVDTs into the data acquisition system, to monitor the motion of the foils, allowed the study of the propulsion performance of different oscillating motions for a given foil geometry.

Mounting the foils in a streamlined central pod, fairing the lower drive shafts and encasing the upper portion of the drive shafts, which operated inside the tunnel, in a fairing ens.red that the flow disturbances around the foils were kept to a minimum. Also the total width of the foils and pod was 222mm while the maximum heave amplitude was 110mm to ensure that the foils were not operated in the boundary layer along the tunnel walls. Thus, this system can be used to study the flow characteristics around oscillating foils for varied foil geometry's, oscillating motions, and speeds of advance.

The insertion of the pivot and link in the forward drive shaft and pins connecting the drive shafts to the mounting pod allowed the drive shafts to be oscillated out of phase with each other. This allowed the foil's pitching axis to be moved along the nose tail chord line of the foils and made it possible to oscillate the foils with a heaving, pitching, or a combination pitching and heaving motion. It was found that the dynamometer could produce a pure heaving motion with a maximum heave amplitude of 110mm and a combined heaving and pitching motion with a maximum pitch angle amplitude of 23°, where the maximum displacement of either drive shaft did not exceed

110mm. The system was not capable of a pure pitching motion. However, by requesting a very small heave amplitude (less than 1mm) a good approximation of a pure pitching motion could be achieved. It may be possible to rectify this problem by modifying the motion subroutine SMALLSIN so that if a heave amplitude of zero is requested a set of modified equations can be used to calculate the required displacements.

The control system was capable of producing a good approximation of the desired motion utilising the available Unidex motion controller commands. If the number of segments which the motion cycle was divided into was chosen correctly the root mean squares error in the obtained motion (for the summation of the variations of the obtained amplitudes from the desired amplitudes over an entire cycle) could be as low as 2.3% of the requested amplitude while the percent error in the obtained oscillating frequency could be as low as 3.6%.

Care had to be taken, when selecting the number of segments per cycle to divide the motion into in order to get a smooth approximation of the desired motion. Too few segments resulted in a poor approximation while too many segments resulted in oscillating frequencies below those requested and in some cases an irregular motion due to excessive accelerations. Accelerations in excess of 38.5 cycles/second/second caused the motion to become irregular while accelerations above 60 cycles/second/second resulted in a fully irregular motion.

The motion control program was capable of allowing the pitching axis of the foils to be moved along the nose tail chord line of the foils. However, the pitching axis could not be moved continuously, since some locations resulted in phase angles between pitch and heave which were very small. Since the phase angles were produced by adding the phase, in seconds, to the time value fed into Equation 4.12 and 4.13 the time per segment had to be less than the phase difference between the two drive shaft. For some pitching axis locations this required the motion to be divided into too many segments.

If more subroutines can be acquired from the manufacturer of the motion controller it may be possible to modify the motion control program so that it produces a motion in which the pitching axis can be moved continuously. Additional subroutines may also allow the production of motions which do not require the motors to stop at the end of each segment. This would allow the obtained frequencies and amplitudes to be closer to the desired motion and may eliminate the noise from the output signals.

Overall the dynamometer was capable of fulfilling the goals of the project. The system was capable of producing an infinite range of oscillating motions for the foils, allowed the measurement of the developed thrust from the foils and the power supplied to oscillate them, and provided a means of studying the flow characteristics around oscillating foils. However, some modifications to the system are required to improve its performance.

The frictional resistance of the seals around the drive shafts was too great to allow accurate data to be obtained from the load cells. Therefore, these seals should be removed during the propulsion performance tests and the tests carried out at the towing tank.

The data from the strain gauged section had a high noise to signal ratio as can be seen from Figure 5.9. This was caused by mechanical noise resulting from the motors starting and stopping at the ends of each segment of the motion. In order to achieve accurate data this source of noise will have to be eliminated or reduced. This problem will be addressed again in the recommendations chapter (Chapter 7).

Chapter 7

Recommendations

The dynamometer is capable of fulfilling its intended purposes. However, there are some modifications which can be carried out on the design of the dynamometer and the motion control program which could improve the dynamometer's performance. These are listed below in the order of their importance.

1) The drive shaft seals should be removed and the propulsion efficiency tests should be carried out in the towing tank. The cavitation tunnel should be used to study the flow around the foils and the cavitation and stall characteristics of different foils and foil motions. Removing these seals will reduce frictional forces being picked up by the load cells and a more accurate measurement of the oscillating force transmitted to the foils will be possible. To run the test in the towing tank one of two things may be done. 1) The seals could be removed from their housings. This will destroy them but they are relatively inexpensive. 2) The window port can be removed from the bottom of the mounting bracket and a new base attached with a new set of teflon bushings/linear bearing to align the drive shafts.

2) The mechanical noise in the oscillating motions must be eliminated or reduced. Check with AeroTech the manufacturers of the motors and controller to see if the motion equation can be directly programmed into the motion controller in a similar manner as the cosine velocity profile command which is incorporated

into their list of commands. It has not been possible so far to build up a completely smooth oscillating motion from the available commands. A set of commands based on new subroutines from the manufacturer of the controller should allow the motions to be built up without the motors stopping during the motion (except at the reversal points). This would eliminate most of the vibrational problems and allow a more accurate approximation to the desired motion and eliminate the noise from the data signals.

3) The source of the noise in the strain gauge signal must be determined and eliminated. A set of test runs should be conducted for a range of operating conditions and a power spectrum density analysis carried out to verify that the starting and stopping of the motors is the cause of the noise. As a further check, sample signals from the strain gauged section should be collected for a condition where the system is in the fully operational state with the motors powered down and the lower assembly struck to induce vibration. These signals should then be analysed to determine the natural vibrational frequency of the lower assembly of the dynamometer. If the natural vibrational frequency of the lower assembly is the same as the frequencies of the noise in the strain gauge signals, then the natural vibrational frequency of the lower assembly must be increased or decreased. All the dynamometer's components (such as the timing belts and pulleys) should be analysed separately to determine if they give rise to the frequencies of the noise as found from the power spectrum density analysis.

4) The system should be run with the seals and bushings removed and the results compared to test run with the bushing and seals in place to separate the influence of the friction forces from the dynamic forces. Also, the test foils and pod should be replaced with a dummy equivalent mass having a shape which, minimises the hydrodynamic forces and a series of test runs in water made to determine the magnitude of the dynamic and friction loads.

5) The system should have been run dry to eliminate the hydrodynamic forces. This will help in identifying the source of the noise in the strain gauge signals.

6) A set of tests should be conducted periodically to calibrate the frictional forces in the bushings and seals, and the dynamic loads. This can be done by running the dynamometer in a fully operational state, but with the water drain from the cavitation tunnel (or by replacing the foils and pod with a mass which minimises the hydrodynamic forces and then running the tests in water) to separate the hydrodynamic loads from the dynamic loads. A set of tests should also be conducted with the dynamometer in a fully operational state, but without any test foils to calibrate the thrust/drag forces on the lower assembly of the dynamometer.

7) Although the limit switches mounted on the dynamometer ensured that the drive shafts could not have a displacement greater than 110mm it was found that if the motion controller's storage buffers became over loaded the relative displacements between the two drive shafts could be large enough to cause

damage to the dynamometer. Therefore, a feed back mechanism should be developed to restrict the relative displacement between the two drive shaft to eliminate this potential danger.

8) Any new test motion or test conditions should be first run with the pod removed to ensure that if the motion malfunctions the two shafts can move independently of each other and not damage the dynamometer.

9) When a new operator is getting used to using the dynamometer he/she should disconnect the pod and run a number of test conditions to familiarise him/herself with the function of the apparatus without the risk of damaging the dynamometer.

10) If after the mechanical noise in the motion is eliminated, the obtained frequencies are below the requested frequencies, then a calibration of the obtained frequencies should be carried out. This would allow a requested frequency sufficiently above the desired value to be fed into the motion control program to produce the desired frequency.

11) The subroutine SMALLSIN should be modified to allow a pure pitching motion. This may be possible by adding an "if" statement which will detect if a heave amplitude of zero has been requested and then use a different set of equations to calculate the displacements. This set of equations should define the displacements in terms of the pitch amplitude, phase angle between the drive

shafts, location of the drive shafts relative to the mid chord of the foils, and oscillating frequency.

12) New motion subroutines should be programmed to produce a large amplitude sinusoidal motion with variable phase angle between pitch and heave, a cycloidal motion, an elliptical motion, etc.

13) Over time the drive pulleys begin to slip on the motor's drive shafts. To prevent this from happening a keyway should be cut in the pulleys as shown in Figure 7.1.

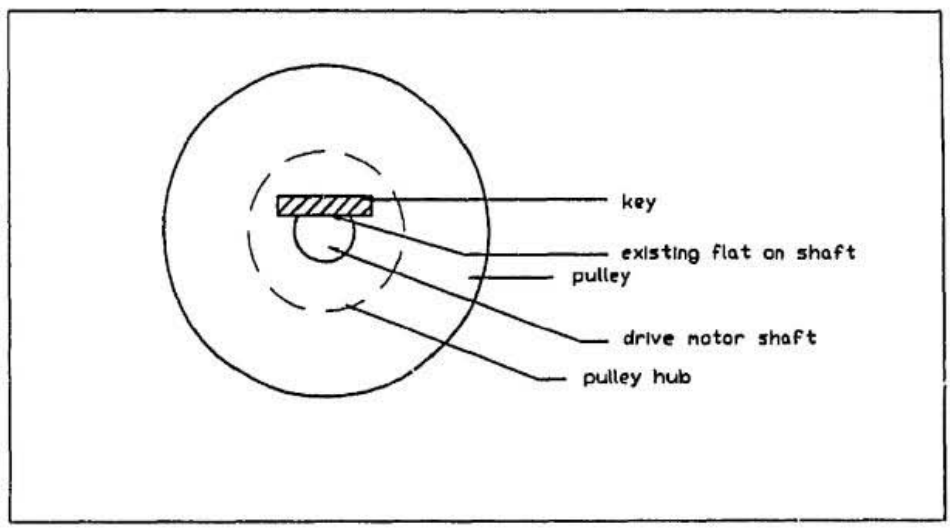

Figure 7.1 Pulley Key

14) Currently the edge of the faired section of the lower forward drive shaft binds up against the edge of the groove in the mounting pod when a pitch angle greater than 23° is requested. To increase the maximum achievable pitch angle

the corners can be machined off the drive shaft or the groove in the mounting pod can be extended.

15) To decrease inertia loading on the motors the drive shafts should be replaced with hollow ground hardened shafts. The pod was made of stainless steel , since it had to be corrosion resistant and tough due to the frequent changing of test foils. Although the original foils were made from brass future foils will be made from lighter materials and some will be flexible. The original foils were made of brass so that they could be used to make molds for the flexible foils and to reduce initial costs.

16) To allow the dynamometer to be aligned along the centre line of the tunnel, it is necessary to grind down the heads of the two bolts at the lower end of the mounting bracket. This will allow the dynamometer to be rotated. Currently the dynamometer is slightly misaligned by approximately 1°.

17) If the drive shafts are replaced with hollow shafts, the lead wires from the strain gauges should be brought up through the inside of the aft drive shaft. This will 1) reduce the amount of drag on the aft drive shaft, 2) reduce the flow disturbances due to the flexing loop of wire coming off the strain gauged section (see Figure 3.6), and 3) reduce the wear on the connection of the lead wires to the strain gauge terminal block since the wires will not be flexing as the drive shaft moves.

18) The load cells used to measure the power transmitted by the shafts to the foils experience a varying force due to the flexing of the cables connecting the load cells to the amplifiers. To reduce the magnitude of this force and to make it a constant offset instead of a varying offset, the cables should be looped back to and clamped to the drive shafts.

19) If the above recommendations do not improve the dynamometer's ability to measure the thrust/drag forces on the test foils then the dynamometer can be loaded onto the tow tank's carriage and the thrust/drag forces measured by independent force transducers. Two possible set-ups for doing this are presented in Figures 7.2 and 7.3. The first method would required the entire dynamometer to be supported by two very thin wide flexible sheets of material in such away that the dynamometer can move easily in the fore and aft direction but be rigid in the lateral direction (see Figure 7.2). The second method would involve mounting the dynamometer on two frictionless tables to allow motions in the fore and aft direction but not in a lateral direction (see Figure 7.3). The thrust/drag forces for both set-ups could be measured by independent force transducers attached to the fore and aft ends of the dynamometer. Note, that conducting propulsion efficiency tests is only one of the functions of the dynamometer. Therefore, any changes to the dynamometer must not limit its abilities to perform the other functions as listed earlier in this thesis.

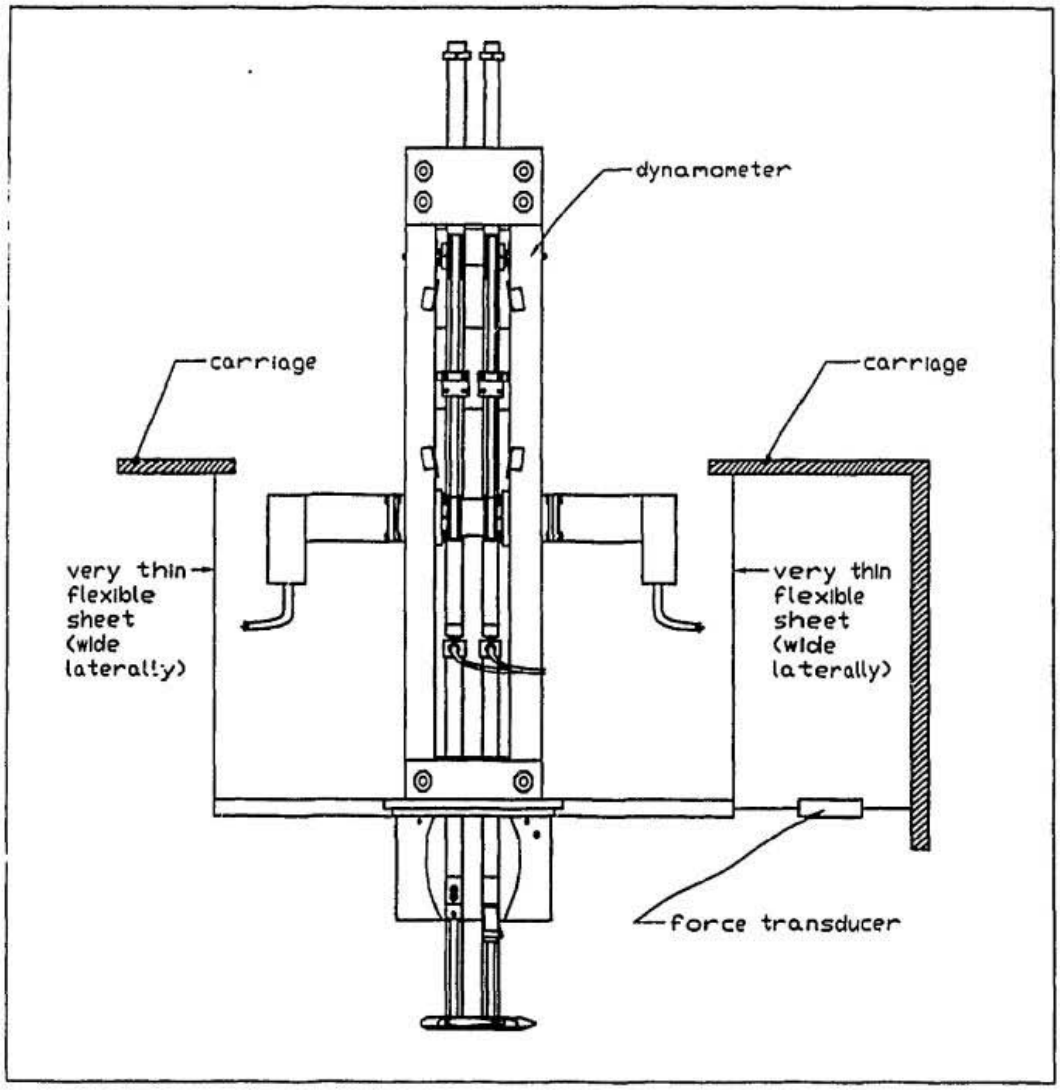

Figure 7.2 Alternative 1 Set-up for efficiency tests

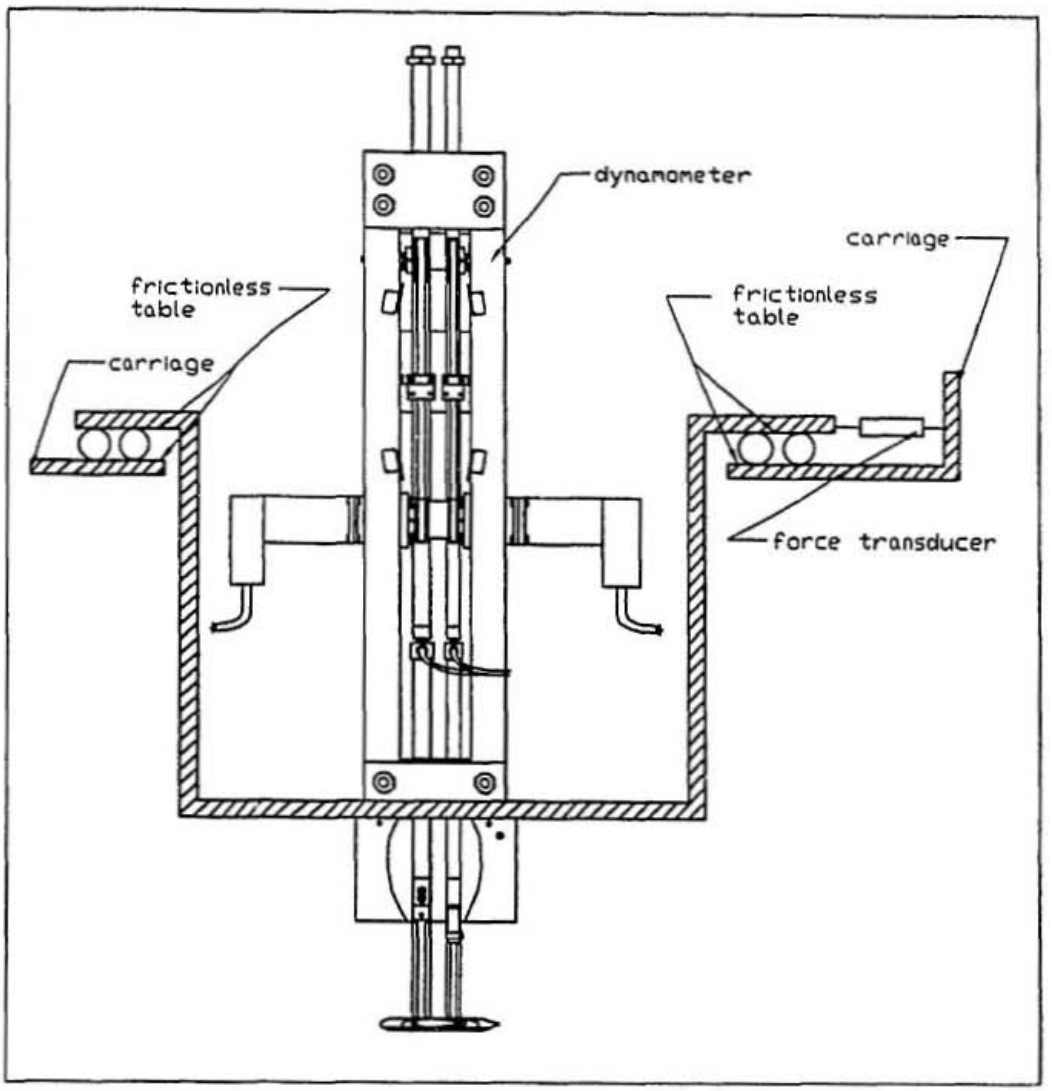

Figure 7.3 Alternative 2 Set-up for efficiency tests

References

Barnary, S (1887). "Marine Propellers," E. and F.N. Spon, 125, Strand, London. New York 35, Murray Street.

Beer, F and Johnston, E (1981). "Mechanics of Materials," McGraw-Hill Ryerson Ltm., Toronto.

Beer, F and Johnston, E (1977a). "Vector Mechanics For Engineers, Statics," McGraw-Hill Ryerson Ltm., Toronto

Beer, F and Johnston, E (1977b). "Vector Mechanics For Engineers, Dynamics," McGraw-Hill Ryerson Ltm., Toronto.

Bose, N (1993). "Propulsive Performance of Chordwise Flexible Oscillating Foils Using a Time-Domain Panel Method," 2nd Marine Dynamics Conf., Vancouver

Bose, N (1992). "A Time-Domain Panel Method for Analysis of Foils in Unsteady Motion as Oscillating Propulsors," Proc. 11th Australian Fluid Mechanics Conference, University of Tasmania, Hobart.

Bose, N, and Lien, J (1989). "Propulsion of a Fin Whale (Balaenoptera physalus): Why the Fin Whale is a Fast Swimmer," Proc. R. Soc. Lond., B237. 175-200.

Chopra, MG & Kambe, T (1977). "Hydromechanics of Lunate-Tail Swimming Propulsion, Part 2," J. Fluid Mech., Vol.79, pp.49-69.

Chopra, MG (1976). "Large Amplitude Lunate Tail Theory of Fish Locomotion," J. of Fluid Mech., Vol.74, pp.49-69

Chopra, MG (1974). "Hydromechanics of Lunate-Tail Swimming Propulsion," J. Fluid Mech., Vol.64, pp. 375-391.

Dally, J.W., Riley, W.F (1965). "Experimental Stress Analysis" McGraw-Hill Book Company, New York

Earle, J.E (1983). "Engineering Design Graphics," Addison-Wesley Publishing Company, Don Mills, Ontario.

Gambell, R (1985). "Fin whale *Balaenoptera Physalus*. In Handbook of Marine Mammals (ed. S.H. Ridgeway & R. Harrison)," pp.3171-3192. Toronto, Ontario: Academic Press.

Grue, J, Mo, A, and Palm, E (1988). "Propulsion of a Foil Moving in Water Waves," J. Fluid Mech., Vol.186, pp. 393-417.

Harvald, Sv Aa (1983). "Propulsion. In Resistance and Propulsion of Ships," John Wiley and Sons, Toronto.

Hoar, WS. and Randall, DJ (1978). "Fish Physiology, Vol. VII, Locomotion," Academic Press.

Hoppe, KG (1989). "The Dynamo-Elastic Oscillating Foil Propeller," Schiff & Hafen, pp.54-58, 60-61.

Katz, J (1981). "A Discrete Vortex Method for the Non-Steady Separated Flow Over an Airfoil," J. Fluid Mech., Vol.102, pp.315-328.

Katz, J, and Weihs,D (1979). "Large Amplitude Unsteady Motion of a Flexible Slender Propulsor," J. Fluid Mech., Vol.90, pp.713-723.

Katz, J, and Weihs,D (1978). "Hydrodynamic Propulsion by Large Amplitude Oscillation of an Airfoil with Chordwise Flexibility," J. Fluid Mech., Vol.88, pp.485-497.

Krebs, JR and Davies, NB (1978). "Behavioral Ecology: An Evolutionary Approach, (494 pages.)," Sunderland, Massachusetts: Sinauer Associates.

Kshatriya, M, and Blake, RW (1988). "Theoretical Model of Migration Energetics in the Blue Whale, *Balaenoptera musculus*," J. Theor. Biol., Vol. 133, pp.479-498.

Lai, P, Bose, N, and McGregor, R (1993). "Wave Propulsion from a Flexible-Armed, Rigid-Foil, Propulsor," Marine Tech., Vol.30, January 1993.

Lai, P, Bose, N, and McGregor, R (1989). "Experimental Investigation of Oscillating Foil Propellers," 22nd American towing tank conf., ATTC conf., St. John's, Newfoundland, Canada., 7 pages.

Lighthill, MJ (1970). "Aquatic Animal Propulsion of High Hydromechanical Efficiency," J. Fluid Mech., Vol.44, pp. 265-301.

Lighthill, MJ, (1969). "Hydromechanics of Aquatic Animal Propulsion," Annual Review of Fluid Mech., Vol.1, pp. 413-446

Lighthill, MJ (1960). "Note on the Swimming of Slender Fish," J Fluid Mech, Vol.9, pp. 305-317.

Liu, P. and Bose, N (1993). "Propulsive Performance of Three Naturally Occurring Oscillating Propeller Planforms," Ocean Engineering, Vol.20, No 1, pp.57-75.

Martini, L (1984). "Practical Seal Design," Marcel Dekker Inc, New York.

Munday, A, and Farrar, R (1979). "An Engineering Data Book," University of Southampton.

Popular Mechanics (1995). "Tech Update, Charlie the K-Tuna. In Popular Mechanics," January, 1995

Rawson, KJ, and Tupper, EC (1984). "Basic Ship Theory, Vol.II," John Wiley and Sons, New York.

Ray, GC, Mitchell, ED, Wartzok, D, Kozick, VM and Maiefsk, R (1978) "Radiotracking of a Fin Whale (*Balaenoptera physalus*). In Science," Wash. 202, pp.521-524.

Saunders, HE (1957). "Hydrodynamics in Ship Design," Soc. Naval Arch. and Mar. Engrs., Jersey City.

Shigley, J, and Mischke,A (1989). "Mechanical Engineering Design," McGraw-Hill Book Company, New York, 5th ed.

Siegel, M, Maleev, V, Hartman, J (1965). "Mechanical Design of Machines," International Textbook Company, New York, 4th ed.

Spotts, M (1978). "Design of Machine Elements," Prentice-Hall Inc., Englewood Cliffs, New Jersey, 5th ed.

Steidel, R, (1989). "An Introduction to Mechanical Vibrations," John Willey & Sons, 3rd ed.

Taggart, R (1969). "Marine Propulsion: Principles and Evolution," Gulf Publishing Company, Houston, 368 pages.

Thornton, P.A. and Coangelo, V.J (1985). "Foundamentals of Engineering Materials," Prentice-Hall, Inc., Englewood Cliff, N.J.

Triantafyllou, G, Triantafyllou, M, and Grosenbaugh (1993). "Optimal Thrust Development in Oscillating Foils With Application to Fish Propulsion," J. of Fluids and Structures, Vol.7, pp.205-224.

Ullman, D (1992). "The Mechanical Design Process," McGraw-Hill Inc, New York.

van Manen, JD (1973). "Non-Conventional Propulsion Devices," Symposium on Marine Propellers, Vol.20, N.226, pp.225-245

van Manen, JD, and van Oossanen, P (1988). "Propulsion. In Principles of Naval Architecture Vol.II (ed. E.V. Lewis)," Soc. Naval Arch. and Mar. Engrs., Jersey City, pp.127-254.

Wu, TY (1971c). "Hydromechanics of Swimming Propulsion. part 3. Swimming and Optimum Movement of Slender Fish With Side Fins," J. of Fluid Mech., Vol.46, pp. 545-568.

Wu, TY (1971b). "Hydromechanics of Swimming Propulsion. part 2. Some Optimum shape problems," J. of Fluid Mech., Vol.46, pp. 521-544.

Wu, TY (1971a). "Hydromechanics of Swimming Propulsion. part 1. Swimming Flexible Plate at Variable Forward Speeds in an Invisid Fluid," J. of Fluid Mech., Vol.46, pp. 337-355.

Wu, TY (1961). "Swimming of a Waving Plate," J. of Fluid Mech., Vol.10, pp.321-344.

Yamaguchi, H, and Bose, N (1994). "Oscillating Foils for Marine Propulsion," Proceedings of the fourth International Offshore and Polar Engineering Conference Osaka, Japan.

Yamamoto, I, Terada, Y, Nagamatu, T, and Imaizumi, Y (1993) "Research on an Oscillating Fin Propulsion Control System," Mitsubishi Heavy Industries, LTD., Japan.

Appendix A
Design Drawings

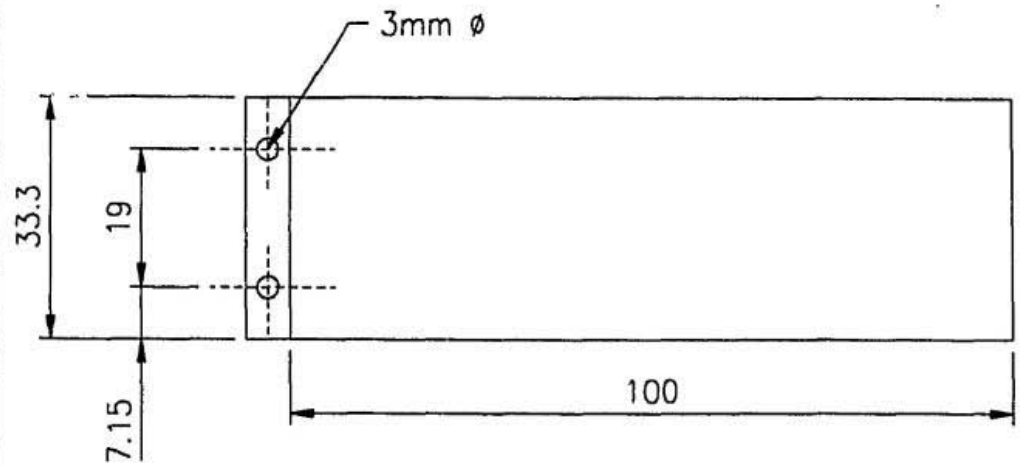

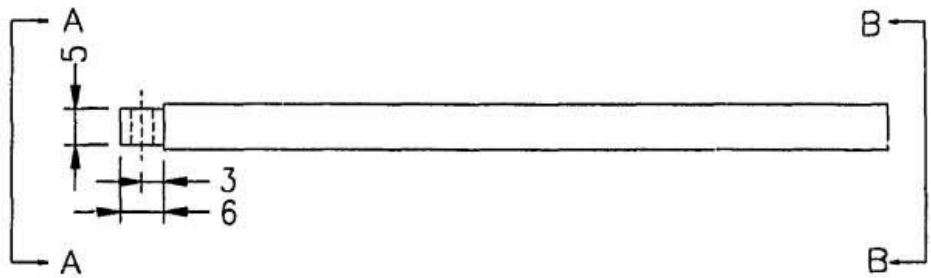

SECTION A–A SECTION B–B

NOTE:
1. ALL DIMENSIONS ARE IN mm
2. TWO OFF
3. FOIL HAS A NACA 0019 SECTION
4. FOIL TO BE CNC MACHINED
5. MATERIAL BRASS

Foil 1

Drawing No.	Part No.	Drawn BY:	Designed BY:
A–001	1	David Greening	David Greening

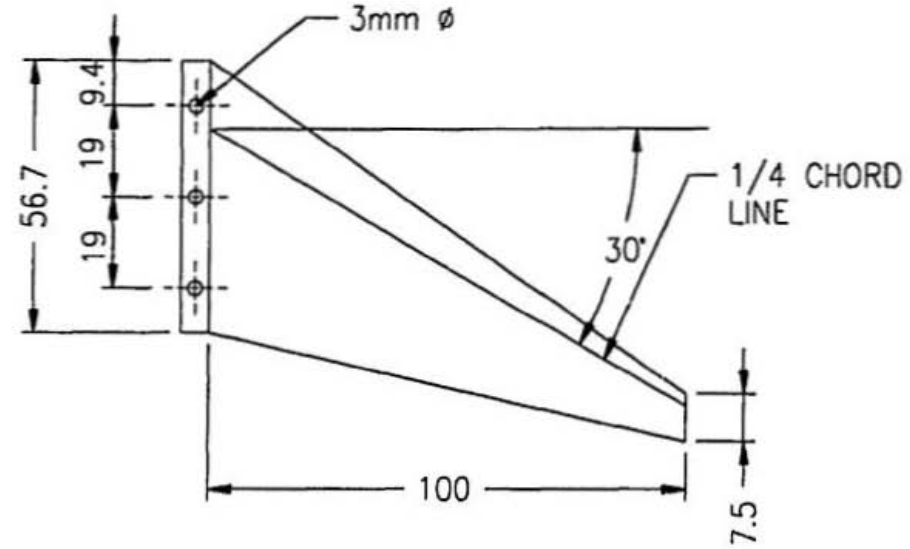

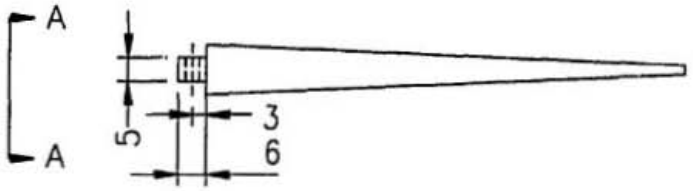

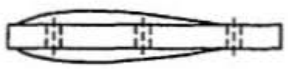

SECTION A–A

NOTE:

1. ALL DIMENSIONS ARE IN mm
2. TWO OFF
3. FOIL HAS A NACA 0019 SECTION
4. FOIL TO BE CNC MACHINED
5. MATERIAL BRASS

FOIL 2

Drawing No.	Part No.	Drawn BY:	Designed BY:
A–002	1	David Greening	David Greening

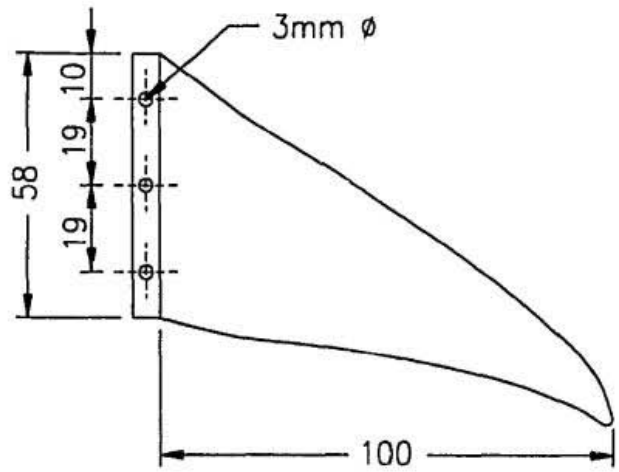

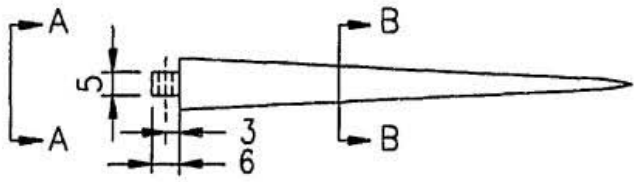

SECTION A–A SECTION B–B

NOTE:

1. ALL DIMENSIONS ARE IN mm
2. TWO OFF
3. FOIL HAS A NACA 0019 SECTION
4. FOIL TO BE CNC MACHINED
5. MATERIAL BRASS

FOIL 3

Drawing No.	Part No.	Drawn BY:	Designed BY:
A–003	1	David Greening	David Greening

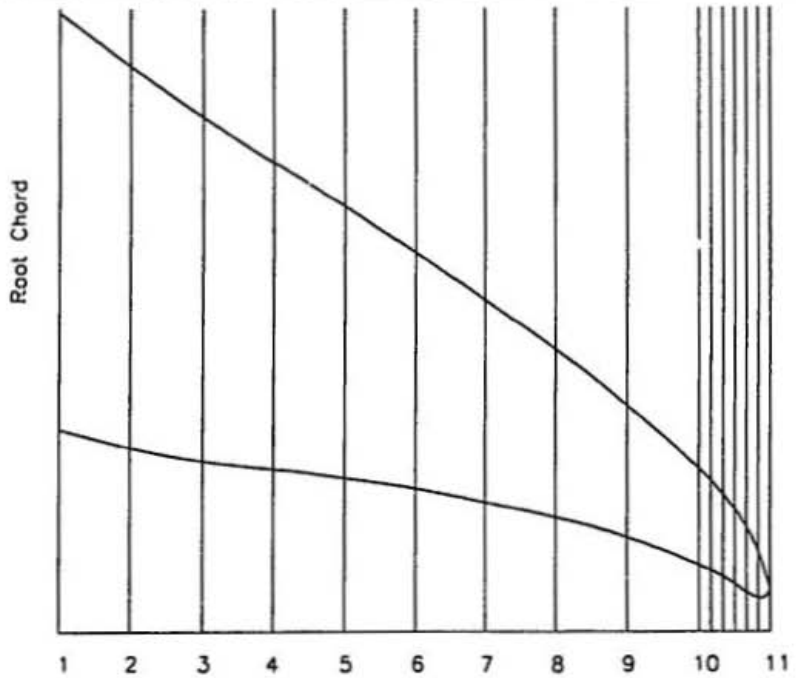

Table Of Offsets

Station	Distance Of Leading Edge From Datum	Distance Of Trailing Edge From Datum
1 centre	86.0	28.0
2	78.7	25.3
3	71.3	23.3
4	65.3	22.7
5	59.3	21.3
6	52.7	20.0
7	46.0	18.0
8	39.3	16.0
9	31.3	13.3
10	22.7	9.3
10 1/6	21.0	8.5
10 1/3	19.0	7.7
10 1/2	17.0	6.7
10 2/3	14.7	5.3
10 5/6	11.7	4.7
11 tip	6.0	6.0

Note:
1. Stations are equally spaced at 10 mm
2. All Measurements are in mm

FOIL 3

Drawing No.	Part No.	Drawn BY:	Designed BY:
A-004	1	David Greening	David Greening

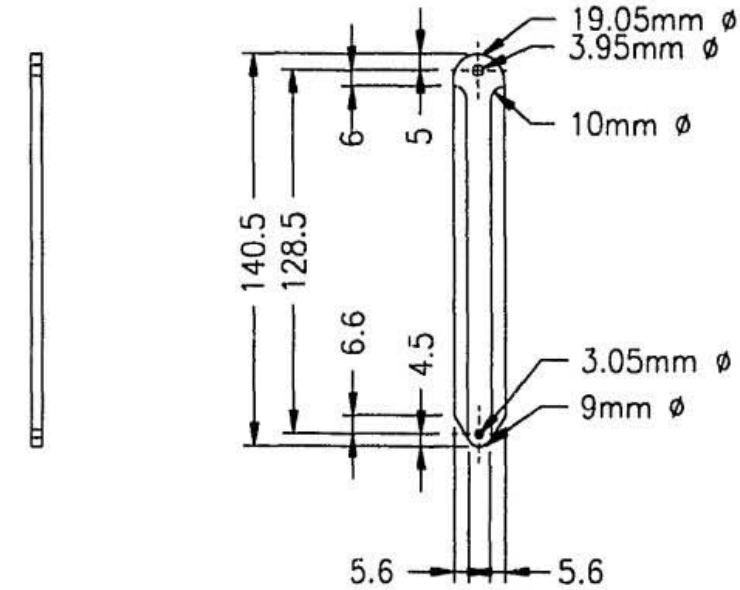

Front View

Side View

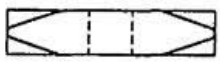

Top View

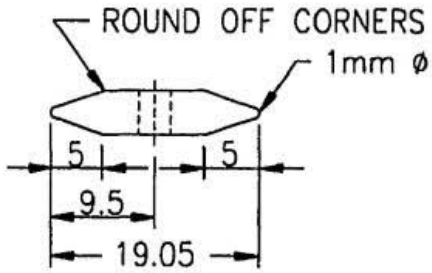

Bottom View

NOTE:

1. ALL DIMENSIONS ARE IN mm
2. ONE OFF
3. MATERIAL STAINLESS STEEL
4. UPPER PIN ROTATES WITH THE SHAFT WHILE SHAFT ROTATES AROUND THE LOWER PIN

LOWER SECTION OF THE FORWARD DRIVE SHAFT

Drawing No.	Part No.	Drawn BY:	Designed BY:
A-005	3	David Greening	David Greening

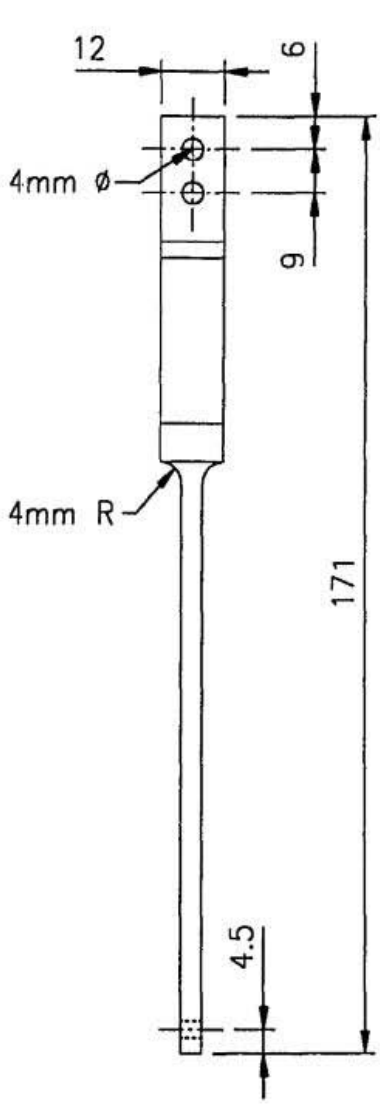

FRONT VIEW

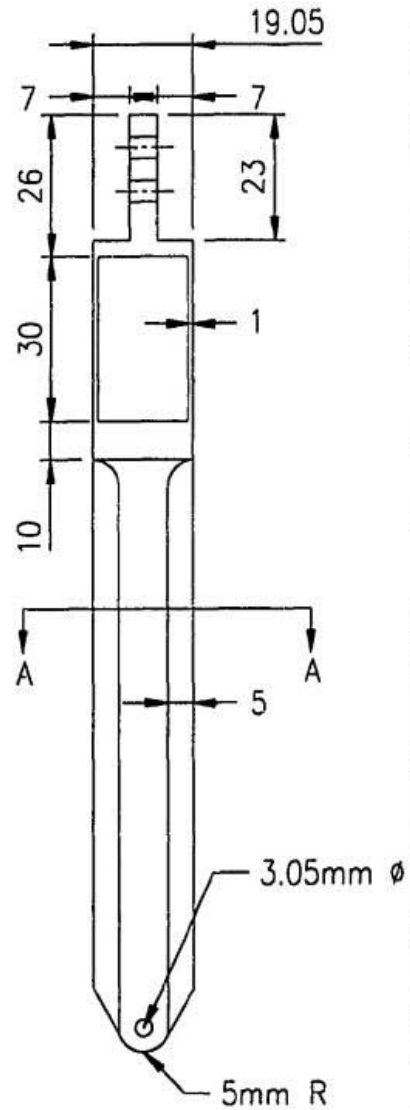

SIDE VIEW

NOTE:

1. ALL DIMENSIONS ARE IN mm
2. ONE OFF
3. ONE 8mm LONG 3mm ø PIN
4. STRUT TO ROTATE ABOUT PIN
5. MATERIAL STAINLESS STEEL

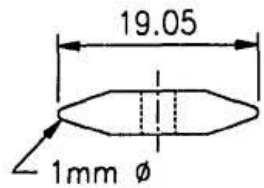

SECTION A-A

LOWER SECTION OF AFT DRIVE SHAFT

Drawing No.	Part No.	Drawn BY:	Designed BY:
A-006	5	David Greening	David Greening

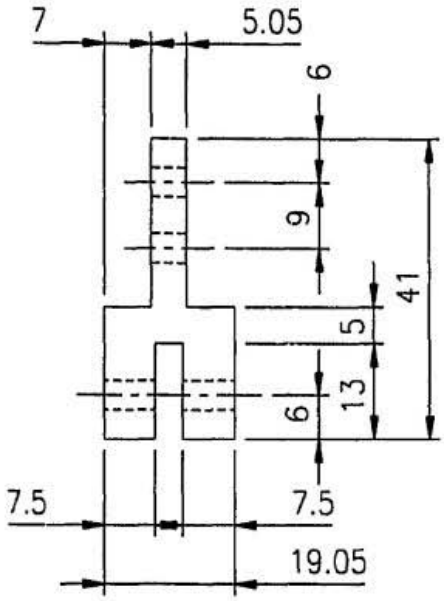

Front View

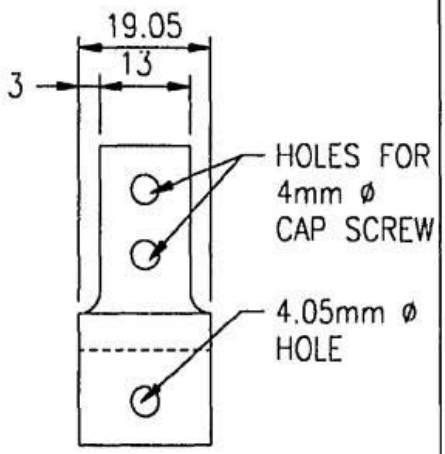

Side View

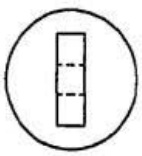

Top View

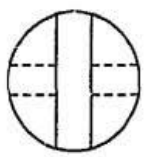

Bottom View

NOTE:

1. ALL DIMENSIONS ARE IN mm
2. ONE OFF
3. MATERIAL STAINLESS STEEL

LOWER PORTION OF PIVOT JOINT

Drawing No.	Part No.	Drawn BY:	Designed BY:
A-007	4	David Greening	David Greening

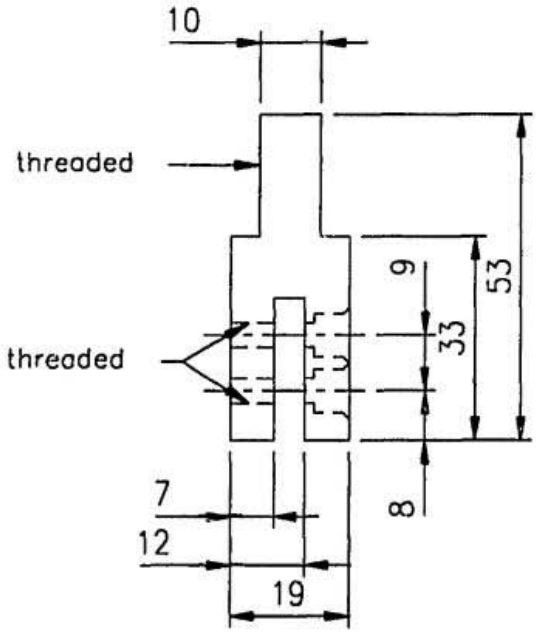

Front View

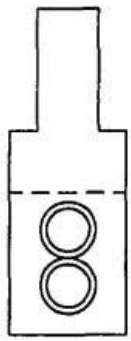

Side View

NOTE:

1. ALL DIMENSIONS ARE IN mm
2. ONE OFF
3. SLOT TO BE CUT TO A DEPTH OF 23mm
4. SCREW TO BE COUNTER SUNK COMPLETELY BELOW SURFACE
5. MATERIAL 3/4 in. ø STAINLESS STEEL ROD
   AND TWO OFF 4mm CAP SCREWS

UPPER PORTION OF PIVOT JOINT

Drawing No.	Part No.	Drawn BY:	Designed BY:
A-008	6	David Greening	David Greening

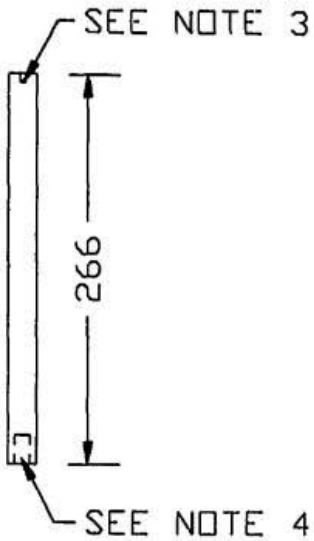

INTERMEDIATE
DRIVE SHAFT

NOTE:

1. ALL DIMENSIONS ARE IN mm
2. TWO OFF EACH
3. DRILL AND TAP FOR A 6-32 SCREW TO A DEPTH OF 10mm
4. DRILL AND TAP FOR A 10mm Ø INSERT
5. MATERIAL STAINLESS STEEL

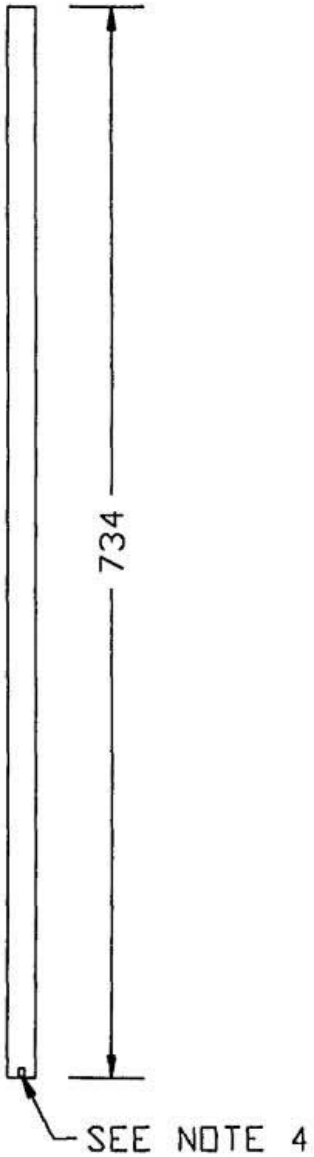

UPPER DRIVE
SHAFT

INTERMIDIATE AND UPPER DRIVE SHAFTS

Drawing No.	Part No.	Drawn BY:	Designed BY:
A-009	7 & 10	David Greening	David Greening

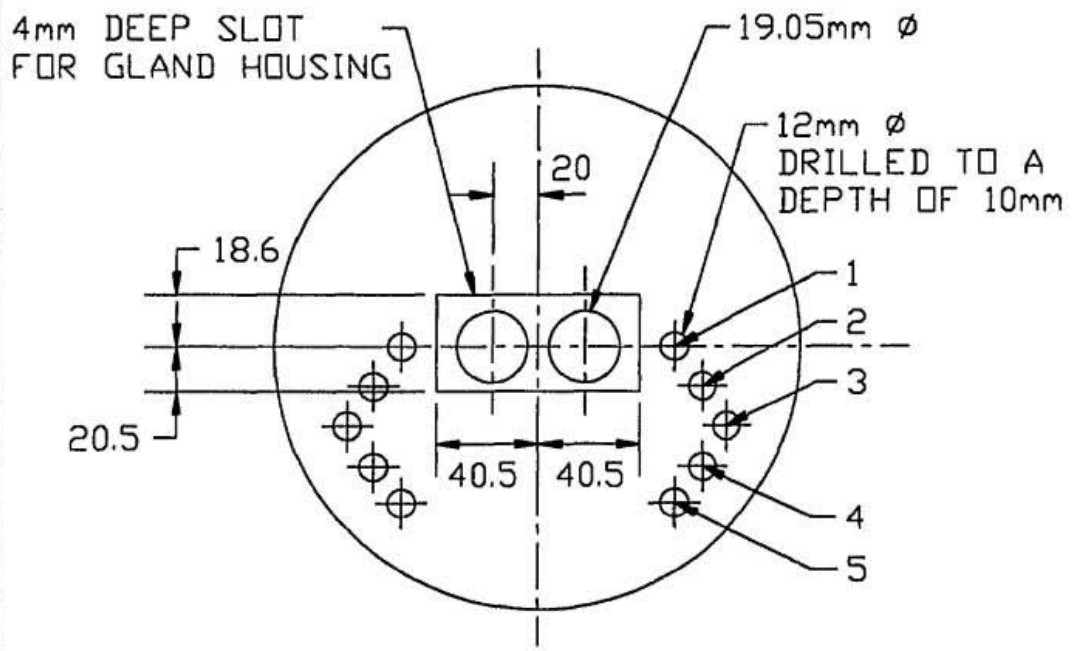

PLAN VIEW
LOOKING DOWN

NOTE:

1. ALL DIMENSIONS ARE IN mm
2. ONE OFF
3. HOLES 2 & 4 DRILLED FOR DOWELS
4. HOLES 1,3, & 5 DRILLED & TAPPED
5. MATERIAL BRASS

HOLE #	DISTANCE OF CL	DISTANCE OFF CL
1	0	59
2	17.3	71
3	34.5	82
4	52.2	71
5	67.9	59

WINDOW PORT

Drawing No.	Part No.	Drawn BY:	Designed BY:
A-010	11	David Greening	David Greening

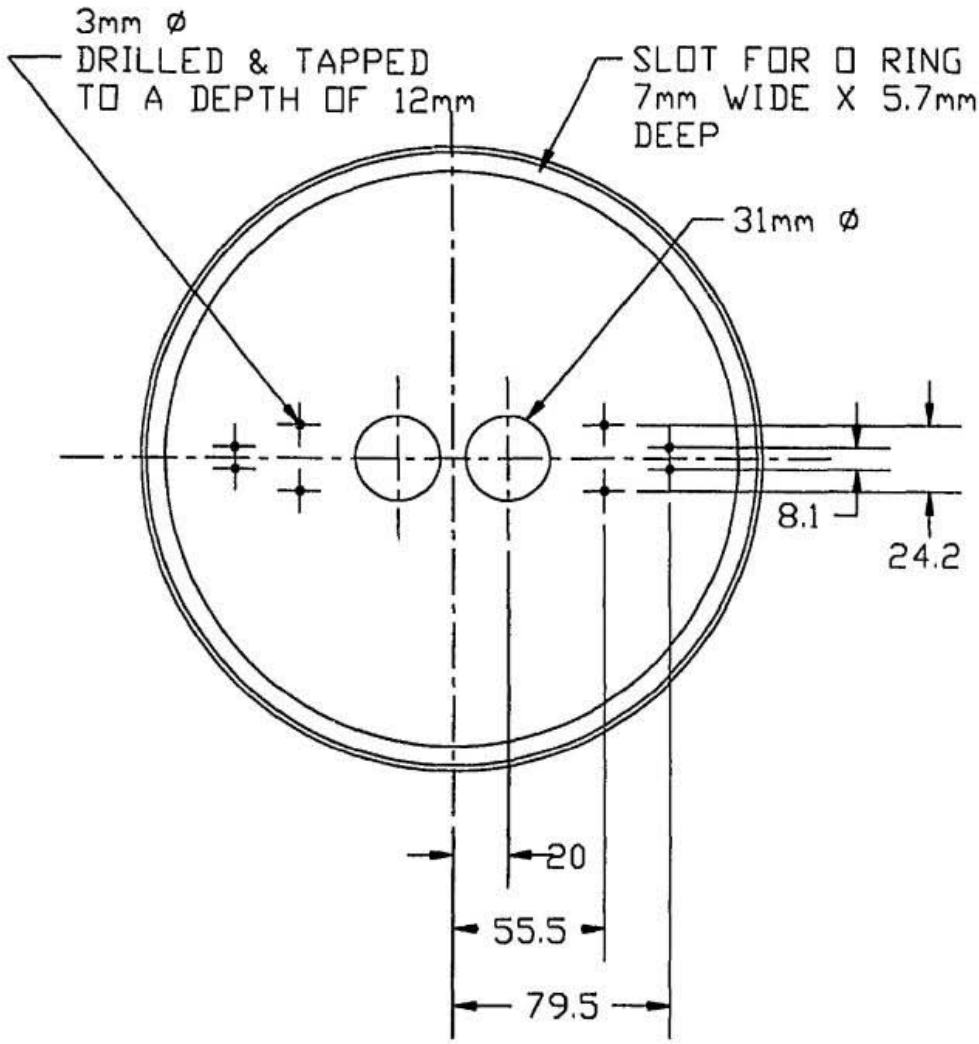

NOTE:

1. ALL DIMENSIONS ARE IN mm
2. ONE OFF
3. PORT ø IS 228mm
4. MATERIAL BRASS

WINDOW PORT

Drawing No.	Part No.	Drawn BY:	Designed BY:
A-011	11	David Greening	David Greening

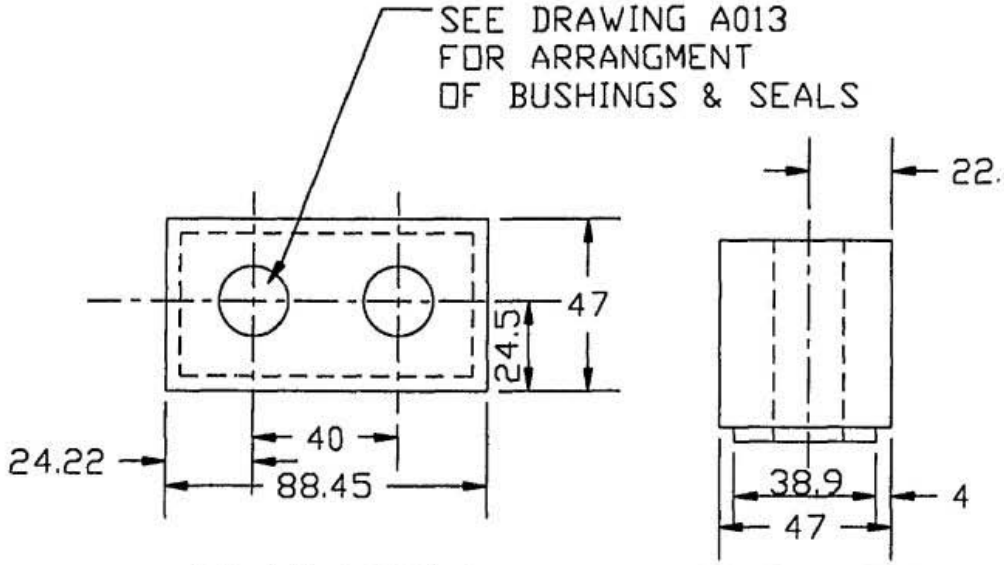

PLAN VIEW

END VIEW

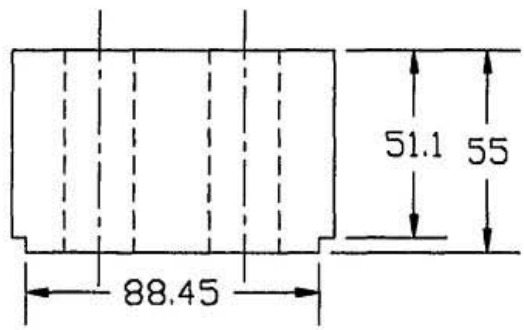

PROFILE VIEW

NOTE:

1. ALL DIMENSIONS ARE IN mm
2. ONE OFF
3. THE SLOTS FOR THE BUSHING & SEALS ARE TO BE MACHINED AFTER THE HOUSING IS SILVER SOLDERED TO THE WINDOW PORT TO ENSURE ALIGNMENT
4. MATERIAL BRASS

BUSHING AND GLAND HOUSING

Drawing No.	Part No.	Drawn BY:	Designed BY:
A-012	15	David Greening	David Greening

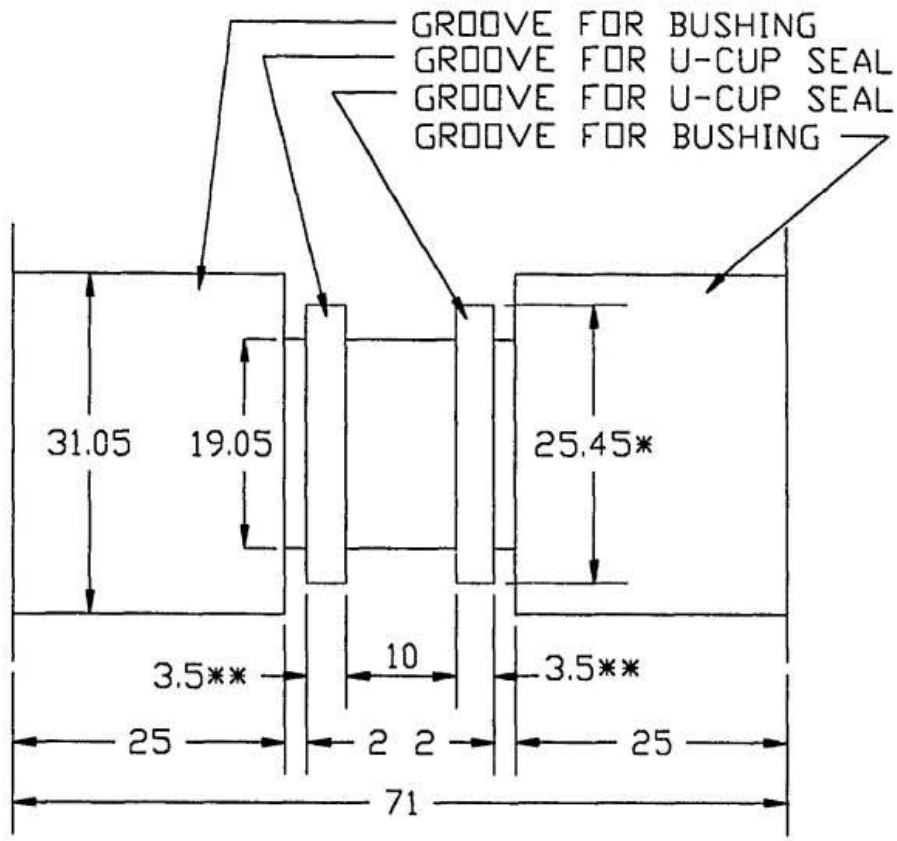

NOTE:

1. ALL DIMENSIONS ARE IN mm
2. ONE OFF
3. * GROOVE ø IS 1" TO 1.008"
4. ** GROOVE ø IS 0.138" TO 0.153"
5. MATERIAL BRASS

BUSHING AND GLAND HOUSING

Drawing No.	Part No.	Drawn BY:	Designed BY:
A-013	15	David Greening	David Greening

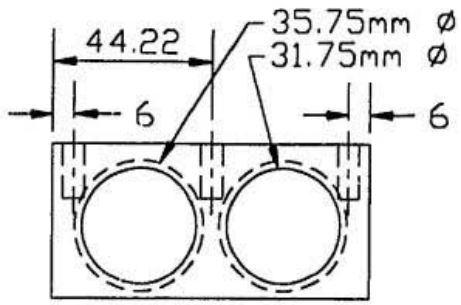

PLAN

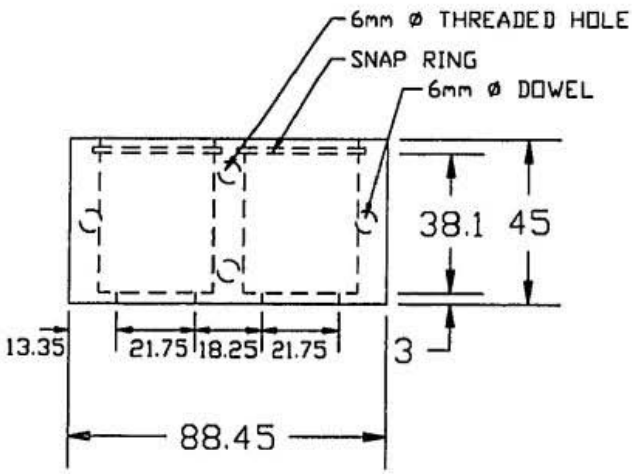

PROFILE

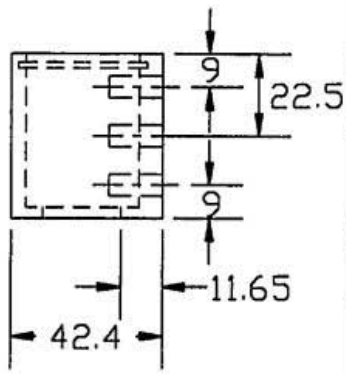

SIDE

NOTE:

1. ALL DIMENSIONS ARE IN mm.
2. TWO OFF
3. MATERIAL MILD STEEL

LINEAR BEARING BRACKET

Drawing No.	Part No.	Drawn BY:	Designed BY:
A-014	17	David Greening	David Greening

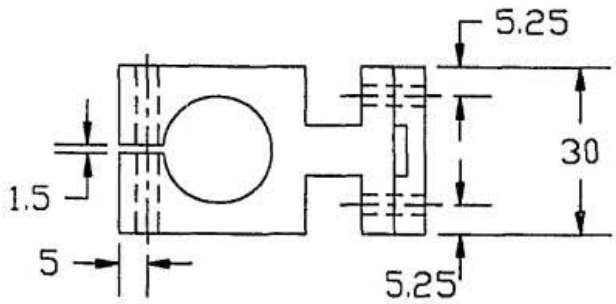

PLAN VIEW

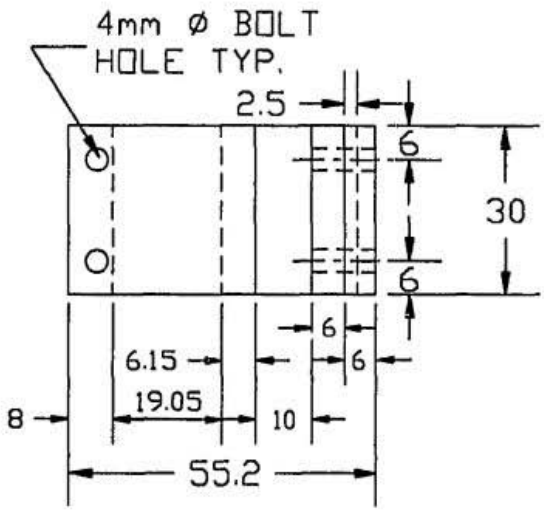

FRONT VIEW

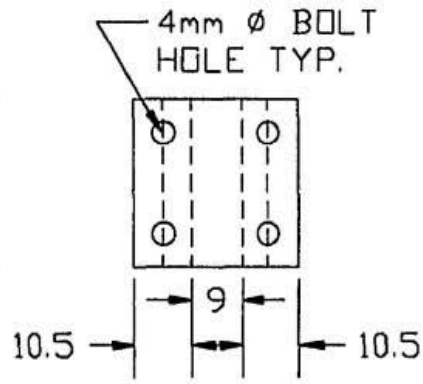

SIDE VIEW

NOTE:

1. ALL DIMENSIONS ARE IN mm
2. TWO OFF
3. MATERIAL ALUMINUM

DRIVE SHAFT TO DRIVE BELT CONNECTION

Drawing No.	Part No.	Drawn BY:	Designed BY:
A-015	21	David Greening	David Greening

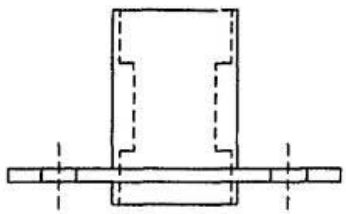

TOP VIEW
SHAFT HOUSING

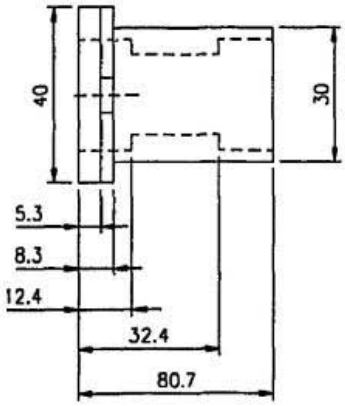

PROFILE VIEW
SHAFT HOUSING

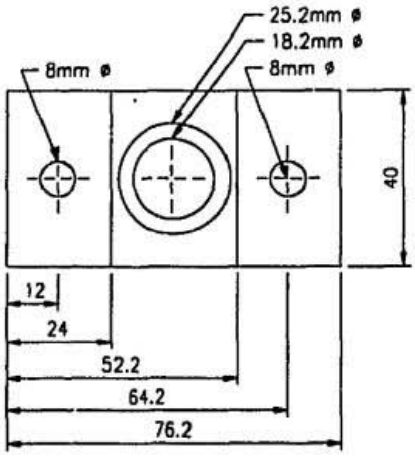

FRONT VIEW
SHAFT HOUSING

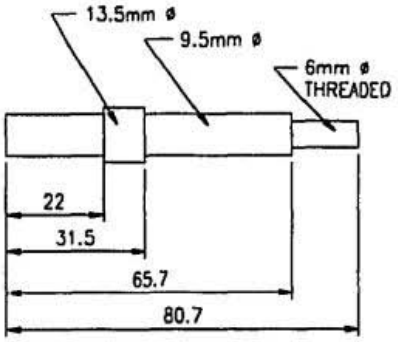

PROFILE VIEW
SHAFT

NOTE:

1. ALL DIMENSION ARE IN mm
2. TWO OF EACH
3. MATERIAL MILD STEEL

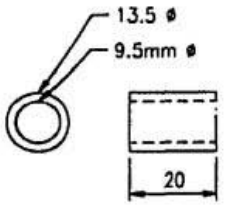

BEARING SPACER

UPPER DRIVE SHAFT & HOUSING

Drawing No.	Part No.	Drawn BY:	Designed BY:
A-016	22 & 23	David Greening	David Greening

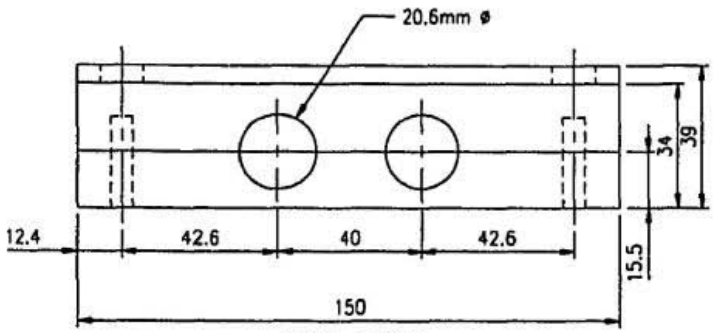

TOP VIEW
LVDT BRACKET

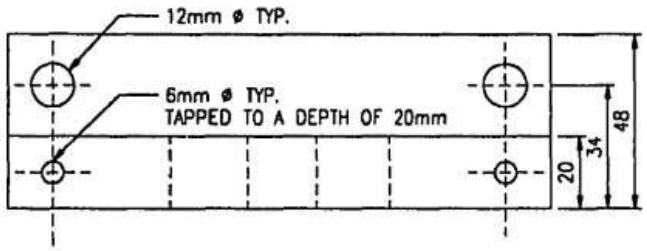

FRONT VIEW
LVDT BRACKET

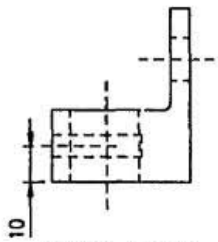

SIDE VIEW
LVDT BRACKET

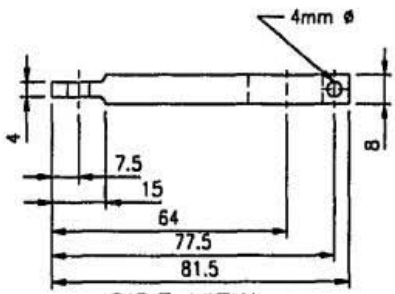

SIDE VIEW
CONNECTION

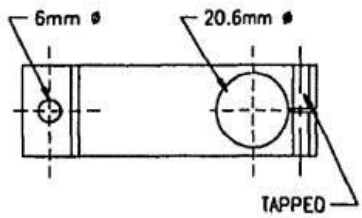

TOP VIEW
CONNECTION

NOTE:

1. ALL DIMENSIONS ARE IN mm
2. NEED TWO OFF EACH
3. MATERIAL ALUMINUM

LVDT BRACKET & CONNECTION

Drawing No.	Part No.	Drawn BY:	Designed BY:
A-017	27 & 28	David Greening	David Greening

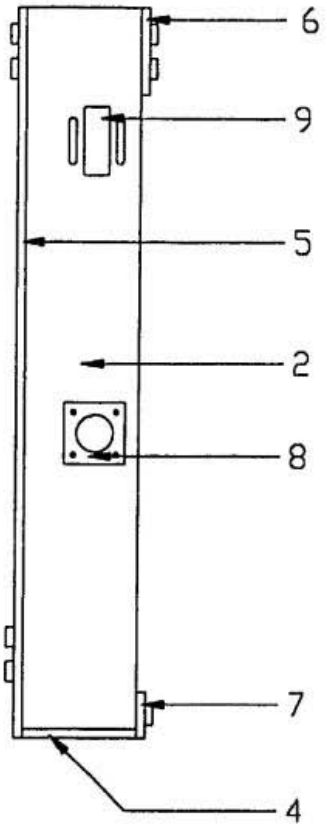

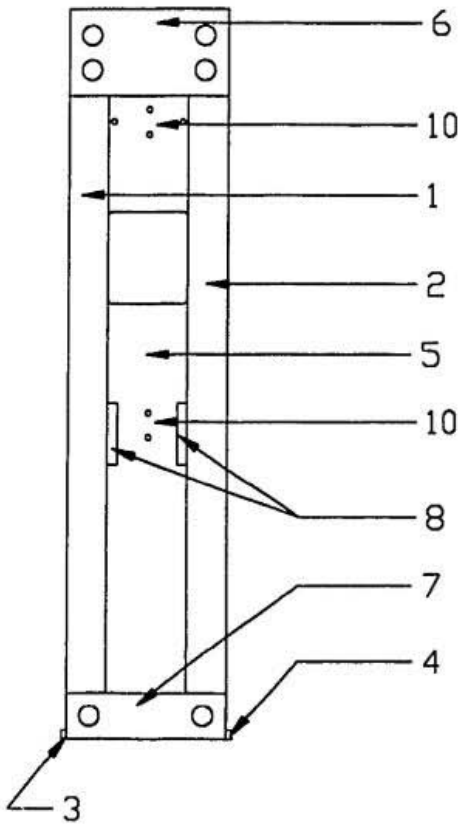

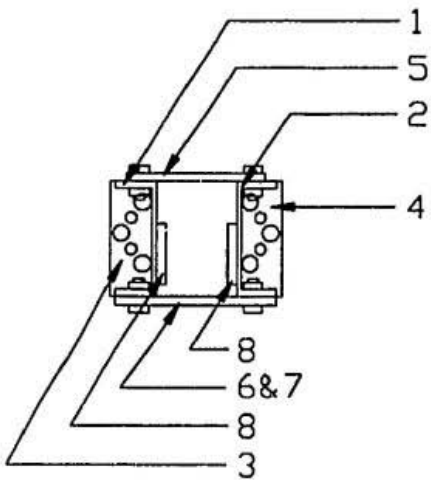

1 CHANNEL 1
2 CHANNEL 2
3 CONNECTION PLATE 1
4 CONNECTION PLATE 2
5 MOUNTING PLATE
6 BRACING PLATE 1
7 BRACING PLATE 2
8 MOTOR MOUNTING PLATE
9 LOCATION OF UPPER SHAFT HOUSING
10 LOCTAION OF LINEAR BEARINGS

MOUNTING BRACKET

Drawing No.	Part No.	Drawn BY:	Designed BY:
A-018	32	David Greening	David Greening

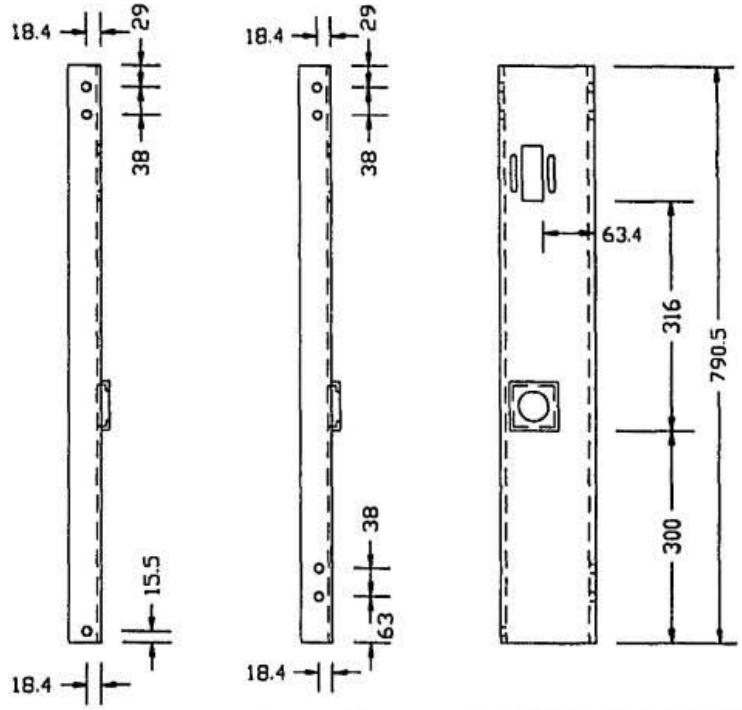

NOTE:

1. ALL DIMENSIONS ARE IN mm
2. ONE OFF CHANNEL 1
   ONE OFF CHANNEL 2
3. CHANNEL 1 SHOWN
   CHANNEL 2 IS A MIRROR IMAGE OF CHANNEL 1
4. MATERIAL MILD STEEL CHANNEL ASTM A36 C130X10

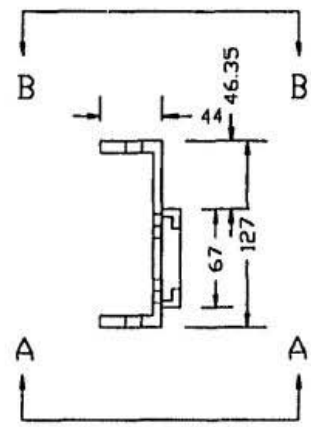

PLAN VIEW

MOUNTING BRACKET (CHANNEL 1&2)

Drawing No.	Part No.	Drawn BY:	Designed BY:
A-019	32	David Greening	David Greening

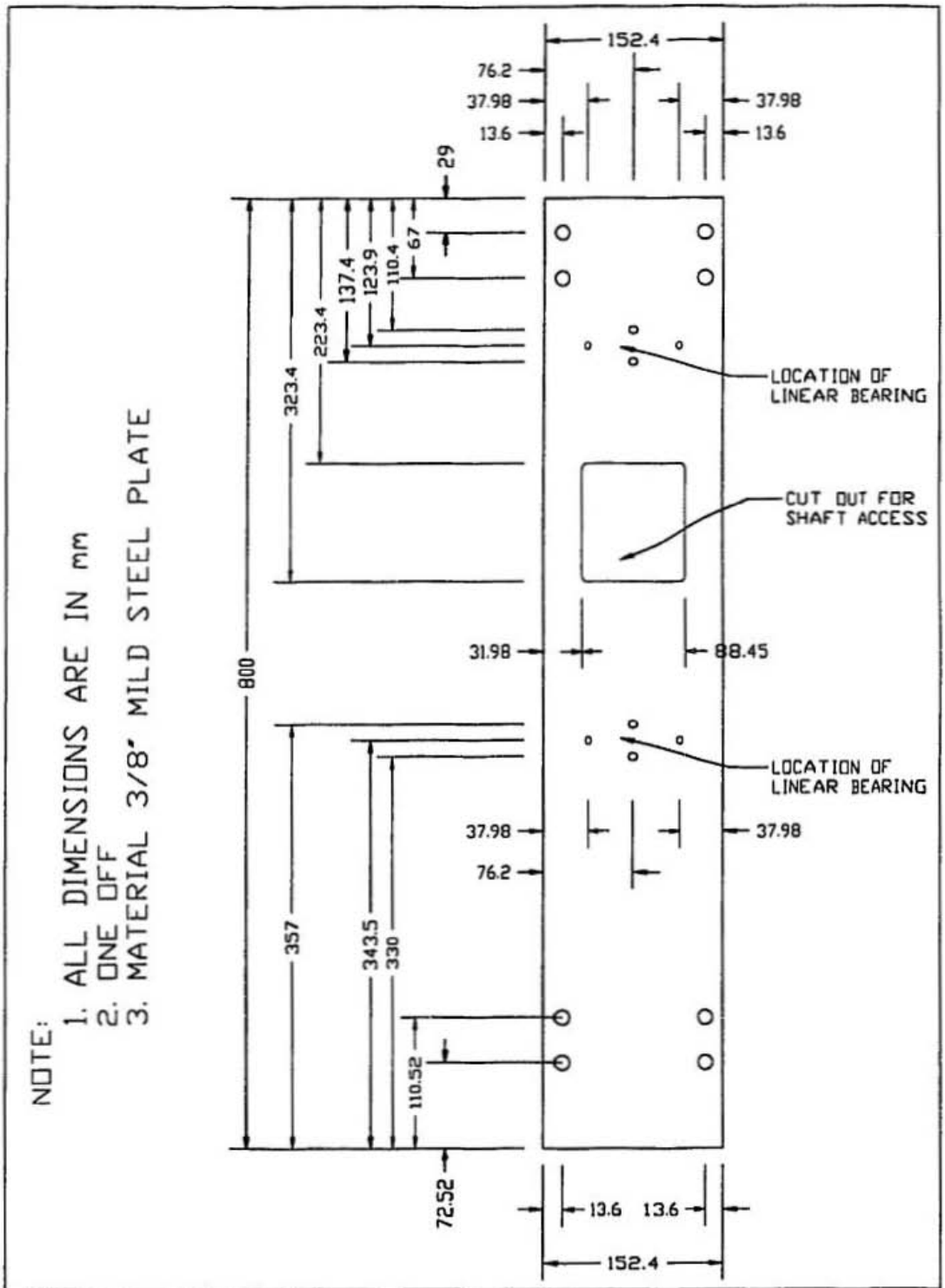

MOUNTING BRACKET (MOUNTING PLATE)

Drawing No.	Part No.	Drawn BY:	Designed BY:
A-020	32	David Greening	David Greening

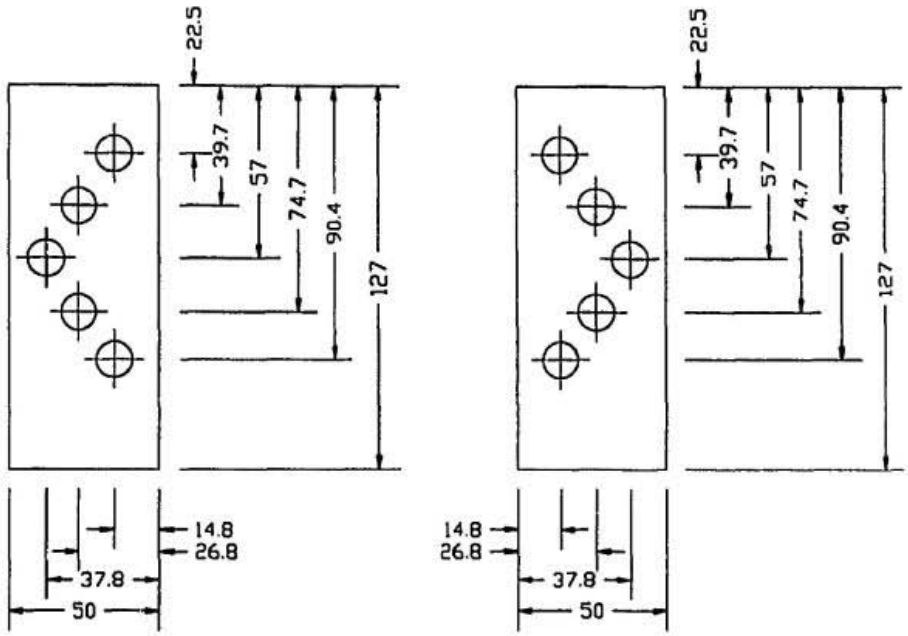

CONNECTION PLATE 1 CONNECTION PLATE 2

NOTE:

1. ALL DIMENSIONS ARE IN mm
2. ONE OFF EACH
3. ALL HOLES ARE 12mm ø
4. MATERIAL 3/8" MILD STEEL PLATE

MOUNTING BRACKET (CONNECTION PLATE)

Drawing No.	Part No.	Drawn BY:	Designed BY:
A-021	32	David Greening	David Greening

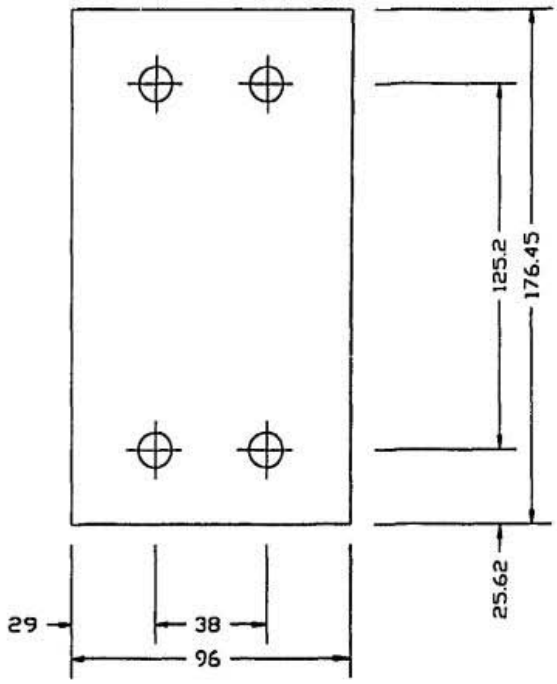

BRACING PLATE 1

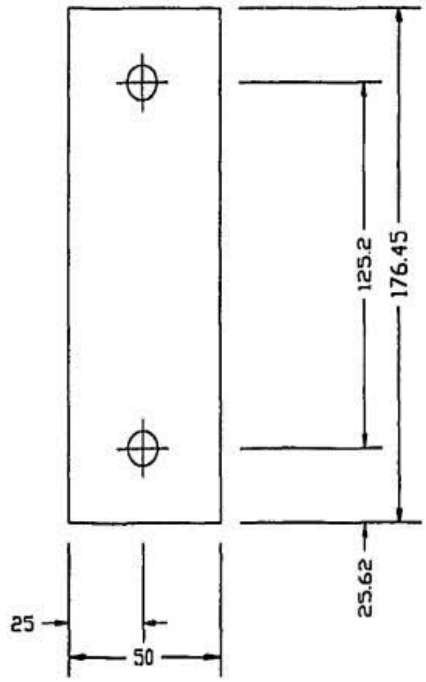

BRACING PLATE 2

NOTE:

1. ALL DIMENSIONS ARE IN mm
2. ONE OFF EACH
3. ALL HOLES ARE 12mm ø
4. MATERIAL 3/8" MILD STEEL PLATE

MOUNTING BRACKET (BRACING PLATE)

Drawing No.	Part No.	Drawn BY:	Designed BY:
A-022	32	David Greening	David Greening

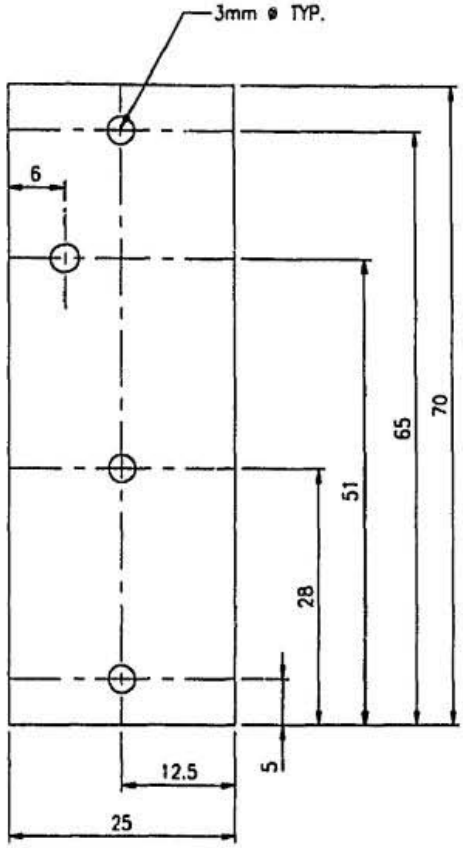

LIMIT SWITCH
BRACKET

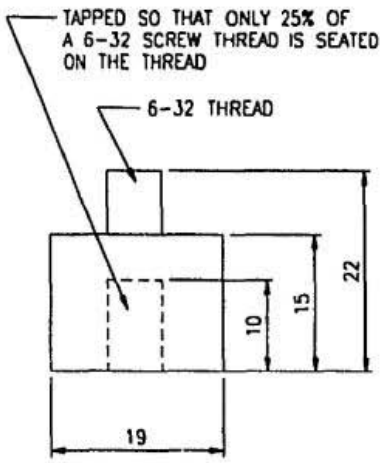

LOAD CELL TO
DRIVE SHAFT INSERT

NOTE:

1. ALL DIMENSIONS ARE IN mm
2. FOUR OFF EACH
3. MATERIAL FOR LIMIT SWITCH BRACKET ALLUMINUM
4. MATERIAL FOR INSERT TEFLON

LIMIT SWITCH BRACKET & LOAD CELL INSERT

Drawing No.	Part No.	Drawn BY:	Designed BY:
A-023	9 & 30	David Greening	David Greening

Appendix B
List of Parts and Suppliers for Maintenance Purpose

Part number	Part	Supplier
1	foils	designed by author and manufactured by Dominis Engineering
2	mounting pod	designed by author and manufactured by Memorial University of Newfoundland's (MUN'S) Technical Services
3	lower drive shaft	designed by author and manufactured by MUN'S Technical Services
4	pivot joint	designed by author and manufactured by MUN'S Technical Services
5	strain gauged section	designed by author and strain gauge section manufactured by MUN'S Technical Services. Gauges (model CEA-06-062UW-350) supplied and installed by Measurements Group U.K. LTD
6	drive shaft connection inserts	designed by author and manufactured by MUN'S Technical Services.
7	intermediate drive shafts	designed by author and manufactured by MUN'S Technical Services. 3/4" ground shaft supplied by Fred C. Morrison Ltd.
8	load cells	supplied by Hoskin Scientifique LTEE Sensotec model 31 0-10lbs
9	load cell to drive shaft inserts	designed by author and manufactured by MUN'S Technical Services
10	upper drive shafts	designed by author and manufactured by MUN'S Technical Services. 3/4" ground shaft supplied by Fred C. Morrison Ltd.
11	window port	designed by author and manufactured by MUN'S Technical Services
12	window port o-ring	designed by author and manufactured by MUN'S Technical Services
13	bushings	designed by author and manufactured by MUN'S Technical Services
14	drive shaft seals	supplied by Dowty Silcofab 3/4" x 1" x 1/8" U-Cup part number 15-024100-125
15	bushing and drive shaft seals housing	designed by author and manufactured by MUN'S Technical Services

Part number	Part	Supplier
16	linear bearings	supplied by Fred C. Morrison Ltd. Thompson Linear Ball Bearings part number A-122026 CLBB-750
17	linear bearing brackets	designed by author and manufactured by MUN'S Technical Services
18	DC servo drive motors	Supplied by Areotech D-C servo motor & motion controller Unidex 14 desktop U14S
19	pulleys	supplied by Fred C. Morrison Ltd. 2" timing belt pulley part number 54692
20	drive belts	supplied by Fred C. Morrison Ltd. 9mm wide timing belt part number 54797
21	drive belt to drive shaft connectors	designed by author and manufactured by MUN'S Technical Services
22	upper pulley shafts	designed by author and manufactured by MUN'S Technical Services
23	upper pulley shaft housings	designed by author and manufactured by MUN'S Technical Services
24	rotary bearings	supplied by Fred C. Morrison Ltd. Thompson radial Bearings part number 50605 catalogue number C4ADS
25	fairing	designed by author and manufactured by MUN'S Technical Services
26	LVDT	supplied by RDP Electrosense Inc. +- 6" LVDT number DCT6000
27	LVDT brackets	designed by author and manufactured by MUN'S Technical Services
28	LVDT to drive shaft connections	designed by author and manufactured by MUN'S Technical Services
29	limit switches	supplied by MUN'S Electrical Engineering Department. Electro Sonic mechanical micro switch.
30	limit switch bracket	designed by author and manufactured by MUN'S Technical Services
31	limit switch flags	designed by author and manufactured by MUN'S Technical Services

Part number	Part	Supplier
32	mounting bracket	designed by author and manufactured by MUN'S Technical Services

List Suppliers

Areotech
Optikon Corporation Ltd.
410 Conestogo Road, Waterloo, Ontario,
Canada, N2L 4E2
telephone number (519) 885-2551
fax number (5129) 885-4712

Dominis Engineering Ltd.
5515 Canotek Rd., Unit 15, Gloucester, Ontario
Canada, K1J 9L1
telephone number (613) 747-0193
fax number (613) 746-3321

Dowty Silcofab
335 Woodlawn Road West, Guelph, Ontario,
Canada, N1H 7K9
telephone number (519) 822 8913
fax number (519) 822-6675

Fred C. Morrison Ltd.
1256 Topsail Rd., Mount Pearl, Newfoundland,
Canada, A1L 1C9
telephone number (709) 364-7959
fax number (709) 364-9422

Hoskin Scientifique LTEE
5683 Pare, Montreal, Quebec,
Canada, H4p 1S1
telephone number (514) 735-5267
fax number 05-826781

Measurements Group U.K. LTD
Stroudley Rd., Basingstoke, Hants,
United Kingdom, RG24 0FW
telephone number (0256) 462131
fax number (0256) 471441

RDP - Electrsenes INC
R.D.S. Route 100 Pottstown, Pennsylvania,
U.S.A. 19464
telephone number (915) 469-0450
fax (915) 469-0852

Appendix C
Flow Charts for Motion Control Program

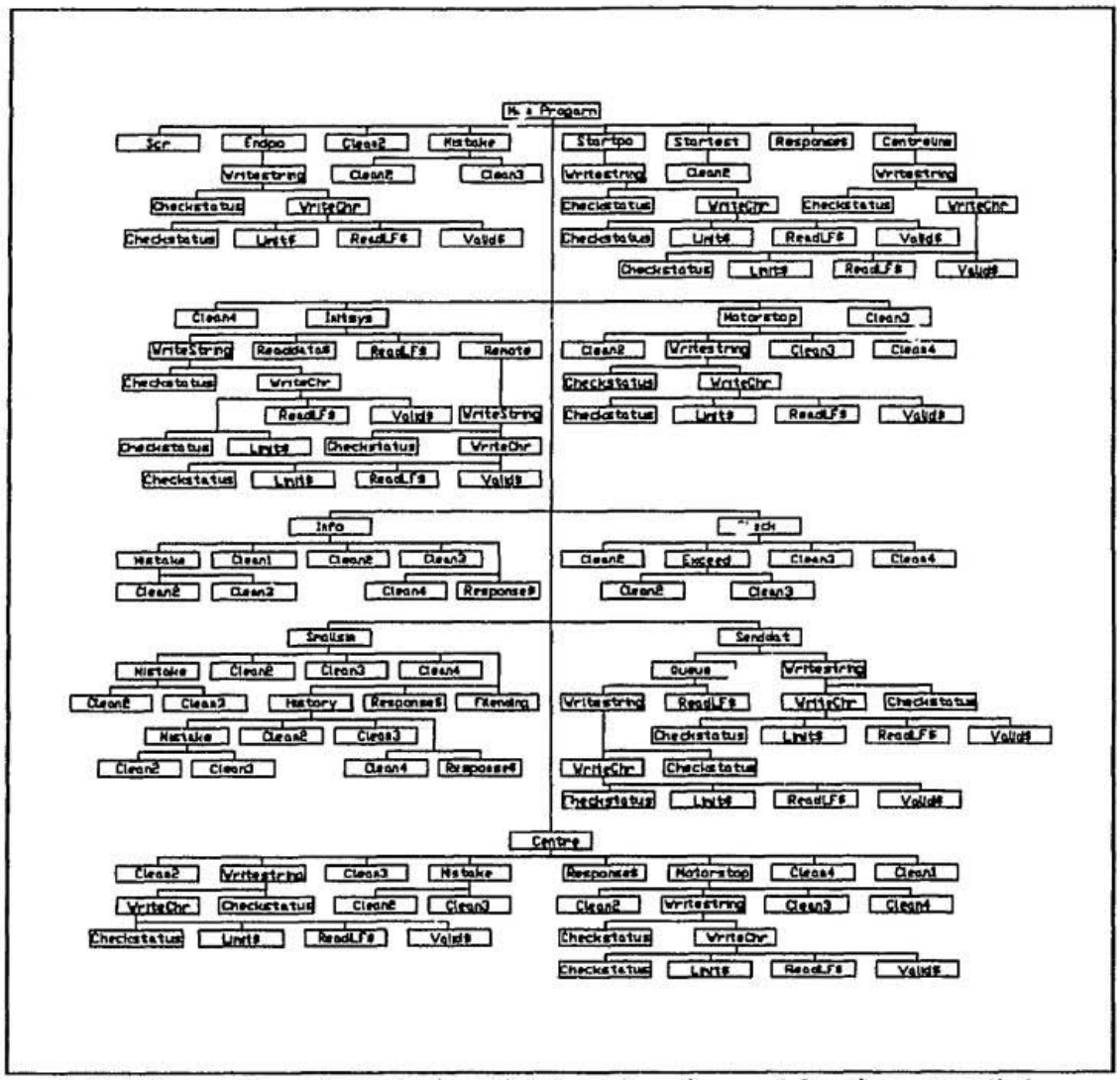

This figure shows the order in which the subroutines and functions are called

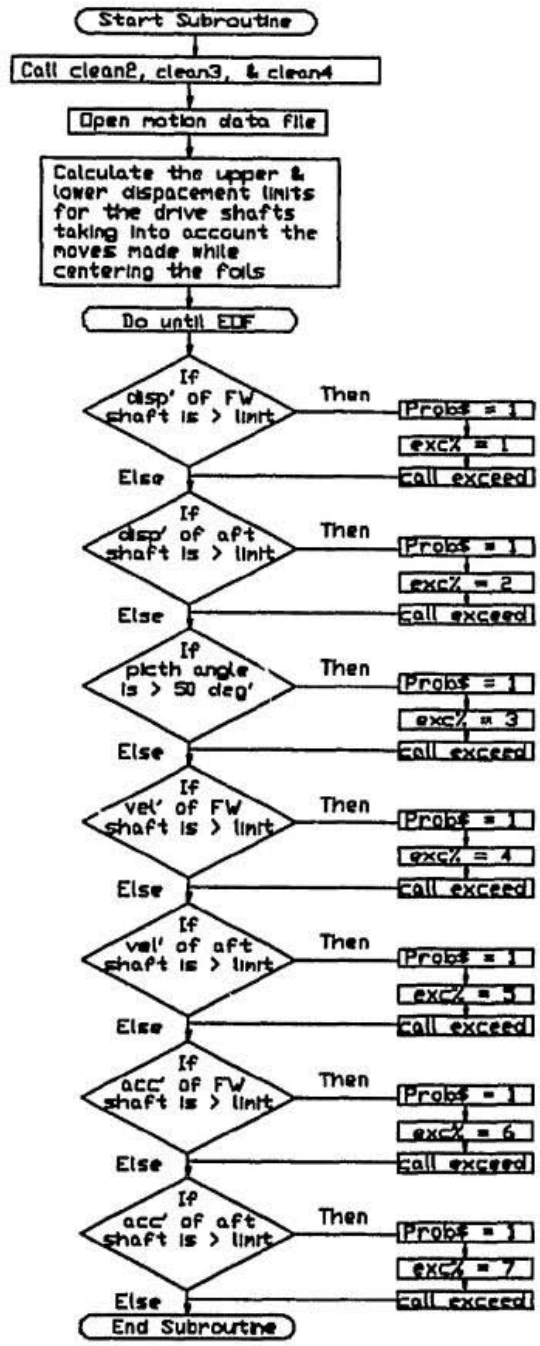
Start Subroutine
Call clean2, clean3, & clean4
Open motion data file
Calculate the upper & lower dispacement limits for the drive shafts taking into account the moves made while centering the foils
Do until EOF
If disp' of FW shaft is > limit
Then
Prob$ = 1
exc% = 1
Else
Call exceed
If disp' of aft shaft is > limit
Then
Prob$ = 1
exc% = 2
Else
Call exceed
If pitch angle is > 50 deg'
Then
Prob$ = 1
exc% = 3
Else
Call exceed
If vel' of FW shaft is > limit
Then
Prob$ = 1
exc% = 4
Else
Call exceed
If vel' of aft shaft is > limit
Then
Prob$ = 1
exc% = 5
Else
Call exceed
If acc' of FW shaft is > limit
Then
Prob$ = 1
exc% = 6
Else
Call exceed
If acc' of aft shaft is > limit
Then
Prob$ = 1
exc% = 7
Else
Call exceed
End Subroutine

CHECK

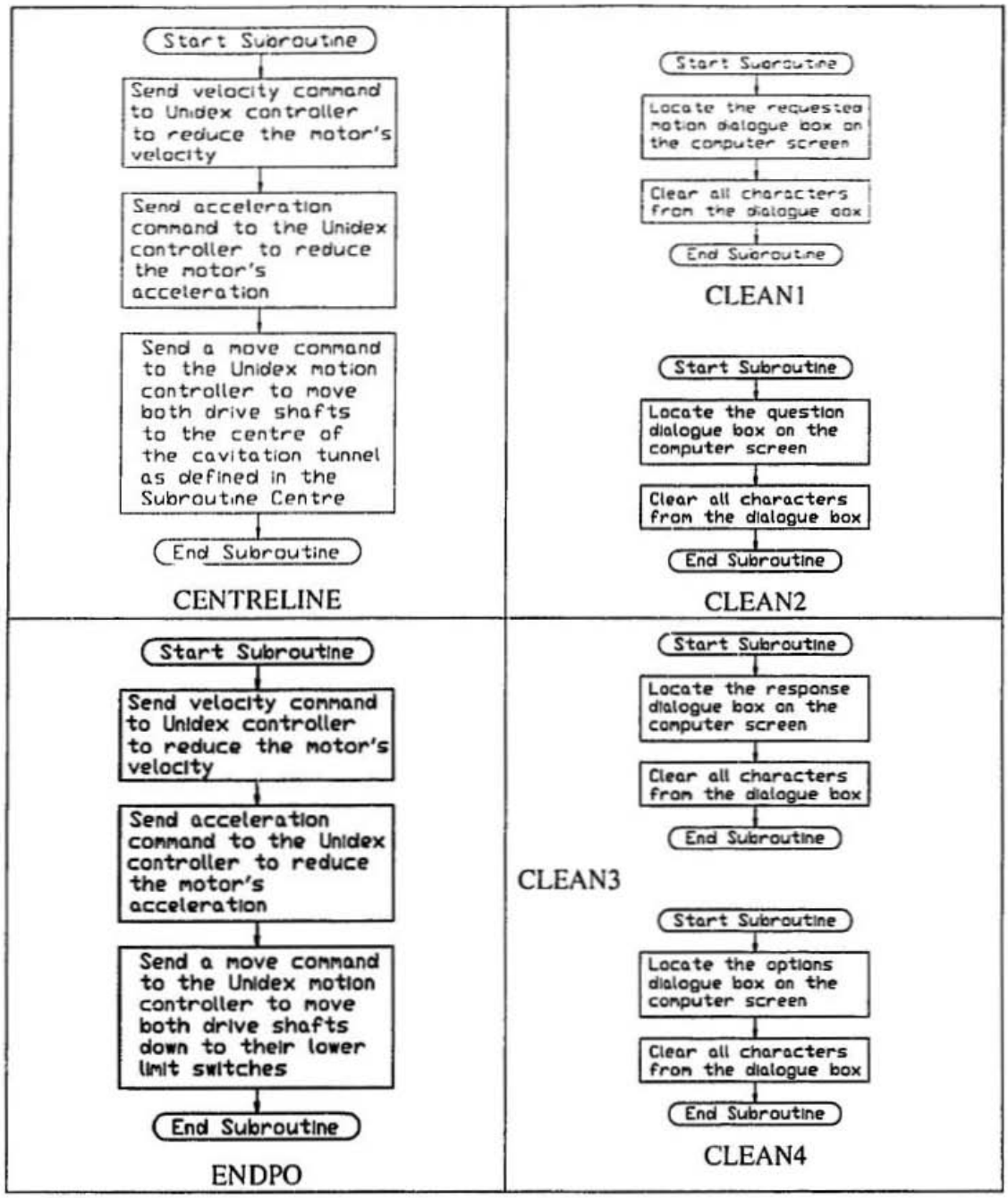
Start Subroutine
Send velocity command to Unidex controller to reduce the motor's velocity
Send acceleration command to the Unidex controller to reduce the motor's acceleration
Send a move command to the Unidex motion controller to move both drive shafts to the centre of the cavitation tunnel as defined in the Subroutine Centre
End Subroutine
CENTRELINE
Start Subroutine
Locate the requested motion dialogue box on the computer screen
Clear all characters from the dialogue box
End Subroutine
CLEAN1
Start Subroutine
Locate the question dialogue box on the computer screen
Clear all characters from the dialogue box
End Subroutine
CLEAN2
Start Subroutine
Send velocity command to Unidex controller to reduce the motor's velocity
Send acceleration command to the Unidex controller to reduce the motor's acceleration
Send a move command to the Unidex motion controller to move both drive shafts down to their lower limit switches
End Subroutine
ENDPO
Start Subroutine
Locate the response dialogue box on the computer screen
Clear all characters from the dialogue box
End Subroutine
CLEAN3
Start Subroutine
Locate the options dialogue box on the computer screen
Clear all characters from the dialogue box
End Subroutine
CLEAN4

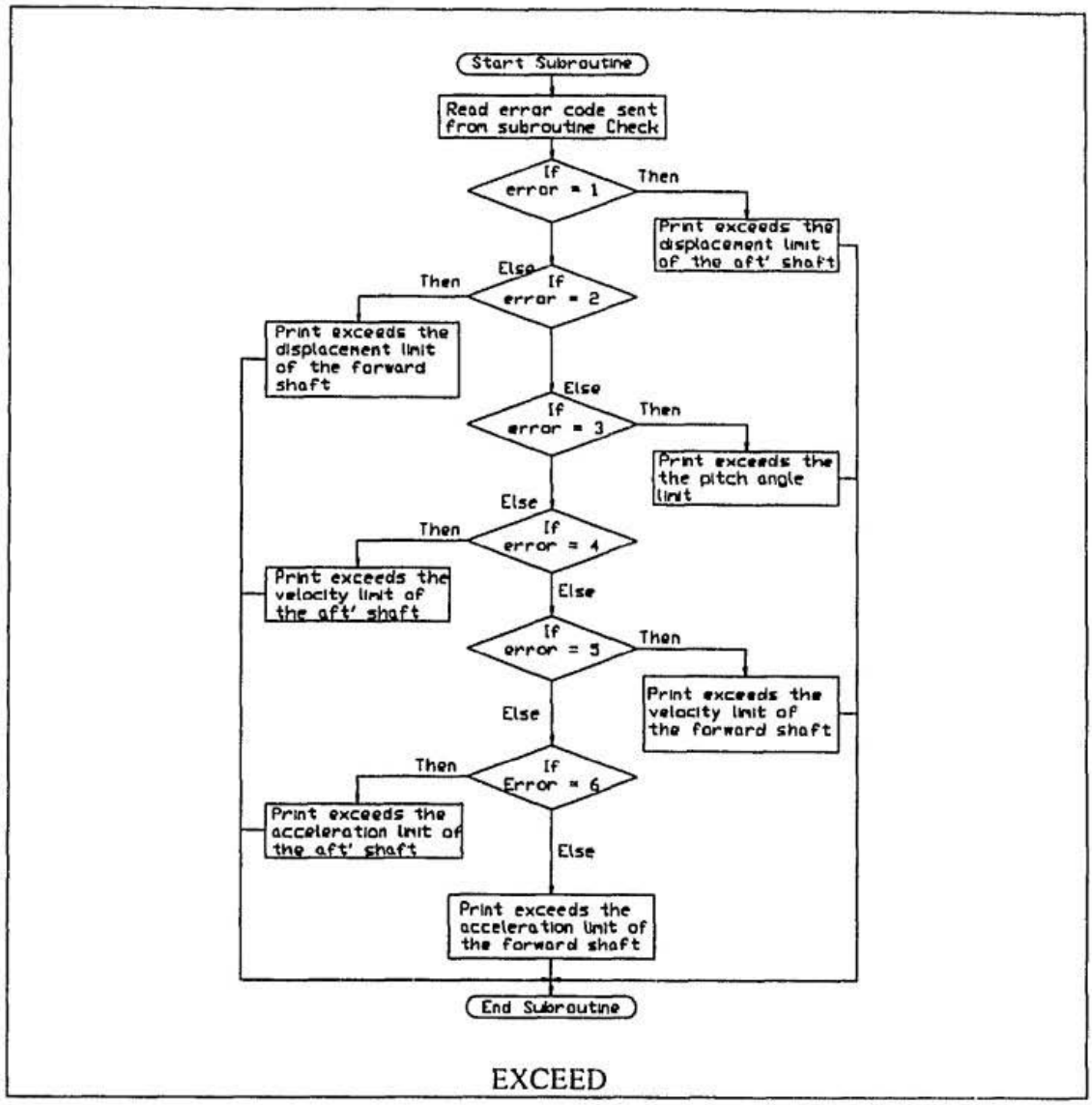
Start Subroutine
Read error code sent from subroutine Check
If error = 1
Then
Print exceeds the displacement limit of the aft' shaft
Else
If error = 2
Then
Print exceeds the displacement limit of the forward shaft
Else
If error = 3
Then
Print exceeds the the pitch angle limit
Else
If error = 4
Then
Print exceeds the velocity limit of the aft' shaft
Else
If error = 5
Then
Print exceeds the velocity limit of the forward shaft
Else
If Error = 6
Then
Print exceeds the acceleration limit of the aft' shaft
Else
Print exceeds the acceleration limit of the forward shaft
End Subroutine

EXCEED

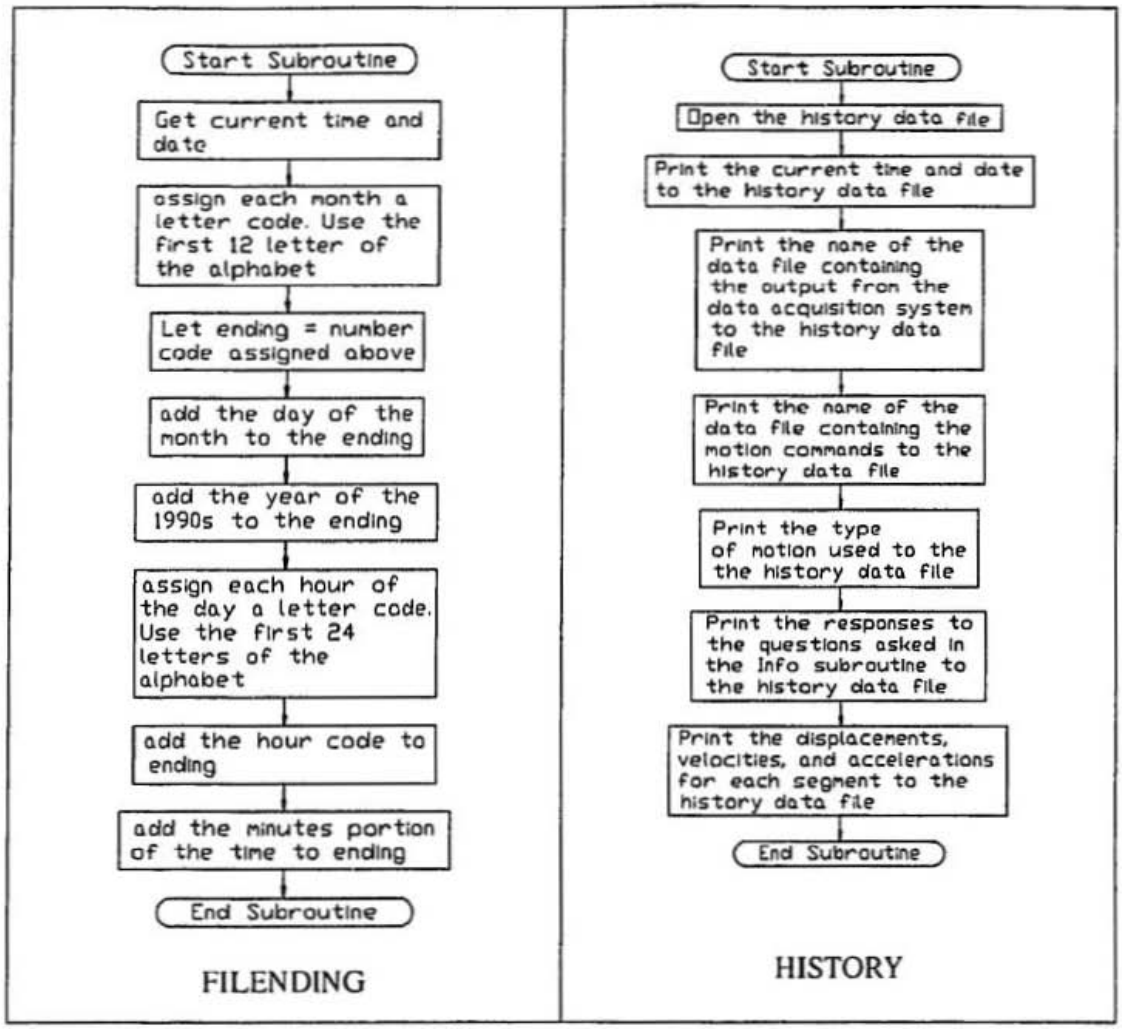
Start Subroutine
Get current time and date
assign each month a letter code. Use the first 12 letter of the alphabet
Let ending = number code assigned above
add the day of the month to the ending
add the year of the 1990s to the ending
assign each hour of the day a letter code. Use the first 24 letters of the alphabet
add the hour code to ending
add the minutes portion of the time to ending
End Subroutine
FILENDING
Start Subroutine
Open the history data file
Print the current time and date to the history data file
Print the name of the data file containing the output fron the data acquisition system to the history data file
Print the name of the data file containing the motion commands to the history data file
Print the type of motion used to the the history data file
Print the responses to the questions asked in the Info subroutine to the history data file
Print the displacements, velocities, and accelerations for each segment to the history data file
End Subroutine
HISTORY

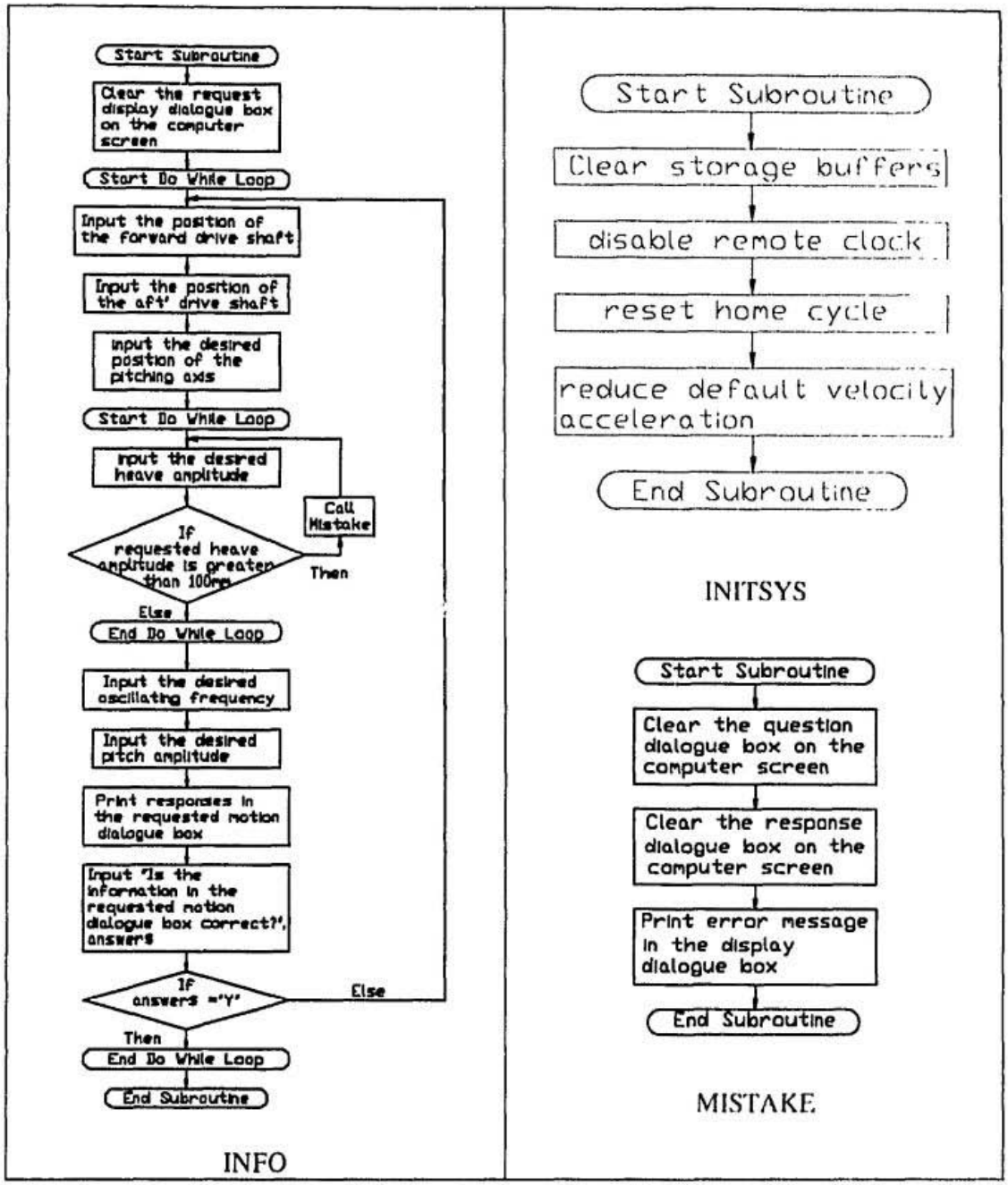
Start Subroutine
Clear the request display dialogue box on the computer screen
Start Do While Loop
Input the position of the forward drive shaft
Input the position of the aft' drive shaft
Input the desired position of the pitching axis
Start Do While Loop
Input the desired heave amplitude
Call Mistake
If requested heave amplitude is greater than 100mm
Then
Else
End Do While Loop
Input the desired oscillating frequency
Input the desired pitch amplitude
Print responses in the requested motion dialogue box
Input "Is the information in the requested motion dialogue box correct?", answers
If answers ="Y"
Else
Then
End Do While Loop
End Subroutine
INFO
Start Subroutine
Clear storage buffers
disable remote clock
reset home cycle
reduce default velocity acceleration
End Subroutine
INITSYS
Start Subroutine
Clear the question dialogue box on the computer screen
Clear the response dialogue box on the computer screen
Print error message in the display dialogue box
End Subroutine
MISTAKE

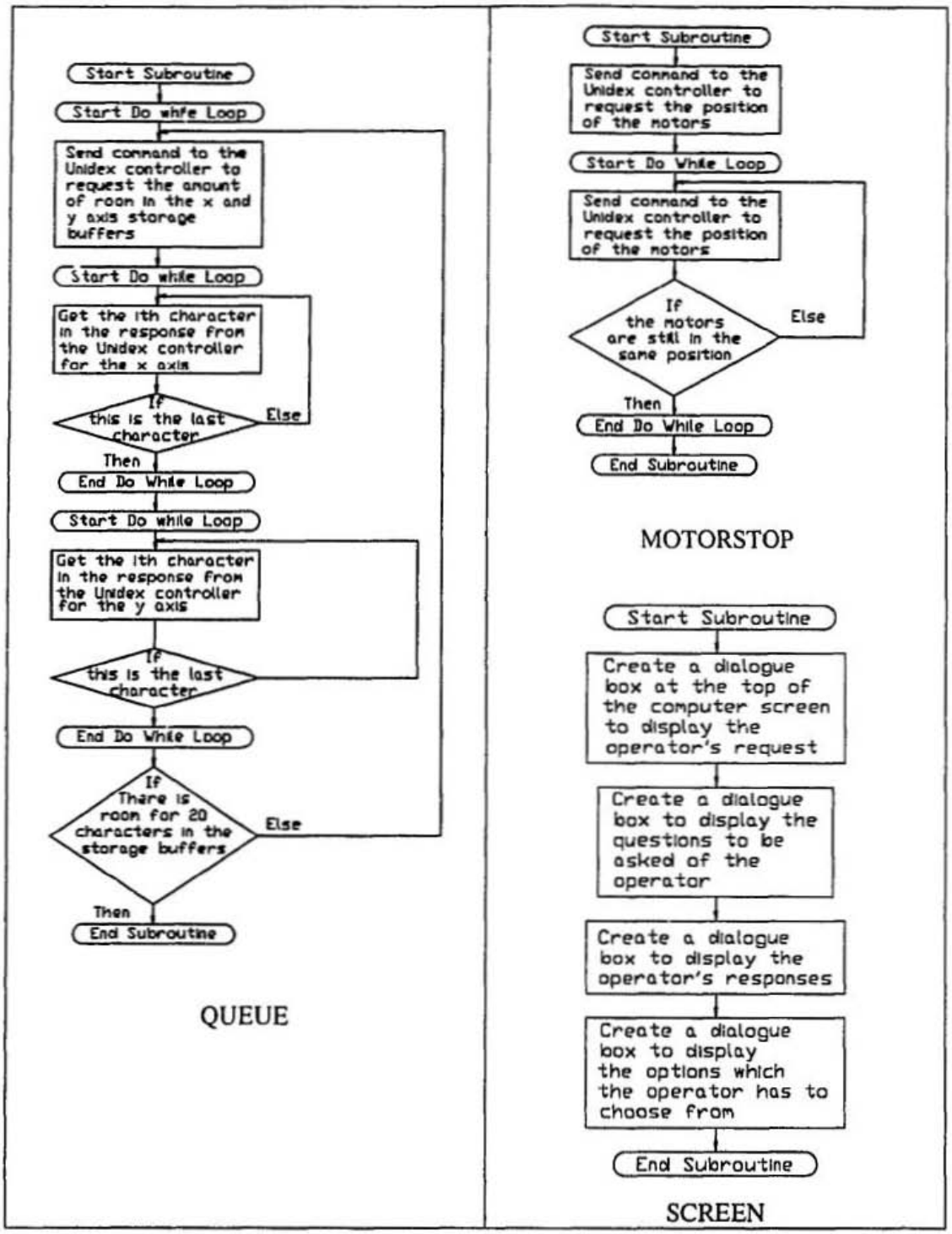
Start Subroutine
Start Do while Loop
Send command to the Unidex controller to request the amount of room in the x and y axis storage buffers
Start Do while Loop
Get the ith character in the response from the Unidex controller for the x axis
If this is the last character
Else
Then
End Do While Loop
Start Do while Loop
Get the ith character in the response from the Unidex controller for the y axis
If this is the last character
End Do While Loop
If There is room for 20 characters in the storage buffers
Else
Then
End Subroutine
QUEUE
Start Subroutine
Send command to the Unidex controller to request the position of the motors
Start Do While Loop
Send command to the Unidex controller to request the position of the motors
If the motors are still in the same position
Else
Then
End Do While Loop
End Subroutine
MOTORSTOP
Start Subroutine
Create a dialogue box at the top of the computer screen to display the operator's request
Create a dialogue box to display the questions to be asked of the operator
Create a dialogue box to display the operator's responses
Create a dialogue box to display the options which the operator has to choose from
End Subroutine
SCREEN

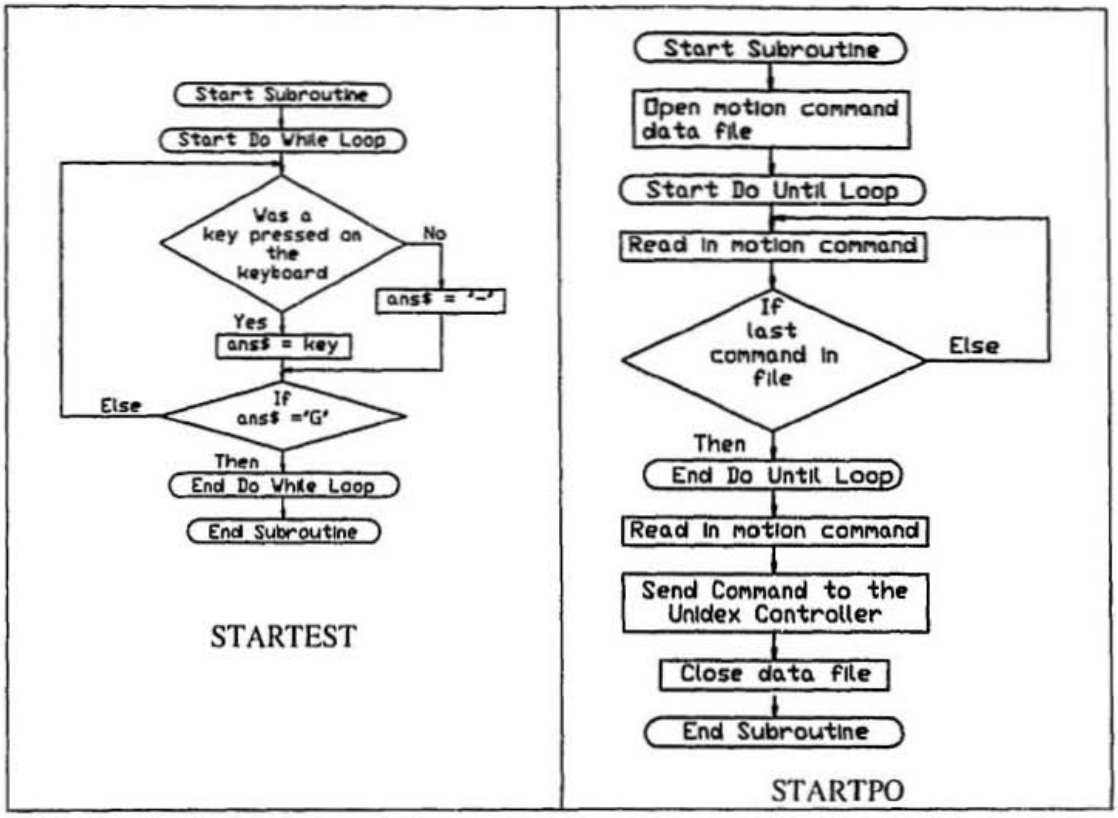
Start Subroutine
Start Do While Loop
Was a key pressed on the keyboard
No
ans$ = '-'
Yes
ans$ = key
If ans$ ='G'
Else
Then
End Do While Loop
End Subroutine
STARTEST
Start Subroutine
Open motion command data file
Start Do Until Loop
Read in motion command
If last command in file
Else
Then
End Do Until Loop
Read in motion command
Send Command to the Unidex Controller
Close data file
End Subroutine
STARTPO

Appendix D
Design Calculations

Development of Equation 4.5

Equation 4.5 is used to account for the errors in the obtained pitch angle amplitude due to the link in the forward drive shaft. Figure D.1 shows the layout of the lower assembly of the dynamometer.

AB = 40mm
= distance between drive shafts

BD = 131.5mm
= length of the link in the forward drive shaft.

α_d = desired pitch angle amplitude

α_o = the obtained pitch angle amplitude

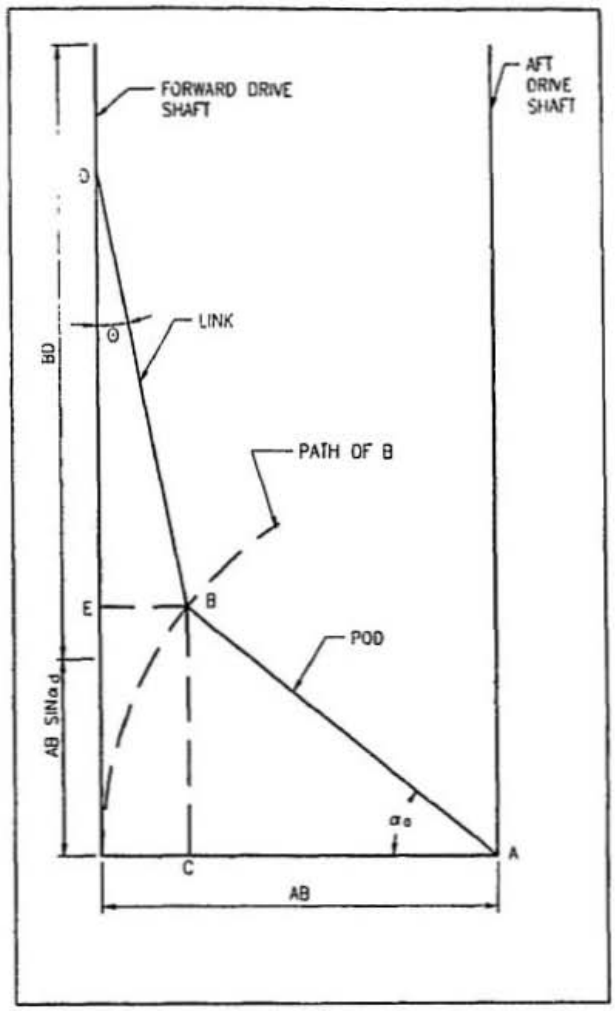

Figure D.1

Consider the movement of the link BD

Y_{BL} = the vertical component of the motion of point B on the link

$= AB\sin\alpha_d + BD - BD\cos\theta$ (D.1)

X_{BL} = the horizontal component of the motion of point B on the link

$= BD\sin\theta$ (D.2)

Consider the movement of the link AB

Y_{BP} = the vertical component of the motion of point B on the pod

$= AB\sin\alpha_o$ (D.3)

X_{BP} = the horizontal component of the motion of point B on the pod

$$= AB - AD\cos\alpha_o \quad (D4)$$

The point B on the pod and on the link are coincident. Therefore,

$$Y_{BL} = Y_{BP} \quad \text{and} \quad X_{BL} = X_{BP}$$

Equating Equations (D.1) and (D.3) gives

$$AB\sin\alpha_d + BD - BD\cos\theta = AB\sin\alpha_o \quad (D.5)$$

Equating Equations (D.2) and (D.4) gives

$$BD\sin\theta = AB - AD\cos\alpha_o \quad (D.6)$$

Solving Equation (D.6) for θ and Equation (D.5) for α_d gives

$$\theta = \arcsin[(AB - AD\cos\alpha)/BD] \quad (D.7)$$

$$\alpha_d = \arcsin[(AB\sin\alpha_o - BD + BD\cos\theta)/AB] \quad (D.8)$$

Now that θ and α_d are defined in terms of known variables the desired pitch angle amplitude can be fed into Equation (D.8) as α_o and angle α_d can be calculated and fed into the motion program to develop a motion with a pitch angle amplitude of α_o.

Estimation of the expected loads on the strain gauged section and load cells

The following two approaches were used to determine the loads:

1) work back from the motors to determine the maximum forces which the motors can exert on the drive shaft.

2) look at the foils to determine the maximum expected thrust loads from the foils.

Approach 1

Motor parameters:

peak torque 2.52Nm

continuous torque	0.35Nm
continuous power output	146 watts

Note:

- the motors have a 10:1 gear box with an efficiency of 90%

- the power from the motors will be transmitted to the drive shafts through 2in (50.8mm) diameter pulleys. For these calculations it will be assumed that there is no other efficiency looses in the system besides the gear box. This will result in over estimating the loads which the motors can transmit to the foils.

The peak force transferred to the drive shaft from the motors is given by Equation D.9.

$$F_{pm} = (T_p * R_g \eta_g)/R \qquad \text{(Siegel 1965)} \qquad \text{(D.9)}$$

Where:

T_p = motor peak torque
R_g = gear box ratio
η_g = efficiency of gear box
R = Radius of pulley

$F_{pm} = (2.52)(10)(0.9)/(0.0254)$
$= 893N$
$= 91Kg$
$= 201lbs$

The continuous force transferred to the drive shaft from the motors is given by

$F_{cm} = (T_c * R_g \eta_g)/R$
$= (0.35)(10)(0.9)/(0.0254)$
$= 12.4N$
$= 13Kg$
$= 28lbs$

The maximum force transmitted to the each drive shafts will be 893N. However, the maximum continuous force transmitted will be 124N.

Approach 2

The thrust developed by an oscillating foil is given by Equation D.10 (van Manen et al.1988)

$$\text{Thrust} = 1/2 C_t \rho U_t^2 S \qquad (D.10)$$

Where:

C_t = the thrust coefficient of the foils
ρ = the density of the water in the tunnel
U_t = the water flow velocity in the tunnel
S = the surface area of the test foils

The power absorbed by the foils is given by Equation (D.11)

$$\text{Power} = F U_t/\eta \qquad \text{(Beer and Johnston 1977b)} \qquad (D.11)$$

Where:

F = force
U_t = velocity of the water flowing pass the foils
η = foil propulsive efficiency

Consider the forces produced by a small test foil and a large test foil.

Foil 1 Parameters:

Aspect Ratio	= 8
span	= 0.2m
heave amplitude	= 0.1m
plan from area	= $0.005m^2$
chord	= 0.025m

Foil 2 Parameters:

Aspect Ratio	= 4
span	= 0.2m
heave amplitude	= 0.1m
plan from area	= $0.01m^2$
chord	= 0.05m

Consider two different test conditions (See Bose and Lien 1989). Note, that the coefficients given in Bose and Lien 1989 are based on mean values found from averaging the unsteady sinusoidal loads on an oscillating foil similar to the ones that will be tested with this dynamometer. They already include the effects of lift and added virtual mass. It would have been preferable to use maximum values. However, this was not possible since data for the maximum values were not available.

Condition 1) Maximum efficiency (η) of 80% for:

advance ratio (J)	= 7
induced angle of attack (θ_a)	= 20°
pitch amplitude	= 1.25°
thrust coefficient (C_t)	= 0.5
velocity of tunnel water (U_t)	= 5 m/s

Condition 2) Maximum efficiency (η) of 80% for:

advance ratio (J)	= 2.5
induced angle of attack (θ_a)	= 20°
pitch amplitude	= 50°
thrust coefficient (C_t)	= 1.0
velocity of tunnel water (U_t)	= 5 m/s

Note, the maximum expected tunnel velocity is 3m/s. A velocity of 5m/s was used in these calculations as an extreme case.

Look at foil 1 condition 1

The advance ratio of an oscillating foil is given by Equation D.12 (See Bose and Lien 1989).

$$J = \text{advance ratio} = \pi U_t/(\omega h) \qquad (D.12)$$

Where:

U_t = velocity of water passing the test foil
ω = oscillating frequency of the foil
h = heave amplitude of the test foil

$\omega = \pi(5)/(7*0.1)$
$= 22.4$radians/second
$= 3.6$rps

For an oscillating motion defined by Equation D.13 the maximum heave velocity and acceleration is given by equations D.14 and D.15 respectively.

$$\text{heave} = a\sin(\omega t) \quad \text{(D.13)}$$

$$\text{velocity} = a\omega\cos(\omega t) = 0.1(22.4)(1) = 2.2\text{m/s} \quad \text{(D.14)}$$

$$\text{acceleration} = -a\omega^2 \sin(\omega t) = -0.1(22.4)^2(1) = 50.2\text{m/s}^2 \quad \text{(D.15)}$$

$\text{Thrust} = 1/2C_t\rho U_t^2 A$
$= 0.5(0.5)(1000)U_t^2(0.005)$
$= 1.25U^2$ N

Look at foil 1 condition 2

$\omega = \pi(5)/(2.5*0.1)$
$= 62.8$radians/second
$= 10$rps

$\text{velocity} = a\omega\cos(\omega t) = 0.1(62.8)(1) = 6.3\text{m/s}$

$\text{acceleration} = -a\omega^2 \sin(\omega t) = -0.1(62.8)^2(1) = 394.4\text{m/s}^2$

$\text{Thrust} = 1/2C_t\rho U_t^2 A$
$= 0.5(1)(1000)U_t^2(0.005)$
$= 2.5U^2$ N

Look at foil 2 condition 1

$\omega = \pi(5)/(7*0.1)$
$= 22.4$radians/second
$= 3.6$rps

$\text{velocity} = a\omega\cos(\omega t) = 0.1(22.4)(1) = 2.2\text{m/s}$

$\text{acceleration} = -a\omega^2 \sin(\omega t) = -0.1(22.4)^2(1) = 50.2\text{m/s}^2$

Thrust = $1/2C_t\rho U_t^2A$
$= 0.5(0.5)(1000)U_t^2(0.005)$
$= 2.5U^2$ N

Look at foil 2 condition 2

$\omega = \pi(5)/(2.5*0.1)$
$= 62.8$radians/second
$= 10$rps

velocity = $a\omega\cos(\omega t) = 0.1(62.8)(1) = 6.3$m/s

acceleration = $-a\omega^2 \sin(\omega t) = -0.1(62.8)^2(1) = 394.4$m/s^2

Thrust = $1/2C_t\rho U_t^2A$
$= 0.5(1)(1000)U_t^2(0.01)$
$= 5U^2$ N

Based on the above calculations the power required to drive the foils under the different conditions as defined by Equation D.11 can be rewritten as follows.

Power (W) = U_tT/η

$= Ku_t^3/0.8$ where: K=1.25, 2.5, and 5 (D.16)

and the forces developed in the drive shafts can be defined as

Force (F) = W/V_s (D.17)

The power required to drive the foils and the axial forces developed in the drive shafts for the different test conditions are listed in Table D.1.

Table D.1

	Power (W)				Force (Kg)			
U_t m/s	foil 1 cond' 1	foil 1 cond' 2	foil 2 cond' 1	foil 2 cond' 2	foil 1 cond' 1	foil 1 cond' 2	foil 2 cond' 1	foil 2 cond' 2
1	1.56	3.1	3.1	6.25	**1.56**	**3.1**	**3.1**	**6.25**
2	12.5	25.0	25.0	50.0	**6.25**	**12.5**	**12.5**	**25.0**
3	42.2	84.4	84.4	168.8	**14.1**	**28.1**	**28.1**	56.3
4	100.0	200.0	200.0	400.0	25.0	50.0	50.0	100.0
5	195.3	390.6	390.6	781.2	39.1	78.1	78.1	156.2

Note, that due to the limitation of the motors only the bolded forces are obtainable. From Table D.1 we see that the maximum value of U_t for which all the test conditions are possible is 2m/s.

Development of spread sheet to estimate loads

Considering both the forces produced by a typical test foil and the limitations of the motors a spread sheet can be developed to determine the expected loads on the drive shafts and strain gauged section.

Look at a typical test foil with:

aspect ration = 6.0
span = 0.1m
chord (root) = 0.333m
maximum heave amplitude = 0.1m
surface area = $0.0333m^2$

Typical test conditions:

velocity of water in tunnel varies from 0 to 3m/s

maximum heave amplitude is 0.1m

maximum heave acceleration = F_{max}/m

$= 2*12.6/5 = 5.0m/s^2$

where:

m = mass of oscillating components and is assumed to be 5Kg. Note, there are two motors carrying the 5KG load and that it is assumed that each motor will carry half the load.

The Dynamic load (F_d)

The mean dynamic loads produced by the foils can be calculated using the Equations D.10, 18, and 19.

Mean Power = $W = Tu_t/\eta$ (Beer and Johnston 1977b) (D.18)

Mean Force = W/V_t (Vertically along drive shaft) (Beer and Johnston 1977b) (D.19)

The mean thrust developed by the foils can be estimated using the Equation D.10 and data from (C_t and η values) Bose and Lien 1989. Note that the coefficients taken from (Bose and Lien 1989) are based on mean values found from averaging the unsteady sinusoidal loads on an oscillating foil similar to the ones that will be tested with this dynamometer. They already include the effects of lift and added virtual mass.

Equations 10, 18, and 19 give the mean values of thrust, power, and axial force in the drive shafts. It would have been preferable to have estimates for the peak values, since they will impact the design of the load cells, strain gauges, and drives shaft. However, this was not possible, since data related to peak loads were not available. It should be noted, however, that the actual test condition which will be used with the dynamometer will produce loads which are lower than the test conditions used in this analysis.

Inertia Load (F_i)

The inertia load acting vertically on the drive shafts produced by the oscillating assembly are given by Equation D.20 .

Force = ma

$= m_a a_s$ (D.20)

Where:

m_a = the mass of the oscillating assembly
a_s = the acceleration of the drive shaft

The added virtual mass associate whit any body accelerating through a fluid also adds to the inertia loads. However, in this analysis these loads are included in the calculation of the thrust loads which is used in the calculation of the dynamic loads. The added virtual mass is defined in Equation D.21 and the inertia force associate with it can be calculated by multiplying the mass by the acceleration of the drive shaft.

$$\text{added virtual mass} = \pi C^2 S \rho \qquad \text{(Harvald 1983)} \qquad \text{(D.21)}$$

Where:

C = the chord length of the foil
S = the span of the foil
ρ = the density of the fluid

Total axial force in the drive shafts

The total axial force in the drive shafts is given by Equation D.22. Note that the calculated forces will be carried by two drive shafts. However, the force will not always be split evenly between the two shafts.

$$F_T = F_d + F_i \qquad \text{(D.22)}$$

The thrust and axial forces for three different water tunnel velocities (1, 2, and 3m/s) were calculated using a spread sheet based on the above equations. The results for a tunnel water velocity of 1m/s is presented in Table D.2. To save space only the 1m/s spread sheet is included, since it contains the maximum possible axial and thrust loads which can be expected.

Table D.2 Expected loads

Column 1 = advance ratio	Column 10 = thrust (N)
Column 2 = pitch angle amplitude (^{0})	Column 11 = dynamic force (N)
Column 3 = thrust coefficient	Column 12 = inertia force (N)
Column 4 = efficiency	column 13 = total axial force (N)
Column 5 = heave amplitude (m)	Column 14 = required power (W)
Column 6 = velocity of water in the tunnel (m/s)	Column 15 = possible heave accelerations (m/s^2)
Column 7 = oscillating frequency (rads/s)	Column 16 = axial forces (N)
Column 8 = heave velocity (m/s)	Column 17 = possible required power (W)
Column 9 = heave acceleration (m/s^2)	Column 18 = possible conditions for the motors

1	2	3	4	5	6	7	8	9	10	11	12	13	14	15	16	17		
2.5	50	0.85	0.83	0.2	1	6.3	1.3	7.9	28.3	27.1	39.5	66.6	83.7	N	Y	Y	N	
2.5	50	0.85	0.83	0.4	1	3.1	1.3	3.9	28.3	27.1	19.7	46.9	58.9	Y	Y	Y	Y	
2.5	50	0.85	0.83	0.6	1	2.1	1.3	2.6	28.3	27.1	13.2	40.3	50.6	Y	Y	Y	Y	
2.5	50	0.85	0.83	0.8	1	1.6	1.3	2.0	28.3	27.1	9.9	37.0	46.5	Y	Y	Y	Y	
2.5	50	0.85	0.83	1	1	1.3	1.3	1.6	28.3	27.1	7.9	35.0	44.0	Y	Y	Y	Y	
2.5	40	1.29	0.8	0.2	1	6.3	1.3	7.9	43.0	42.7	39.5	82.2	103.3	N	Y	Y	N	
2.5	40	1.29	0.8	0.4	1	3.1	1.3	3.9	43.0	42.7	19.7	62.5	78.5	Y	Y	Y	Y	
2.5	40	1.29	0.8	0.6	1	2.1	1.3	2.6	43.0	42.7	13.2	55.9	70.2	Y	Y	Y	Y	
2.5	40	1.29	0.8	0.8	1	1.6	1.3	2.0	43.0	42.7	9.9	52.6	66.1	Y	Y	Y	Y	
2.5	40	1.29	0.8	1	1	1.3	1.3	1.6	43.0	42.7	7.9	50.6	63.6	Y	Y	Y	Y	
2.5	30	1.52	0.78	0.2	1	6.3	1.3	7.9	50.6	51.6	39.5	91.1	114.5	N	Y	Y	N	
2.5	30	1.52	0.78	0.4	1	3.1	1.3	3.9	50.6	51.6	19.7	71.4	89.7	Y	Y	Y	Y	
2.5	30	1.52	0.78	0.6	1	2.1	1.3	2.6	50.6	51.6	13.2	64.8	81.4	Y	Y	Y	Y	
2.5	30	1.52	0.78	0.8	1	1.6	1.3	2.0	50.6	51.6	9.9	61.5	77.3	Y	Y	Y	Y	
2.5	30	1.52	0.78	1	1	1.3	1.3	1.6	50.6	51.6	7.9	59.5	74.8	Y	Y	Y	Y	
2.5	20	2	0.74	0.2	1	6.3	1.3	7.9	66.6	71.6	39.5	111.1	139.6	N	Y	Y	N	
2.5	20	2	0.74	0.4	1	3.1	1.3	3.9	66.6	71.6	19.7	91.4	114.8	Y	Y	Y	Y	max
2.5	20	2	0.74	0.6	1	2.1	1.3	2.6	66.6	71.6	13.2	84.8	106.5	Y	Y	Y	Y	
2.5	20	2	0.74	0.8	1	1.6	1.3	2.0	66.6	71.6	9.9	81.5	102.4	Y	Y	Y	Y	
2.5	20	2	0.74	1	1	1.3	1.3	1.6	66.6	71.6	7.9	79.5	99.9	Y	Y	Y	Y	
3	50	0.23	0.86	0.2	1	5.2	1.0	5.5	7.7	8.5	27.4	35.9	37.6	N	Y	Y	N	
3	50	0.23	0.86	0.4	1	2.6	1.0	2.7	7.7	8.5	13.7	22.2	23.3	Y	Y	Y	Y	
3	50	0.23	0.86	0.6	1	1.7	1.0	1.8	7.7	8.5	9.1	17.6	18.5	Y	Y	Y	Y	
3	50	0.23	0.86	0.8	1	1.3	1.0	1.4	7.7	8.5	6.9	15.4	16.1	Y	Y	Y	Y	
3	50	0.23	0.86	1	1	1.0	1.0	1.1	7.7	8.5	5.5	14.0	14.6	Y	Y	Y	Y	
3	40	0.58	0.86	0.2	1	5.2	1.0	5.5	19.3	21.4	27.4	48.9	51.2	N	Y	Y	N	
3	40	0.58	0.86	0.4	1	2.6	1.0	2.7	19.3	21.4	13.7	35.2	36.8	Y	Y	Y	Y	
3	40	0.58	0.86	0.6	1	1.7	1.0	1.8	19.3	21.4	9.1	30.6	32.0	Y	Y	Y	Y	
3	40	0.58	0.86	0.8	1	1.3	1.0	1.4	19.3	21.4	6.9	28.3	29.6	Y	Y	Y	Y	
3	40	0.58	0.86	1	1	1.0	1.0	1.1	19.3	21.4	5.5	26.9	28.2	Y	Y	Y	Y	
3	30	0.92	0.82	0.2	1	5.2	1.0	5.5	30.6	35.7	27.4	63.1	66.1	N	Y	Y	N	
3	30	0.92	0.82	0.4	1	2.6	1.0	2.7	30.6	35.7	13.7	49.4	51.7	Y	Y	Y	Y	
3	30	0.92	0.82	0.6	1	1.7	1.0	1.8	30.6	35.7	9.1	44.8	46.9	Y	Y	Y	Y	
3	30	0.92	0.82	0.8	1	1.3	1.0	1.4	30.6	35.7	6.9	42.5	44.5	Y	Y	Y	Y	
3	30	0.92	0.82	1	1	1.0	1.0	1.1	30.6	35.7	5.5	41.2	43.1	Y	Y	Y	Y	
3	20	1.27	0.79	0.2	1	5.2	1.0	5.5	42.3	51.1	27.4	78.5	82.2	N	Y	Y	N	
3	20	1.27	0.79	0.4	1	2.6	1.0	2.7	42.3	51.1	13.7	64.8	67.9	Y	Y	Y	Y	
3	20	1.27	0.79	0.6	1	1.7	1.0	1.8	42.3	51.1	9.1	60.3	63.1	Y	Y	Y	Y	
3	20	1.27	0.79	0.8	1	1.3	1.0	1.4	42.3	51.1	6.9	58.0	60.7	Y	Y	Y	Y	
3	20	1.27	0.79	1	1	1.0	1.0	1.1	42.3	51.1	5.5	56.6	59.3	Y	Y	Y	Y	
4	40	0.12	0.84	0.2	1	3.9	0.8	3.1	4.0	6.1	15.4	21.5	16.9	Y	Y	Y	Y	

Table D.2 Continued

4	40	0.12	0.84	0.4	1	2.0	0.8	1.5	4.0	6.1	7.7	13.8	10.8	Y	Y	Y	Y
4	40	0.12	0.84	0.6	1	1.3	0.8	1.0	4.0	6.1	5.1	11.2	8.8	Y	Y	Y	Y
4	40	0.12	0.84	0.8	1	1.0	0.8	0.8	4.0	6.1	3.9	9.9	7.8	Y	Y	Y	Y
4	40	0.12	0.84	1	1	0.8	0.8	0.6	4.0	6.1	3.1	9.1	7.2	Y	Y	Y	Y
4	30	0.37	0.87	0.2	1	3.9	0.8	3.1	12.3	18.0	15.4	33.5	26.3	Y	Y	Y	Y
4	30	0.37	0.87	0.4	1	2.0	0.8	1.5	12.3	18.0	7.7	25.7	20.2	Y	Y	Y	Y
4	30	0.37	0.87	0.6	1	1.3	0.8	1.0	12.3	18.0	5.1	23.2	18.2	Y	Y	Y	Y
4	30	0.37	0.87	0.8	1	1.0	0.8	0.8	12.3	18.0	3.9	21.9	17.2	Y	Y	Y	Y
4	30	0.37	0.87	1	1	0.8	0.8	0.6	12.3	18.0	3.1	21.1	16.6	Y	Y	Y	Y
4	20	0.65	0.84	0.2	1	3.9	0.8	3.1	21.6	32.8	15.4	48.2	37.9	Y	Y	Y	Y
4	20	0.65	0.84	0.4	1	2.0	0.8	1.5	21.6	32.8	7.7	40.5	31.8	Y	Y	Y	Y
4	20	0.65	0.84	0.6	1	1.3	0.8	1.0	21.6	32.8	5.1	37.9	29.8	Y	Y	Y	Y
4	20	0.65	0.84	0.8	1	1.0	0.8	0.8	21.6	32.8	3.9	36.7	28.8	Y	Y	Y	Y
4	20	0.65	0.84	1	1	0.8	0.8	0.6	21.6	32.8	3.1	35.9	28.2	Y	Y	Y	Y
5	30	0.08	0.86	0.2	1	3.1	0.6	2.0	2.7	4.9	9.9	14.8	9.3	Y	Y	Y	Y
5	30	0.08	0.86	0.4	1	1.6	0.6	1.0	2.7	4.9	4.9	9.9	6.2	Y	Y	Y	Y
5	30	0.08	0.86	0.6	1	1.0	0.6	0.7	2.7	4.9	3.3	8.2	5.2	Y	Y	Y	Y
5	30	0.08	0.86	0.8	1	0.8	0.6	0.5	2.7	4.9	2.5	7.4	4.6	Y	Y	Y	Y
5	30	0.08	0.86	1	1	0.6	0.6	0.4	2.7	4.9	2.0	6.9	4.3	Y	Y	Y	Y
5	20	0.33	0.86	0.2	1	3.1	0.6	2.0	11.0	20.3	9.9	30.2	19.0	Y	Y	Y	Y
5	20	0.33	0.86	0.4	1	1.6	0.6	1.0	11.0	20.3	4.9	25.3	15.9	Y	Y	Y	Y
5	20	0.33	0.86	0.6	1	1.0	0.6	0.7	11.0	20.3	3.3	23.6	14.8	Y	Y	Y	Y
5	20	0.33	0.86	0.8	1	0.8	0.6	0.5	11.0	20.3	2.5	22.8	14.3	Y	Y	Y	Y
5	20	0.33	0.86	1	1	0.6	0.6	0.4	11.0	20.3	2.0	22.3	14.0	Y	Y	Y	Y
6	20	0.15	0.86	0.2	1	2.6	0.5	1.4	5.0	11.1	6.9	17.9	9.4	Y	Y	Y	Y
6	20	0.15	0.86	0.4	1	1.3	0.5	0.7	5.0	11.1	3.4	14.5	7.6	Y	Y	Y	Y
6	20	0.15	0.86	0.6	1	0.9	0.5	0.5	5.0	11.1	2.3	13.4	7.0	Y	Y	Y	Y
6	20	0.15	0.86	0.8	1	0.7	0.5	0.3	5.0	11.1	1.7	12.8	6.7	Y	Y	Y	Y
6	20	0.15	0.86	1	1	0.5	0.5	0.3	5.0	11.1	1.4	12.5	6.5	Y	Y	Y	Y
7	20	0.08	0.83	0.2	1	2.2	0.4	1.0	2.7	7.2	5.0	12.2	5.5	Y	Y	Y	Y
7	20	0.08	0.83	0.4	1	1.1	0.4	0.5	2.7	7.2	2.5	9.7	4.3	Y	Y	Y	Y
7	20	0.08	0.83	0.6	1	0.7	0.4	0.3	2.7	7.2	1.7	8.8	4.0	Y	Y	Y	Y
7	20	0.08	0.83	0.8	1	0.6	0.4	0.3	2.7	7.2	1.3	8.4	3.8	Y	Y	Y	Y
7	20	0.08	0.83	1	1	0.4	0.4	0.2	2.7	7.2	1.0	8.2	3.7	Y	Y	Y	Y

The maximum expect thrust and axial loads are 66.6N and 91.4N respectively. Note, that the axial load is going to be carried by two drive shafts.

Sizing the drive shafts

The dynamometer was designed to have hollow drive shafts but, hollow shafting could not be obtained in time or at an acceptable cost. Note, that the calculations below were done for a 3/4in. diameter shaft, However, calculations were also done for shaft diameters of 3/8 and 1/2in.. It was found that only the 3/4in. diameter shaft could meet

the deflection criteria. Note that the 3/4in. shaft can be replaced by tubing in the future, when funds are available. The layout of the drive shaft can be seen in Figure D.2.

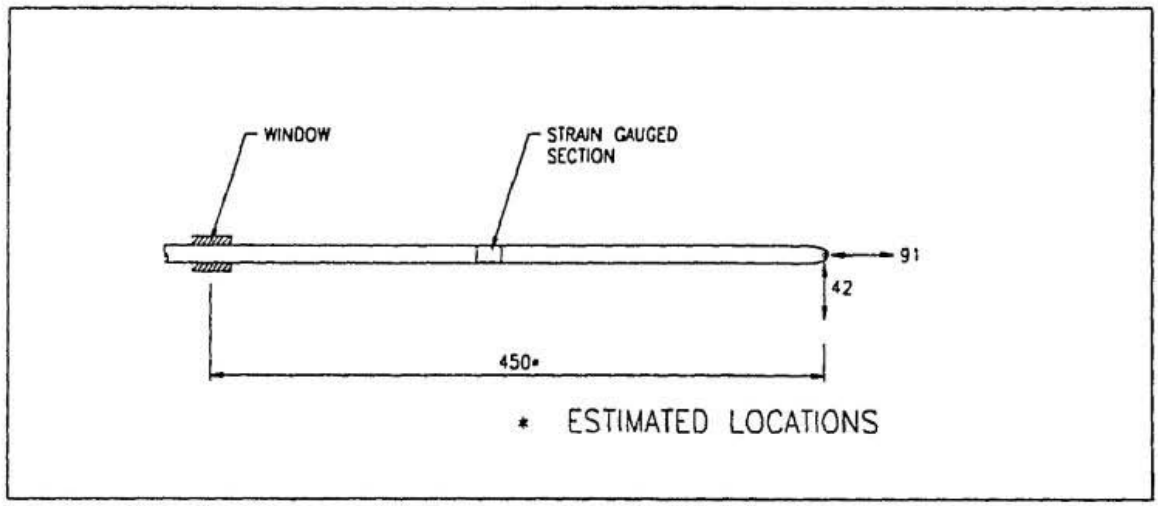

Figure D.2

The following assumptions were made in sizing the shaft:

- the bushings in the window eliminates all the bending loads from being transmitted from the portion of the drive shafts below the window to the portion of the drive shafts above the window
- the maximum load on the drive shafts occur at the maximum possible displacement of the foils. (200mm below there equilibrium position) This is not true but it ensure that the shafts will be able to carry the expected loads.
- the drive shafts have a constant cross section.

Check to ensure that the stress developed by the expected loads do not exceed the allowable stress in the lower section of the drive shafts.

Note

$P/A + MC/I \leq \sigma_{all}$ (Beer & Johnston 1981) (D.23)

Calculate the slenderness ratio to determine if this is a short or intermediate column.

Slenderness ratio = L_e/r (Beer & Johnston 1981) (D.24)

$r = \sqrt{(J_o/A)}$ (Beer & Johnston 1981) (D.25)
= radii of gyration

$Jo = 1/2\ \pi r^4$
$= 1/2\pi\ (9.525)^4$
$= 12.929 \times 10^{-9} m^4$

$A = \pi r^2$
$= \pi\ (0.009525)^2$
$= 285.02 \times 10^{-6}\ m^2$

$r = \sqrt{(12.929 \times 10^{-9}/285.02 \times 10^{-6})}$
$= 6.735 \times 10^{-3} m$

L_e = effective length
= 900mm assuming one fixed and one free end.

Slenderness ratio = $900 \times 10^{-3} / 6.735 \times 10^{-3}$
= 133

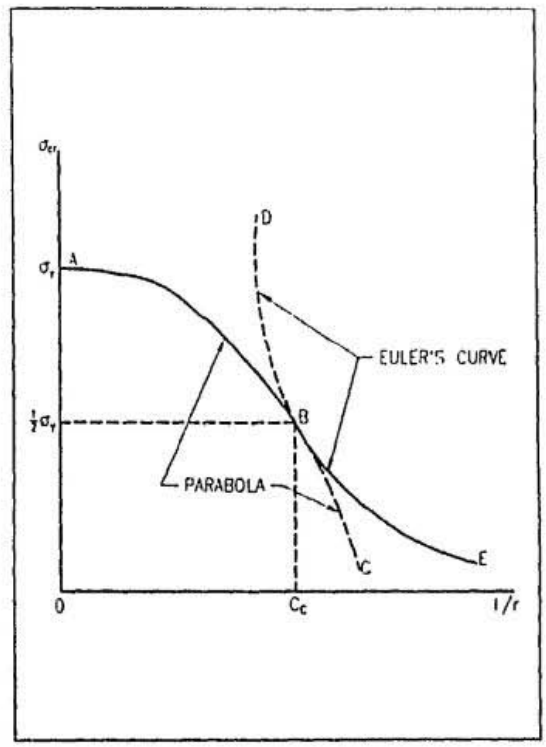

Figure D.3

To determine if the column strength will depend on the modulus of elasticity E or the yield strength σ_y the value of C_c must be calculated. See Figure D.3.

$C_c = \sqrt{(2\pi^2 E/\sigma_y)}$ (Beer and Johnston 1981) (D.26)

= 122.5

σ_y = 275MPa
E = 209GPa

Since $L_e/r < C_c < 200$ this can be considered a short column. Therefore,

σ_{all} = allowable stress
= σ_{cr}/F.S.

where:

F.S. = the safety factor = 2

$\sigma_{all} = \sigma_y/F.S.[1-1/2((L/r)/C_c)^2]$
(Bear & Johnston 1977a)
= 56.4MPa

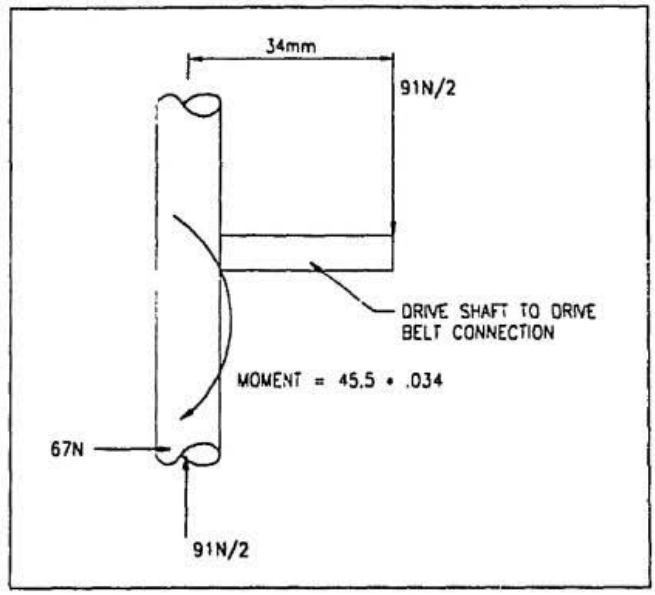

Figure D.4

Since this value is less than the allowable stress for compression, it may be used to determine the maximum permissible load using the allowable stress method of analyzing a column (Equation D.23).

$P/A + MC/I \leq \sigma_{all}$

$A = 285.02 \times 10^{-6}\ m^2$
$M = 67 * 0.450$ (worst case)
$C = 9.525 \times 10^{-3} m$
$I = 6.465 \times 10^{-9} m^4$

$P/285 \times 10^{-6} + [(67)(0.73)(9.525 \times 10^{-3})]/6.465 \times 10^{-9} \leq 83.6MPa$

Therefore,

$P \leq 3414N$

Therefore, a 3/4in. shaft can carry the expected loads in the lower portions of the drive shafts.

Check to ensure that the stresses developed by the expected loads do not exceed the allowable stress in the portions of the drive shafts above the window (See Figure D.4).

$L_e = 336mm$ assuming one fixed end : one pined end

$L_e/r = 336 \times 10^{-3}/6.735 \times 10^{-3}$
$= 50$

Since $L_e/r < C_c < 200$ this can be considered a short column. Therefore,

σ_{all} = allowable stress
$= \sigma_{cr}/F.S.$

where:

F.S. = the safety factor = 2

$\sigma_{all} = \sigma_y/F.S.[1-1/2((L/r)/C_c)^2]$ (Bear & Johnston 1977a)
$= 126MPa$

Since this value is less than the allowable stress for compression, it may be used to determine the maximum permissible load using the allowable stress method of analyzing a column (Equation D.23).

$P/A + MC/I \leq \sigma_{all}$

$A = 285.02 \times 10^{-6}\ m^2$
$M = P \times 0.340$ (worst case)
$C = 9.525 \times 10^{-3}m$
$I = 6.465 \times 10^{-9}m^4$

$P/285 \times 10^{-6} + [P(34 \times 10^{-3})(9.525 \times 10^{-3})]/6.465 \times 10^{-9} \leq 126MPa$

Therefore,

$P \leq 2351N$

Therefore, a 3/4in. shaft can carry the expected loads.

Check the angular deflection at the window port when the shaft is at its maximum deflection (See Figure D.5).

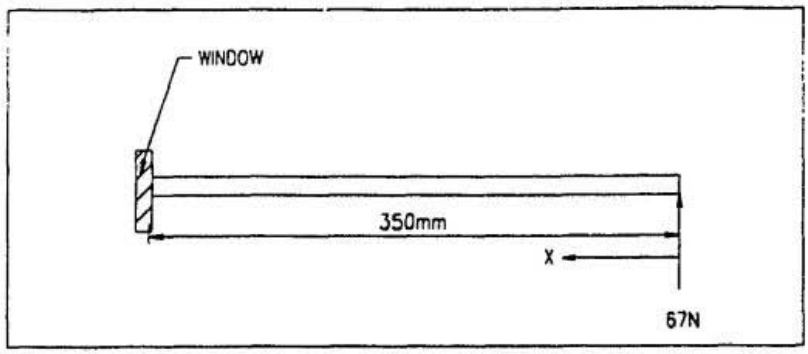

Figure D.5

The equation of the elastic curve is given by:

$$y = (P/6EI)(x^3 - 3Lx^2) \qquad \text{(Beer \& Johnston 1981)} \qquad (D.27)$$

The slope at a point x is given by

$$\theta = dy/dx = (PL^2/2EI) \qquad \text{(Beer \& Johnston 1981a)} \qquad (D.28)$$
$$= 0.003^{\circ}$$

The deflection at the free end is given by

$$y = 0.71mm$$

These deflections are not excessive and should not be a problem.

Determine the natural oscillating frequency of the drive shafts

Model the shaft as a mass at the end of a uniform conti-levered beam (Including the mass of the beam).

Natural oscillating frequency $= \omega_n = \sqrt{(3EI/(m + (33/100)m_s l^2))}$ (Steibel 1971) (D.29)

$$E = 207MPa$$

$I = 6.465 \times 10^{-9} m^4$

M_s = mass of shaft

$= \pi r^2 l \rho$ $\quad l = 150, 250$ and 350

$= 0.38$kg for upper limit of motion

$= 0.56$kg for equilibrium position

$= 0.79$kg for lower limit of foils

M = 1/2 (mass of pod & 2 foils)

$= 0.242$kg

$\omega_n = 60.2$ radians/second for upper limit of motion

$\omega_n = 26.3$ radians/second for equilibrium position

$\omega_n = 14.9$ radians/second for the lower limit of motion

Note: The natural frequencies of the drive shafts. Should be the same about an axis parallel to and perpendicular to the water flow. However, this will not actually be the case. Since the lower sections of the drive shafts are not symmetrical about both these axis and also the shafts are connected by the pod, a test should be carried out on the dynamometer to measure the natural frequencies of both shafts about both axis.

The transfer ratios for the above frequencies are:

$$T.R. = \left| 1/(1 - \omega^2/\omega_n^2) \right| \qquad (D.30)$$

Where

ω = the forcing oscillating frequency

ω_n = natural frequency of the drive shaft

For upper limit of motion and maximum forcing frequency.

$T.R. = | 1/(1-6.28^2/60.2^2| = 1.01$

For lower limit of motion and max. forcing frequency

$T.R. = | 1/(1-6.28^2/14.9^2| = 1.2$

This will be the highest transfer ratio for the drive shafts. Therefore, the desired oscillating frequencies should not cause excessive vibration. It should be noted, that the water will have a damping effect on the motion.

The following calculations were done to:

- ensure the strain gauged section would not fail under the expected loads.
- ensure that sufficient strain would be produced in the strain gauged section to allow measurement of the expected loads, and
- ensure that the natural vibrational frequency of the strain gauged section is outside the operational frequency of the dynamometer.

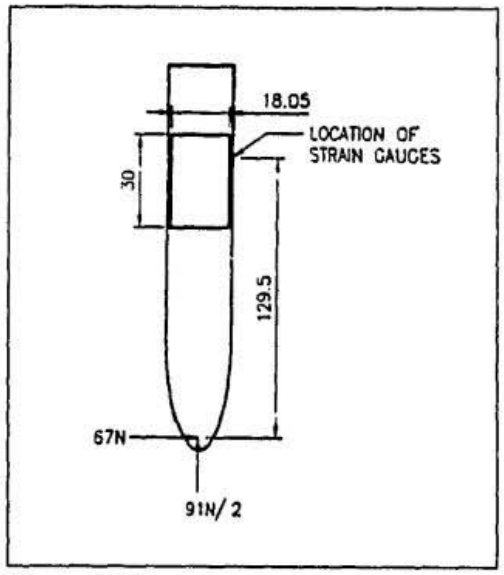

Figure D.6

Check to ensure that the reduced section will not fail

The moment (M) developed at the 1/4 length of the reduced section is given by:

$$M = F\,d \qquad \text{(Beer \& Johnston 1977a)} \qquad \text{(D.31)}$$

Where:

F = applied force
d = distance between the point of application and the location at which the moment is being calculated.

Note: If the strain gauged section is considered to have two fixed ends (See Figure D.6), then the maximum bending moment will occur at the 1/4 length of the section (Beer & Johnston 1981).

$$M = 67 * 0.1295$$
$$= 8.7 \text{ Nm}$$

This bending moment will produce tension (F_T) on the left hand member and compression (F_C) in the strain gauged section as shown in Figure D.7 and calculated below.

$$F_T = F_C = M/d$$

Where:

d = the distance between the centres of the two 1mm reduced sections

$$F_T = F_C = 8.7/0.018$$
$$= 483N$$

There will also be tension and compression loads (F_a) due to axial loading as shown in Figure D.2.

$$Fa = 91N$$

The total maximum axial load on the reduced 1mm section is (F)

$$F = 483 + 1/2\ (91)$$
$$= 528.5N$$

To account for the dynamic loading, a 1.5 load factor is applied to the local load to give.

$$F' = F * \text{load factor}$$
$$= 528.5 * 1.5$$
$$= 793\ N$$

The strain gauged section is made out of stainless steel with the following properties (Thornton and Coangelo 1985).

Yield stress = 275MPA
Young's modulus = 207GPa

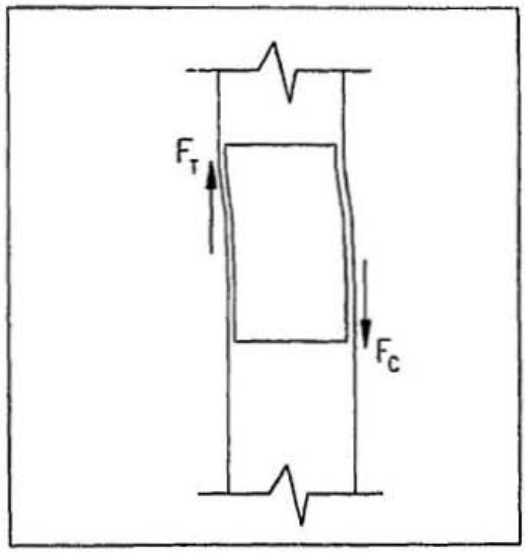

Figure D.7

The required area to prevent yielding of the strain gauged section taking into account the axial load resulting from the bending moment produced by the thrust force is

$$A = F/\sigma_y \qquad \text{(Beer \& Johnston 1981)} \qquad \text{(D.32)}$$
$$= 793/275$$
$$= 2.88mm^2$$

The area of the reduced section as designed is (A_d)

$$A_d = (12)(1)$$
$$= 12mm^2$$

Therefore, the section should not fail under the axial loads.

Check to ensure that the reduced section will not fail in buckling.

If each of the 1 mm thick reduced sections are considered as a column then by the allowable stress method of analyzing a column (Equation D.23) the critical load is:

$$P_{cr} = (\sigma_y - MC/I)A \qquad \text{(Beer \& Johnston 1981)} \qquad \text{(D.33)}$$
$$= 6.6MN$$

$$M_x = 67(0.1295)/2 = 4.32Nm$$

This is much higher than the expected axial load which will be developed in the reduced section. Therefore the reduced section will not fail.

Check to see if vibration will be a problem.

Consider the reduced section as a uniform conti-levered beam with a mass (lower drive shafts, foils and pod) at its end.

Look at only 1mm x 12 mm beam to estimate $\omega_{nx\text{-}x}$ and $\omega_{ny\text{-}y}$ for free vibration (See Figure D.8).

Natural frequency = $\omega_n = \sqrt{\ } K/M$ (Steidel 1989) (D.34)

Where:

K = F/L = stiffness
= load/unit displacement

M = Mass at the lower drive shafts, mounting pod and two foils

K_{xx} = F/L
= $12EI/L^3$ (Munday & Farrar 1979)
= $12\ (207x10^9)\ (1x10^{-12})\ /\ (30x10^{-3})^3$
= 9.2×10^4 N/m

M = 0.762 Kg

$\omega_{nx\text{-}x} = \sqrt{(\ 9.2x10^4/(0.762/2))}$
Only half the mass is carried by the aft shaft
= 491 radians/second

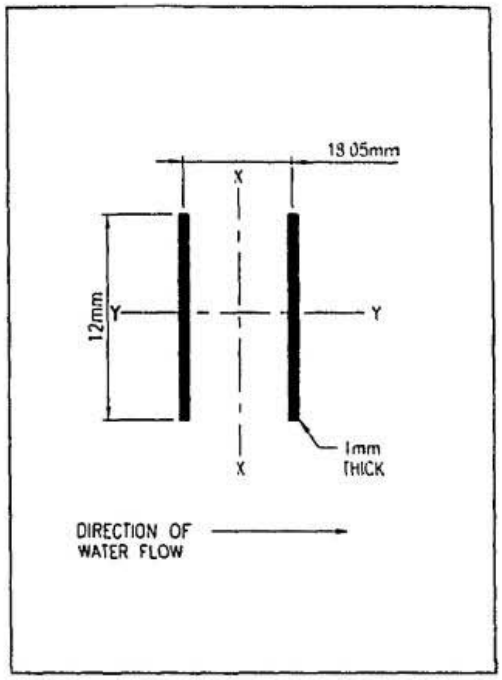

Figure D.8 Plan View of cut through strain gauged section

$K_{y\text{-}y} = FL$
$=12(207x10^9)(1.44x10^{-10})/(30x10^{-3})^3$
= 13248000

$\omega_{ny\text{-}y} = \sqrt{(13248000/\ (0.762/2))}$ = 5897 radians/second

Note: that if the stiffness of both 1 mm sections had been considered these natural frequencies would be higher. Therefore, the strain gauged section should not develop noise in the signals from the strain gauges.

Check to ensure that sufficient strain will be developed in the strain gauged section

The following analysis takes into account the lateral displacement of the strain gauged section when calculating the bending moment at the 1/4 span point of the section. The differential equation for the elastic curve is

$d^2y/dx^2 = M_x/EI$ (Munday and Farrar 1979) (D.35)

From Figures D.9 and D.10 it can be seen that

$$M_x = M - Fx \qquad \text{(Munday and Farrar 1979)} \qquad \text{(D.36)}$$

Therefore,

$$EId^2y/dx^2 = M - Fx \qquad \text{(D.37)}$$

Integrating twice with respect to x gives the elastic curve for the 1 mm thick section.

$$EIy = 1/2M_x^2 - 1/6\,Fx^3 + C_1x + C_2 \qquad \text{(D.38)}$$

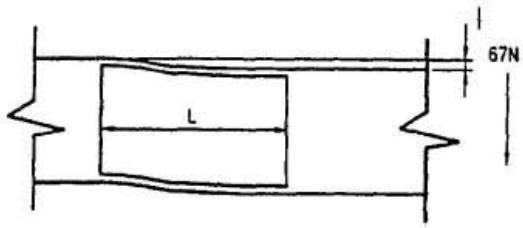

Figure D.9

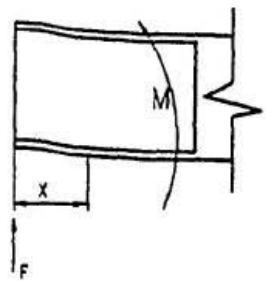

Figure D.10

Note:

At $x = L$ $\quad y = 1$

$x = 0.8L$ $\quad dy/dx = \text{slope} = 0$ $\quad C_2 = 0$

Thus equation (D.38) reduces to

$$EIy = 1/2\,M_x^2 - 1/6\,Fx^3 + C_1x \qquad \text{(D.39)}$$

At $x = l/2$ $\quad d^2y/dx^2 = 0$

Therefore,

$$M = Fl/2$$

At $x = L$ $\quad dy/dx = 0$

$$C_1 = 0$$

Thus equation (D.39) reduces to

$$EIy = 1/4\ FLx^2 - 1/6Fx^3 \qquad (D.40)$$

At $X = L$ $\quad y = l$

Thus equation (D.40) can be re-written as

$$F = 12EIl/L^3 \qquad (D.41)$$

Substituting equation (D.41) into equation (D.36) gives

$$M_x = (12EIl/L^2)(L/2 - x) \qquad (D.42)$$

At $x = L/4$ the bending moment is

$$M_x = 3EIl/L^2 \qquad (D.43)$$

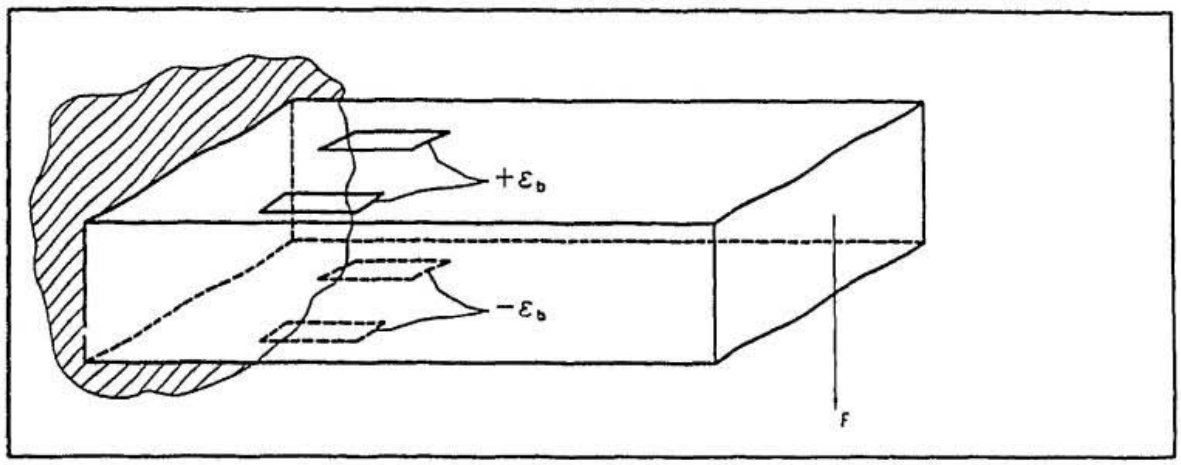

Figure D.11

The bending moment (M_x) at the 1/4 span position of the strain gauged section is

$$M_x = 3(207\times10^9)(1\times10^{-12})(0.36\times10^{-3})/(30\times10^{-3})^2$$
$$= 0.75\text{N.m}$$

$$l = FL^3/12EI \qquad \text{(Munday \& Farrar 1979)}$$
$$= (33.5)\,(0.03)^3/[12(207\times10^9)\,(1\times10^{-12})]$$
$$= 0.36\text{mm}$$

The stress in the 1 mm thick section is given by Equation D.44.

$$\sigma = My/I \qquad \text{(Beer \& Johnston 1981)} \qquad (D.44)$$
$$= (0.75)\,(0.5\times10^{-3})/1\times10^{-12}$$

$= 3.6x10^8 N/m^2$
$= 360MPa$

$\varepsilon = \sigma/E$ (Beer & Johnston 1981) (D.45)
$= (360x10^6/207x10^9$
$= 1.7x10^{-3}$
$= 1700mstrain$

For the full wheatstone bridge (See Figure D.11)

Determine the output voltage from the strain gauges

$\Delta E/V = 1/4[\Delta R_1/R_1 - \Delta R_2/R_2 + \Delta R_3/R_3 - \Delta R_4/R_4]$ (Dally & Riley 1965) (D.46)

Where:

ΔE = the output voltage
R_i = gauge resistance
ΔR_i = change in gauge resistance due to strain

Note, for a wheatstone bridge $\Delta R_i/R_i$ are all equal and additive. Therefore,

$\Delta E/V = \Delta R/R = 2\varepsilon_b$ (Dally & Riley 1965) (D.47)
$= 2(1.7 \times 10^{-3})$
$= 2.4mV/V$

If the bridge is excited by 5V rms and amplified with a gain of 1000

Then

ΔE = the output voltage
$= (5 \times 2.4)(1000) = 12$ volt

This is sufficient to allow the measurement of the expected loads.

Natural oscillating frequency of the mounting bracket

Determine the natural oscillating frequency of the mounting bracket about an axis 'x' parallel to the water flow and an axis 'y' perpendicular to the water flow (See Figure D.12).

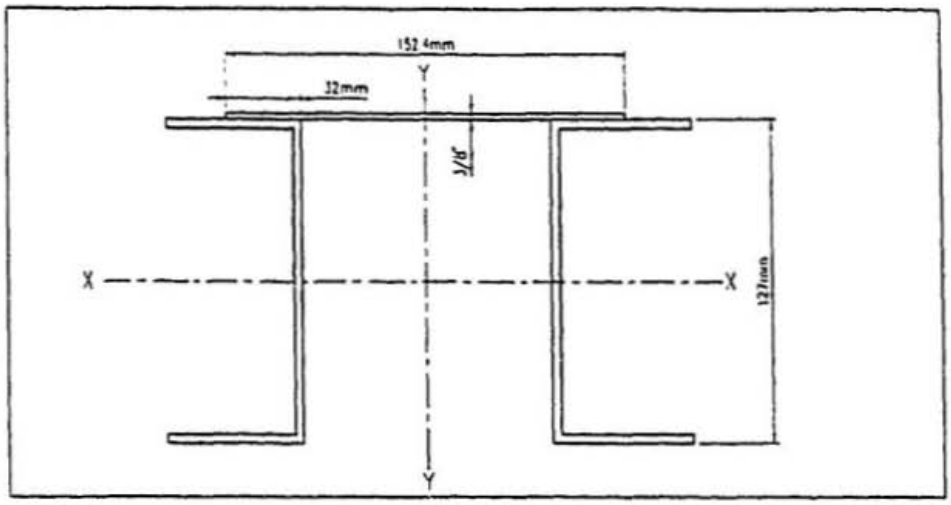

Figure D.12

Calculate Ixx

Table D.3

Item	Area	Y	AY	I	Y_{NA}	AY_{NA}^2
	mm^2	mm	mm^3	mm^4	mm	mm^4
44 x 8.2	356.4	-59.45	-21,188	1,948.6	-83.45	2,481,935
127 x 4.8	609.6	0	0	819,353.0	-24	351,130
44 x 8.1	356.4	-59.45	-21,188	1,948.6	-83.45	2,481,935
44 x 8.1	356.4	59.45	21,188	1,948.6	35.45	447,889
127 x 4.8	609.6	0	0	819,353.0	-24	2,481,935
44 x 8.6	356.4	59.45	21,188	1,948.6	35.45	447,889
152.4 x 9.5	1,447.8	68.25	98,812	10,888.7	44.25	2,834,883
	4,092.6		98,812	1,657,389.1		11,527,596.0

$Y_{NA} = 98812/4092.6$
$= 24mm$

$I_{xx} = (1/12)bh^3$

$I_{total} = 1,657,389 + 11,527,596$
$= 13,184,985mm^3$

μ = weight/unit length
= 32.1 Kg/m

$\omega_{nxx} = 3.515\sqrt{(EIg/\mu l^4)}$ (Steidel 1971) (D.48)

$E = 209GPa$

$= 3.515\sqrt{(209x10^9)(3184985x10^{-9})(9.81)/(32.1)(0.8)^4}$
$= 45343$ radians/second

$T.R._{xx} = |1/(1-6.282^2/45343^2)|$
$= 1$

Calculate Iyy

Table D.4

Item	Area	Y	AY	I	Y_{NA}	AY_{NA}^2
	mm^2	mm	mm^3	mm^4	mm	mm^4
44 x 8.1	356.4	-66.2	-23,594	57,499	66.2	1,561,902
127 x 4.8	609.6	-46.6	-28,407	1,170	46.6	1,323,783
44 x 8.1	356.4	-66.2	-23,594	57,499	66.2	1,561,902
44 x 8.1	356.4	66.2	23,594	57,499	66.2	1,561,902
127 x 4.8	609.6	46.6	28,407	1,170	46.6	1,323,783
44 x 8.1	356.4	66.2	23,594	57,499	66.2	1,561,902
152.4 x 9.5	1,447.80	0	0	2,780,181	0	0
	4,092.6			3,012,517.0		8,895,174.0

$Y_{NA} = 0$

$I_{yy} = (1/12)b^3h$

$I_{total} = 3012517+8895174$
$= 11907691 mm^3$

μ = weight/unit length
= 32.1 Kg/m

$\omega_{nyy} = 3.515\sqrt{(EIg/\mu l^4)}$

E = 209GPa

$= 3.515\sqrt{(209x10^9)(11907691x10^{-9})(9.81)/(32.1)(0.8)^4}$
= 43091 radians/second

$T.R._{yy} = |1/(1-6.282^2/43091^2)|$
= 1

Vibration should not be a problem since the transmission ratios are 1.

Estimation of F_{HR} on the aft drive shaft

The rotational displacement, velocity, and acceleration for link 'A' about point 'C' (See Figure 3.8) is given by Equations D.49, D50, and D.51 (Beer and Johnston 1977b).

Rotational displacement of link 'B' about 'C' = Amp sin(ωt) (D.49)

Rotational velocity of link 'B' about 'C' = Amp ωcos(ωt) (D.50)

Rotational acceleration of link 'B' about 'C' = -Amp ω^2sin(ωt) (D.51)

Where: Amp = the amplitude of the motion. The maximum expected amplitude of the dynamometer's motion is 30° (0.52radians/second)

Assuming constant rotation the centripetal acceleration (A_c) is given by

$A_c = \Omega^2 r$ (Beer and Johnston 1977b) (D.52)

and the centripetal force (F_c) is defined as

$F_c = m\Omega^2 r$ (Beer and Johnston 1977b) (D.53)

Where:

Ω = the angular velocity of link 'B'
$= (Amp\omega)^2$
ω = rotational frequency (maximum assumed to be 3.14radians/second)
r = distance from joint 'C' to the centre of gravity of the link.
= 0.05m
m = mass of link 'B' (0.25Kg)

$F_c = (0.25)(0.52 \times 3.14)^2(0.05)$
$= 0.03N$

This is relatively low (0.06% of the expected axial force and 0.04% of the thrust force) due to the low frequencies of oscillation.

Estimation of the maximum load in the direction of the water flow carried by the forward drive shaft.

The maximum angle between the link in the forward drive shaft and the vertical is approximately 3°. Assumming an axial load of 45.5N in the forward drive shaft, then the maximum load in the direction of the water flow carried by the forward drive shaft will be

$F_{fsh} = 45.5 \sin(3)$
$= 2.4N$

Since the maximum expected thrust force is 67N, the forward drive shaft will carry a maximum of 3.6% of the thrust force.